New materials for micro-scale sensors and actuators. An engineering review

S.A. Wilson, R.P.-J. Jourdain, Q. Zhang, R.A. Dorey, C.R. Bowen, Magnus Willander, Qamar Ul Wahab, M. Willander, S.M. Al-hilli, O. Nur, E. Quandt, C. Johansson, E. Pagounis, M. Kohl, J. Matovic, B. Samel, der Wijngaart W. van, Edwin Jager, D. Carlsson, Z. Djinovic, M. Wegener, C. Moldovan, E. Abad, M. Wendlandt, C. Rusu and K. Persson

Original Publication:

S.A. Wilson, R.P.-J. Jourdain, Q. Zhang, R.A. Dorey, C.R. Bowen, Magnus Willander, Qamar Ul Wahab, M. Willander, S.M. Al-hilli, O. Nur, E. Quandt, C. Johansson, E. Pagounis, M. Kohl, J. Matovic, B. Samel, der Wijngaart W. van, Edwin Jager, D. Carlsson, Z. Djinovic, M. Wegener, C. Moldovan, E. Abad, M. Wendlandt, C. Rusu and K. Persson, New materials for micro-scale sensors and actuators. An engineering review, 2007, Materials science & engineering. R, Reports, (56), 1-129.
http://dx.doi.org/10.1016/j.mser.2007.03.001

New Materials for Micro-scale Sensors and Actuators – An Engineering Review

Edited by:

Stephen Wilson
Microsystems and Nanotechnology Centre, Materials Department, Cranfield University, Bedfordshire MK43 0AL United Kingdom

and

Chris Bowen
Materials Research Centre, Department of Mechanical Engineering, University of Bath, Bath, BA2 7AY United Kingdom

Abstract

This paper provides a detailed overview of developments in transducer materials technology relating to their current and future applications in micro-scale devices. Recent advances in piezoelectric, magnetostrictive and shape-memory alloy systems are discussed and emerging transducer materials such as magnetic nanoparticles, expandable micro-spheres and conductive polymers are introduced. Materials properties, transducer mechanisms and end applications are described and the potential for integration of the materials with ancillary systems components is viewed as an essential consideration. The review concludes with a short discussion of structural polymers that are extending the range of micro-fabrication techniques available to designers and production engineers beyond the limitations of silicon fabrication technology.

Keywords

Piezoelectric, magnetic, shape memory, polymer, microstructure, microtechnology

Table of Contents

10	**Shape memory materials** **10.1 Shape Memory Alloys** **10.2 Micro-scale applications of SMA** **10.3 Shape memory polymers** **10.4 SMP applications in MST**
11	**Expandable polymer micro-sphere composites** **11.1 Direct mixing of the microspheres in liquid** **11.2 Surface immobilization of the microspheres by incorporation in photoresist** **11.3 Surface immobilization of the microspheres through self-assembly on a chemically altered surface** **11.4 Incorporation of the microspheres in a paste** **11.5 Incorporation of the microspheres as a composite in a polymer matrix**
12	**Electro-active polymers - General**
13	**Electro-active polymer micro-actuators** **13.1 Conjugated Polymer Actuators** **13.2 Fabrication of PPy-Microactuators** **13.2 Operation and Performance** **13.3 Applications and Devices**
14	**Electrochromic / electroluminescent polymers** **14.1 Electrochromic materials** **14.2 Electrochromic devices** **14.3 Electroluminescent materials** **14.4 Electroluminescent devices**
15	**Ferroelectrets – Cellular piezoelectric polymers** **15.1 Foam preparation and optimization** **15.2 Void charging in cellular space-charge electrets** **15.3 Piezoelectric properties** **15.4 Applications of ferroelectrets**
16	**Conductive polymers** **16.1 Mechanism of polymer conductivity – role of doping** **16.2 Conductive polymeric materials - examples** **16.3 Applications of conductive polymers in sensors and actuators**
17	**Photopatternable polyimides** **17.1 Properties of polyimides** **17.2 Processing of polyimides** **17.3 Polyimide applications**
18	**Structural Polymers** **18.1 Selection of Materials** **18.2 Applications**

List of Contributing Authors

Dr Stephen A. Wilson (Corresponding Author)
Dr Renaud P-J Jourdain, Dr Qi Zhang
Dr Robert A. Dorey

Microsystems and Nanotechnology Group
Materials Department
Cranfield University
Cranfield
Bedfordshire
United Kingdom
MK43 0AL
Tel: +44 (0)1234-750111 Ext2505
Fax: +44 (0)1234-751346
e-mail: s.a.wilson@cranfield.ac.uk

CRB

MW

EQ

CJ

EP

MK

JM

WvW

CKM

Dr. Edwin W. H. Jager, Daniel Carlsson
Micromuscle AB
Westmansgatan 29
58216 Linköping
Sweden
Tel. +46-13-3420053
Fax. +46-13-3420059
e-mail: edwin.jager@micromuscle.com,
daniel.carlsson@micromuscle.com

ZD

Dr Michael Wegener
Applied Condensed-Matter Physics
Department of Physics
University of Potsdam
Potsdam

Germany
14469
Tel: +49 (0)331-9771144
Fax: +49 (0)331-9771577
e-mail: mwegener@uni-potsdam.de

CM

EA

Dr Michael Wendlandt
Micro and Nanosystems
Department of Mechanical Engineering
ETH Zurich
8092 Zurich
Switzerland
Tel: +41 (0)632 47 05
Fax: +41 (0)632 14 62
e-mail: wendlandt@micro.mavt.ethz.ch

1 Introduction

A material can be said to be ‘new’ or ‘novel’ until it finds its way into mainstream engineering technology. The distinguishing criterion is not whether the end-use is in consumer products, sophisticated, specialised or niche applications, but whether materials performance is predictable and reliable. By implication, quality and processing must be well understood and commercial supplies readily available. For these reasons, the time-scale in which a material remains new is related directly to the commercial interest that has evolved and consequently to the business opportunities that the material has inspired in its conceptual form.

A new material that promises to provide tangible improvements over the established norm will soon attract commercial interest and its’ potential use will come under scrutiny. The first questions to be raised relate to possible integration into existing systems or possible creation of a new product line. If technological barriers to integration exist, be these either real or perceived, then commercial interest will immediately cool. For the particular case of micro-systems technology (MST), where the creation of fine scale integrated systems is a key motivational factor, the potential costs of product development can often overshadow any improvements in performance that might be gained. This is partly a consequence of local integration with microelectronics and packaging and it is partly due to the capital equipment costs involved. In the main, however, it is due to the time and uncertainty involved in establishing a new fabrication route that meets predefined standards of quality and reliability. Hence to gain acceptance in micro-technology the new material must offer performance advantages and be compatible with various ancillary systems components and packaging. In all cases it is highly probable that production will entail a lengthy sequence of process steps and consequently the material will need to tolerate repeated thermal cycling as system fabrication proceeds. It is not uncommon for the materials covered in this review, namely transducer materials, to rely on some aspect of their micro-structural composition that is highly sensitive to processing conditions. As an example, effects of size or morphology are often critical and optimum performance can be impaired by excursions outside a limited temperature range. Therefore the processes involved in creating the material may only be one part of the equation and compatibility with secondary systems fabrication processes is equally essential.

Full-integration of micro-electronic and micro-mechanical components on a single wafer has been achieved commercially using silicon processing technology. Some examples of products made in this way include micro-gyroscopes and micro-mirror arrays. However, whilst this integrated design approach appears to be commercially attractive it has proven to be relatively rare owing to its complexity and high development costs. Furthermore, due to processing restrictions the mechanical components of these devices are often constructed simply from silicon and silicon oxide with selective metallization. An alternative approach is via a hybrid design where component parts are created separately for subsequent assembly into a complete system. For small or medium-scale batch production this is an attractive option, as it removes many of the restrictions imposed by the need for process compatibility. Furthermore test procedures can be performed at the wafer-scale before final assembly to enhance quality and overall yield. It is in this context that new transducer materials have the best chance of success. Key considerations are the availability of material-specific replication

technologies, device-specific geometric requirements (feature types, planar or 3D, aspect ratios), the required dimensional tolerances and accuracy, surface quality or integrity, volumetric production rate and, often of secondary importance in this context, cost.

Overall it can be said that the most significant barriers to progress are firstly the availability of production technologies and secondly the availability of knowledge. This article therefore seeks to review recent developments in transducer materials technology and to place them in the context of their current and future applications in micro-scale systems fabrication. In addition to examining recent advances in piezoelectric, magnetostrictive and shape memory alloys systems, emerging transducer materials such as magnetic nanoparticles, expandable micro spheres and conductive polymers are also discussed. Their underlying properties, transducer mechanism and end applications are described, along with the processing technologies to form them in particulate, bulk or film geometry. Aspects of processing that may influence integration of the materials with their related components are viewed as an essential consideration. From a global perspective there are of necessity some important omissions. It seems certain that materials incorporating carbon nanotube technology and nanocomposites will reach industrial maturity in the very near future and that their impact will be significant. This subject matter has been extensively reviewed elsewhere and the materials are not covered in this review. Rather the intention is to highlight a range of materials that could be used in conjunction with the standard the micro-fabrication techniques that are available to designers and production engineers to extend the range of devices that can be made beyond the limitations of silicon fabrication technology.

2 Ferroelectric ceramics

Stephen A. Wilson, Renaud P-J Jourdain, Qi Zhang and Robert A. Dorey – Cranfield University, United Kingdom

Polycrystalline lead zirconate titanate (PZT) ceramics are of major importance in microtechnology, particularly in the field of sensors and actuators, because of their superior piezoelectric and pyroelectric properties and their high dielectric constants [1]. Devices that incorporate these materials as their active component include micro-pumps and valves, ultrasonic motors, thermal sensors, probes for medical imaging and non-destructive testing, accelerometers and quite recently a new range of electronic components that includes filters, memory devices and switches. New applications continue to emerge and a major research effort has been underway to address the manufacturing technology required to incorporate these materials with associated structural components and electronic circuitry at the wafer scale. Two distinct approaches are available which have very different process requirements and which consequently require different fabrication techniques. The bottom-up approach is by thin film deposition, performed via spin coating of a sol-gel precursor or sputtering. Thin film compositions have been developed that have greatly reduced processing temperatures (600-700 ºC) in comparison to standard bulk ceramic sintering (1100-1400 ºC) and this has led to commercialization by the major electronics corporations in the form of ferroelectric memories and electronic components. A single layer is typically around 0.1 micron and films are built up to the required thickness by depositing several layers in succession.

The processing issues that surround production of electromechanical devices on the micro-scale are arguably even more complex however, due to the range of ancillary system components that are needed. The available force that can be generated by the ceramic is directly related to the amount of electro-active material that is available and many piezoelectric devices with potential commercial applications such as micro-pumps require much thicker films to be effective, typically in the size range 10 - 80 microns. These values have been achieved by multi-layer deposition using composite thick film techniques and significant progress has been made, which makes these materials suitable for a number of applications. This technique is detailed below. In practice residual tensile stress is a critical issue, inherent to the process, which becomes progressively more significant as film thickness increases. Tensile stresses result from substrate clamping as the material crystallizes at elevated temperatures often leading to reduced fracture toughness or cracking and somewhat lower electro-active coefficients.

The alternative, top-down approach for micro-scale device fabrication is by assembly of net shape components, usually by adhesive bonding. This is routinely adopted for one-off device fabrication in the research environment. On the wafer scale there are important questions of positional accuracy both laterally and in terms of parallelism with underlying materials. This becomes more significant as layer thicknesses are reduced below ~80 microns. The nature of the bond is of critical importance to device performance and hence the surface roughness and particularly the flatness of the ceramic component are very significant. Recently it has been shown that bulk PZT ceramics can be thinned in-situ to thicknesses well below 50 microns, using ultra-precision grinding, after bonding to wafer-scale components [2]. This technique has

several advantages: a) the electro-active properties of the ceramic can be fully exploited; b) films can be made in the 20 - 50 micron thickness range, which is difficult to achieve by other methods; c) ceramic films can be engineered into residual compression to optimize device performance; d) the machining techniques can be used in sequence with standard micro-fabrication processes, such as photolithography, without the need for a high temperature excursion, thereby extending design flexibility and the range of devices that can be produced; e) PZT films in this thickness range can be can be activated well below 100V, this is highly significant in commercial terms as they are then compatible with current CMOS drive circuitry. Recent research work is this area has lead to major improvements in technique and the method can be considered viable for flexible, batch-scale assembly and systems integration. The key issues that are involved in producing exceptionally smooth, flat surfaces in PZT by means of ultra-precision grinding have been discussed by Arai [3-5]

As noted, ferroelectric ceramics are of widespread technological importance and for this reason they remain the subject of intense research activity. Materials development has focussed on three particular areas. One of these can be said to be market-driven through strong commercial interest in new fuel injection systems for motor vehicles. This is a high power, high temperature, low voltage application which is satisfied by multi-layer ceramic stacks. The ceramic layers are typically less than 50 microns in thickness and they are co-fired with metallic interlayers to produce an inter-digitated structure. As the layers are thin a low applied voltage can be used to generate a strong electric field in the ceramic [4]. A further area of both commercial and technological interest is in high frequency medical ultrasonics for imaging and ultrasound-guided therapy. This also tends to be a high power application where the goal is to reduce the energy losses that result from internal power dissipation. These can generate significant amounts of heat leading to thermal instability and loss of performance [6-8].

The second major area of research is pushed by new technology that has emerged in the form of ferroelectric single crystal materials. This type of material has recently become available in commercial quantities and the electro-active properties exhibited are a marked extension beyond those of conventional polycrystalline ceramics. The crystals are relaxor ferroelectric materials and they are typically based on the lead magnesium niobate – lead titanate (PMN-PT) solid solution, although many other compositions are also in research. Relaxors are characterised by a diffuse dielectric phase transition, that is to say their dielectric permittivity is both frequency and temperature dependent. Their physical behaviour is as yet not fully understood but, importantly, they are found to exhibit very large dielectric permittivities and very high piezoelectric coefficients. In operation their electro-mechanical behaviour is predominantly electrostrictive in nature resulting in exceptionally low hysteretic losses even at high frequencies. Whilst these materials have shown clear superiority for some electro-acoustic applications, their adoption for use in actuators is still at a very early stage. The upper temperature limit of operation can be relatively low at around 50-80°C and this, together with a marked environmental variability of properties, clearly imposes some restrictions on design. Nevertheless these materials do show very interesting new capabilities and they are an exciting technological innovation [9-15]

The third main focus of research is driven by environmental concerns over the industrial use of compounds containing lead. Whilst it can be argued that the toxicity of lead-containing ceramics or glasses is very significantly reduced in comparison to that of the

base metal, there is pressure to reduce its consumption. This has led to a concerted effort world-wide to identify equivalent electro-active materials that are lead-free. To-date, despite some significant investment of time and resources, little progress has been made in developing materials that are able to outperform standard PZT ceramics. Several interesting compositions have been identified, however, that have useful transducer properties and work seems sure to continue [16-20].

2.1 Piezoelectric Properties and Potential Applications of Ferroelectric Thin Films

Thin films are generally considered to have thicknesses less than 1μm. Interest in ferroelectric thin films has been considerable over the last 20 years, driven by the possibility of using them for non-volatile memory applications and new microelectromechanical systems (MEMS). Thin film piezoelectric materials offer a number of advantages in MEMS application, due to the large displacements that can be generated, the high available energy densities, as well as high sensitivity sensors with wide dynamic ranges, and low power requirements [21].

Piezoelectric MEMS devices contain at least two elements: a bulk silicon frame and a piezoelectric deflection element built onto it, which also has electrodes to apply or detect voltage potentials. The silicon substrate often provides only the structural element, defining the mechanical properties, while the added functional material such as piezoelectric thin films provide a direct transformation between a driving signal or a read-out signal and a sensor or an actuator parameter.

A sampling of recent developments in piezoelectric devices using thin films includes a variety of actuators and sensors. These include lead zirconate titanate (PZT) based ultrasonic micromotors [22-24], cantilever actuators, probes for atomic force microscopy [25], micropumps [26], ultrasonic transducers for medical applications [27-28], uncooled thermal imaging as pyroelectric arrays [29-30]. The aims of this section are as follows:

- To introduce the current fabrication techniques for piezoelectric thin films
- To discuss the important piezoelectric coefficients and the key issues or factors influencing the piezoelectric properties of ferroelectric thin films
- To discuss the piezoelectric thin film poling and reliability issues

Thin film deposition

Most of the existing physical and chemical coating techniques have been investigated for the deposition of PZT. The physical methods include ion beam sputtering [31], rf magnetron sputtering [32-33], dc magnetron sputtering [34] and pulsed laser deposition (PLD) [35-37]. Chemical methods include metal-organic chemical vapour deposition (MOCVD) [38-42] and chemical solution deposition (CSD) [43-44]. Today there is a clear trend to apply MOCVD or CSD since a particular advantage with MOCVD is that conformal coating of three-dimensional objects is possible. CSD is a low cost technique for small-scale production, as required in the sensor industry. Since for CSD the film is initially amorphous, post-annealing treatments are necessary to crystallize the film. All the other methods described above allow in situ growth. Although the CSD technique seems very different from the vacuum deposition techniques like sputtering or PLD, there are nevertheless some common features:

- The crystallinity and texture of the film are strongly dependent on the crystal structure of the substrate, for example: lattice parameters and thermal expansion coefficients matching, surface defects etc.
- The quality of the interface is dependent on the substrate chemistry, for example: reactivity of the substrate surface with the deposited phase constituents, diffusion coefficients etc.
- The lattice energy has to be brought to the system, either thermally or by a physical way, since the initial state is a disordered one (gas or liquid phase, plasma, particle beam etc.).
- Nucleation and growth of the perovskite require a precise stoichiometry, otherwise competing phases with fluorite ($Pb_{2+x}Ti_{2-x}O_{7-y}$) and pyrochlore ($PbTi_3O_7$) structures will nucleate [45].
- The growth is nucleation controlled [46-47].

Piezoelectric properties of ferroelectric thin films

The piezoelectric properties of ferroelectric materials, such as $PbZr_{1-x}Ti_xO_3$, are highly dependent on composition [21]. A schematic diagram of the lead zirconate (PZ) – lead titanate (PT) phase diagram is shown in Figure 2.1. PZT has two main ferroelectric phases; rhombohedral for $x < 0.48$ and tetragonal for $x > 0.48$ under standard conditions. The rhombohedral phase is divided into 'high temperature' and 'low temperature' phases with crystal symmetries R2m and R3c respectively. The boundary between the tetragonal and rhombohedral phases is sharply defined and virtually independent of temperature and the boundary is known as the morphotropic phase boundary (MPB). The boundary was defined by Jaffe et al. [48] to be at a composition of 53 % Zr and 47% Ti in PZT ceramics, and is defined as the point of equal coexistence for tetraganol / rhombohedral phases. In bulk ceramics, maxima in the piezoelectric coefficients are generally observed at the MPB. The same behaviour is often [49-55], but not universally [54-56], reported in thin films.

In MEMS technology, most of the piezoelectric thin films are polycrystalline materials. The piezoelectric effect is averaged over all the grains. The optimum piezoelectric properties of ferroelectric materials can only be obtained for polycrystalline materials after an appropriate 'poling' treatment. Poling is able to switch internal polarisation to the direction of applied field. As a result, there is a net polarisation and a net piezoelectric effect. This can simplify processing, since single crystals are not required for good electromechanical properties.

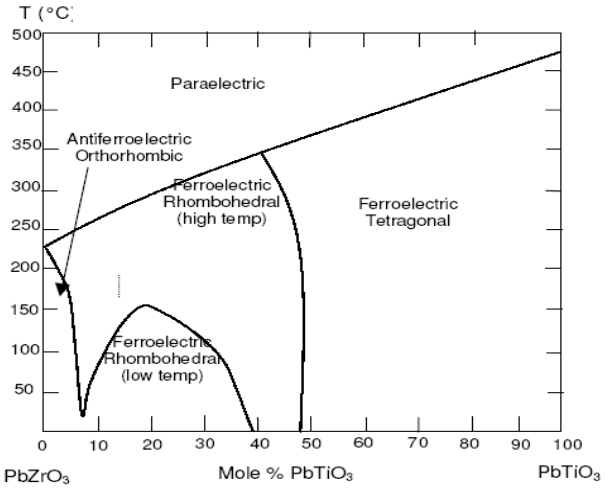

Figure 2.1 Phase diagram of the PbZrO3 - PbTiO3 system [48]

The piezoelectric properties of films are almost always smaller than those of corresponding bulk ceramics. This is due to substrate clamping, which reduces the amount of strain which the film can exhibit for a given applied electric field or stress [56-57]. The film is part of the composite structure consisting of the piezoelectric film and silicon substrate. The film is clamped in the film plane, but free to move in out-of-plane direction. Therefore the clamping effect is thickness dependent, and the piezoelectric coefficient, such as $d_{33,f}$, increases with increasing thickness over a range of film thickness [21, 58-62]. In thin film ceramics, it is conventional to assign the index 3 to the poling direction, usually perpendicular to the film plane. The directions of 1, 2 are therefore in the plane of the film. In a polycrystalline film, directions 1 and 2 are equivalent which implies that the in-plane strains (d_{31} and d_{32}) due to an applied electric field though the film thickness (E_3) are isotropic and $d_{31} = d_{32}$.

The relative coefficients of piezoelectric thin films are the effective values of $d_{33,f}$ and $e_{31,f}$, which are obtained as follows from the bulk tensor properties [63-64]:

$$d_{33,f} = d_{33} - 2s^E_{13}d_{31}/(s^E_{11}+s^E_{12}) \quad (1)$$

$$e_{31,f} = d_{31}/(s^E_{11}+s^E_{12}) \quad (2)$$

The $d_{33,f}$ coefficient can be directly measured as the strain per unit electric field through the film thickness (x_3/E_3) provided that $x_1=x_2=\sigma_3=0$, where x_1 and x_2 are in-plane strains, σ_3 off-plane stress, x_3 is off-plane strain and s^E_{ij} is a compliance of the thin film. This measurement has been achieved with a double-beam Mach-Zehnder interferometer [45] that measures the thickness change of a film clamped on a much thicker substrate (assuring $x_1=x_2=0$) at $\sigma_3=0$. The measurement of the transverse piezoelectric coefficient $e_{31,f}$ has been undertaken with a cantilever bending method, collecting the charges as a function of x_1 and x_2 at zero σ_3 and electric field [66].

Apart from mechanical clamping due to the inert substrate, there are several other factors which influence the piezoelectric response of ferroelectric thin films, including orientation of the film [67-70], grain size [71], the level of polarization and breakdown field strength [72-73]. The influence of defects on the domain-wall contributions to the piezoelectric effect in thin films has not yet been studied in detail. Thus, it is presently

not clear whether, for example, the effect of acceptor and donor dopants on the properties of PZT films would lead to the same effects as in bulk materials.

Film orientation can have a substantial effect on piezoelectric coefficients. Piezoelectric coefficients are optimized when the polarization axis, namely c-axis or (001), is perpendicular to the film surface. It has been recently demonstrated [58] that the sol-gel derived PZT thin films with higher c-axis orientation exhibited larger piezoelectric coefficients. For random polycrystalline films, poling is often necessary to reorient the domains along the poling direction.

In many of the structures applied to MEMS technology, the piezoelectric film is part of a composite structure, i.e. the piezoelectric film is clamped to another elastic body. The coupling coefficient not only depends on the material parameters, but film stresses also play a role and such film stresses introduced during processing at elevated temperature are unavoidable. The residual stress can be as high as 10-100 MPa [74], which induces a pre-strain, or a pre-curvature to micromechanical structures. This stress has to be taken into account in the design phase of the devices.

Poling and reliability issues

The effects of poling in thin films differ from that in ceramics, since the clamping effect of the substrate pins the motion of a-domains [75-76]. In bulk ceramics, the clamping is effectively zero, and domains are relatively free to move in alignment with the poling field. There are few studies to date that are specifically related to thin film poling for piezoelectric measurement, but it is well known that the strain induced by poling can be close enough to the tensile strength of the film which can induce cracking or delamination. Poling usually takes place at elevated temperatures (<150 ºC) at high field (200-300 kV/cm) as this increases domain wall mobility and enables better alignment along the field direction. Some examples of PZT thin film devices are shown in Figures 2.2 and 2.3.

A further important point of performance is stability during operation and with time. The effective measured piezoelectric coefficients decay with time after poling in a process known as piezoelectric ageing, during which the domains in the poled sample revert to a more thermodynamically stable configuration. Depolarization (fatigue) may occur and, if integration of the film into the MEMS structure is not optimised, delamination of the PZT film or the electrodes may occur [77]. From an industrial point of view, the evaluation of ageing and fatigue is certainly an important task, however, only a limited studies have been reported so far [78-80].

Summary – ferroelectric thin fims

Ferroelectric thin films continue to represent an area of dynamism and technical advance in MEMS. Over the last 20 years, considerable progress has been made in optimizing the deposition conditions for thin films to improve the available piezoelectric activity although the growth of good quality PZT thin films still requires some effort. In processing such films, wet chemical methods continue to appear attractive for many applications. Recently, the attention has shifted from preparing novel ferroelectric films to the integration of such films in complex devices.

The overall estimation of performance is best seen in device applications since the performance of the devices depends not only on the properties of the materials, such as,

film orientation, grain size, thickness etc., but also the composite structure of the devices in many cases.

In the future, the materials community requires greater knowledge of, and ability to control, the microstructure of films, and much more effective interaction with device technologists. Much greater attention will have to be directed to cost including both the films and device or system.

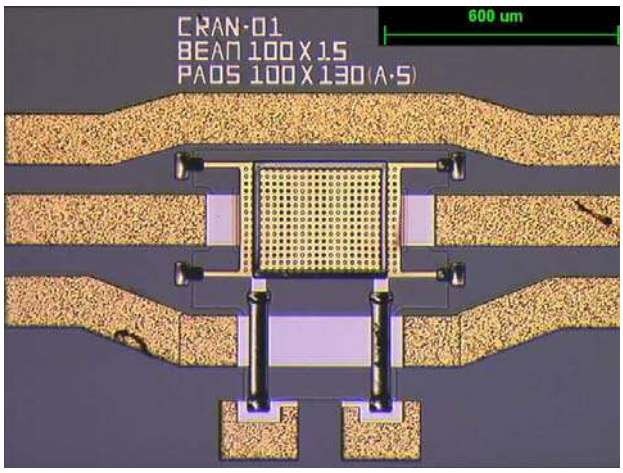

Figure 2.2 a) RF MEMS series switch – Image courtesy of Glenn Leighton, Materials Department Cranfield University

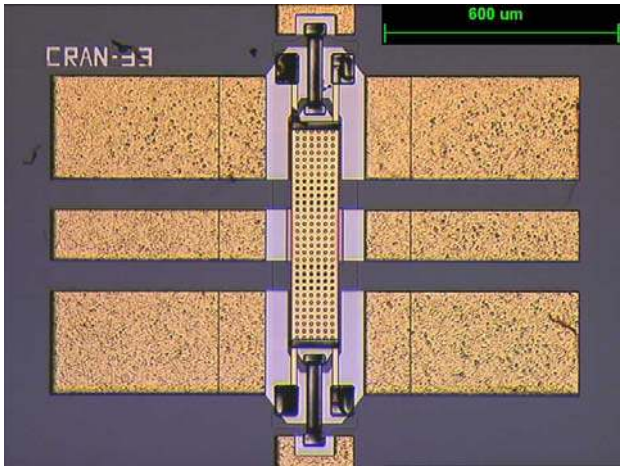

Figure 2.2 b) RF MEMS shunt switch – (Image courtesy of Glenn Leighton, Materials Department Cranfield University)

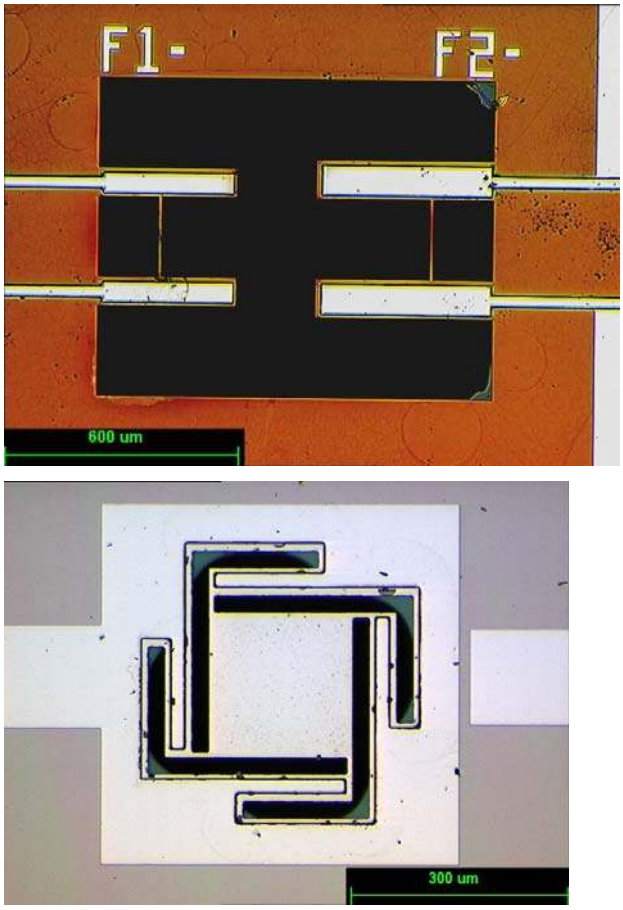

Figure 2.3 PZT actuated coupled cantilever bandpass filters / Parallel plate variable capacitor actuated by four PZT cantilever unimorphs PZT thin film. (Images courtesy of Glenn Leighton, Materials Department Cranfield University)

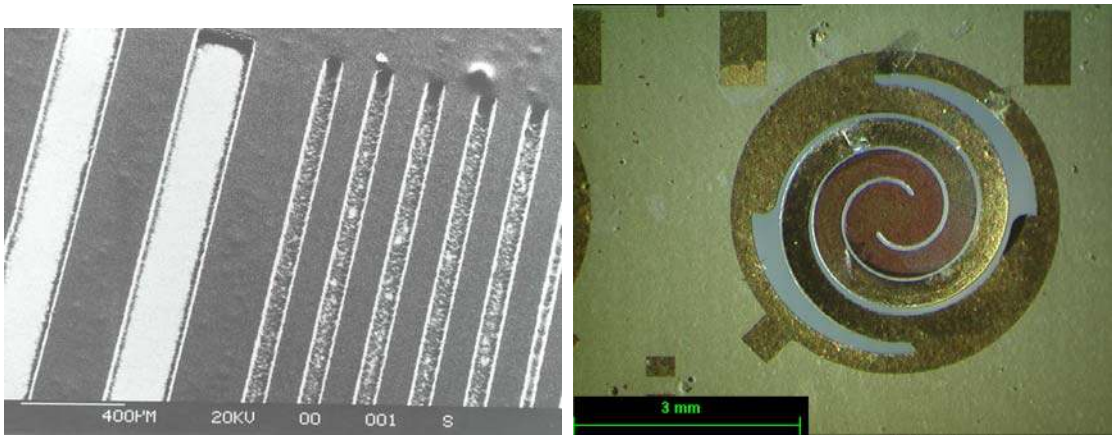

Figure 2.4: a) Test structures patterned by powder blasting and b) a spiral cantilever unimorph device – 10 micron thick film PZT deposited on a 20 micron silicon membrane

2.2 Thick Film Fabrication for micro-scale sensors

Thick films are generally considered to be those with thicknesses greater than 1μm, however, such a definition is imprecise as many thin film technologies can now achieve film thicknesses in excess of 1 μm. Thick films are required to increase the amount of

functional material present in order to achieve higher displacements or increased power compared to thin films, e.g. for acoustic transducers or micro pumps. For the purposes of this discussion, PZT thick films will be considered to be those that are formed using a powder suspension based processing route. These suspensions are typically made up of the desired ceramic powder (to impart the required functional properties), a carrier fluid, and additives designed to improve the stability of the ink and processing of the ceramic material. For further information on issues associated with thick film processing and patterning of thick film structures the reader is directed towards an earlier review [81].

Deposition techniques

Many different forming techniques can be used to deposit thick films due to the ability to tailor the fluidic characteristics (e.g, surface tension, viscosity, shear behaviour) of the powder suspensions. Despite the difference in processing techniques the general processing stages are retained. Firstly, a suspension of the powder is deposited onto a substrate. Drying of the suspension then causes solvents and other additives to be removed. Finally a high temperature stage is used to sinter the film.

Screen printing is the most widely used thick film deposition technique [82] due to the ability to simultaneously create the thick film and pattern it. During the printing process, ink (containing the powder suspension) is forced though a fine mesh to deposit it onto the desired substrate. The mesh can be selectively masked off to enable a desired pattern to be created. The rheology of the ink is such that it does not pass though the mesh when at rest. When a shear stress is applied by the 'squeegee' of the screen printing device the viscosity decreases by shear thinning and the ink passes through the mesh. The ultimate resolution of the screen printing process is limited by the resolution of the mesh and the flow of the ink once printed.

Once the ink has been printed it is dried to remove the solvents. Subsequent layers can then be deposited prior to removing the organic components, such as polymers and modifiers, at temperatures between 350 and 600ºC. Final sintering occurs at temperatures between 850 and 950ºC.

Inks with lower powder loadings and viscosities (and less shear thinning behaviour) are used with processes such as *spin coating* [83], *dip coating* [84], and *spray coating* [85-86]. All of these techniques result in the formation of continuous films. By further reducing the powder loading (typically below 1 vol% [87]) *electrophoretic deposition* (EPD) can be used to create continuous films. In EPD a DC electric field (either constant field or constant current density) is used to attract charged ceramic particles to a substrate [88-89] with the advantage that complex geometries can be coated [90]. The limitation of the EPD process is that the substrate must be conducting, which may present difficulties in MEMS devices, and high density systems (e.g. lead based) are difficult to stabilise [88]. A thorough review of the electrophoretic deposition technique, as applied to many ceramic oxide films, is given by Sarkar and Nicholson [91].

Inks

In addition to using different deposition routes, it is also possible to use inks based on different principles – non-fugitive binders, fugitive binders, and transformation binders. The most straightforward ink type is the *non-fugitive binder* type where the binder remains within the system and forms the structural component of the film. Paints typify such systems, where an organic binder is used to bind the film together and bond the

film to the substrate. PZT paints have been used to construct strain sensors on large structures [92]. The advantage of such systems is that no (or minimal) heating is required for processing the films. This means that the films can be applied to delicate substrates or large structures where it would be impractical to apply a post heat treatment. The disadvantage is that the low percentage (often little more than 50%) and low interconnectivity of active material within the films means that the functional properties of the films are significantly below those of bulk materials and conventionally sintered thick films.

The majority of ceramic powder processing is based on *fugitive binder* systems where a temporary binder is used to impart limited strength to the system while it is shaped and handled. Subsequent thermal processing is then used to remove the binder and cause sintering of the ceramic phase. These fugitive binder inks use the same principle with inks containing the powder, and organic binder, a carrier fluid, and additives. The carrier fluid (usually water or a solvent) allows the powder to be handled conveniently and shaped. Once the film has been deposited and the carrier fluid removed through evaporation, the film is held together and to the substrate by the fugitive binder phase. To enhance the sintering kinetics of the system, and lower the sintering temperature, a sintering aid is often added to the ink. These sintering aids form a liquid at temperatures in the region of 700-900ºC, which initially facilitates the reorientation of the ceramic particles to enhance the packing. Once reorientation has occurred the liquid phase sintering aid also acts as a fast diffusion path for atomic species and so encouraging the densification process to occur.

The sintering temperature of bulk PZT is typically between 1100 and 1300ºC. With liquid phase sintering aids these temperature scan be lowered to between 800 and 900ºC. Examples of sintering aids used for lead based piezoelectric materials include PbO [93-96], PbO-Cu_2O [83; 97-98], $Pb_5Ge_3O_{11}$ [99-101], $LiBiO_2$-CuO [102], PbO-PbF_2 [103-105], Bi_2O_3-B_2O_3-CdO [103; 106-107], Borosilicate Glass [106;108-109; 96], Li/PbO [88] and PbO/TiO_2 [110]. Although sintering aids significantly reduce the sintering temperature and enhance densification the presence of significant levels of non/low-function material within the thick film can reduce the resultant functional and piezoelectric properties. Furthermore, as sintering aids enhance the degree of solution-reprecipitation of the major phase (i.e. PZT) there is a large degree of atomic mixing. This may affect the electromechanical properties of the ceramic. i.e. if a soft doped PZT is the major phase, but the sintering aid contains a significant proportion of hard dopants then the sintered PZT material will behave as a hard doped material. Care should therefore be taken when selecting the appropriate sintering aid.

Transformation binders

A third type of ink is an evolution of thin film sol-gel processing – often termed composite sol gel [99; 111-112]. Unlike the fugitive binder inks, these *transformation binders* use a metallorganic system (e.g. sol gel) to replace the organic binder and carrier fluid. In these systems, following deposition and evaporation of the solvent, the sol gel material gels and binds the ceramic particles to each other and to the substrate. Subsequent heating then causes the sol to transform to an amorphous oxide ceramic and subsequently to a polycrystalline ceramic, which fully integrates with the ceramic powder. Due to the high reaction kinetics of the sol gel material it is possible to produce thick films at temperatures as low as 600ºC. The density of the films can also be varied

by changing the proportion of sol to powder present in the ink and through using repeated infiltration steps [97] to enhance the green density.

As with the fugitive binder inks, sintering aids can also be added to further enhance to the densification of the systems [83; 97; 100]. As it is necessary to melt the sintering aids, typical processing temperatures are above 700ºC when sintering aids are used.

In addition to the ability to process films at lower temperatures it is also possible to create composite structures where the composition of the powder is different to that of the sol gel material [83], which offers the potential to tailor the behaviour of the film.

A variation of the composite sol-gel route is to use conventional thick film processing followed by infiltration of the oxide ceramic producing sol to increase the green density of the film [113]. Subsequent sintering is then enhanced due to the presence of the highly sinterable sol-gel derived nanophase

Electrical properties of PZT thick films

As the functional properties of ceramics depend strongly on the composition, dopant level, film stress state, film thickness, processing temperature and substrate materials it is very difficult to find meaningful comparisons from literature. In general it can be stated that film properties are relatively independent of the route used to produce the films. The major factors affecting the properties are the sintering aid – with lower properties being exhibited as the percentage of sintering aid increases above the optimum level (typically 2-10 vol%). For a given sintering temperature better properties are found in films containing the sintering aid with the lower melting point or activity.

When compared to comparable bulk ceramics, the relative permittivity of thick films can approach that of the bulk for certain compositions. However, piezoelectric and ferroelectric properties are typically reduced to between 1/4 and 1/3 those of the bulk ceramic [114; 103; 113; 115] due to a combination of domain clamping and the presence of secondary phases.

Summary – ferroelectric thick films

A number of thick film deposition techniques have been presented which can themselves be used with different types of ink. Through the appropriate selection of process and ink it is possible to tailor the process for a wide range of applications.

Very low temperature (<100ºC) processing can be accomplished using paint type systems. Such systems exhibit very much lower electromechanical properties than do bulk ceramics. To improve the functional properties of the system it is necessary to use higher processing temperatures (650-950ºC). Such processing temperatures require the use of a liquid phase sintering aid or sol gel material to lower the processing temperature from 1200ºC typically used for processing functional ceramics. The reduction in temperature means that these materials can be successfully integrated into microsystems.

[1] N.Setter, Journal of the European Ceramic Society 21 (2001) 1279-1293
[2] S.A.Wilson, R.Jourdain, R.W.Whatmore, P.Morantz, J.Corbett, M.J.Hucker, C.Warsop, Proceedings of Actuator 2006 10th International Conference on New Actuators 14-16th June 2006 Bremen, Germany 748-751

[3] S.Arai, J.Corbett, R.W.Whatmore, S.A.Wilson, J.Hedge, Proceedings of the 4th International Conference of the European Society for Precision Engineering and Nanotechnology, May30th-June3rd 2004 Glasgow UK 201-203
[4] K.Uchino, Proceedings of Actuator 2006 10th International Conference on New Actuators 14-16th June 2006 Bremen, Germany 48-57
[5] K.Uchino, Proceedings of Actuator 2004 9th International Conference on New Actuators 14-16th June 2004 Bremen, Germany 38-47
[6] C.A.Randall, A.Kelnberger, G.L.Yanmg, R.E.Eitel, T.R.Shrout, Journal of Electroceramics 14 (2005) 177-191
[7] S.Zhang, R.Xia, L.Lebrun, D.Anderson, T.R.Shrout, Materials Letters 59 (2005) 3471-3475
[8] K.A.Snook, T.R.Shrout, K.K.Shung, IEEE Transactions on Ultrasonics, Ferroelectrics and Frequency Control 53 Issue 2 February (2006) 300-308
[9] S.Zhang, C.A.Randall, T.R.Shrout, IEEE Transactions on Ultrasonics, Ferroelectrics and Frequency Control 52 Issue 4 April (2006) 564-569
[10] L.E.Cross, Japanese Journal of Applied Physics 34 5B (1995) 2525-2532
[11] G.Xu, Z.Zhong, Y.Bing, Z-G Ye, G.Shirane, Nature Materials 5 (2006) 134-140
[12] Z.Kutznjak, J.Petzelt, R.Blinc, Nature, London 441 Issue 7096 22nd June (2006) 956
[13] P.Marin-French, S.Cochran, K.Kirk, Journal of Materials Science: Materials in Electronics 15 (2004) 715-720
[14] S.Park, T.R.Shrout, IEEE Transactions on Ultrasonics, Ferroelectrics and Frequency Control 44 September (1997) 1140-1147
[15] J-S Park, J-H Kim, Smart Materials and Structures 14 (2005) 745-753
[16] S.Zhang, T.R.Shrout, 2006 US Navy Workshop on Acoustic Transduction Materials and Devices, Penn State University, State College Pennsylvania 9-11th May (2006)
[17] Y.Saito, H.Takao, T.Tani, T.Nonoyama, K.Takatori, T.Homma, T.Nagaya, M.Nakamura, Nature, London 432 Issue.7013 November 4th (2004) 84-87
[18] Y.Guo, K.Kaikamoto, H.Ohsato, Applied Physics Letters 85 No.18 1st November (2004) 4121-4123
[19] E.Hollenstein, M.Davis, D.Damjanovic, N.Setter, Applied Physics Letters 87 No.18 31st October (2005) 182905
[20] T.Takenaka, H.Nagata, Journal of the European Ceramics Society 25 Issue12 (2005) 2693-2700
[21] S.Trolier-Mckinstry, P. Muralt, Journal of Electroceramics, 12 (2004) 7-17
[22] P. Muralt M. Kohli, T. Maeder, A. Kholkin, K. Brooks, N. Setter, R. Luthier, Sensors and Actuators A 48 Issue 2 (1995) 157-165
[23] M.A. Dubois, P Muralt, IEEE Trans. Ultrasonics, Ferroelectrics, Frequency Control 45 Issue 5 (1998) 1169-1177
[24] P. Muralt, Proceedings of ISAF '96, edited by B. M. Kulwicki, A. Amin, A. Safari (IEEE, Piscataway, 1996) 145
[25] Y. Miyahara T. Fujii, S. Watanabe, A. Tonoli, S. Carabelli, H. Yamada, H. Bleuler, Applied Surface Science 140 Issues 3-4 (1999) 428-431
[26] M. Koch, N. Harris, R. Maas, A. G. R. Evans, N. M. White, A. Brunnschweiler, Measurement Science and Technology, 8 (1997) 49-57
[27] P. Muralt, J. Baborowski, Journal of Electroceramics, 12 (2004) 101-108

[28] P. Muralt, N. Lederman, J. Baborowski, A Barzegar,S.Gentil, B. Belgacem, S. Petitgrand, A. Bosseboeuf, N. Setter, IEEE Transactions on Ultrasonics Ferroelectrics and Frequency Control 52 Issue 12 (2005) 2276-2288
[29] R.W.Whatmore, Ferroelectrics, 118 (1990) 241
[30] L.L. Sun, W.G.Liu, O.K.Tan, W.Zhu, Materials Science and Engineering B 99 (2003) 173-178
[31] R.N. Castellano and L.G. Feinstein, J. Appl. Phys. 50 June (1979) 4406-4411
[32] S.B. Krupanidhi, N. Maffeo, M. Sayer, K. El-Asselet, J. Appl. Phys. 54 November (1983) 6601-6609
[13] S. Hiboux, P. Muralt, Ferroelectrics, 224 (1999) 315
[34] K. Sreenivas, M. Sayer, P. Garrett, Thin Solid Films, 172 Issue 2 (1989) 251-267
[35] S. Otsubo, T. Maeda, T. Minamikawa, Y. Yonezawa, A. Morimoto, T. Shimizu, Japanese J. Appl. Phys., 29 Part 2 No.1 January 20th (1990) L133-L136
[36] H. Buhay, S.Sinharov, W.H.Kasner, M.H.Francome, D.R.Lampe, E.Stepke, Applied Physics Letters 58 Issue 14 April 8th (1991) 1470-1472
[37] D. Roy, S.B. Krupanidhi, J. P. Dougherty, J. Appl. Phys., 69 Issue 11 June 1st (1991) 7930-7932
[38] B. S. Kwak, E.P. Boyd. A. Erbil, Applied Physics Letters 53 Issue 18 October 31st (1988) 1702-1704
[39] K. Sreenivas, M. Sayer, D.J. Baar, M. Nishioka, J. Appl. Phys. 54 (1988) 6601
[40] S.L. Swartz, D.A. Seifert, F.T. Noel, Ferroelectrics 93 (1989) 37
[41] C.J. Brierley, C. Trundle, L. Considine, R.W. Whatmore, F.W. Ainger, Ferroelectrics 91 (1989) 181
[42] M. Okada, K. Tominaga, T. Araki, S. Katayama, Y. Sakashita, Japanese Journal of Applied Physics 29 (1990) 718
[43] K.D. Budd, S.K. Dey, D.A. Payne, Brit. Ceram. Proc. 36 (1985) 107
[44] S.K. Dey, K.D. Budd, D.A. Payne, IEEE Trans. on Ultrasonics Ferroelectrics and Frequency Control 35 (1988) 80
[45] R.D. Klissurska, K.G. Brooks, I.M. Reaney, Cz. Pawlaczyk, M. Kosec, N. Setter, J. Amer. Ceram. Soc. 78 (1995) 1513
[46] C.K. Kwok and S. B. Desu, J. Mater. Res. 7 (1994) 1728
[47] H. Habata, Appl. Phys. Lett. 59 (1991) 2354
[48] B. Jaffe, W. R. Cook, H. Jaffe, Piezoelectric Ceramics (Academic Press, New York (1971)
[49] H.D. Chen, K.R. Udayakumar, C.J. Gaskey, L.E. Cross, Appl. Phys. Lett., 67 (23) (1995) 3411
[50] A. Seifert, N. Ledermann, S. Hiboux, J. Baborowski, P. Muralt, N. Setter, Integrated Ferroelectrics 35 (1-4) (2001) 1889
[51] F. Xu, R.A. Wolf, T. Yoshimura, S. Trolier-McKinstry, Proc. 11th Int. Symp. Electrets (2002) 386
[52] R.A. Wolf and S. Trolier Mckinstry, J. Appl. Phys. 95 (3) (2004) 1397
[53] T.Haccart, C. Soyer, E. Cattan, D. Remiens, Ferroelectrics 254 (1-4) (2001) 185
[54] I. Kanno, H. Kotera, K. Wasa, T. Matsunaga, T. Kamada, R. Takayama, J. Appl. Phys. 93 (7) (2003) 4091
[55] D.-J. Kim, J–P. Maria, A. I. Kingon, S.K. Streiffer, J. Appl. Phys. 93 (2003) 5568
[56] K. Lefki, G.J.M. Dormans, J. Appl. Phys. 76 (1994) 1764

[57] D.Damjanovic, K.G. Brooks, A. Kholkin, M. Kohli, T. Maeder, P. Muralt, N. Setter, in Materials for Smart Systems, edited by E.P. George, S. Takahashi, S. Troiler-Mckinstry, K. Uchino, M. Wun-Fogle, MRS, Boston MA (1994) 429.
[58] N. Ledermann, P. Muralt, J. Baborowski, S. Gentil, K. Mukati, M. Cantoni, A. Seifert, N. Setter, Sensors and Actuator A 105 (2003) 162
[59] P. Muralt, Integrated Ferroelectrics, 17 (1997) 297
[60] H.D. Chen, K.R. Udayakumar, C.J. Gaskey, L.E. Cross, J.J. Bernstein, L.C. Niles, J. Amer. Ceram. Soc. 79 (1996) 2189
[61] A.L. Kholkin, A.K. Tagantsev, K.G. Brooks, D.V. Taylor, N. Setter, in ISAF '96, edited by B.M. Kulwicki, A. Amin, A Safari, IEEE East Brunswick NJ (1996), 351
[62] F.Chu, F.Xu, J. Shepard, S. Trolier-Mckinstry, in Ferroelectric Thin Films VI, edited by R.E. Treece, R.E. Jones, C.M. Foster, S.B. Desu, I.K. Yoo, MRS Boston MA, (1998) 409
[63] P. Muralt, A. Kholkin, M. Kohli, T. Maeder, Sensors and Actuators A 53 (1996) 397
[64] K. Lefki, G.M. Dormans, J. Appl. Phys. 76 (1994) 1764
[65] A.L. Kholkin, C. Wütrich, D.V. Taylor, N. Setter, Rev. Sci. Instr. 67 (1996) 1935
[66] M.-A. Dubois, P. Muralt, Sensors and Actuators A 77 (1999) 106
[67] A. Seifert, N. Ledermann, S. Hiboux, J. Baborowski, P.Muralt, N. Setter, Integrated Ferroelectrics 35(1-4) (2001) 1889
[68] F.Xu, R.A. Wolf, T. Yoshimura, and S. Trolier-Mckinstry, Proc. 11th Int. Symp. Electrets (2002) 386
[69] K. Kakimoto, H. Kakemoto, S. Fujita, Y. Masuda, J. Am. Ceram. Soc. 85 (4) (2002) 1019
[70] J. Marshall, Q. Zhang, Z. Huang, R.W. Whatmore, Ferroelectric, 1 (2005) 318
[71] B.A. Tuttle, T.J. Garino, J.A. Voight, T.J. Headley, D. Dimos, M.O. Eatough, Science and Technology of Electroceramic Thin Films edited by O.Auciello, R. Waser, Kluwer Academic Publishers, The Netherlands (1995) 117
[72] F. Jona, G. Shirane, Ferroelectric Crystals Pergamon Press, New York (1962).
[73] T.M. Shaw, S. Trolier-McKinstry, P.C. McIntyre, Ann. Rev. Mater. Sci. 30 (2000) 263
[74] G.A.C.M. Spierings, J.M. Breed, M.J.E. Ulenaers, P.J. van Veldhoven and P.K. Larsen, Microelectronic Engineering 29 (1995) 235
[75] K. Lefki and G. J. M. Dormans, J. Appl. Phys. 76 (1994) 1764
[76] D. Damjanovic, K.G. Brooks, A. Kholkin, M. Kohi, T. Maeder, P. Muralt, N. Setter, in Materials for Smart Systems, edited by E.P. George, S. Takahashi, S. Troiler-McKinstry, K. Uchino, M. Wun-Fogle MRS, Boston MA (1994) 429.
[77] J. H. Jang and K. H. Yoon, Appl. Phys. Lett., 75 (1999) 130
[78] P. Muralt, A. Kholkin, M. Kohli, T. Maeder, K.G. Brooks, R. Luthier, Integrated Ferroelectrics 11 (1995) 213
[79] A. Kholkin, E.L. Colla, K. Brooks, P. Muralt, M. Kohli, T. Maeder, D. Taylor, N. Setter, Microelectronic Engineering 29 (1995) 261
[80] N. Ledermann, P. Muralt and A. Dommann, Proc. 2nd Int. Conf. on Integrated Micro/Nanotechnology for Space Applications MNT'99, Pasadena April 1999 The Aerospace Corporation (1999) 250-257.
[81] R.A. Dorey, R.W. Whatmore, J. Electroceramics 12 [1-2] (2004) 19
[82] R.A.Dorey, R.W. Whatmore, S.P. Beeby, R.N. Torah, N.M. White, Integrated Ferroelectrics 54 (2003) 651

[83] R.A. Dorey, S.B. Stringfellow, R.W. Whatmore, J. Euro.Ceram.Soc. 22 (2002) 2921
[84] A.L. Kholkin, V.K. Yarmarkin, A. Wu, P.M. Vilarinho, J.L. Baptista, Integrated Ferroelectrics 30 (2000) 245
[85] T. Olding, M. Sayer, D. Barrow, Thin Solid Films 581 (2001) 398
[86] M. Kobayashi, T.R. Golding, M. Sayer, C.-K. Jen, Ultrasonics, 39 (2002) 675
[87] G. Wang, P.S Nicholson, J. Amer. Ceram. Soc. 84 (2001) 1977
[88] J. Van Tassel, C.A. Randall, J. Euro.Ceram.Soc. 19 (1999) 955
[89] T.G. Sweeney, R.W. Whatmore, Ferroelectrics 187 (1996) 57
[90] J. Ma, W. Cheng, J. Amer. Ceram. Soc., 85, 1735, (2002)
[91] P. Sarkar, P.S. Nicholson, J.Amer. Ceram.Soc., 79 (1996) 1987
[92] J.M. Hale, B. de Poumeyrol, Proc. Ferroelectrics UK 2000 Eds N.M.Alford, E.Yeatman Woodhead Publ. Cambridge UK (2000) 205
[93] T. Futakuchi, K. Nakano, M. Adachi, Jap. J. Appl. Phys. 39 (2000) 5548
[94] V. Farrari, D. Marioli, A. Taroni, E. Ranucci, Sensors and Actuators B 68 (2000) 81
[95] G. De Cicco, B. Morton, D. Dalmonego, M. Prudenziati, Sensors and Actuators 76 (1999) 409
[96] M. Prudenziati, B. Morten, De Cicco, Microelectronics International 38 (1995) 5
[97] D.L. Corker, Q. Zhang, R.W. Whatmore, C. Perrin, J. Euro. Ceram. Soc. 22 (2002) 383
[98] D.L. Corker, R.W. Whatmore, E. Ringgaard, W.W. Wolney, J. Euro. Ceram. Soc. 20 (2000) 2039
[99] P. Tran-Huu-Hue, F. Levassort, F.V. Meulen, J. Holc, M. Kosec, M. Lethiecq, J. Euro. Ceram. Soc. 21 (2001) 1445
[100] T. Hayashi, T. Inoue, Y. Akiyama, J. Euro. Ceram. Soc. 19 (1999) 999
[101] F.F.C. Duval, R.A. Dorey, Q. Zhang, and R.W. Whatmore, J. Euro. Ceram. Soc. 23 Issue 11 (2003) 1935
[102] X.X. Wang, K. Murakami, O. Sugiyama, and S. Kaneko J. Euro.Ceram.Soc. 21 (2001) 1367
[103] S. Le Dren, L. Simon, P. Gonnard, M. Troccaz, and A. Nicolas, Mat.Res.Bull., 35, 2037, (2000)
[104] C. Lucat, F. Menil, R. Von Der Muhll, Meas. Sci. Techn. 8 (1997) 38
[105] T. Sweeney, PhD Thesis Cranfield University UK, (1998)
[106] E.S. Thiele, N. Setter, J. Amer. Ceram. Soc. 83 (2000) 1407
[107] M.-C. Wang, M.-S. Huang, N.-C. Wu, J. Euro. Ceram. Soc. 21 (2001) 695
[108] S.P. Beeby, A. Blackburn, N.M. White, J. Micromech. Microeng. 9 (1999) 218-229
[109] R. Maas, M. Koch, N.R. Harris, N.M. White, A.G.R. Evans, Materials Letters 31 (1997) 109
[110] M. Prudenziati, Thick Film Sensors Elsevier NL (1994) 113
[111] D.A. Barrow, T.E. Petroff, R.P. Tandon, M. Sayer, J. Appl. Phys. 81 (1997) 876
[112] M. Lukacs, M. Sayer, S. Foster, Integrated Ferroelectrics, 24 (1999) 95
[113] H.J. Kim, Y.-B. Kim, J.-Y. Kang, T.S. Kim, Integrated Ferroelectrics, 50 (2002) 11
[114] L. Simon, S. Le Dren, P. Gonard, J. Euro. Ceram. Soc. 21 (2001) 1441
[115] X.N. Jiang, C. Sun, Z. Zhang, B. Xu, Y.H. Ye, Sensors and Actuators, 87 (2000) 72

3. Piezoelectric semiconductors

Christopher R. Bowen – University of Bath UK

Piezoelectric semiconductors, including the Group III-V materials such as GaAs (see Table 3.1), have attracted growing in interest for MEMS applications where one particular advantage is their compatibility with conventional processing technologies for integrated circuit technology. Unlike perovskite materials such as PZT described earlier, the materials are not ferroelectric in nature and cannot be poled. Therefore interest in these materials is primarily in the form of thin films that are epitaxially grown on a substrate. Although reported research [1,2] on specific semiconductor materials, such as those with the noncentrosymmetric wurtzite crystal structure (Figure 3.1), such as GaN, ZnO, CdS and ZnS, often refer to their 'high' piezoelectric coefficients it should be stressed that the coefficients are considerably lower than those of ferroelectric ceramics such as PZT. Nevertheless, published research on MEMS based devices using the piezoelectric or pyroelectric properties of such materials is growing and the aim of this section is to provide an overview of the most common materials and their potential advantages and applications. Table 3.1 presents a summary of dielectric, piezoelectric and mechanical properties of a range of piezoelectric semiconductors, along with the properties of a PZT for a direct comparison. The d_{ij} coefficients (strain per unit field) are low compared to PZT indicating a low level of strain for actuator applications. It is of interest to note the much lower relative permittivity of these materials compared to PZT, which can lead to high g_{ij} coefficients ($g_{ij} = d_{ij}$/permittivity), which is measure of the electric field per unit stress for sensor.

3.1 Group III-V nitrides (GaN/AlN)

The piezoelectric effect in III-V nitrides, such as GaN, has been of primary interest because of its influence of the behaviour of field electric transistors and light emitting diodes. [1]. However interest has gown in utilising the piezoelectric coefficients of these materials to develop MEMS systems, sensors and actuators which can take advantage of the inherent wide band gap (3.4eV for GaN), chemical and radiation inertness and high temperature properties of GaN. The wide band gap makes it a candidate material for high-power and high-temperature or radiation resistant electronics, particularly above 180°C, which can degrade conventional silicon based transistors. Depending on whether the growth of GaN is in the [0001] direction (when its crystal structure is wurtzite) or [111], when in a zinc blend crystal structure, the material exhibits a strong lattice polarisation, which has been reported to be ideal for piezoelectric based transducers or pyroelectric sensors at temperatures in excess of 300ºC [1].

Shur et al. [1] recently reported data on the performance of preliminary devices based on GaN. The pyroelectric effect in GaN thin films was used to generate an electric charge in response to flow of heat at temperatures up to 300ºC. In addition to the primary pyroelectric effect the secondary pyroelectric effect was considered where a charge is developed as a result of a piezoelectric induced thermal strain. For fast heat transfer, the primary effect was dominant and experimentally determined pyroelectric coefficients for n-type GaN were ~10^4 V/mK, comparable to typical pyroelectric ceramics such as PZT and $BaTiO_3$. Modelling results, with electrode contact along the

c-axis, predicted that the potential sensitivity of GaN could be increased up to $7x10^5$ V/mK, which is greater for other high temperature ferroelectric pyroelectric materials such as $LiTaO_3$ [1].

Relatively little work has examined the development of strain sensors or actuators based on GaN. Strittmatter [2] stated that one possible reason for this is that, compared to conventional ferroelectric ceramics, the movement of free charge carriers in GaN can potentially negate any piezoelectric charge that is developed as a result of a force or strain. To minimise this effect, Strittmatter used Schottky diodes on n-GaN to hinder the screening effect and examined the electrical response of a GaN cantilever as a result of an applied strain. It was concluded that the voltage generated was a direct result of the piezoelectric effect and was not piezoresistive in nature. The use of GaN solid state sensors for harsh environments, including space, aerospace and homeland defence has been reviewed by Pearton et al [3] and free standing GaN cantilevers have been produced on silicon substrates [4]. Little data is provided on GaN actuation, apart from extensional measurement of films to characterise the relatively small d_{33} coefficients (compared to PZT) of these materials [5].

Another group wide band gap (6eV) III-V nitride, AlN, has been considered for surface wave technology in thin film form due to its high piezoelectric coefficients for MEMS applications. Low deposition temperatures (<500ºC) enable compatibility with conventional integrated circuit technology [6, 7] and the large band gap provides high resistivity that minimises dielectric losses [16]. Iborra [7] examined the use of RF-sputtering to produce thin films with low residual stress and high c-axis orientation to optimise the piezoelectric properties. Preliminary test structures consisting of AlN/polysilicon bimorphs were fabricated, although no actuation results were reported. Cochran et al. [8] recently reported the use of thick AlN films (>5μm) for bulk acoustic wave resonators, with its high Curie temperature, low permittivity and low losses being cited as potential advantages for such applications.

3.2 Group III-V materials

GaAs has also attracted interest for microsensors and microactuation due to its piezoelectric properties and high band gap (1.4eV), also enabling operation temperatures of 300ºC. To increase temperature stability AlGaAs heterostructures have been used to increase the band gap and increase resistivity [9] in an attempt to reduce noise and increase temperature stability. Kumar [10] examined $Al_xGa_{1-x}As$ films due to their low defect density and ability to integrate lattice-matched electrodes for the manufacture of released beams will low stress gradients, coupled with the ability to directly integrate with electronics and optoelectronics. Released beams of $Al_{0.3}Ga_{0.7}As$ with integrated electrodes and piezoelectric layers were produced, although no actuation data was reported.

3.3 ZnO materials

Zinc oxide is another semiconducting and piezoelectric material that has potential applications in optoelectronics, piezoelectric sensors, resonators, surface acoustic wave devices and transducers [11,12]. Examination of Table 3.1 reveals that it has relatively high piezoelectric coefficients, along with its wide band gap (3.4eV), near UV emission and transparency to visible light. A range of piezoelectric nanostructures including

springs, helices, rings and bows can be formed due to polar-surface dominated growth mechanism of ZnO. Figure 3.2 shows some of the ZnO nanostructures, synthesised by thermal evaporation of solid powders. Its relatively high piezoelectric coefficient (Table 1) provide a means to develop electro-mechanical coupled sensors and actuators at the nano-scale [11,12]. It has been reported that the piezoelectric coefficient of a polar nanobelts is approximately three times greater than that of the bulk material [12].

ZnO has been also used in more conventional thin film form (~0.5μm thick), sputtered onto a 1.5μm silicon nitride membrane, to develop a piezoelectric micromachined membrane acoustic devices, e.g. miniature microphones or loudspeakers for a cellular phone or earphone [13]. The maximum displacement of the membrane was 1μm at 7.3kHz with an input drive of $15V_{0\text{-}P}$. For this material, cantilever actuators based on ZnO have been manufactured and characterised. DeVoe et al. [14] produced 500μm long ZnO cantilever actuators by surface micromachining to validate a novel modelling methodology for cantilever actuators, with experimentally measured deflections of up to 400nm. Minne et al. [15] produced cantilevers for atomic force microscopy, with a deflection of over 4μm at dc conditions and 30μm at resonance with applied electric fields up to 10^7 V/m. Trolier-Mckinstry and Muralt [16] have provided a good overview of ZnO thin film MEMS, along with a comparison and discussion of AlN and PZT based films, along with the appropriate figures of merit to compare materials for particular applications.

Summary – piezoelectric semi-conductors

Piezoelectric semiconductors such as those in Table 3.1 are attracting growing in interest for MEMS applications due to their compatibility with conventional processing technologies for integrated circuit technology and wide gap for use in harsh environment. The piezoelectric ‘d’ coefficients are lower than many ferroelectric materials and research on actuator applications to date is limited. The low permittivity results in high ‘g’ coefficients indicating potential for sensor applications.

In addition to piezoelectric properties, materials such as ZnO nano-rods can be employed as bio-chemical sensor to improve the physiological sensors sensitivity and selectivity. These advances and others possible with engineered applications of functional multi-scale materials will open many new opportunities for sensors in biomedical applications.

Material	GaN	AlN	CdS	ZnS	GaAs	ZnO	InN	PZT5H
Relative permittivity	9 [19]	8.5 [20]	9.35 [24]	8.7 [24]	12.5 [24]	9.15 [24]		700 [25]
d_{33} pC/N	3.7 [5]	5 [5]	10.3 [24]	3.23 [24]		11.67 [24]		593 [25]
d_{31} pC/N	-1. [5]	-2 [5]	-5 [24]	-1.13 [24]		-5.43 [24]		-274 [25]
d_{15} pC/N	3.1 [18]	3.6 [18]	-14 [24]	-2.8 [24]		-11.34 [24]		741 [25]
e_{33}	1 [1]	1.55 [1]	1.32 [22]		-0.185 [1]	1.32 [1]	0.43 [1]	23.3 [25]
e_{31}	-0.36 [1]	-0.58 [1]	-0.074 [22]		0.093 [1]	-0.57 [1]	-0.22 [1]	-6.5 [25]
e_{15}	-0.3 [1]	-0.48 [1]			0.093 [1]	-0.48 [1]	-0.22 [1]	17 [25]
S_{11} (pPa^{-1}) / C_{11} (GPa)	C_{11} 390] [19]	C_{11} 410 [21]	S_{11} 20.69 [24]	S_{11} 11.12 [24]	S_{11} 12.64 [24]	S_{11} 7.86 [24]	C_{11} 190 [23]	C_{11} 126 [25]
S_{12} (pPa^{-1}) / C_{12} (GPa	C_{12} 145 [19]	C_{12} 149 [21]	S_{12} -9.99 [24]	S_{12} -4.56 [24]	S_{12} -4.23 [24]	S_{12} -3.43 [24]	C_{12} 104 [23]	C_{12} 79.5 [25]
S_{13} (pPa^{-1}) / C_{13} (GPa	C_{13} 106 [19]	C_{13} 99 [21]	S_{13}-5.81 [24]	S_{13}-1.4 [24]	S_{13} -4.23 [24]	S_{13} -2.21 [24]	C_{13} 121 [23]	C_{13} 8.5 [25]
S_{33} (pPa^{-1}) / C_{33} (GPa)	C_{33} 398 [19]	C_{33} 389 [21]	S_{33} 16.97 [24]	S_{33} 8.47 [24]	S_{33} 12.64 [24]	S_{33} 6.94 [24]	C_{33} 182 [23]	C_{33} 117 [25]
S_{44} (pPa^{-1}) / C_{44}(GPa)	C_{44} 105 [19]	C_{44} 125 [21]	S_{44} 66.49 [24]	S_{44} 34.4 [24]	S_{44} 18.6 [24]	S_{44} 23.6 [24]	C_{44} 10 [23]	C_{44} 23 [25]

Table 3.1. Collated data of piezoelectric materials. In some cases data from the stiffness matrix [S] is shown rather than compliance [C]

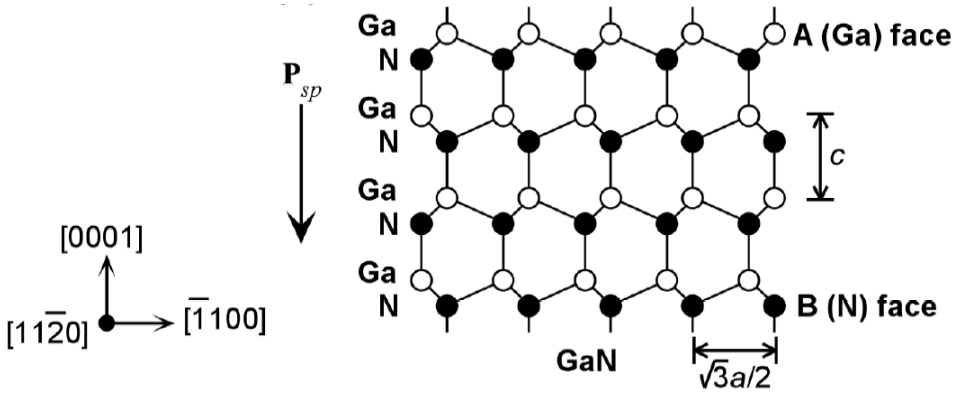

Figure 3.1 Schematic diagram of the GaN wurtzite crystal structure. [17]

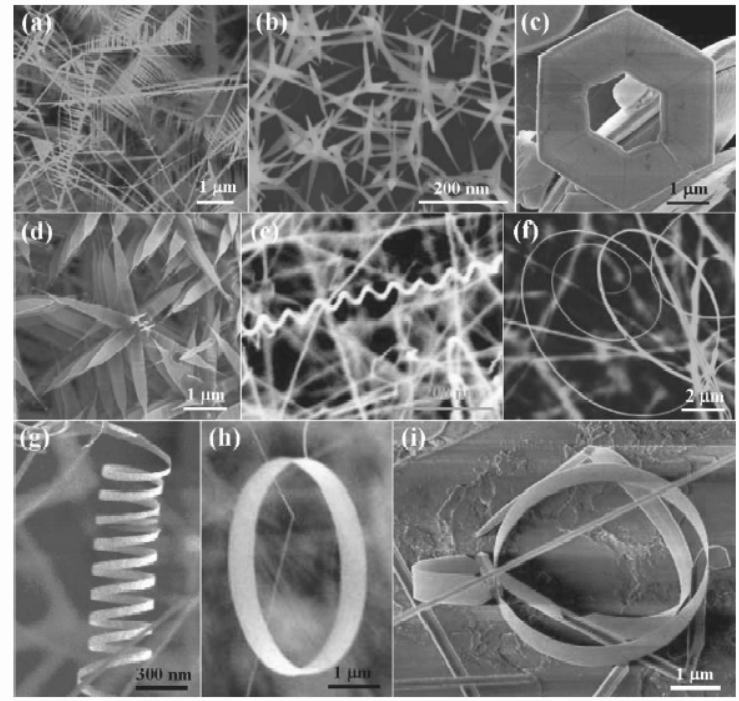

Figure 3.2 ZnO nanostructures synthesised by thermal evaporation of solid powders. (a)nanocombs (b) tetraleg (c) hexagonal disks (d) nanopropellers (f) nanospiral (g) nanosprings (h) single crystal nanoring (i) combination of rods, bow and ring.

[1] M.S. Shur, A.D. Bykhovski and R. Gaska, "Pyroelectric and piezoelectric properties of GaN-based materials", MRS Internet J.Nitride Semicond. Res., (1999), 4S1, G1.6
[2] R.P. Strittmatter, R.A. Beach, J. Brooke, E.J. Preisler, G.S.Picus and T.C.McGill, "GaN schottky diodes for piezoelectric strain sensing", J. App. Phys., (2003), 93, 5675-5681
[3] S.J. Pearton, B.S. Kang, S.K. Kim, F. Ren, B.P. Gila, C.R. Abernathy, J.S. Lin and S.N.G. Chu., "GaN-based diodes and transistors for chemical, gas, biological and pressure sensing", J. Phys.- Cond. Matt., (2004), 16 (29): R961-R994
[4] S. Davies, T.S. Huang, M.H. Glass, A.J. Papworth, T.B. Joyce and P.R. Chalker, "Fabrication of GaN cantilevers on silicon substrates for microelectromechanical devices", App. Phys. Lett., 84, (2004), 2566-2568
[5] I.L. Guy, S. Muensit and E. Goldys, "Extensional piezoelectric coefficients of GaN and AlN", Applied Physics Letters, (1999), 75, 4133-4135
[6] M.A. Dubois and P. Muralt, "Stress and piezoelectric properties of aluminium nitride thin films deposited onto metal electrodes by pulsed direct current reactive sputtering", J. App. Phys., (2001) 89, 6389-6395
[7] E. Iborra, J. Olivares, M. Clement, L. Vergara, A. Sanz-Harvas and J. Sangrador, "Piezoelectric properties and residual stress of sputtered AlN thin films for MEMS applications", Sensors and Actuators, (2004), A 115, 501-507
[8] C.K. Lee, S. Cochran, A. Abrar, K.J. Kirk and F. Placido, "Thick AlN films deposited by room-temperature sputtering for ultrasonic applications". Ultrasonics, (2004), 42, 485-490 (2004)
[9] K. Fricke, "Piezoelectric properties of GaAs for application in stress transducers", J. App. Phys., 70(2), (1991), 914-918,

[10] P. Kumar, L. Li, L. Calhoun, P. Boudreaux and D. DeVoe "Fabrication of piezoelectric $Al_{0.3}Ga_{0.7}As$ microstructures", Sensors and Actuators, (2004), A 115 96-103
[11] Z.L. Wang, "Self-assembled nanoarchitectures of polar nanobelts/nanowires", J. Mat. Chem. 15, (2005), 1021-1024
[12] M.H. Zhao, Z.L.Wang and S.X. Mao, "Piezoelectric characterisation of individual zinc oxide nanobelt probed by piezoresponse force microscopy, Nano. Lett., (2004), 5, 587-590
[13] S.C. Ko, Y.C. Kim, S.S. Lee, S.H. Choi, S.R. Kim, "Micromachined piezoelectric membrane acoustic device", Sensors and Actuators, (2003), A. 103, 130-134
[14] D.L. DeVoe and A.P. Pisano, "Modeling and optimal design of piezoelectric cantilever microactuators", J. Micromech. Systems, 6, (1997), 266-270
[15] S.C. Minne, S.R. Manalis and C.F. Quate, "Parallel atomic force microscopy using cantilevers with integrated piezoresistive sensors and integrated piezoelectric actuators", App. Phys. Lett, 67, (1995), 3918-3920
[16] S.Trolier-McKinstry and P.Muralt, "Thin film piezoelectrics for MEMS", Journal of Electroceramics, (2004), 12, 7-17
[17] E.T.Yu, "Spontaneous and piezoelectric polarization effects in nitride heterostrucutres" in III-V Nitride Semiconductors: Applications and Devices. E.T.Yu and O.Manasreh, eds., Taylor and Francis, 2003, pp161-191
[18] S.Muensit, E.M.Goldys and I.L.Guy, "Shear coefficients of gallium nitride and aluminium nitride" App. Physics Letters, 75, 1999, 3965-3967
[19] Polian, A., M. Grimsditch, I. Grzegory, Elastic constants of gallium nitride, J. Appl. Phys. 79(6) (1996), 3343-3344
[20] Goldberg Yu. in Properties of Advanced Semiconductor Materials GaN, AlN, InN, BN, SiC, SiGe . Eds. Levinshtein M.E., Rumyantsev S.L., Shur M.S., John Wiley & Sons, Inc., New York, 2001, 31-47.
[21] McNeil, L.E, Grimsditch M., French R.H., J. Am. Ceram. Soc. 76, 5 (1993), 1132-1136.
[22] Ce–Wen Nan, Theoretical approach to the coupled thermal-electrical-mechanical properties of inhomogeneous media, Phys. Rev. B 49, 12619-12624, 1994
[23] Sheleg, A.U., Savastenko V.A., Izv. Akad. Nauk SSSR. Neorg. Mater. 15 (1979), 1598.
[24] www.efunda.com, accessed 1 July 2005
[25] H. A. Kunkel, S. Locke, and B. Pikeroen, IEEE Trans. Ultra. Ferro. Freq. Cont. 37, 316 (1990).

4 Zinc Oxide structures for chemical sensors

M. Willander, S.M. Al Hilli, O. Nur – Gothenburg University, Sweden

In addition to useful piezoelectric properties zinc oxide has attracted interest for applications in chemical sensing. There is an increased demand for selective, sensitive, time domain chemical sensors for physiological environments, primarily due to the interest in human health care and the need for new drug discovery. Almost all chemical and biochemical reactions involves a process were the acidity (pH) is subjected to relatively small changes, sometimes, even momentarily. In real physiological mediums, the problem is made complicated by the fact that the pH changes have to be detected in volumes that are relatively small. This implies that the new needed sensors have to also be small in dimensions. In general, when objects are scaled down isomorphically (i.e. all dimensions are scaled uniformly) the change in length, area and volume ratios increase as we scale down and this render surface effects to be significant. This alters the relative influence of the different physical effects in question in an unexpected way. If the object (e.g. analyte) in question shrinks to the same length scale as the effective boundary layer then continuum theories break down and the laws of micro scaling no longer apply. For the analyte in question, the total sample size needed for the detection is determined by the analyte concentration [1,2]. One important property of scaled objects (sensors), of particular interest, is the sensitivity of these scaled sensors. Obviously a sensor with a wide dynamic range for the detection sensitivity is indeed an aim of the scientific community. Before proceeding, we define the sensors of interest here to be those called electrochemical sensors. It is important to mention that electrochemical sensors are more flexible to miniaturization and usually provide a large dynamic range. They are further divided into conductometric, poteniometric, and amperometric. An electrochemical sensor is a sensor that deals with the electron transfer, electron consumption, or generation during a chemical or bio-chemical process. It is also important to note that, a poteniometric sensor measuring a voltage such as the ion sensitive filed effect transistor (ISFET) or ion selective electrode (ISE), are scale invariant; while amperometric and conductometric sensors on the other hand measures currents and are sensitive to miniaturization. The reduction in sensor size can lead to beneficial effects. To illustrate this, we consider the sensitivity of a sensor as we miniaturize our electrodes. If the size of the sensing electrodes is reduced to sizes comparable to the thickness of the diffusion layer, and the electrodes are kept isolated, non-linear diffusion, caused by curvature effects, needs to be considered. Analysis of such situation showed that as the non linear curvature effects become more and more pronounced, more diffusion takes place, i.e. diffusion occurs from all directions and analyte collection increasingly persist. This leads to more analyte supply to the electrode; this is an example of a beneficial un-expected effect. This implies that as we scale down our sensing electrodes and keep them ‘’isolated’’ the sensitivity is significantly enhanced. In fact it has been demonstrated experimentally that if a single ion is located near a single electron transistor (SET), detection is achieved with a change of the conduction current. In addition to this, nano-electrodes have relatively large surface area that makes them attractive for pH and other chemical sensing. In addition, the possibility to control their nucleation sites makes them one of the best candidates to develop high-density sensor arrays. Miniaturization is also a mixed issue for both the sensor and analyte. Hence the analyte concentration is an important

parameter to consider. As mentioned above, sometimes we are faced by the fact that the analyte to be detected has relatively low concentration (≈ fL), and this implies the need for a large sample volume to achieve detection. Large volumes are again not in our control, especially if we deal with a real physiological medium, e.g. human body analyte.

In this section, we will briefly discuss the properties and use ZnO nano-rods (with few nanometers in diameter and micrometers of length) for chemical sensing purpose. Experimental results from growth as well as theoretical results on sensing using different approaches will be presented.

3.3 Synthesis and properties of ZnO nano-structures

Zinc oxide (ZnO) is a direct band gap semiconductor (3.37 eV at room temperature) and having large exciton binding energy (60 meV), exhibiting near UV emission, transparent conductivity and piezoelectricity. Of interest to this section are the bio-safe and bio-compatible properties of ZnO. In addition ZnO is a polar semiconductor, which means that the outer surface can be controlled to have a neutral, positive (Zn^+ terminated), or negative charge (O^-). This besides the possibility of other non-polar surfaces, which are also of interest to chemical sensing as will shown below. This combines with the bio-safe and biocompatible properties imply that ZnO is quite suitable for chemical sensors for physiological mediums.

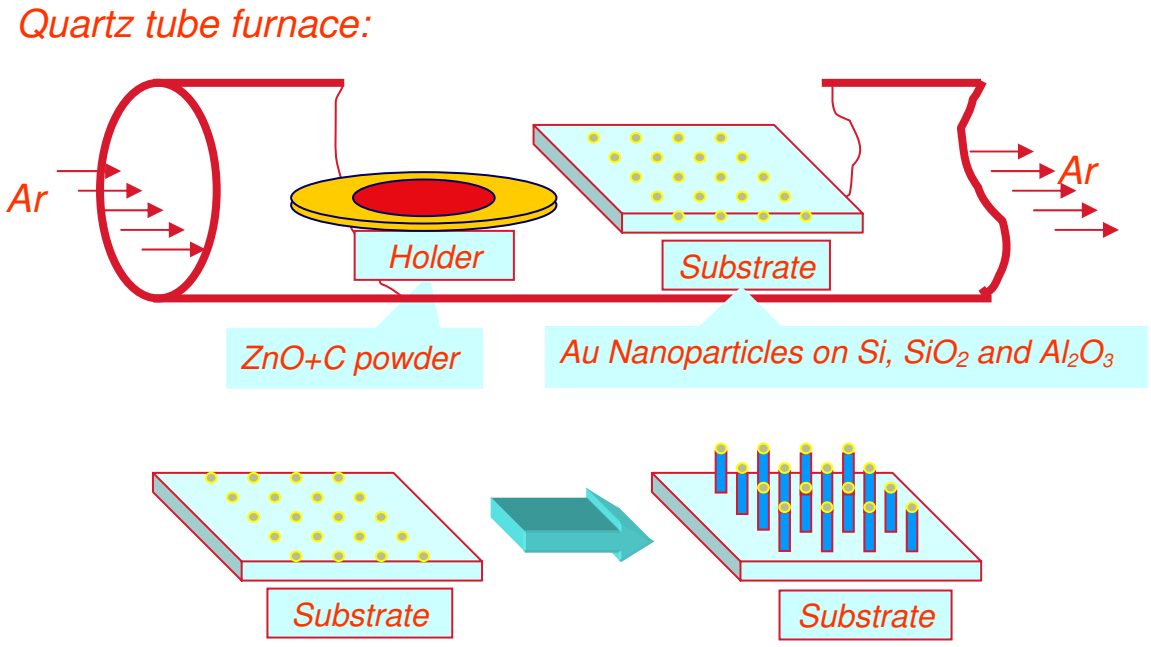

Figure 4.1: Schematic diagram of a typical chamber of the synthetic growth of ZnO nanostructures.

A variety of ZnO nano-structures (nanometer of diameter and micrometer of length) have been synthesized using different techniques. Nano-structure geometries include nano-rods, nano-wires, nano-belts, nano-rings, nano-tubes [3,4]. The most commonly investigated growth technique is through vapor phase nucleation. The vapour species are first generated by evaporation, chemical reduction and gaseous reaction. They are then transported and condensed onto the substrate. This is illustrated in Figure 4.1.

Figure 4.2 shows an example of well aligned ZnO nano-wires grown on sapphire [4]. Although this technique has been extensively studied the exact mechanism of growth by the vapor phase technique is, as yet, not well understood.

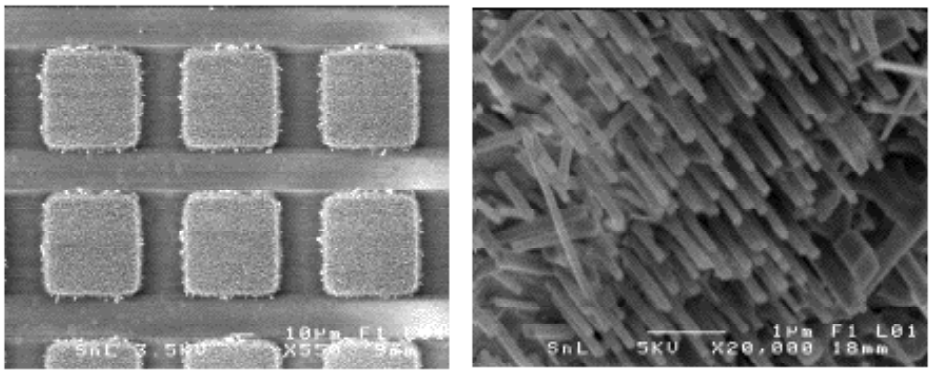

(a) **(b)**

Figure 4.2: SEM images of c-axis oriented ZnO nano-wires grown on patterned sapphire substrate, a) a low magnification image showing nanowires grown in squares, b) higher magnification image showing nanowires within one square [4].

The unique characteristics of nanoscale materials make them a perfect choice for the sensors world. Integrating them into existing sensors can increase the devices' sensitivity, selectivity, and speed. In addition, the large surface area to volume ratios greatly facilitates sensor miniaturization with benefits discussed above. Because of the minuscule size of nanoscale materials, their chemical and physical properties differ from those of their bulk counterparts and therefore behave differently. One of these properties is an ability to be functionalized or custom-designed to attract specific molecules; another is an extremely high surface area tucked into a tiny space. Researchers are integrating functionalized ZnO nanorods into variety of sensor applications to meet urgent needs in fields ranging from biomedicine to biochemistry [4-8]. The scientific community goal is to lay foundation for a miniaturized sensor that uses smallest sample size to detect the smallest concentration of molecules of interest.

The electrochemical potential method and the site binding method applied to investigate a material behavior is a function of its extensive exterior surface area. The advantage of this technique is that you can employ many of them (nanorods) together so you get the same benefits of low volume and high reactivity. Since ZnO nanorods are conductive, they can provide a signal each time a target substance (proton) binds to the surface layer of the nano-rod [9-11].

[1] M. Willander and O. Nur, Nanoscale Sensors: Scaling issues and challenging limitations. The Dekker Encyclopedia of Nanoscience and Nanotechnology, Marcel Dekker, New York, USA, Editors James A. Schwartz, Cristian Contescu, and Karol Putyers, to appear in 2006.
[2] M. Willander and O. Nur, Silicon Based Devices: Chemical Sensing, Invited, The

Dekker Encyclopedia of Nanoscience and Nanotechnology, Marcel Dekker, New York, USA, Editors James A. Schwartz, Cristian Contescu, and Karol Putyers, to appear (2006).
[3] Z. L. Wang, Materials Today 7, 26 (2004)
[4] Q.X. Zhao, M. Willander, R. Morjan, Q.H. Hu and E.E.B. Campbell, "Optical Recombination of ZnO Nanowires Grown on Sapphire and Si Substrates", Appl. Phys. Lett. 83,165 (2003)
[5] P.D. Batista and M. Mulato, ZnO extended-gate field effect transistors as pH sensors, Appl. Phys. Lett. 87 143508 (2005)
[6] B.S. Kang and F. Ren, pH measurements with single ZnO nanorods integrated with a microchannel, Appl. Phys. Lett. 86, 112105 (2005).
[7] Olga Dulub, Bernd Meyer and Ulrike Diebold, Observation of the dynamical change in a water monolayer adsorbed on a ZnO surface, Phys. Rev. Lett. 95, 136101 (2005).
[8] M. Arab, D. Bougeard and K.S. Smirnov, Molecular dynamics study of the structure and dynamics of Zn^{+} ion in water, Chem. Phys. Lett. 379 (2003) 268-276.
[9] William W. Porterfield, Inorganic Chemistry a unified Approach, Academic press, Inc., P.335, 1993.
[10] D. E. Yates, S. Levine and T. W. Healy, ´´ Site-binding model of the electrical double layer at the metal oxide/water interface,´´ J. Chem. Soc. Faraday Trans. I, vol. 70, p. 1807, 1974.
[11] Werner Stumm, Chemistry of the solid-water interface, John Wiley & Sons, Inc., 1992, p. 43-86.

5 *Silicon Carbide for chemical sensing devices*

M. Willander, O. Nur – Gothenburg University and Q.Wahib –- Linköping University Sweden

Silicon carbide (SiC) is the only compound that exists in the Si-C two atom system. However, it exists in more than 180 poly-types. These all consist of identical closely packed Si-C double layers, whose stacking sequence differs along a certain direction. The nearest neighbor arrangement of atoms is identical in the crystal structures. Each carbon atom is tetrahedrally surrounded by four Si atoms, and each Si atom is tetrahedrally bonded to four carbon atoms by sp^3 hybrid orbitals [1]. The ionicity of SiC is 12%. The next nearest neighbors may be placed in two different possible ways. These are respectively the cubo-octahedral or the hexagonal cubo-octahedral. Single crystalline SiC exists in cubic (C), hexagonal (H), and rhombohedral (R) structures. Moreover all the poly-types are divided into two families. The α-SiC and the β–SiC families. The β–SiC family has only one member and it is the only poly-type that exists in the cubic structure, referred to as 3C-SiC (three layers cubic). It is the simplest and the most well known among all the poly-types. Despite the large lattice mismatch with Si (20%), the cubic structure is in fact important since it enables the materials to be grown epitaxially on Si. The growth of a device quality 3C-SiC/Si heterostructure presents the possibility of monolithic integration with other standard Si electronic components. The other poly-types, belonging to the α-SiC family exist in the other two crystal structures mentioned above. Amongst these, the 2H, 4H, 6H, and 16R are the most commonly occurring poly-types. The number denotes the number of the repeated layers, which in some poly-types reaches a few hundreds of repeated sequences. Although the chemical bonding and thermodynamics of the different poly-types seem to be the same, some of the physical properties such as bandgap and electronic properties differ very strongly. This implies that we can consider all of the poly-types as belonging to the same family of semiconductors having almost the same lattice parameters and similar chemical properties, but with different physical and electronic properties. This is of great interest as the combination of different SiC poly-types can lead to heterojunctions among the same family. In general all the poly-types of SiC are characterized physically by a wide bandgap. The 2H poly-type has the largest bandgap (3.33 eV), while the 3C poly-type has a bandgap of (2.39 eV). Beside the large bandgap, SiC is an excellent radiation-resistant material, having a high Debye temperature and high thermal conductivity. It is important to also note that it is straightforward to grow high quality oxide on SiC. These properties make SiC an attractive semiconductor material for many application areas, which include, power electronics, high frequency devices, and sensors. The later is of interest to this section. Comparing the physical properties of the different wide bandgap semiconductors, it can be concluded that there is no competition based on physical properties alone. The physical properties of all wide bandgap semiconductors are similar, apart from the offered direct and indirect bandgap which influences the quantum efficiency in optoelectronic devices. Significantly SiC demonstrates high chemical stability and it is a chemically an inactive material, making it a durable and appropriate choice for sensors operating under harsh conditions, e.g. operating at high temperature. High chemical stability also suggests that this material can be used for applications in medicine and ecological engineering fields and SiC has long been recognized as an excellent material for the realization of Micro-Electro-Mechanical Systems (MEMS) operating in harsh conditions. This is due to its unique

mechanical strength combination with chemical inertness [2]. In this section we will restrict the discussion in the sections below towards chemical sensors.

The growth of single crystalline SiC and device processing technology research has been going on for few decades and remains an active area of research. It has attracted many research laboratories around the world since the mid-80s. The growth of different poly-types (both bulk as well as thin films) has reached a device quality material for many applications. Since semiconductor crystal quality is an important factor we will discuss some important facts regarding SiC single crystal growth. We first briefly describe the growth development of single crystalline SiC (bulk and thin films), then the general principles of chemical gas sensors are mentioned. This will be followed by some specific examples that utilize SiC as a chemical sensor. Finally, some ‘’exotic’’ chemical sensors based on new and/or innovatively engineered SiC will be given.

5.1 SiC single crystal growth

As mentioned above, the possible device applications utilizing SiC are many and, depending on the application, there is an acceptable degree of crystalline quality for efficient and long life time component. Figure 5.1 shows a high resolution cross-sectional transmission electron micrograph (HR-TEM) from a 4H-SiC along the 0001 plane. The image shows the presence of stacking faults that can lead to current degradation with time. The presence of such stacking faults is the major reason for the lack of availability of commercial SiC devices for high power applications.

Figure 5.1: High resolution cross sectional transmission electron microscope (HR-TEM) view of 4H SiC along the 0001.

The sublimation technique for single crystalline semiconductors is one of the oldest growth techniques used for bulk SiC [3]. These initial efforts resulted in high purity α-SiC single crystals. However, the crystals were random in size and the control over the grown poly-type was poor. This technique was later modified to include seeded growth [4], which resulted in more control of the particular poly-type grown and was adopted by many researchers. Using the seeded sublimation technique, large single-crystal blues

of pure 6H-SiC poly-type with diameter up to 40 mm as well as 4H-SiC were demonstrated [5-6] and doping of this large single crystal to tailor electrical properties was possible. Although the modified seeded sublimation growth method has demonstrated control over the poly-type, along with possibility of obtaining lightly doped and highly doped crystals, the structural quality regarding the density of dislocations was not promising. A severe problem was the density of micropores and micropipes (around 10^2 cm^{-2}). This density of defects is a severe limitation on the use of these crystals and it can cause degradation in device performance, especially for high power electronics. Many other techniques were proposed to grow well controlled high quality single crystal SiC and chemical vapor deposition (CVD) has been recently favoured. It is the most advanced epitaxial technique and is the most widely used technique for commercialization [7]. As mentioned above the 3C-SiC is of special interest due of the possibility of epitaxial growth on Si and hence monolithic integration with other Si standard devices. Although the lattice mismatch between 3C-SiC and Si is relatively large, different methods have been employed to produce device quality 3C-SiC/Si heterostructures. Some early results can be found in [7-9]. One approach adopted to reduce the lattice mismatch, is to use off-axis substrates to eliminate the anti-phase boundaries which are the main type of intrinsic defect in the grown 3C-SiC layers [10]. A second approach is the use of elastic substrates to release stress due to the relatively large lattice mismatch [11]. It should be noted that elastic substrates e.g. Silicon On Insulator (SOI) becomes viscous at temperatures approaching the growth temperature and hence their use will not lead to any temperature modification.

The first commercial SiC substrates became available during the late 80s and early 90s. This has stimulated the research on SiC-based device technology and triggered a global interest. The status of SiC single crystal grown epitaxial layer today is to a large extent acceptable for almost all applications. Until 5 years ago the density of dislocations, micropipes and micropores, although low, were still unacceptable. Today these un-wanted structural imperfections are completely eliminated and only few stacking faults (as those shown in Fig. 1) are present. It is important to note that although stacking faults can cause degradation in device performance for high power applications, they are not of significant concern when considering SiC chemical sensors.

Although SiC based devices demonstrate significant advantages and potential the projected realization for commercial products has not matched initial expectations. This is due to many factors. For the specific case of SiC based chemical sensors, although stable performance up high temperatures has been demonstrated, mounting and packaging of the sensor is providing a further challenge for a wide range of commercial products. This issue is elaborated below when discussing specific SiC chemical sensors.

5.2 Gas sensor principles

The first pioneering work on chemical sensors was demonstrated during the early 70s. Two main different devices were demonstrated, these were the ion sensitive field effect transistors (ISFET) for pH sensing of electrolytes [12], and Pd gate MOSFETs for gas sensing [13]. Of particular interest here is the gas sensor MOSFET based on pure Si Pd-gate MOSFET. The principle of operation was based on the fact that Pd is a catalytic metal that dissociates the ambient gas to ions. These travel by diffusion to the metal-oxide interface where an electrically polarized layer is formed (for the first Pd MOSFET hydrogen was the ambient gas). This layer stimulates a change in the electrical

characteristics of the MOS device, and hence a sensing mechanism is established. In the case of MOS based sensors this is observed as a shift of the C-V characteristics due to the voltage modification of the dipole layer. Demonstration of this first solid state electronic chemical sensor has stimulated the scientific community and many research papers are published. Gas sensitivity and operating conditions using different catalytic metals were also demonstrated as will be discussed in the next section. Based on the same principle, two other devices employing SiC were demonstrated with excellent performance. These are the Metal Insulator Semiconductor Schottky diode (MIS) and the Schottky diode. The MIS Schottky usually employs a thin (0.15-0.2 nm) silicon dioxide layer to avoid pinning the barrier height.

5.3 SiC gas sensor development

Although the successful demonstration of the first gas sensor using pure Si found many application areas; Si-based MOS sensors cannot operate at temperatures above 280^{o}C.

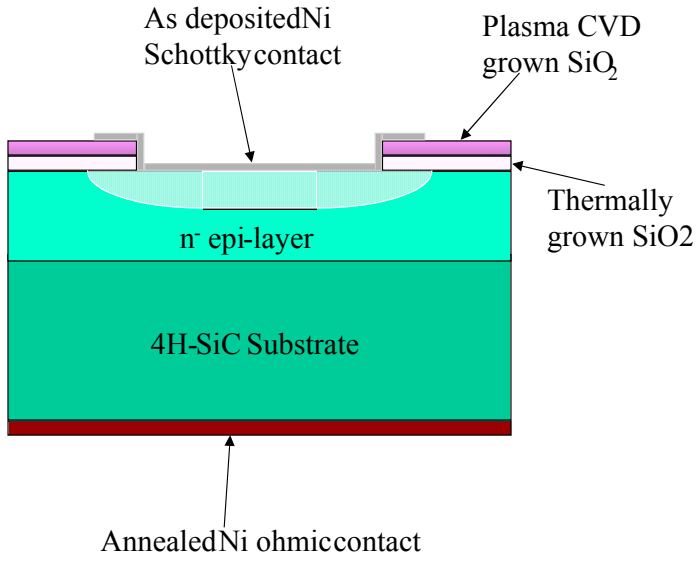

Figure 5.2: Schematic diagram showing a typical high temperature Schottky based gas sensor. As seen the processing steps required to such sensor are quite simple. Here the top contact choice can be any appropriate catalytic metal depending on the sensitivity.

Many gaseous systems of interest have an operating enviroment well in excess of the Si working temperature. High temperature gas sensors, for example, are of great interest for large scale commercial applications such as continuous monitoring of exhaust gases emerging from combustion processes in car engines. The requirements here are very demanding. To monitoring car exhaust gases, an efficient sensor will have a working temperature as high as 900 ^{o}C for 4000 hours or alternatively 160000 km. The response to a change between oxidizing and reducing atmospheres must be within 10 ms. SiC with its large bandgap and chemical inertness is the best among the wide bandgap semiconductors for this type of application.

The first MOS SiC based sensor was demonstrated on commercial 6H-SiC with Pt used as the catalytic gate metal [14, 15]. This sensor has been operated at temperatures as

high as 800^{o}C. The sensitivity to hydrogen was studied over a wide temperature range. Although MOSFET based devices have been demonstrated employing both the 4-H and 3C families, 3C-SiC has a higher electron mobility. Hence it has the potential to provide a more efficient MOS device. However, the lack of 3C-SiC wafers (substrates) has led to high temperature sensor research focusing on the H family. The earliest reported SiC MOS-based sensors showed promising results and they were used to study the reactions of catalytic metals at temperatures well above the operating temperature for Si MOS (280 ^{o}C). The sensors enabled the study of the hydrocarbon dissociation, which usually occurs at temperatures above 350 ^{o}C. The SiC based MOS sensor has provided detailed information on the decomposition of different hydrocarbons e.g. methane, ethane, propane and butane [15]. Since this early work, different groups have presented investigations that provided knowledge of high temperature chemical gas sensing and recent studies can be found in [16-20]. The development of SiC based devices has shown promising results with stable operation demonstrated for temperatures up to 600^{o}C. The effects of operating temperature, catalytic metal employed, and physical structure of the sensor on selectivity and sensitivity have been investigated for many gaseous environments. As a result of these valuable efforts, sensor arrays can be fabricated for the purpose of sensing gas mixtures. However, it should be noted that at high temperatures the band offset between the SiC and the SiO_2 decreases, and as a result the devices are increasingly susceptibile to charge injection from the semiconductor into the oxide. This is understood to be the main reason for sensor failure at high temperatures (above 600^{o}C). By engineering the physical parameters of the device in such a way to minimize the electric field at the SiC-SiO_2 interface, stability above 600 ^{o}C can be achieved. This issue is important with regard to the long term stability of these sensors. The use of nano-particles embedded in the oxide has been suggested as a possible method for increasing the long term stability at relatively high temperatures. In addition to the SiC MOS sensor, MIS Schottky and Schottky fabricated on SiC were employed as gas sensors. Early wok on these devices can be found in [21-22]. It is important to note that Schottky contact is a majority carrier mechanism and hence a fast response is expected. The Schottky based sensor is also the most simple structure to fabricate. Figure 5.2 shows a typical Schottky based SiC based high temperature gas sensor. Both devices show stable operation, but at temperatures below the maximum theoretical temperature associated with SiC physical properties. More device engineering research is needed in order to have stable operation at extremely high temperature.

5.4 Other innovative SiC based chemical gas sensors

We have provided a brief example of the use of SiC in an innovative way to demonstrate a highly sensitive sensor. It is known that as the sensing element dimensions are reduced, the more sensitive is the device. Most recently an innovative sensor based on porous SiC was demonstrated [23]. This was sensitive to ammonia for levels as low as 0.5 ppm. The sensor was fabricated employing a relatively very simple process. SiC thin film was deposited on Si using chemical vapor deposition. The SiC was made porous by electrochemical etching. Finally, Al electrodes were deposited to contact to both the porous-SiC and back side of the Si wafer. The exact sensing mechanism of this device is not yet completely understood, however one possible explanation could be due to changes in the depletion layer upon decomposition of ammonia and the subsequent adsorption of the hydrogen.

Conclusions

Progress in crystal growth and processing methods has ensured the availability of device quality wafers and thin epitaxial layers with precise control of doping, oxidation and metallization. The wide bandgap, combined with chemical inertness results in SiC being the best material for gas sensing in harsh and/or at high temperatures. The physical parameters of SiC enable it to function for temperatures as high as 1000 ^{o}C. However, testing in research laboratories has shown long term stability is curently restricted to 600^{o}C. More research into the physical design could push the sensor performance up to much higher temperatures. Development is also required in the areas of mounting and packaging of this type of sensor system [24].

[1] Y. M. Tairov and M. Willander, ‘’Silicon carbide: material and device properties’’, In High Temperature Electronics, 1st Edition, Electronics Materials 2, Edited by M. Willander and H. L. Hartnagel, Chapman & Hall (1997).
[2] C. Zorman, A.J. Fleischman, A. S. Dewa, M. Mehregany, C. Jacob, S. Nishino, P. Pirouz, J. Appl. Phys. **78**, 5136 (1995).
[3] J. A. Lely, Darstellung von Einkristalln von Silizum Karbid und Beherrschung von Art und Menge der eingebauten Verunreinigungen. Ber. Deutsch. Keram. Ges. **32**, 229 (1955).
[4] Y. M. Tairov, and V. F. Tsverkov, J. Crysl. Growth **43**, 209 (1978).
[5] D. L. Barret, J. P. McHugh, H. M. Hopgood, R. H. Hopkins, P. G. McMullin, and R. C. Clarke, J. Crystal Growth **128**, 352 (1993).
[6] M. Kanaya, J. Takahashi, Y. Fujiwara, and A. Moritani, Appl. Phys. Lett. **58**, 56 (1991).
[7] S. Nishino, J. A. Powel, and H. A. Will, Appl. Phys. Lett. **45**, 460 (1983).
[8] Q. Wahab, L. Hultman, J. E.-Sundgren, and M. Willander, Material Science and Engineering **B11**, 61 (1992).
[9] Q. Wahab, M. R. Sardela, Jr., L. Hultman, A. Henry, M. Willander, E. Janzen, and J. E.-Sundgren, Appl. Phys. Lett. **65**, 725 (1994).
[10] R. F. Davis, J. Palmour, and J. A. Edmound, Diamond. Rel. Mat. **1**, 109 (1992).
[11] S. I. Romanov, V. I. Mashonov, L. V. Sokolov, A. Gutakovski and O. P. Pchelyakov, Appl. Phys. Lett. 75, 4118 (1999).
[12] P. Bergveld, IEEE Trans. Biomed. Eng. **17**, 70 (1970).
[13] I. Lundström, M. S. Shivaraman, and C. M. Svensson, J. Appl. Phys. **46**, 3876 (1975).
[14] A. Arbab, A. Spetz, Q. Ul Wahab, M. Willander, and I. Lundström, Sens. Mater. **4**, 173 (1993).
[15] A. Arbab, A. Spetz, and I. Lundström, Sensors and Actuators **B 15-16**, 19 (1993).
[16] A. Spetz, L. Unene, H. Sevenningstorp, P. Tobias, L.-G. Ekedahl, O. Larsson, A. Göras, S. Savage, C. Harris, P. Mårtensson, R. Wigren, P. Salomonsson, B. Häggendahl, P. Ljung, M. Mattsson, and I. Lundström, Phys. Stat. Sol. **(a) 185**, 15 (2001).
[17] J. Schalwig, P. Kreisl, S. Ahlers, G. Muller, IEEE Sensor Journal **2**, 394 (2002).
[18] S. A. Khan, E. A. De Vasconcelos, H. Uchida, and T. Katsube, Sensors and Actuator **B92**, 181 (2003).
[19] S. Roy, C. Jacob, and S. Basu, Sensors and Actuator **B94**, 298 (2003).

[20] O. Casals, B. Barcones, A. Romano-Rodriguez, C. Serre, A. Perez-Rodriguez, J. R. Morante, P. Godignon, J. Montserrat, and J. Millan, Sensors and Actuators **B109**, 119 (2005).
[21] M. Karlsteen, A. Baranzahi, A. Spetz, M. Willander, and I. Lundström, J. Electronic Materials **24**, 853 (1995).
[22] J. W. Palmour, D. g. Waltz, J. A. Edmond, C. H. Carter, Jr., G. Gati, and S. J. Przyblko, Trans. 2nd Int. Conference. on High Temperature Electronics **1**, X123 (1995).
[23] E. J. Connolly, B. Timmer, H. T. M. Pham, J. Groeneweg, P. M. Sarro, W. Olthuis, and P. J. French, Sensors and Actuators **B109**, 44 (2005).
[24] M.Willander, M.Friesel, Q-U Wahab, B.Straumal, 'Silicon carbide and diamond for high temperature device applications' Journal of Materials Science: Materials in Electronics 17 pp1-25 (2006)

6 Magnetostrictive Thin Films

Eckhard Quandt - Stiftung CAESAR, Bonn, Germany

Interest in magnetostrictive thin films has rapidly grown over the last ten years due to their potential as actuators for powerful transducer systems in microsystems [1] or as miniaturized sensors monitoring strains [2] or magnetic fields using multiferroic composites [3]. These developments are based on the direct magnetostrictive (Joule) or indirect magnetostrictive (Villari) effect, respectively. Figure 6.1 shows the principle of both effects in the case of thin films with an in-plane anisotropy perpendicular to the applied field or stress.

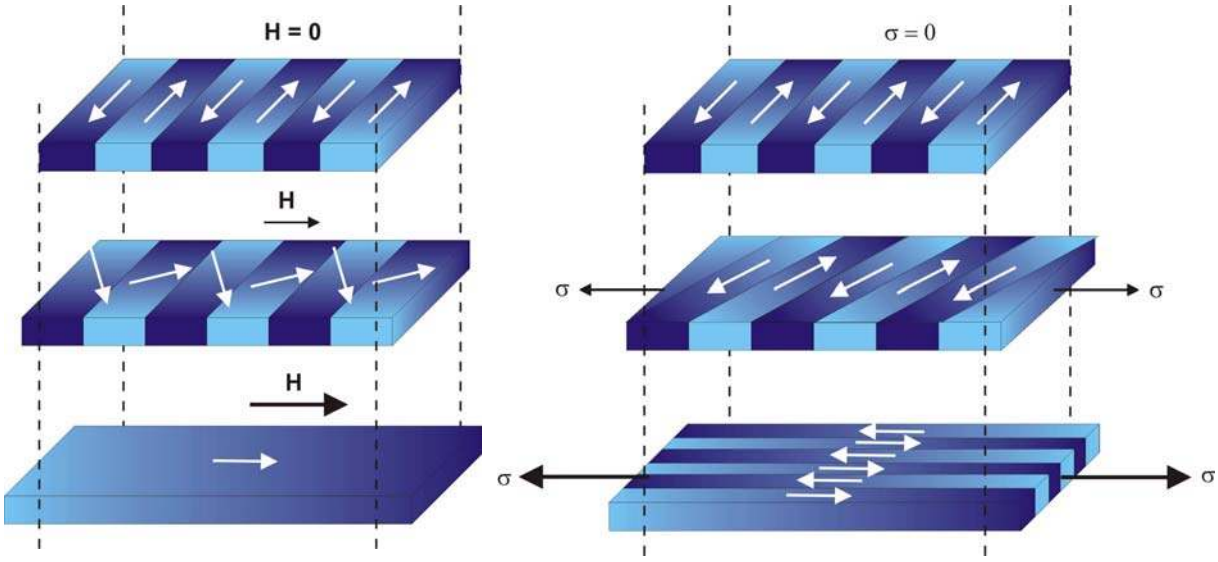

Figure 6.1: Schematic behavior of positive magnetostrictive thin films upon magnetization (left) or application of a tensile stress (right). White arrows indicate orientation of domain.

While the direct effect results in a change of dimension of the material due to domain alignment, which is the origin of any solid state actuator, the situation for the inverse effect is more complicated since it may consist of 180° domain walls, as shown in Figure 6.1. In that case it is obvious that the strain or stress does not result in a net magnetization of the sample but may lead to a rotation of the magnetic domains. To use this effect as a sensor mechanism for mechanical quantities it is necessary to combine the inverse magnetostriction with further effects being themselves sensitive to the orientation of magnetic domains. The effects to be combined with inverse magneto-striction are magnetoresistive effects, especially GMR (giant) or TMR (tunnel) effects [4], magnetoimpedance [5], or inductance using microinductors [6,7].

In the following sub-chapters the materials development for giant magnetostrictive materials, their use as micro-actuators, and magnetostrictive sensor using inductive, impedance or resistive effects are described in more detail.

6.1 Giant magnetostrictive thin films

The development of giant magnetostrictive thin film materials at room temperature is based on rare earth-transition metal alloys. These alloys offer the best possibility to develop giant magnetostriction at room temperature or above, since the highly aspherical 4f orbitals of the rare earths, which are the origin of the large magnetostriction, remain in an oriented state due to the strong coupling between the rare earth and the Fe or Co moments. An important development task for giant magnetostrictive materials has been their optimization in terms of their magnetostriction to magnetic anisotropy ratio in order to attain large strains at moderate magnetic fields. In bulk materials this was achieved by using cubic compounds, the rare earth-Fe_2 Laves phases, in which the second order anisotropy constant vanishes along with Tb-Dy alloying to compensate the fourth order anisotropy constant [8]. In the case of thin films, amorphous $(Tb,Dy)_x(Fe,Co)_{1-x}$ films [9] or particularly novel TbFe/FeCo multilayers [10] represent the most promising approaches to combine soft magnetic and giant magnetostrictive properties.

Since the magnetic saturation field is proportional to the ratio of the anisotropy and the saturation magnetization, two approaches are possible: the decrease of the anisotropy e.g. by using amorphous magnetic materials or the increase of the saturation magnetization. Using multilayers it is possible to engineer novel composite materials which show enhanced magnetizations in comparison to classic thin film magnetostrictors [11]. To create such a material two materials have to be combined: One material is the giant magnetostrictive amorphous TbFe alloy which should be combined with a material that is magnetically soft with a very high magnetization and preferably a magnetostrictive (e.g. FeCo). By fabricating layers with thicknesses smaller than the ferromagnetic exchange length and domain wall width, domain wall formation at the interfaces is prevented. The magnetic properties of such an exchange-coupled multilayer system are determined by the average of each individual layer. Together with the reduction in anisotropy this increase in magnetization results in a significant reduction in the magnetic saturation field. Figure 6.2 compares the magnetoelastic coupling coefficient, the product of the magnetostriction and the effective Young's modulus, of a TbFe/FeCo multilayer film with a nanocrystalline TbDyFe film and a TbFe single layer film.

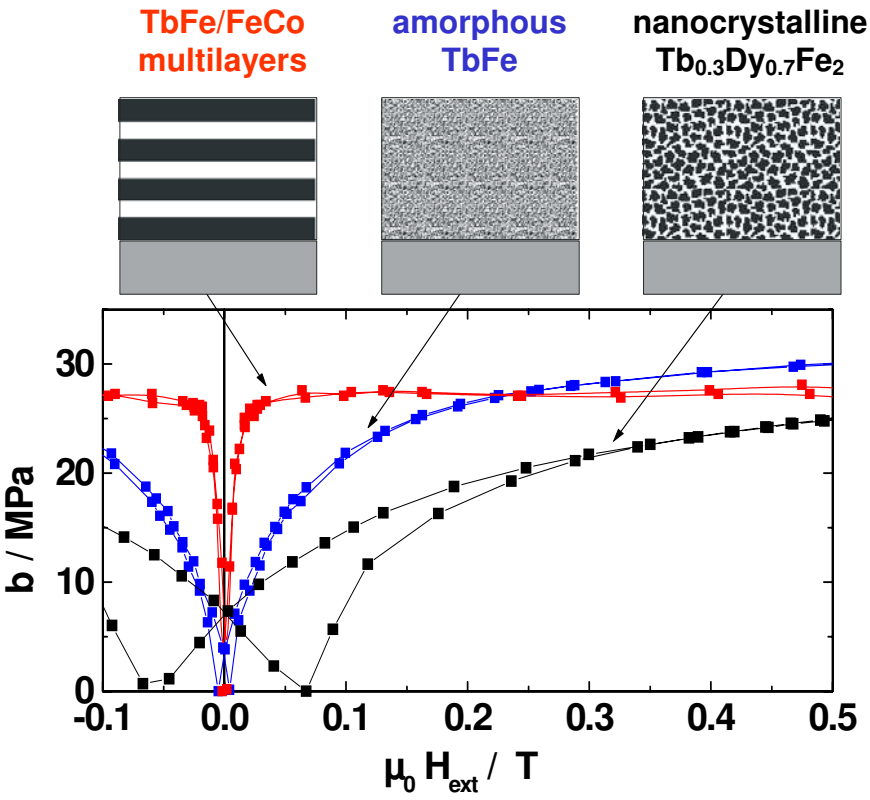

Figure 6.2 - Comparison of the magnetoelastic coupling coefficient of a TbFe/FeCo multilayer film, a nanocrystalline TbDyFe film, and a TbFe single layer film.

The fabrication of giant magnetostrictive thin films has only been realized by PVD-techniques until now, the most prominently used being magnetron sputtering using either mosaic type or composite targets as well as multitarget arrangements. Other PVD-techniques include electron beam evaporation, laser ablation and ion beam sputtering. The amorphous films are generally deposited onto unheated or cooled substrates while for crystalline films heated substrates for a single-step-process are used as an alternative to a post-deposition crystallization treatment.

For developing devices, the orientation of the magnetic easy axis and of the domains in the demagnetized state is of special importance since maximum magnetostriction is only obtained by 90° rotations of the magnetic domains, while 180° rotations do not result in any magnetostrictive strain. Considering that magnetostrictive thin film actuators are in general driven by a single magnetic field, whose direction is fixed in relation to the actuator and in-plane in order to avoid large demagnetization losses, the optimized demagnetized state should consist of domains with an in-plane easy axis being oriented perpendicular to the driving field direction (see Figure 6.1). This initial state can be obtained by a post-deposition annealing process under an in-plane magnetic field which is oriented under 90° towards the driving field direction [12].

6.2 Magnetostrictive thin film actuators

Magnetostrictive thin films form have predominantly been used as various micro-actuators for applications in microsystem technology [1] which are based on a bending transducer principle consisting of a film/substrate composite with the substrate being in

general non-magnetostrictive. Different geometries and boundary conditions are common, the most important being cantilevers, membranes and plates. Magnetostriction in the film causes the film/substrate composite to bend, similar to the bending of a bimetallic transducer. Commonly, the most important feature of these micro-actuators is the possibility of a remote-controlled operation.

In the case of cantilever actuators different applications have been realized, normally by using Si micro-machining for the fabrication of the cantilevers. The large bending or deflection of these cantilevers were used in the application of fluid jet deflectors controlling up to 500 ml/s [13], for magnetic field measurements by detecting the deflection of the cantilever optically, as well as for optical 2D micro-mirrors which employ bending and torsional vibrations driven by two differently oriented magnetic fields [14]. Furthermore, special attention has been paid to the development of thermal drift-free actuators either realized by a special design of the micro-machined substrate or by combining positive and negative magnetostrictive materials in a bimorph structure. Magnetostrictive membranes have been used for fluidic micro-components such as micro-valves or micro-pumps, whereas the deflection of the membrane is either used to close or to open the valve outlet or to induce a pressure rise in the pumping chamber [15]. Free plates with magnetostrictive coatings have been employed for the realization of traveling machines or for ultrasonic motors [16]. Both linear and rotating standing wave motors were realized with micro-machined Si or Ti substrates using a propulsion mechanism of vibrating teeth on a friction layer. The ultrasonic motors were operated by ac magnetic fields in combination with a magnetic bias field.

6.5 Magnetostrictive magnetoresistive sensors

The motivation to use the inverse magnetostriction for mechanical sensing is driven by their high sensitivity, small sizes, high spatial resolution, along with their cost-effective fabrication by thin film technology. These general advantages are especially fulfilled in the case of sensors combining magnetostrictive and magnetoresistive effects.

Giant magnetoresistive (GMR) or tunnel magnetoresistive (TMR) stacks are well known as highly sensitive magnetic field sensors [17,18]. The GMR or TMR structures consist in principal of a magnetic reference layer and a magnetic sensing layer which are separated by a metallic non-magnetic layer (typically Cu) in the case of GMR sensors and a very thin non-conducting layer (Al_2O_3 or MgO barrier) in the case of TMR sensors. For TMR sensors resistivity changes $\Delta R/R$ of up to 350% have been obtained in the case of epitaxial MgO tunnel barriers between the high resistivity state (antiparallel orientation of the two magnetic layers) and the low resistivity state (parallel orientation). The GMR effect has been found in exchange-coupled structures such as Fe/Cr-multilayers with $\Delta R/R$ as large as 220 at 1.5 K and 42 at room temperature [19].

Initial investigations that combine GMR structures with magnetostrictive phenomena have been limited to NiFe sensing layers of varying compositions [20-22]. A significant enhancement of stress sensitivity of GMR structures could be achieved by using highly magnetostrictive materials such as $Fe_{50}Co_{50}$ as a free layer [23]. The most important increase in sensitivity compared to magnetostrictive GMR sensors could be achieved by using TMR sensors in combination with highly magnetostrictive materials such as crystalline $Fe_{50}Co_{50}$ [24] or amorphous $(Fe_{90}Co_{10})_{78}Si_{12}B_6$ [25].

For strain sensor applications the gauge factor (GF) which is defined as:

$$GF = \left(\frac{\Delta R}{R}\right) \Big/ \Delta\varepsilon \qquad \text{Eqn 6.1}$$

is the important parameter for the classification of different sensors and demonstrates this enhancement. While FeCo/Cu/Co GMR-trilayer systems show gauge factors of approximately 30 (ΔR/R of 3% upon 0.1% strain), the TMR sensor with $Fe_{50}Co_{50}$ reaches values up to 600 (ΔR/R of 25% upon 0.04% strain).

The potential application areas are manifold. The positive features are the very small size, for example TMR stacks have been demonstrated with junctions sizes as small as 50nm×50nm [26], the high sensitivity which also enables a reduction of the total sensor size and the large variety of substrates (e.g. Si, glass, diamond, polymer). The fabrication processes are in general compatible to both Si–micromachining and CMOS-technology offering the possibility to design highly integrated sensors.

6.6 Magnetostrictive magnetoimpedance sensors

These sensors profit from their high sensitivity, their possibility of remote interrogation [27,28], and the cost effective fabrication of melt-spinned wires and ribbons. The giant magnetoimpedance (GMI) effect is widely considered as a high-frequency analogy of the GMR effect: a type of side effect of the skin effect. The sensitivity as a field sensor can reach 100 %/Oe [29], which is typically at least one order of magnitude higher than that of GMR sensors. Sensors based on the GMI effect use magnetic ribbons or wires produced by melt spinning techniques [30], glass covered magnetic wires [31,32] or magnetic thin films [33,34]. In the case of magnetostrictive GMI sensors for stress/strain measurements the magnetic material has either a positive or negative magnetostriction. As the skin depth is dependent on the permeability a change in permeability due to magnetostriction results in corresponding magnetoimpedance changes. Therefore, a general condition is that the skin depth is smaller than the cross sectional dimension of the material (wire, ribbon, film) in order to have a strong impedance dependency on changes in the skin depth.

GMI thin film micro-strain sensors were e.g. achieved using FeCoBSi materials. The sensor consists of a millimeter-sized meander-like structure on a 20mm×4mm and 150µm thick glass cantilever. A change in impedance of about 46 % was observed with 100MHz driving frequency at a strain of 0.03% [35].

6.5 Magnetostrictive inductive sensors

Since one of the consequences of the inverse magnetostrictive effect is the change in permeability, inductive elements with magnetostrictive cores offer the possibility to produce magnetostrictive strain sensors. The application of a strain results in a change of permeability of the magnetostrictive core. This leads to a change of inductance L that, for example, can be monitored by electrical resonance measurements [36]. These measurements use resonant circuits (so called LC-tags, consisting of a capacitance C and an inductance L) where L is changed due to its magnetostrictive core. A particular benefit of this approach is the possibility to operate these sensors by remote interrogation using either radar reflectivity or inductive coupling.

Micro-inductors with incorporated magnetic thin films have been widely investigated in the past 10 years due to their potential as integrated components in micro-electronic

devices. Four general types of magnetic thin film inductors [37] have been investigated in detail: strip line inductors with magnetic sandwich layers [38-40], spiral inductors with magnetic sandwich layers [41-43], solenoid inductors [44,45], and toroid inductors [46]. In principle, the same approaches can be also used in the case of mechanical sensors; the main difference is merely the replacement of the magnetic core by a magnetostrictive one. Another design aspect is the orientation of the magnetic easy axis which should be well-defined with respect to the direction of the applied stress in order to guarantee a reproducible and optimized sensor behavior. Therefore approaches which can be operated with a uniaxial anisotropy, as with a strip-line or the solenoid inductor are of more general interest for sensors.

An example of an inductive strain sensor was realized using a magnetostrictive LC-circuit based on a strip-line type inductor [47]. Here the magnetic easy axis is aligned parallel to the strip, optimally aligned to the exciting high frequency magnetic field. When a tensile stress is applied perpendicular to the strip (for a positive magnetostrictive material) the permeability and therefore the inductance of the strip will increase resulting in a decrease of the resonance frequency. Similarly, a compressive stress leads to a stabilization of the easy axis and decreases of the permeability along the hard axis resulting in an increase in resonance frequency. Millimeter-sized LC resonant circuits have been fabricated in thin film technique on glass wafers [48]. FeCoBSi and FeCo/CoB were used as magnetostrictive materials, demonstrating both high frequency properties and high magnetostriction. The values of the inductance and the capacitance were designed to yield a LC resonance frequency of approximately 500 MHz.

It was demonstrated that this sensor can read by remote interrogation [49,50]. In this case the read out was realized by two pick up coils and a network analyzer. The figure of merit (FoM) which was defined as

$$FoM = \frac{\Delta f}{f_0} \Big/ \Delta\varepsilon \qquad \text{Eqn 6.2}$$

With f_0, Δf, $\Delta\varepsilon$ being the resonance frequency and change in frequency and permeability with the change of strain, respectively. In the sensitive strain range this sensor reached a FoM of approximately 1000. These values are extraordinarily high compared to more traditional strain gauges. A possible application for this type of sensor is the measurement of torque. Torque measurements of up to 200 Nm using a similar sensor are presented in [49].

[1] E. Quandt, A. Ludwig, Sensors and Actuators A 81 (2000), 275-280
[2] M. Frommberger, E. Quandt, Encyclopedia of Sensors (in press).
[3] S. Stein, M.Wuttig,; D.Viehland, E.Quandt, J. Appl. Phys. 97 (2005), 1-3.
[4] P. Grünberg, Phys. Rev. Lett. 57 19, 2442-2445 (1986)
[5] M. Knobel, K.R. Pirota, J. Magn. Magn. Mat. 242-245, 33-40 (2002)
[6]. M. Yamaguchi, Y. Miyazawa, K. Kaminishi, H. Kikuchi, S. Yabukami, K.I. Arai, T. Suzuki, J. Magn. Magn. Mat. 268, 170-177 (2004)
[7]. B. Rejaei, M. Vroubel, Y. Zhuang, J. N. Burghartz, proc. of the 4th topical meeting on silicon monolithic integrated circuits in rf-systems, 100-103 (2003)
[8] A.E. Clark in: Ferromagnetic Materials, Vol. 1, E.P. Wohlfarth (ed.) Amsterdam 1980, S. 531- 586.

[9] N.H.Duc,, K. Mackay, J. Betz, D. Givord, J. Appl. Phys. 79 (1996), 973-76.
[10] E. Quandt, A. Ludwig, J. Appl. Phys. 85 (1999) 6232-37
[11] E.Quandt, A. Ludwig, J. Betz,; K. Mackay, D. Givord, J. Appl. Phys. 81 (1997), 5420-22.
[12] A. Ludwig, E. Quandt, J. Appl. Phys. 87 (2000) 4691-95
[13] G. Flik, M. Schnell, F. Schatz, M. Hirscher, H. Kronmüller, in: Proc. Actuator 94, Bremen 1994, p. 232-235.
[14] T. Bourouina, E. Lebrasseur, G. Reyne, A. Debray, H. Fujita, A. Ludwig, E. Quandt, H. Muro, T. Oki, A. Asaoka, Journal of Microelectromechanical Systems, 11/4 (2002), 355 - 361
[15] W. Pfleging, A Ludwig, E. Quandt, in: Proc. Actuator 98, Bremen, 1998, p. 379-382.
[16] F. Claeyssen, N. Lhermet, J. Betz, K. Mackay, D. Givord, E. Quandt, H. Kronmüller, in: Proc. Actuator 98, Bremen, 1998, p. 375-378.
[17] Ch. Binek, B. Doudin, J. Phys.: Condens. Matter 17, L39-L44 (2005) and references therein.
[18] A. Barthelemy, A. Fert, J-P. Contour, M. Bowen, V. Cros, J.M. De Teresa, A. Hamzic, J.C. Faini, J.M. George, J. Grollier, F. Montaigne, F. Pailloux, F. Petroff, C. Vouille, J. Magn. Magn. Mat. 242–245, 68-76 (2002) and references therein.
[19] R. Schad, C. D. Potter, P. Beliën, G. Verbanck, V. V. Moshchalkov, and Y. Bruynseraede, Appl. Phys. Lett. 64, 3500-3502 (1994)
[20] L. Baril, B.A. Gurney, D.R. Wilhoit, V. Speriosu, J. Appl. Phys. 85, 5139-5141 (1999)
[21] H.J. Mamin, B.A. Gurney, D.R. Wilhoit, and V.S. Speriosu, Appl. Phys. Lett. 72, 3220 (1998)
[22] R.C. O'Handley, J.R. Childress, IEEE Trans. Magn. 31 4, 2450-2454 (1995)
[23] T. Duenas, A. Sehrbrock, M. Löhndorf, A. Ludwig, J. Wecker, P. Grünberg, E. Quandt, J. Magn. Magn. Mat. 242-245, 1132-1135 (2002)
[24] M. Löhndorf, T. Duenas, M. Tewes, and E. Quandt, M. Rührig, J. Wecker, J. Appl. Phys. Lett. 81 2, 313-315 (2002)
[25] M. Löhndorf, T.A. Duenas, A. Ludwig, M. Rührig, J. Wecker, D. Bürgler, P. Grünberg, E. Quandt, IEEE Trans. Magn. 38 5, 2826-2828 (2002)
[26] H. Kubota, Y. Ando, T. Miyazaki, G. reiss, H. Brückl, W. Schepper, J. Wecker, G. Gieres, J. Appl. Phys. 94 3, 2028-2032 (2003)
[27] C. Tyrén, A. Vázquez, C. Quinones, Stress wire antenna, Int. Patent WO 00/57147 (2000)
[28] M. Tewes, M. Löhndorf, A. Ludwig, E. Quandt, in Advanced Microsystems for automotive applications, S. Krueger, W. Gessner (Eds.), Springer Berlin Heidelberg New York, 83-87 (2001)
[29]. A.E. Mahdi, L. Panina, D. Mapps, Sensors and Actuators A 105, 271-285 (2003)
[30] P. Marín, A. Hernando, "Magnetic Microwires: manufacture, properties and applications" in Encyclopedia of Materials: Science and Technology, Elsevier Ltd., 1-9 (2004)
[31] M. Vazquez, Physica B 299, 302-313 (2001)
[32]. H. Chiriac, T. A. Óvári, C. S. Marinescu, J. Appl. Phys. 83 11, 6584-6586 (1998)
[33] Y. Nishibe, N. Ohta, R&D Review of Toyota CRDL 35 4 (2000.12)

[34] H. Yamadera, Y. Nishibe, J. Appl. Phys. 87 9, 5356-5358 (2000) K.-H. Shin, M. Inoue, K.-I. Arai, J. Appl. Phys. 85 8, 5465-5467 (1999)
[35]. C.H. Tyrén, G. Lord, Magnetoelastic stress sensor, US Patent 5297439 (1994)
[36] B. Rejaei, M. Vroubel, Y. Zhuang, J. N. Burghartz, Proc. of the 4th topical meeting on silicon monolithic integrated circuits in rf-systems, 100-103 (2003)
[37] V. Korenivski, J. Magn. Magn. Mat. 215-216, 800-806 (2000)
[38] A. Gromov, V. Korenivski, D. Haviland, R.B. van Dover, J. Appl. Phys. 85 8, 5202-5204 (1999)
[39] T. Saito, K. Tsutsui, S. Yahagi, Y. Matsukura, H. Endoh, T. eshita, K. Hikosaka, IEEE Trans. Magn. 35 5, 3187-3189 (1999)
[40] M. Yamaguchi, K. Suezawa, Y. Takahashi, K.I. Arai, S. Kikuchi, Y. Shimada, S. Tanabe, K. Ito, J. Magn. Magn. Mat. 215-216, 807-810 (2000)
[41]. A.M. Crawford, D. Gardner, S.X. Wang, IEEE Trans. Magn. 38 5, 3168-3170 (2002)
[42] B. Viala, A.S. Royet, R. Cuchet, M. Aid, P. Gaud, O. Valls, M. Ledieu, O. Acher, IEEE Trans. Magn. 40 4, 1999-2001 (2004)
[43] Y. Zhuang, B. Rejaei, E. Boellaard, M. Vroubel, J.N. Burghartz, IEEE Elec. Dev. Lett. 24 4, 224-226 (2003)
[44] K. Shirakawa, H. Kurata, J. Toriu, H. Matsuki, K. Murakami, IEEE Trans. Magn. 27 6, 5432-5434 (1991)
[45] M.G. Allen, IEEE Trans. Magn. 39 5, 3073-3078 (2003)
[46] M. Frommberger, Ch. Zanke, A. Ludwig, M. Tewes, E. Quandt, Microelectronic Engineering 67-68, 588-594 (2003)
[47] M. Frommberger, Ch. Zanke, A. Ludwig, M. Tewes, E. Quandt, Microelectronic Engineering 67-68, 588-594 (2003)
[48] E. Quandt, M. Frommberger, Mat. Trans. 45 2, 244-248 (2004)
[49] M. Frommberger, M. Tewes, A. Ludwig, Ch. Zanke, E. Quandt, Trans. Magn. Soc. Japan 3, 115-117 (2003)

7 Magnetic properties of magnetic nanoparticles

Crister Johansson - Imego AB, Gothenburg, Sweden

7.1 Single domains

This section will discuss the basic magnetic properties of magnetic nanoparticles and different applications where they are used. Spherical magnetic nanoparticles with diameters smaller than about 30 nm are singledomains [1]. The critical singledomain size depends on the material and the geometry of the particles. The definition of a singledomain is that all spins in the particle have the same direction giving a total magnetic moment of the particle being the sum of all the spins. Thus, the magnetic moment is proportional to the product of the volume and a material parameter called the *intrinsic spontaneous magnetization* of the singledomain. Above the critical single domain size the particles consist of polydomains, meaning that the particles are splitted up into several domains with different spin directions. Table 1 shows the critical single domain size and the intrinsic spontaneous magnetization for some typical magnetic material.

The intrinsic spontaneous magnetization of singledomains with sizes in the nanometre range is in most cases different than the corresponding value of the bulk material. This has been explained by a surface effect or the effect of the small size of the nanoparticles [2]. The surface effect becomes considerable since the number of surface spins becomes comparable to bulk spins for particles with sizes in the nanometre range. The spins at or close to the particle surface may become canted resulting in that the surface spins are not oriented in the same directions as the bulk spins. This results in that the intrinsic magnetization is less than the value for the bulk material.

Material	d_S *(nm)*	d_B *(nm)*	M_s *(kA/m)*
Fe_3O_4	70	15	390
γ-Fe_2O_3	70	20	320
Fe	50	15	1500
Co	30	7	1300
$CoFe_2O_4$	90	10	380
FePt	50	5	420

Table7.1 The single domain/polydomain transition diameter, d_s, the superparamagnetic transition diameter (or the blocking diameter), d_B, at room temperature, and the intrinsic spontaneous magnetization, M_s, at room temperature with respect to the magnetic material is presented in the following table. The M_s values are given for small magnetic nanoparticles (which is usually smaller than the corresponding values for bulk values as explained in the text). The diameter d_B is explained in the text.

Since the magnetic moment of the singledomains is proportional to the volume of the particle, the magnetic moment of the single domain is very large compared to the individual magnetic moments of the ions of ordinary paramagnetic substances. As a result, the magnetic energy (even at moderate external magnetic fields) becomes comparable to the thermal energy. This implies that magnetic saturation is achieved at moderate fields and a high magnetic susceptibility is obtained for the particle system even at room temperature. When the relaxation time, a measure of the time for magnetization reversal, of the singledomain system is less than the measuring time (the measuring time is a characteristic time for the used detection method) the particle system is called *superparamagnetic* [3]. The magnetization of the superparamagnetic singledomain system can be calculated with the Langevin function averaged over a domain size distribution [4]. This model can be further modified for magnetic single domain interactions and magnetic anisotropy [5,6].

7.2 Néel relaxation

In a singledomain particle system where the particles are placed in a solid matrix such that the magnetic particles cannot physically rotate, the only change of the direction of the magnetic moment of the particle comes from an internal rotation of the magnetic moment over an energy barrier. This type of magnetic relaxation is named Néel relaxation. The value of the energy barrier is depending on the material and size of the nanoparticle; along with the applied external magnetic field and the magnetic interactions between the nanoparticles that also changes the energy barrier. The magnetic moment can relax (or rotate) over the energy barrier during a specific time (the relaxation time) if there is enough thermal energy available. The magnetic relaxation time of magnetic nanoparticles can approximately be considered as the time for the magnetic moment of the nanoparticle to rotate from one easy axis direction to the other easy axis direction. The Néel relaxation time, τ_N, is dependent on the temperature, T, the magnetic anisotropy, K (which is dependent on the material, size, and the geometry of the nanoparticles) and the volume of the nanoparticles, V. The Néel relaxation time in zero magnetic field and for non-interacting nanoparticles can be expressed by [7]:

$$\tau_N = \tau_0 e^{\frac{KV}{k_B T}} \qquad \text{Eqn 7.1}$$

where k_B is the Boltzmann constant and τ_0 a characteristic relaxation time in the range of 10^{-9} s and 10^{-12} s [5,8]. Since the Néel relaxation time depends exponentially on the energy barrier, the Néel relaxation time varies drastically with the size of the nanoparticles as can bee seen in Figure 7.1. The Néel relaxation time changes from very low values of about nanoseconds up to several thousands of years when the size of the nanoparticles changes. This enables control of the relaxation time and magnetic properties of the nanoparticles and ultimately the design of magnetic nanoparticles for specific applications.

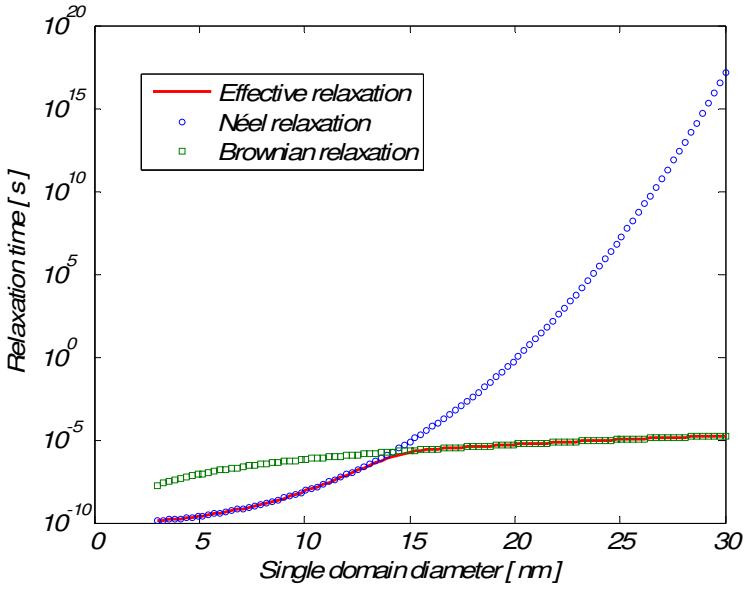

Figure 7.1: The plot shows how the Néel relaxation time (blue circles) and Brownian relaxation time (green rectangles) varies with the diameter of the single domains. The parameters used in the plot are typical data of single domains of maghemite (γ-Fe_2O_3) at room temperature. A size dependence of the magnetic anisotropy has also been taken into account in this plot. The Brownian relaxation time is plotted for nanoparticles placed in water at room temperature with a hydrodynamic size of 20 % larger than the actual domain size. The effective relaxation time (red line) is the relaxation time the particles will undergo when placed in, as in this case, water. Nanoparticles in a solid matrix will always only relax with the Néel relaxation

Magnetic nanoparticles with long Néel relaxation times can be used in data storage systems where it is crucial to have small regions of magnetic material with stable magnetic moment directions. The two directions of the magnetic moments of the magnetic nanoparticles enable the storage of binary data as zeros (0) and ones (1). The directions of the magnetic moment of the nanoparticles must be stable with time since otherwise the information would be lost. Today the research of using magnetic nanoparticles for information storage is under great development [9, 10].

Magnetic nanoparticles can be subdivided into particles that are thermally blocked or superparamagnetic [3,8]. Thermally blocked particles have magnetic relaxation times that are longer than the measurement time (the characteristic time for the used detection method) and superparamagnetic particles that have magnetic relaxation times that are short compared to the measurement time. The size that divides the particles into superparamagnetic and thermally blocked particles is given in table 1 (diameter d_B), and is dependent on material and temperature. If the nanoparticles are placed in a solid matrix the thermally blocked nanoparticles will exhibit remanence and coercivity while the superparamagnetic particles will not show any remanence and coercivity, e.g. the coercivity and remanence for a nanoparticle system depends on the magnetic relaxation compared to the measuremet time. Coercivity is the field that brings the magnetization to zero value and the remanance is the residual magnetization of the particle system after being magnetized with an external magnetic field. Thermally blocked particles can

then used in data storage systems and it is the direction of the remanence that yields the information and the coercivity gives the necessary magnetic field to write data to the information storage system.

7.3 Brownian relaxation

If the nanoparticles are placed in a carrier liquid the particles can rotate and another relaxation mechanism enter, the Brownian relaxation. The Brownian relaxation time, τ_B, is dependent on the viscosity of the liquid, η, the hydrodynamic volume, V_h, of the particles and the temperature. The Brownian relaxation time can be expressed as [11]:

$$\tau_B = \frac{3V_h\eta}{k_BT} \qquad \text{Eqn 7.2}$$

The variation of Brownian relaxation time with nanoparticle size can also bee seen in Figure 7.1. The Brownian relaxation time depends also on the size of the nanoparticle but not as dramatically as the Néel relaxation time. The effective (or the total relaxation time) of the nanoparticles placed in the liquid is a combination of the Néel and Brownian relaxation time. The mechanism by which that the nanoparticle system relaxes is the mechanism with shortest relaxation time. By setting the Néel relaxation time equal to the Brownian relaxation time it is possible to determine a critical nanoparticle diameter that divides particles which relaxes with the Néel relaxation (internal relaxation of the particle magnetic moment) or with the Brownian relaxation (where the direction of the particle magnetic moment follows the rotation of the particle). For magnetic nanoparticles of maghemite at room temperature in water, the crossover between the two relaxation mechanism occurs at 15 nm (see Figure 7.1). Today, most of the magnetic nanoparticles in medicine and biomedicine use maghemite or magnetite nanoparticles equal to or below a diameter of about 10 nm [12]. The magnetic nanoparticles in these size ranges have short relaxation times, μs or less. In magnetic separation techniques in biomedical applications the size of the total magnetic particles can be 1 μm or even larger. In this case the particle is built up of several magnetic nanoparticles in the range of 10 nm in a polymer matrix. Using these small nanoparticles, with short relaxation times, agglomeration of particles after the particle system has been exposed to a magnetic field gradient (which is used in the magnetic separation process) is prevented. Magnetic nanoparticles with sizes of about 10 nm and below are also used as contrast agents in Magnetic Resonance Imaging (MRI) [12].

7.4 Biosensor methods using magnetic nanoparticles

Magnetic nanoparticles in biosensor applications have been used for several years. Different detection techniques are being used in these applications, very sensitive SQUID (Superconducting Quantum Interference Device) sensors [13], GMR (Giant Magnetic Resistance) sensors [14,15], Flux-gate magnetometers [16] and induction techniques [17]. Both the Néel and the Brownian relaxation are used in these biosensor applications in order to detect the presence of different bio substances in a liquid. The methods that uses SQUID sensors and Flux-gate magnetometers measures the magnetization decay of magnetic nanoparticles after they have bounded to a rigid surface (due to the presence of a specific substance in the liquid) and magnetized by a external field. In this case the Néel relaxation should be long enough which sets a lower limit of the size magnetic nanoparticles according to Figure 7.1. In the case of the GMR technique the magnetic nanoparticles is superparamagnetic with no remanence and

consequently the particle system must be magnetized during the measurement is performed. This is achieved by an external magnetic field with a field direction not oriented in the sensitive direction of the GMR sensors.

In the biosensor method using induction techniques to detect the Brownian relaxation [17], the Néel relaxation time must be larger than the Brownian relaxation time. Then, the orientation of the magnetic moment of the particle changes with the same rate as the rotation rate of the particle itself, e.g. the Brownian relaxation is detected by magnetic detection. This put a lower limit of the sizes of the nanoparticles. From Figure 7.1 the lowest size at room temperature for maghemite nanoparticles is about 15 nm. The magnetic nanoparticles in this biosensor method must then be larger than 15 nm. The method is based on measurements how the Brownian relaxation time changes when different substances in a liquid binds to the surface of the particles. The magnetic response, $\chi(f)$, at different excitation frequencies, f, of the applied field is measured and analyzed by a model including a distribution of Brownian relaxation times (mostly due to a spread in particle sizes) according to:

$$\chi(f) = \int \chi(f, \tau_B) f(\tau_B) d\tau_B \qquad \text{Eqn 7.3}$$

where $\chi(f, \tau_B)$ is the frequency dependent Debye response and $f(\tau_B)$ the distribution function (a log-normal distribution is used in the model) of the Brownian relaxation time. The Brownian relaxation time can be translated to a size of the particle (Eqn.7.2) and the size distribution of the particle system can be determined. When the excitation frequency approaches $1/(2\pi\tau_B)$ the imaginary part of the magnetic response is at its maximum. The result in figure 2 shows the imaginary part of the magnetic response versus excitation frequency when different amounts of PSA (Prostate Specific Antigen) are absorbed on the surface of the particles.

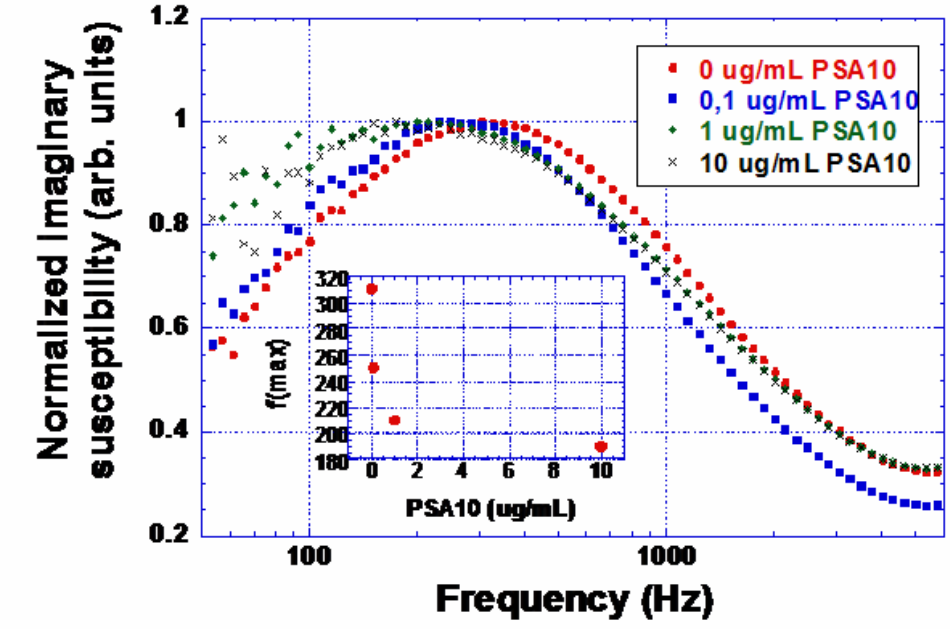

Figure 7.2. The plot shows the normalized imaginary part of the magnetic response versus the excitation frequency at different amounts of absorbed PSA (Prostate Specific

Antigen) to the surface of the particles. The inset figure shows how the frequency where the imaginary part of the magnetic response is at its maximum (f_{max}) varies with the PSA concentration.

From Figure 7.2 we can see that increasing the amount of PSA bounded to the particle surfaces gives a frequency shift of the magnetic response towards lower frequencies. This is due to that the hydrodynamic size of the particles increases and thereby the Brownian relaxation time increases, meaning a decrease in the corresponding Brownian relaxation frequency, $1/(2\pi\tau_B)$. From Figure 7.2 (inset) we can also see that that the shift in the Brownian relaxation frequency is saturated at higher PSA concentration. At this high PSA concentration in the liquid the surfaces of the particle system are saturated with PSA. The dynamic range of the concentration detection is determined by the size of the particles (different surface areas) and the number of particles in the liquid. With this biosensor method it is possible to detect different kinds of substances in a liquid [17,18].

Conclusions

We have seen in this chapter that there are large numbers of different applications where magnetic nanoparticles are key components. Depending on the application different kinds of magnetic nanoparticles are used with different magnetic relaxation times. As we have also seen, the magnetic properties of magnetic nanoparticles are closely related to the magnetic relaxation time. The magnetic relaxation can be tailored by changing the size of the nanoparticles or utilising different materials in the particles. Due to this and on the rapid development of nanotechnology, magnetic nanoparticles will be a great tool in different kind of industrial or medical applications as well as very good model systems in more scientific investigations.

[1]. L. Néel, Compt. Rend. 224 (1947) 1488.
[2]. X. Batlle, A. Labarta, Review article in J. Phys. D: Appl. Phys. 35 (2002) R15.
[3]. C. P. Bean, J. D. Livinston, J. Appl. Phys. 30 (1959) 120S.
[4]. R. W. Chantrell, J. Popplewell, S. W. Charles, IEEE Trans. Mag. MAG-14 (1978) 975.
[5]. K. O'Grady, A. Bradbury, S. W. Charles, S. Menear, J. Popplewell, R. W. Chantrell, J. Magn. Magn. Mat. 31-34 (1983) 958.
[6]. C. Johansson, M. Hanson, M. S. Pedersen, S. Mørup, J. Magn. Magn. Mat 173 (1997) 5.
[7]. L. Néel, C. R. Acad. Sci. 228 (1949) 664.
[8]. C. Johansson, M. Hanson, P. V. Hendriksen, S. Mørup, J. Magn. Magn. Mat 122 (1993) 125.
[9]. H. J. Richter, Review article in J. Phys. D: Appl. Phys. 32 (1999) R147.
[10]. A. Moser, K. Takano, D. T. Margulies, M. Albrecht, Y. Sonobe, Y. Ikeda, S. Sun, E. E. Fullerton, Review article in J. Phys. D: Appl. Phys. 35 (2002) R157.
[11]. J. Frenkel, The Kinetic Theory of Liquids, Dover, New York (1955).
[12]. Q. A. Pankhurst, J. Connolly, S. K. Jones, J. Dobson, Review article in J. Phys. D: Appl. Phys. 36 (2003) R167.
[13]. K. Enpuku, T. Minotani, IEICE Trans. Electron. E84-C1 (2001) 43.
[14]. M. Megans, M. Prins, J. Magn. Magn. Mat 293 (2005) 702.

[15]. M. Tondra, A. Popple, A. Jander, R. L. Millen, N. Pekas, M. D. Porter, J. Magn. Magn. Mat 293 (2005) 725.
[16]. F. Ludwig, E. Heim, S. Mäuselein, D. Eberbeck, M. Schilling, J. Magn. Magn. Mat. 293 (2005) 690.
[17]. A. Prieto Astalan, F. Ahrentorp, C. Johansson, K. Larsson, A. Krozer, Biosensors and Bioelectronics 19 (2004) 945.
[18]. K. Petersson, D. Ilver, C. Johansson, A. Krozer. Analytica Chimica Acta, in press.

8 Magnetic Shape Memory Alloys

Emmanouel Pagounis, Laboratory of Materials Science, Helsinki University of Technology, Finland

Magnetic Shape Memory (MSM) materials are a new class of smart, or active, material that change their shape when exposed to moderate magnetic fields (typically < 1 T). The materials return to their original shape when applying a spring force, or when reversing 90 º the direction of the magnetic field. The deformation can be as large as 10 %, generating, thus, motion and force. MSM materials are single crystalline metal alloys, which convert electrical power to mechanical power, and vice versa.

The first report on a large magnetically induced strain in a Dy single crystal is dated back in 1968 [1]. Liebermann et al. [2] reported a giant 3.4 % reversible strain in the magnetically hard direction in a single crystal Dy subjected to a magnetic field of 100 kOe at 4.2 K. Detailed investigation revealed twinning to be the primary deformation mode. It was suggested that the driving force for the observed deformation is the lowering in the magnetostatic and magnetocrystalline anisotropy energies on twinning. However, the magnetic field-induced deformation received significant attention after similar strains were measured in Heusler type non-stoichiometric Ni_2MnGa alloys [3-8]. The exact mechanism of large reversible strains by the application of an external magnetic field is not thoroughly understood yet. It is proposed that this can be due to structural transformations in martensite phases [9-12], twin variant conversion and reorientation [13-16], or by the magnetic force generated due to non-uniform magnetic field, which can deform the martensite and induces twin variant rearrangement [17-19]. The magnetic shape memory effect essentially differs from magnetostriction, even though some effect of magnetostriction may contribute in the early stages of the deformation process. Finally, the effect of internal stresses, caused by structural transformation and alloy processing, in the magnetic field-induced deformation received little attention.

The martensite crystal, after transformation from cubic austenite, consists of the mixture of tetragonal martensite variants, having different c-axis orientation, separated by twin boundaries. In MSM materials the twin boundaries are highly mobile. A simplified representation of the MSM deformation process is given in Figure 8.1, where it is assumed that only two twin variants exist in the material. These variants have different magnetic and crystallographic orientations. When the MSM material is exposed to an external magnetic field the twins in a favourable orientation relative to the field direction “grow” at the expense of other twins. Magnetic field H increases the amount of twin variants of “preferable” orientation, i.e. the twin boundaries move in the material. Steuwer et al. [18] demonstrated that large shape changes in the order of 10^{-2} cannot be achieved by a direct effect of the external magnetic field on twin variant rearrangement. On the other hand, the magnetic force, which is proportional to the magnetic field gradient, can be of a magnitude enough to cause twin variant rearrangement.

The mechanical stress needed to move the twin boundary is called twinning stress, σ_{tw}. This term is important when studying the magneto-mechanical properties of MSM materials. As the Ni-Mn-Ga MSM material has at room temperature a martensitic tetragonal crystal structure (lattice parameters $c/a < 1$, typically 0.94), the material

exhibits a net shape change as a result of the change of the relative amounts of twin variants. That shape change equals the magnitude of the tetragonal distortion:

$\varepsilon_H = (a/c - 1)$ Eqn 8.1

Magnetocrystalline anisotropy has a key role in achieving large magnetic field-induced strains. The energy of a ferromagnetic crystal depends on the direction of the magnetization relative to the crystallographic axes. Tetragonal crystals show a uniaxial anisotropy. In this case, the energy density of the anisotropy is described as $E_a=K_{u1}\sin^2\theta+K_{u2}\sin^4\theta$, where θ is the angle between the *c*-axis (axis of tetragonality) and magnetization direction, K_{u1} and K_{u2} are anisotropy coefficients. A large positive K_{u1} describes crystals with an "easy" axis of magnetization along the *c*-axis. In the case of non-stoichiometric Ni_2MnGa alloys, the value of K_{u1} was determined in the range from 1.3×10^5 to 2.48×10^5 J/m^3 [20-22] for different compositions. In the absence of an applied magnetic field the magnetization vector lies along the easy magnetization axis. In the presence of a magnetic field the magnetization rotates towards the direction of the field and magnetic energy of the variant increases. The maximum energy, which can be stored in the variants is given by the magnetic anisotropy energy, E_a, i.e. the energy originated from the rotation of magnetization vector from the easy magnetization axis to the direction of the field. We can explicitly equal magnetic anisotropy energy with elastic energy due to a twinning stress σ_{tw}. When the magnetic field increases, the difference of magnetic energy given by the magnetic anisotropy energy E_a exceeds the twinning stress energy ($\sigma_{tw}\cdot\varepsilon_H$) that is needed for twin boundary motion, and the twin boundaries are moving. Accordingly, important parameters for an existence of the MSM effect are high saturation magnetization, high magnetic anisotropy and low twinning stress.

8.1 Production and chemical composition

Magnetic Shape Memory materials are currently produced by conventional single crystal growth techniques, such as Bridgman [23,24] or Czochralski [25,26]. The details of the production process are rarely disclosed. After producing the single crystal bars the materials are homogenized at about 1000 °C for 24 h and ordered at 800 °C for another 20 h. Information about the effect of heat treatment on the crystal structure and the transformation temperatures is given in the literature [27-30]. The material is then oriented using X-ray techniques to produce the desired crystallographic structure for the MSM effect. Following the crystal orientation the material is cut and thermo-mechanically treated. The key to obtaining high strains is to cut the samples so that the twin boundaries are aligned at 45° to the sample axis (when magnetic field is applied transverse to the bar).

Studies of MSM alloys focus on ways to produce materials in which short response times are combined with large reversible strains. Several Heusler alloys and intermetallic compounds like Fe-Pd, Fe-Pt, Co-Ni-Al, Fe-Ni-Co-Ti have been investigated in this connection. The most promising results to date have been achieved with the ferromagnetic Heusler alloy Ni2MnGa, and more exactly the family of $Ni_{2+x+y}Mn_{1-x}Ga_{1-y}$. In this alloy magnetically controlled strains of up to 9.5 % have been measured [31].

The MSM effect in these alloys is observed when the material is in its martensite state, therefore its crystal structure is of prime importance. The Ni-Mn-Ga alloys show a

variety of martensitic structures. The crystal structure of the martensite depends strongly on the chemical compositions [32-34]. When the possibility of the MSM effect is studied, the main interest is focused on the ferromagnetic twinned martensitic structures. The crystal structure of martensite affects the magnetic anisotropy [35,36] as well as the magneto-mechanical properties [37-39], and the chemical behaviour [40]. The martensitic structures, transformation temperatures, and the Curie point have been systematically studied as functions of the average number of valence electrons per atom (e/α) [41-44]. It has been suggested (45) that the martensitic transformation temperature increases linearly with the e/α concentration. High transformation temperatures and Curie point are essential requirements in increasing the operating temperature range of MSM materials. Shifts in the $Ni_{2+x+y}Mn_{1-x}Ga_{1-y}$ composition can significantly affect the maximum operating temperature of the MSM material [45], i.e. the maximum austenite start (A_s) temperature. For the time being, the MSM effect has been observed at temperatures of up to 65 °C, however for several applications higher operating temperatures are required.

The most important martensitic structures found in the Ni-Mn-Ga system are the five layered tetragonal martensite (5M), the seven layered near-orthorhombic martensite (7M), and the non-modulated tetragonal martensite (T). The 5M and 7M structures have lattice parameters c/α <1, while the T structure has c/α >1. Among them the 5M martensite has mostly been studied to date, and gives a theoretical maximum field-induced strain of 6 % at room temperature. The 7M structure provides a maximum strain of 10.7 %, while the T structure has so far not demonstrated the MSM effect. The T structure on the other hand has shown a huge 20 % mechanically induced strain [46], but the large twinning stress (> 6 MPa) hinders the magnetic field-induced deformation. The exact crystal structure that appears during cooling depends on the composition of the alloy, the thermo-mechanical treatment, and the thermal stability of the different martensitic phases [47-49]. The T structure is the most stable one and the alloys transforming straight to the T martensite from the parent phase have typically transformation temperatures close or above the Curie point [50-52]. The 5M structure transforms directly from the parent phase at lower temperatures close to the ambient one, while the 7M martensite appears directly from the parent phase in a very narrow temperature range below the Curie point, and is highly compositional dependent [31,53-56]. Even though the 7M structure provides the largest field-induced strain, the magnetic field-induced stress is low, and it needs a higher magnetic field for saturation. These, together with its very narrow composition and temperature range, limit its practical applications to date. In the following text most measurements and experimental results are carried out using MSM materials with 5M martensitic structures.

Among other candidate systems for the MSM effect most attention received the Fe-Pd [57-60], Fe-Pt [61-63], Co-Ni-Al [64-69], Ni_2MnAl [70-72], and Fe-Ni-Co-Ti [73,74]. In these alloys measured field induced strains were demonstrated in the Fe_3Pd alloy [58] and in Co-Ni alloys [75,76]. An advantage of Fe_3Pd alloy is its excellent workability compared to Ni_2MnGa. In addition, attempts to replace the Mn in Ni_2MnGa with Fe or Co have been reported [77-79], as well as the addition of rare earth elements [80,81].

8.2 Magnetic and mechanical measurements

Magnetic and mechanical measurements in MSM materials can be carried out with the set-up described in [82]. Since MSM materials are ferromagnetic and highly anisotropic their magnetization is high, it has a specific saturation value which depends on the direction of the applied field. Figure 8.2 shows the magnetization curve of a Ni-Mn-Ga MSM material. In the first magnetization cycle (Figure.8.2a) the curve exhibits some interesting features. Initially, the increase of magnetization is slow and nearly linear, suggesting that the magnetization process is controlled by magnetization rotation. At approximately 280 kA/m the magnetization suddenly rises and then levels off, indicating the martensitic c-axis, which is the 'easy' magnetization axis of the tetragonal martensitic phase, aligns itself with the external magnetic field. That peculiar shape of the magnetization curve is an indication of the MSM effect. On decreasing the field the magnetization remains at the saturation value towards the lower field. This results in large transient hysteresis at the first quadrant. This hysteresis occurs in the first cycle, while during the second cycle (Figure .8.2b) the magnetization reaches its saturation value in a weak magnetic field. Further magnetization loops show fast saturation without appreciable hysteresis, indicating that the 'easy' axis of magnetization (i.e. the *c*-martensite axis) is now oriented along the field direction (Figure. 8.2b). A slight tilt of the magnetization curve is caused by a demagnetization field. Observed transient behaviour can be, however, easily restored. The saturation value of intrinsic induction B_{is} in Ni-Mn-Ga alloys was measured between 0.6 T and 0.68 T, while the saturation field strength H_s varied between 520 kA/m and 720 kA/m [15, 20, 82]. The changes in the magnetization curve as a function of the strain in a Ni-Mn-Ga MSM material is described in [82].

From the magnetization curve of the MSM material (Figure.8.2a) it is possible to calculate the material's energy product. The magnetic cycle energy density w_{eMSMlim} is determined by the area between "easy" and "hard" magnetic axis (anisotropy energy) [13]. Numeric integration shows that:

$$w_{\mathrm{eMSM\,lim}} = \oint_{0-1.5\,\mathrm{T}} H_{\mathrm{MSM}}\, dB_{\mathrm{MSM}} = 190\ \mathrm{kJ/m^3} \qquad \text{Eqn 8.2}$$

The value of 190 kJ/m^3 for the maximum energy density of the MSM material is an order of magnitude higher than that reported for the highest energy density actuator material so far, Terfenol-D. If we further assume an operating frequency of f = 600 Hz, then the limit average electric power density of MSM-material $p_{\mathrm{eav\,lim}}$ has a value of:

$$p_{\mathrm{eavlim}} = f \cdot w_{\mathrm{eMSMlim}} = 600 \cdot 190 \cdot 10^3 = 114 \cdot 10^6\ \mathrm{W/m^3} = 114\ \mathrm{MW/m^3} \qquad \text{Eqn 8.3}$$

In Figure 8.3 the field-induced MSM strain in a Ni-Mn-Ga alloy under a variety of mechanical loads is shown as a function of the magnetic field. The characteristics of this type of curves depend on the chemical composition of the alloy, its thermal and mechanical history, and the temperature. The measurement curves demonstrate the large work output (force x stroke) capabilities of MSM materials. In the measurements the direction of the magnetic field was perpendicular to the long sample axis and fixed constant compressive stress was applied along the sample axis, i.e. field and loading directions are normal to each other. The expansion is then measured in the stress

direction. The contraction was observed in the field direction so that the volume of the sample remained constant.

It can be seen in Figure 8.3 that the stroke of the MSM material depends on the external load and field. With increasing compressive stress the maximum of field-induced strain decreases and the field needed for straining the material increases. The maximum blocking force for MSM materials was measured between 3 and 9 MPa [4,7,57]. The hysteresis observed in the strain curves indicates that the MSM material possesses also excellent damping capabilities. Using the hysteretic properties in actuator design and biasing permanent magnets, it is possible to reduce the applied current, and, thus, power consumption, while keeping the material in a certain position.

Since MSM-phenomena can be obtained only if the force generated in the material by the magnetic field is larger than the force needed for reorientation of the single martensite variant to another, i.e. the twinning stress σ_{tw}, this value becomes very important in characterizing the MSM material. A low twinning stress corresponds to higher work output (force × stroke) of the MSM material, and also lower activating field. The later is very important in reducing the size and power consumption of an MSM actuating device. Twinning stress values of < 1 MPa are sufficient for actuator operation, however, MSM samples with a twinning stress of < 0.4 MPa will provide significant advantages compared to existing technologies in practical applications. Low twinning stress materials exhibit also smaller hysteresis. The importance of twinning stress can be seen, for example, in the efficiency η_{MSM} of the MSM material, i.e. the ratio of output mechanical energy to input electrical energy. In MSM materials having twinning stress of around 1 MPa (measured in Figure 8.3) the efficiency of the MSM material is about 50 %, while if twinning stress reduces to 0.4 MPa the efficiency increases to 80 %, with the theoretical limit closing to 95 %. Efforts are currently in progress to reduce the twinning stress of the MSM materials. Figure 8.4 presents theoretical calculations on the effect of the material's twinning stress in the activation field and the efficiency (η_{MSM}).

The temperature dependence of the MSM effect is also of importance, however this effect has received little attention to date. Similar to other smart materials, such as piezo-ceramics and magnetostrictives, the properties and performance of Ni-Mn-Ga MSM materials are affected by the operating temperature. It was found that the lattice parameters, which affect the free strain of the material, are highly temperature dependant. For example, in 5M martensites cooling causes a slight increase of the α-axis and a large decrease in c-axis [83,84]. In addition, the twinning stress of Ni-Mn-Ga increases with the decreasing temperature [85]. The lowest twinning stress values for a given alloy composition are measured at temperatures close to the transformation ones. The saturation magnetization and the anisotropy energy of the Ni-Mn-Ga martensite increase when the temperature decreases. These effects have a direct impact on the performance of the MSM materials at different temperatures, as demonstrated in Figure 8.5. For a given alloy composition there is a specific lower temperature where the twinning stress σ_{tw} is high enough and exceeds the magnetic field-induced stress σ_{mag}. Below this temperature no MSM effect is observed [84,85]. In 5M martensites this temperature is between -160 ºC and -20 ºC, depending on the chemical composition, processing, and thermo-mechanical treatment. This critical temperature is important in actuator applications, while in the sensor applications there is no low temperature limit.

The basic equations for MSM materials are summarized in the following [20, 85-88]:

$$\sigma = \pm\sigma_{\mathrm{MSM}} + \sigma_{\mathrm{tw}}(\varepsilon); \qquad \text{Eqn 8.4}$$

$$\sigma_{\mathrm{MSM}} = \sigma_{\mathrm{mag}}\left[1-\left(1-\frac{H}{H_{\mathrm{s}}}\right)^{2}\right]; H \le H_{\mathrm{s}}; \qquad \text{Eqn 8.5}$$

$$\sigma_{\mathrm{MSM}} = \sigma_{\mathrm{mag}}; \qquad H > H_{\mathrm{s}}; \qquad \text{Eqn 8.6}$$

$$\sigma_{\mathrm{mag}} = \frac{K_{\mathrm{u}}}{\varepsilon_0}; \qquad \text{Eqn 8.7}$$

$$K_{\mathrm{u}} = \frac{B_{\mathrm{is}} H_{\mathrm{s}}}{2}; \qquad \text{Eqn 8.8}$$

$$H_{\mathrm{s}} = \frac{B_{\mathrm{is}}}{(\mu_{\mathrm{hd}}-1)\mu_0}; \qquad \text{Eqn 8.9}$$

$$\eta_{MSM} = \frac{\sigma_{mag} - 2\sigma_{tw}}{\sigma_{mag}} \qquad \text{Eqn 8.10}$$

$$\varepsilon_H = \left|\frac{a-c}{c}\right|; \qquad \text{Eqn 8.11}$$

where:
σ – mechanical stress of the MSM-material;
ε – relative strain of the MSM-material;
$\sigma_{\mathbf{MSM}}$ – magnetic field-induced stress of the MSM-material;
$\sigma_{\mathbf{tw}}(\varepsilon)$- twinning stress of the MSM-material as function of the relative strain;
$\sigma_{\mathbf{tw}}$ - twinning stress of MSM material;
$\sigma_{\mathbf{mag}}$ – maximum anisotropic magnetic field-induced stress of the MSM-material;
H and B – magnetic field strength and flux density within the MSM-material;
H_{s} – saturation magnetic field strength (i.e. field strength at which easy direction and hard direction magnetization curves cross each other);
K_{u} – anisotropic energy density of the MSM-material (equal to w_{eMSMlim});
$\varepsilon_0 = \varepsilon_{\mathrm{H}}$ – free strain of the MSM-material;
μ_{hd} – relative permeability of the MSM-material along the magnetic hard axis;
μ_0 – absolute permeability of the vacuum;
$B_{\mathrm{i}} = B - \mu_0 H$ – intrinsic induction within MSM-material;
B_{is} – saturated value of the intrinsic induction;
η_{MSM} – coupling factor (efficiency) of MSM material
a and c –geometric dimensions of the crystallographic axes.

Mechanical and magnetic properties of MSM materials are summarized in Table 8.1. In Table 8.2 the magnetic field-induced strains measured in various Ni-Mn-Ga samples are summarized.

8.3 Magnetic Shape Memory actuators

Magnetic shape memory materials have been developed primarily for actuator applications. The operation principle of an MSM actuator is schematically presented in Figure 8.6. The actuator consists of two coils aligned symmetrically to the MSM element, a prestress mechanism and the appropriate ferromagnetic core (not shown in the drawing). Before applying the magnetic field, the MSM element is aligned with its short martensite crystallographic c-axis along the stick axis (i.e. the direction of pre-stress loading). When a magnetic field is applied the MSM element elongates in the direction perpendicular to the field. When the field is removed the pre-stress mechanism, usually a mechanical spring, contracts the MSM material to its original length. The operation is then continuously repeated. The electric and magnetic circuit of an MSM actuator is modelled in [88].

The basic feature of an MSM actuator is that the magnetic field is applied *perpendicular* to the MSM material. In the topology presented in Figure 8.6 the MSM element is located in the same magnetic circuit with ferromagnetic core and the magnetic field is generated with the coils. The air-gap should be kept as small as possible to eliminate power losses. In actuator design, it is also possible generate the necessary magnetic field using only one coil. The magnetic circuit to drive the MSM stick shall be designed to give field strength on the surface of the sample 300-500 kA/m. This corresponds to a flux density of about 0.6 T on the surface, and of about 1.3 T inside the MSM material. The difference between the external and internal field is due to the demagnetization effect observed in ferromagnetic materials [107]. Lower magnetic fields can be applied when the twinning stress of the MSM material is reduced (see Figure 8.3). This has a direct effect in reducing the size, efficiency, and power consumption of the actuator.

Biasing permanent magnets (PM) are often used to increase the field strength and reduce power consumption of the coils. In this case the mechanical frequency of the device is the same as the electrical frequency at sinusoidal excitation. In practice the permanent magnet generated DC field is half of the maximum magnetic field needed to drive the MSM material. Actuators with PM have usually a reduced size.

The pre-stress on the sample is usually between 0.5 and 1 MPa, a spring or disk spring can be used. Correct pre-stressing is crucial in optimising actuator operation, as it affects the actuator's force and stroke capability (see also Figure 8.3). Both the spring force and the load the actuator is working against should be taken into account in the actuator design. An optimal load to reach maximum magnetic-field-induced strain is about 1 - 1.5 MPa (Figure 8.3), however values of 2 MPa or higher can be reached with proper alloy development and low twinning stress materials [86,106].

The MSM element, the moving mass and the pre-stress spring are the basic components of the mechanical circuit of the MSM actuator. Since the actuator can work at a high frequency, the resonance frequency of the mechanical system is often reached. In case the actuator is used only at a specific frequency and mass the mechanical resonance frequency can also be used to increase the motion of the system.

The properties of the MSM actuator are strongly affected by the core type of the magnetic circuit. In particular, eddy currents have to be minimized in high frequency applications. Figure 8.7 presents a curve, computed from field theory, which shows the field penetration inside the MSM material. It can be seen that, theoretically, with 2.5 mm thickness of the MSM stick the maximum operating frequency can be well above

1000 Hz. In practice current device work is often at lower frequencies due to the existence of eddy currents within the material. Improved magnetic circuit design and a better understanding of the properties of the material should enable higher operating frequencies. Laminated MSM materials can be also used when higher frequencies are required.

The electric circuit connected to the coil senses the construction in Figure 8.6 as an inductor. The magnetic field strength inside the MSM element is roughly dependent only on the applied electric current. The voltage supplied to the coils has a delay before it affects the magnetic field inside the MSM element. Therefore, MSM actuators are best driven with current sources. If the actuator is driven with the voltage source, an additional delay in the operation may exist; as a result best performance is achieved when using a power supply with current controller.

When exposed to a magnetic field the MSM element generates a stress. Stress is a function of the magnetic field strength, which in turn is a function of the input current. Hence, when the current it controlled it is possible to control the MSM actuator's acceleration. This relation affects the position control of the actuator. For position control applications it is beneficial to have an intelligent control algorithm, which takes the relation between current and motion into account.

In Figure 8.8 a response time of 0.7 ms is demonstrated for an MSM actuator, however the shortest rise times to reach strokes of 5 % of the actuating element measured 0.2 ms (39,89). The operating speed of the MSM actuators is limited only by the eddy-currents in the core and the inertia of the moving parts of the actuator. The actuator's acceleration depends also on the moving mass. The largest acceleration is achieved when the moving mass is smallest, theoretically even 10^5 m/s^2 can be reached. In Figure 8 acceleration of 5×10^3 m/s^2 was measured in an MSM actuator. The acceleration of the MSM element affects the maximum operating frequency of the MSM actuator. To date, operating frequencies from DC up to the kHz range have been achieved with MSM actuators [39,89,90,108]. Higher frequencies can be reached with more efficient magnetic circuit design and power electronics. The limiting factor is often the voltage supply's ability to change current in the actuator. Apart from the acceleration, the speed of an MSM actuator is also an important design parameter. In an MSM material a maximum speed of 1.5 m/s was measured (89) with the theoretical limit being the speed of sound (333 m/s).

It is useful to include an external position measurement for position control applications since the motion of the MSM actuator depends on the force the MSM element has to work against. A diagram of a control system for a MSM actuator can be seen in [105]. The control system is designed for a linear motor's MSM actuator, but it is generally usable for any MSM actuator used for position control. Ultra-high (nm) positioning resolution can be achieved, depending on the resolution of the position sensor used.

Hysteresis exists between the strain and the actuator input current, as well as between the strain and stress. Hysteresis is caused by the internal properties of the MSM material, such as twinning. The hysteresis of the MSM material (Figure.8.3) has to be taken into account in the design of a specific MSM actuator application. The hysteresis dampens unwanted mechanical vibrations and higher harmonics of current and in that way eases the control of the application. In addition, it reduces vibrations and overshooting of the MSM actuator in rapid shape changes of the element. An inherent

feature of the MSM actuators is that the stroke can remain in a certain position, even under external load, without using current. This can be achieved using the hysteresis of the MSM material and proper actuator design with biasing permanent magnets.

The magnetic field-induced force of an MSM actuator depends on the cross-sectional area of the MSM element, with a typical blocking stress of 3 MPa. The stroke in turn depends on the length of the MSM element, typically in actuator operation the MSM material produces up to 5 % elongation. These affect the dimensions and performance of the actuator [87]. In actuator operation, MSM materials have demonstrated more than 5×10^8 cycles without deterioration of stroke [109]. These results need yet to be confirmed in practical actuator applications. Fatigue properties and crack propagation in MSM materials have recently being studied in more detail [91,92]. Since the MSM shape change is relatively large, the motion can often be used directly without any mechanical amplification. Hence, the structure of the actuator can be simple and reliable, as backlash and wear problems are eliminated with this kind of construction.

Figure 8.9 summarizes the performance of various actuator technologies [93]. As can be seen the MSM actuators bridge the gap between "smart" and conventional actuator technologies. Compared to conventional actuator technologies (electromagnetic, hydraulics, pneumatics) MSM actuators offer advantages in terms of fast response, reduced size, high operation frequencies, enhanced controllability, reliability and efficiency.

8.4 MSM sensors, thin films and composites

Like most active materials, MSM materials possess also the inverse effect, i.e. mechanical straining of the material causes changes in the surrounding magnetic field. Generally, magneto-elastic materials have been used as sensing elements in force, torque or displacement sensors [110]. The sensor application of MSM materials has not been studied as much as the actuator one, however, studies revealed that MSM materials can be used in applications such as force, position or acceleration sensors [82,86,88]. In these studies it was demonstrated that the MSM material can also be used in direct power generation, as large voltage (100V) signals were induced by fast compressing the material. The voltage signal is directly proportional to the velocity of the compression, as shown in Figure 8.10. A great advantage of the sensor approach is that only low magnetic fields are needed, which simplifies the design process.

As the magnetization depends on the strain state of the MSM material, the most obvious application is in a position sensor. This can be implemented by measuring the magnetization [82] or properties related to it, like the inductance. On the other hand, the material's shape affects the magnetic flux going through it and, due to Faraday's law, the change in flux can be monitored through the induced voltages. Since the induced voltages are proportional to the time derivative of the flux change [88] this phenomenon can be used in a speed sensor.

An interesting area for MSM materials is thin films due the potential for applications in micro-electro-mechanical systems (MEMS) [112-119]. The great challenge here is to grow uniform, defect-free, single crystalline films. Various methods have been used, like ion-beam sputtering [112], epitaxial growth on GaAs [113], pulsed laser deposition [114], r.f.-sputtering [115] and laser-beam ablation [118].

Finally, an area where MSM materials are also finding potential applications is that of ribbons and composites [121-125]. In composite materials MSM alloy in plate, fibre or powder form is combined with the polymer matrix. Accordingly, the selection of a suitable polymer matrix, which will minimize potential reactions and accommodate the strain of the MSM alloy, is of prime importance. MSM composites offer the advantage that less bulk material is needed and high frequencies can be achieved, while the polymer matrix can be used as the return spring force. In these applications the damping capabilities of composite MSM materials have also received attention.

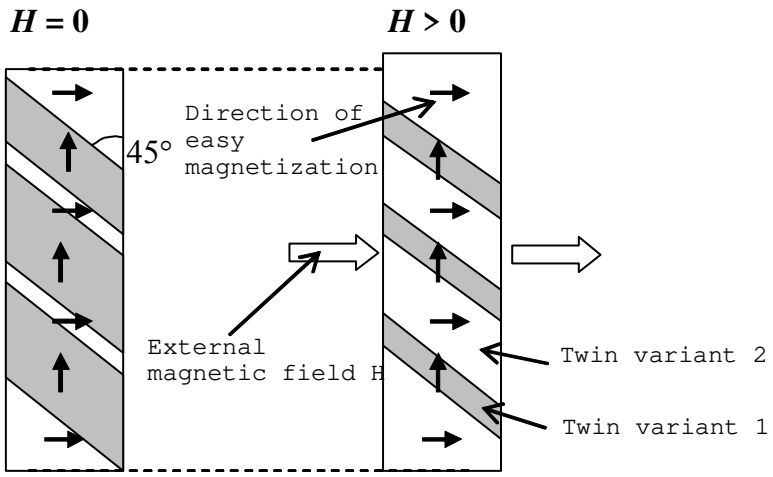

Figure 8.1. Simplified representation of the magnetic-field-induced deformation.

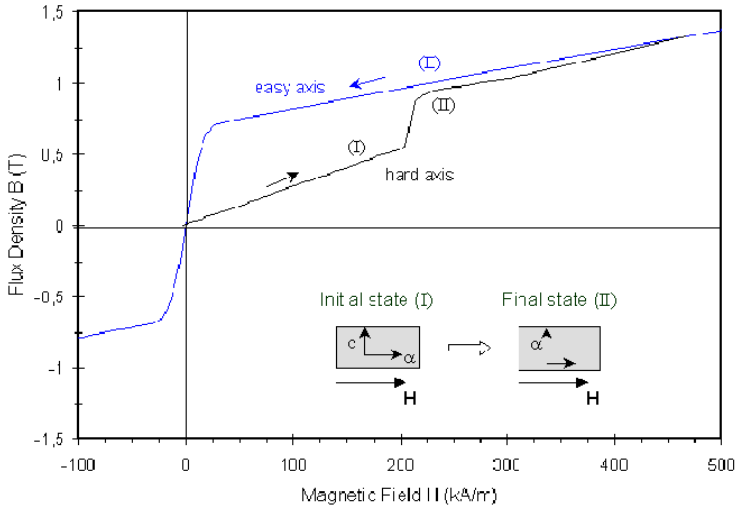

(a)

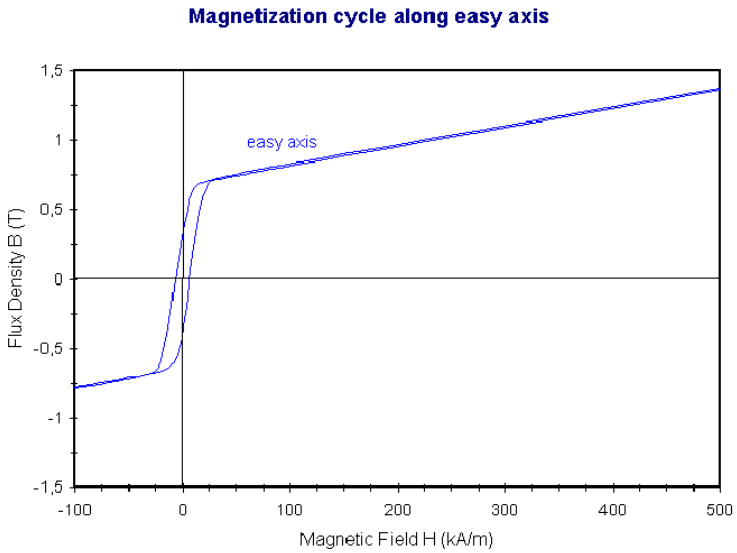

(b)

Figure 8.2: Typical magnetization B-H curve for a Ni-Mn-Ga MSM material, (a) during the first magnetizing cycle, and (b) during the next cycles.

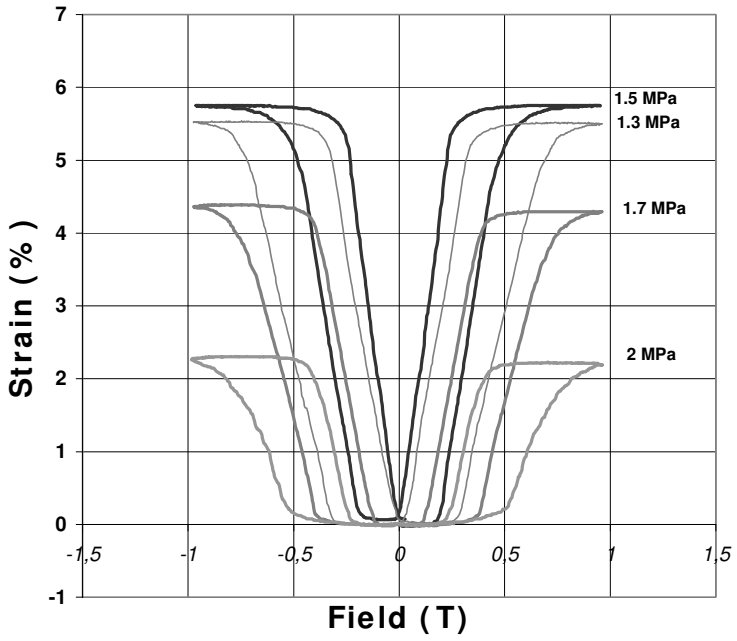

Figure 8.3. Strain output and applied magnetic field at different pre-stress loads in a Ni-Mn-Ga MSM material.

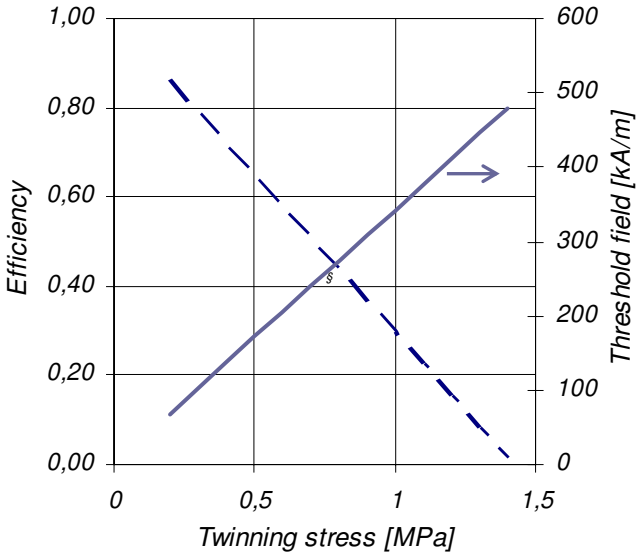

Figure 8.4. Efficiency and threshold activation field as a function of the twinning stress in a Ni-Mn-Ga MSM material.

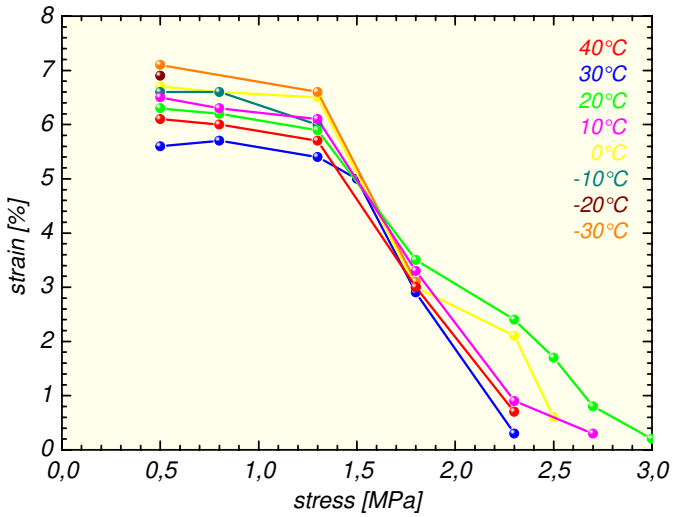

Figure 8.5. Strain vs. stress as a function of the temperature in a Ni-Mn-Ga MSM material (Robert Bosch© with permission)

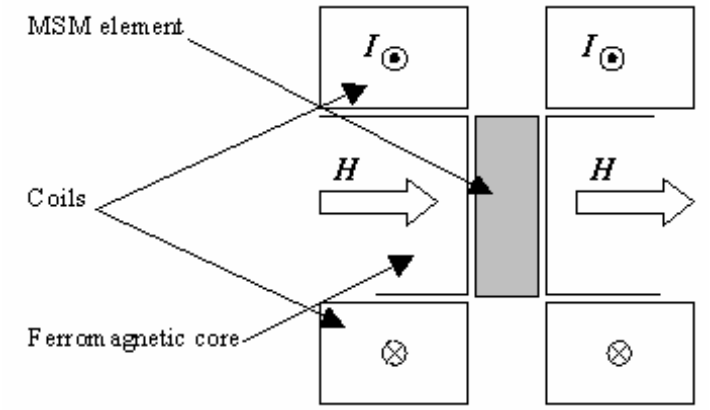

Figure 8.6. Basic structure of an MSM actuator.

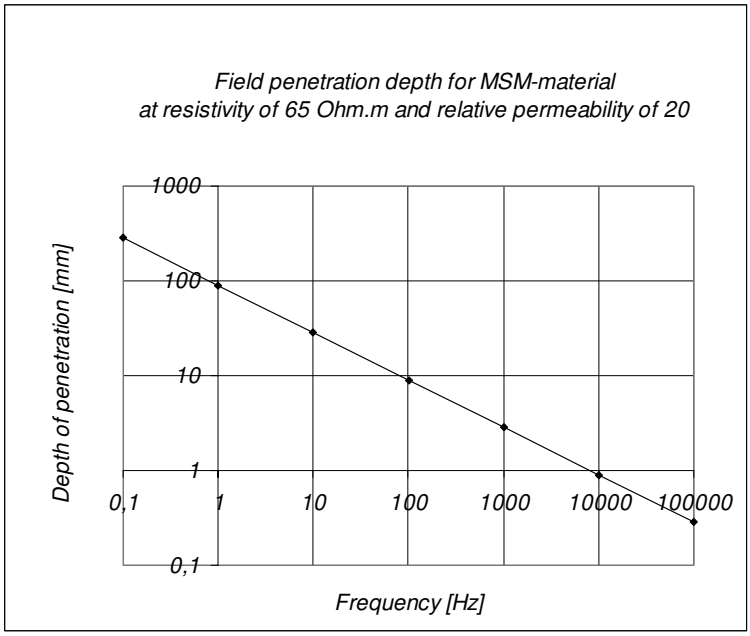

Figure 8.7. Computed field penetration depth for the MSM material as a function of the frequency.

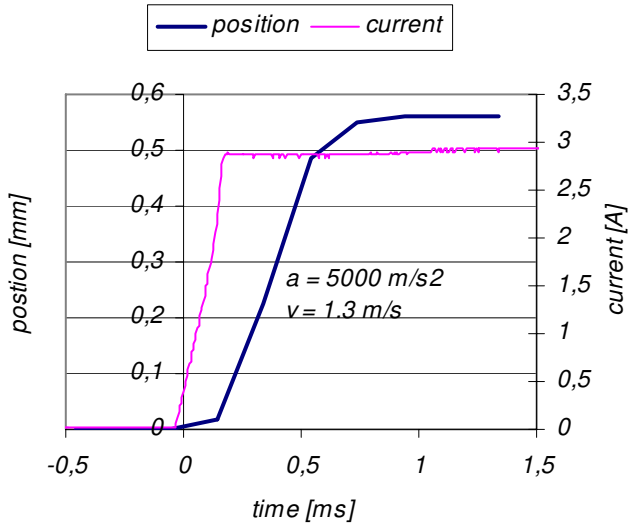

Figure 8.8. Applied current and stroke measured in an MSM actuator with laminated iron core.

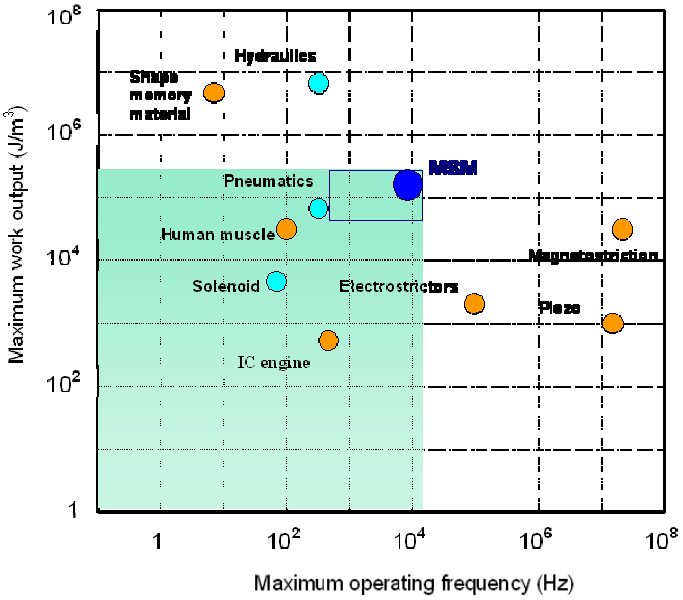

Figure 8.9. Positioning of various actuator technologies. The magnetic shape memory bridges the gap between ‘smart’ and conventional actuator technologies.

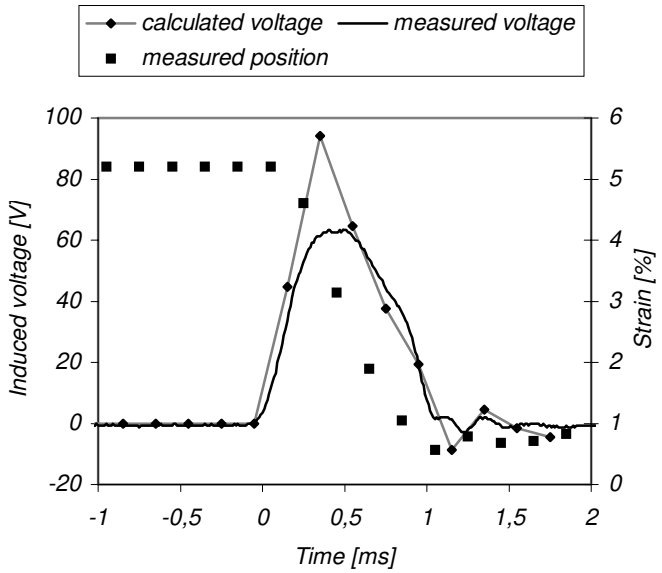

Figure 8.10. Measured and calculated voltage induced by fast compressing a Ni-Mn-Ga MSM material.

1. J.J. Rhyne, S. Foner, E.J. McNiff, R. Doclo, *J. Appl. Phys.*, **39**, 892 (1968).
2. H.H. Liebermann and C.D. Graham Jr., *Acta Metall.*, **25**, 715 (1977).
3. K. Ullakko, J.K. Huang, C. Kantner, R.C. O'Handley and V.V. Kokorin, *Appl. Phys. Lett*., **69**(13), 1966 (1996).
4. R. Tickle, R.D. James, T. Shield, M. Wuttig and V.V. Kokorin, *IEEE Trans. Magn*., **35**, 4301 (1999).
5. R. Tickle and R.D. James, *J. Magn. Magn. Mater.*, **195**, 627 (1999).
6. S.J. Murray, M. Marioni, S.M. Allen and R.C. O'Handley, *Appl. Phys. Lett*., **77**, 886 (2000).
7. O.Heczko, A. Sozinov and K. Ullakko, *IEEE Trans. Magn*., **36**, 3266 (2001).
8. K. Ullakko, E. Pagounis, I. Suorsa, J. Tellinen, I. Aaltio, O. Söderberg, O. Heczko, A. Sozinov, A.A. Likhachev and V.K. Lindroos, *J. Phys. IV France*, **112**, 1217 (2003).
9. T. Kakeshita, K. Shimizu, S. Funada and M. Date, *Trans. of Japan Insitute of Metals*, **25**, 837 (1984).
10. T. Takagi, V. Khovailo, T. Nagatomo, H. Miki, M. Matsumoto, T. Abe, Z. Wang, E. Estrin, A. Vasil'ev, and A. Bozhko, *Trans. Mater. Res. Soc. Jpn*, **26**, 197 (2001).
11. A.A. Cherechukin, I.E. Dikshtein, D.I. Ermakov, A.V. Glebov, V.V. Koledov, D.A. Kosolapov, V.G. Shavrov, A.A. Tulaikova, E.P. Krasnoperov, T. Takagi, *Phys. Lett.* A, **291**, 175 (2001).
12. Chandrashekhar H. Joshi, US patent 6,886,331.
13. R.C. O'Handley, *J. Appl.Phys*., **83**, 3263 (1998).
14. Kari Ullakko, US patent 6,157,101.
15. A.A. Likhachev and K. Ullakko, *Phys. Lett*., **A275**, 142 (2000).
16. A.A. Likhachev, A. Sozinov, K.Ullako, *Mater. Sci. Eng.* A, **378**, 513 (2004).
17. H. Kato and K. Sasaki, *Scripta Mater.*, **48**, 31 (2003).
18. A. Steuwer, T. Mori, H. Kato, T. Wada, *J. Appl. Phys*., **94**, 2761 (2003).

19. Masahiro Ohta, Toru Sukigara, US patent 6,803,846.
20. A.A. Likhachev, A. Sozinov and K. Ullakko, *Proc. SPIE 4333*, 197 (2001).
21. R.D. James, R. Tickle and M. Wuttig, *Mater. Sci. Eng*., **A273-275**, 320 (1999).
22. B.D. Shanina, A. Konchits, S. Kolesnik, V. Gavriljuk, I. Glavatskij, O. Söderberg, V.K. Lindroos, and J. Foct, *J. Magn. Magn. Mater.*, **237**, 309 (2001).
23. D. Schlagel, Y. Wu, W. Zang, and T. Lograsso, *J. Alloys Compounds*, **312**, 77 (2000).
24. O. Söderberg, M. Friman, A. Sozinov, N. Lanska, Y. Ge, and V.K. Lindroos, *Z. Metallk.*, **95**, 724 (2004).
25. G. Liu, J. Chen, Y. Cui, Z. Liu, M. Zhang, G. Wu, E. Bruck, F.R. deBoer, F. Meng, Y. Li, and J. Qu, *Solid State Communications*, **130**, 687 (2004).
26. C. Yu, W. Wang, J. Chen, G. Wu, F. Yang, N. Tang, S. Qi, W. Zhan, Z. Wang, Y. Zheng, and L. Zhao, *J. Appl. Phys.*, **87**, 6292 (2000).
27. J. Soltys, *Acta Phys. Pol*. A, **47**, 521 (1975).
28. P.J. Webster, K.R.A. Ziebeck, S.L. Town, M.S. Peak, *Phil. Mag.* B, **49**, 295 (1984).
29. V. Khovailo, T. Takagi, A. Vasil'ev, H. Miki, M. Matsumoto, R. Kainuma, *Phys. Status Solidi A*, **183**, R1 (2001).
30. K. Tsuchiya, D. Ohtoyo, M. Umemoto, H. Ohtsuka, *Trans. Mater. Res. Soc. Jpn*, **25**, 521 (2000).
31. A. Sozinov, A.A. Likhachev, N. Lanska, K. Ullakko, *Appl. Phys. Lett.*, **80**, 1746 (2002).
32. V.A. Chernenko, V.V. Kokorin, I.N. Vitenko, *Scripta Metall. et Mater*., **33**, 1239 (1995).
33. Overholsen, M. Wuttig, D.A. Neumann, *Scripta Mater.*, **40**, 1095 (1999).
34. J. Pons, V.A. Chernenko, R. Santamarta, E. Cesari, *Acta Mater*., **48**, 3027 (2000).
35. F. Albertini, L. Pareti, A. Paoluzi, L. Morelon, P.A. Algarabel, M.R. Ibarra, L. Righi, *Appl. Phys. Lett.*, **81**, 4032 (2002).
36. A. Sozinov, A.A. Likhachev, K. Ullakko, *IEEE Trans. Magn.*, **38**, 2814 (2002).
37. R.C. O'Handley, S.J. Murray, M. Marioni, H. Nembach, S.M. Allen, J. Appl. Phys., 87, 4712 (2000).
38. G.H. Wu, C.H. Yu, L.Q. Meng, J.L. Chen, F.M. Yang, S.R. Qi, W.S. Zhan, Z. Wang, Y.F. Zeng, L.C. Zhao, Appl. Phys. Lett., 75, 2990 (1999)
39. M. Marioni, R.C. O'Handley, S.M. Allen, S.R. Hall, D.I. Paul, M.L. Richard, J. Feuchtwanger, R. Techapiesancharoenkji, *J. Magn. Magn. Mater.*, **290-291**, 35 (2005).
40. X.W. Liu, O. Söderberg, Y. Ge, A. Sozinov, V.K. Lindroos, *Mater. Sci. Forum*, **394-395**, 565 (2002).
41. V.A. Chernenko, *Scripta Mater.*, **40**, 523 (1999).
42. A.N. Vasil'ev, A.D. Bozhko, V.V. Khovailo, I.E. Dikshtein, S.G. Shavrov, V.D. Buchelnikov, M. Matsumoto, S. Suzuki, T. Takagi, J. Tani, *Phys. Rev.* B, **59**, 1113 (1999).
43. K. Yamaguchi, S. Ishida, S. Asano, *Mater. Trans. JIM*, **44**, 204 (2003).
44. P. Entel, V.D. Buchelnikov, V.V. Khovailo, A.T. Zayak, W.A. Adeagbo, M.E. Gruner, H.C. Herper, E.F. Wassermann, *J. Phys. D: Appl. Phys.*, **39**, 865 (2006).
45. X. Jin, M. Marioni, D. Bono, S.M. Allen, R.C. O'Handley, T.Y. Hsu, *J. Appl. Phys.*, **91**, 8222 (2002).
46. C. Jiang, T. Liang, H. Xu, M. Zhang, G. Wu, *Appl. Phys. Lett*., **81**, 2818 (2002).
47. V.V. Martynov, *J. Phys. IV France*, **5**, 91 (1995).

48. K. Koho, O. Söderberg, N. Lanska, Y. Ge, X. Liu, L.Straka, J. Vimpari, V.K. Lindroos, *Mater. Sci. Eng.* A, **378/1-2**, 384 (2004).
49. A. Sozinov, A. A. Likhachev, N. Lanska, K. Ullakko, *Proc. SPIE*, **4699**, 195 (2002).
50. V.A. Chernenko, C. Segui, E. Cesari, J. Pons, V.V. Kokorin, *Phys. Rev.* B, **57**, 2659 (1999).
51. V.A. Chernenko, J. Pons, C. Segui, E. Cesari, *Acta Mater*., **50**, 53 (2002).
52. O. Söderberg, L. Straka, V. Novak, O. Heczko, S.P. Hannula, V.K. Lindroos, *Mater. Sci. Eng.* A, **386**, 27 (2004).
53. A. Sozinov, A.A. Likhachev, N. Lanska, O. Söderberg, K. Ullakko, V.K. Lindroos, *Mater. Sci. Eng.* A, **378/1-2**, 399 (2004).
54. P. Müllner, V. Chernenko, G. Kostorz, *J. Appl. Phys.*, **95**, 1531 (2004).
55. A. Sozinov, A.A. Likhachev, N. Lanska, K. Ullakko, V.K. Lindroos, *J. Phys. IV France*, **112**, 955 (2003).
56. N. Lanska, O. Söderberg, A. Sozinov, Y. Ge, K. Ullakko, V.K. Lindroos, *J. Appl. Phys.*, **95**, 8074 (2004).
57. R.D. James and M. Wuttig, *Philos. Mag. A*, **77**, 1273 (1998).
58. J. Cui and R.D. James, *IEEE Trans. Magn*., **37**, 2675 (2001).
59. T.W. Shield and J. Cui, *Proc. SPIE*, **4699**, 251 (2002).
60. T. Sakamoto, F. Fukuda, T. Kakeshita, T. Takeuchi, K. Kishio, *J. Appl. Phys*., **93**, 8647 (2003).
61. T. Kakeshita, T. Takeuchi, T. Fukuda, M. Tsujiguchi, T. Saburi, R. Oshima, S. Muto, *Appl. Phys. Lett.*, **77**, 1502 (2000).
62. R. A. Stern, S.D. Willoughby, J.M. MacLaren, J. Cui, Q. Pan, R.D. James, *J. Appl. Phys.*, **93**, 8644 (2003).
63. T. Sakamoto, T. Fukuda, T. Kakeshita, T. Takeuchi, K. Kishio, *J. Appl. Phys.*, **93**, 8647 (2003).
64. K. Oikawa, L. Wulff, T. Ijima, F. Gejima, T. Ohmori, A. Fujita, K. Fukamichi, R. Kainuma, K. Ishida, *Appl. Phys. Lett.*, **79**, 3290, (2001).
65. M. Wuttig, J. Li, C. Craciunescu, *Scripta Mater.*, **44**, 2393 (2001).
66. H. Morito, A. Fujita, K. Fukamichi, R. Kainuma, K. Ishida, K. Oikawa, *Appl. Phys. Lett.*, **81**, 1657 (2002).
67. Y. Murakami, D. Shindo, K. Oikawa, R. Kainuma, K. Ishida, *Acta Mater*., **50**, 2173 (2002).
68. H.E. Karaca**,** I. Karaman , D.C. Lagoudas, H. J. Maier, and Y.I. Chumlyakov, *Scripta Mater.*, **49**, 831 (2003).
69. H.E. Karaca**,** I. Karaman , Y.I. Chumlyakov, D.C. Lagoudas, X. Zhang, *Scripta Mater.*, **51**, 261 (2004).
70. L. Manosa, A. Planes, M. Acet, E. Duman, E. Wassermann, *J. Appl. Phys.* , **93**, 8498 (2003)
71. L. Manosa, A. Planes, M. Acet, E. Duman, E. Wassermann, *J. Magn. Magn. Mater.*, **272-276**, 2090 (2004)
72. T. Büsgen, J. Feydt, R. Hassdorf, S. Thienhaus, M. Moske, M. Böse, A. Zayak, P. Entel, *Phys. Rev.* B, **70**, 014111 (2004).
73. S. Murray, R. Hayashi, M. Marioni, S. Allen, R. O'Handley, *Proc. SPIE,* **3675**, 204 (1999).
74. H. Sehitoglu, I. Karaman, X. Zhang, Y. Chumlyakov, H.J. Maier, *Scripta Mater.*, **44**, 779 (2001).

75. Y. Liu, W. Zhou, B. Jiang, X. Qi, J. Wang and C. Feng, *J. Phys. IV France*, **112**, 1013 (2003).
76. Y. Liu, W. Zhou, X. Qi, B. Jiang, J. Wang and J. Chen, *Appl. Phys. Lett.*, **78**, 3660 (2001).
77. H. Morito, A. Fujita, K. Fukamichi, R. Kainuma, K. Ishida, K. Oikawa, *Appl. Phys. Lett*., **83**, 4993 (2003).
78. Z.H. Liu, M. Zhang, Y.T. Cui, Y.Q. Zhou, W.H. Wang, G.H. Wu, X.X. Zhang, Gang Xiao, *Appl. Phys. Lett.*, **82**, 424 (2003).
79. H. Zheng, M. Xia, J. Liu, Y. Huang, J. Li, *Acta Mater*., **53**, 5125 (2005).
80. K. Tsuchiya, A. Tsutsumi, H. Ohtsuka, M. Umemoto, *Mater. Sci. Eng*. A, **378**, 370 (2004).
81. S. Guo, Y. Zhang, B. Quan, J. Li, Y. Qi, X. Wang, *Smart Mater. Struct*., **14**, S236 (2005).
82. I. Suorsa, E. Pagounis, K. Ullakko, *Appl. Phys. Lett.*, **84**, 4658 (2004).
83. N. Glavatska, G. Mogylny, I Glavatsky, S. Danilkin, D. Hohlwein, A. Beskrovnij, O. Söderberg, V.K. Lindroos, *J. Phys. IV*, **112**, 963 (2003).
84. C. Jiang, J. Wang, H. Xu, *Appl. Phys. Lett.*, **86**, 252508 (2005).
85. O. Heczko and L. Straka, *J. Appl. Phys.*, **94**, 7139 (2003).
86. I. Suorsa and E. Pagounis, *J. Appl. Phys.*, **95**, 4958 (2004).
87. I. Suorsa, E. Pagounis, J. Tellinen, I. Aaltio, K. Ullakko, *Proc. Actuator 2004*, Bremen, Germany, 573 (2004).
88. I. Suorsa, J. Tellinen, K. Ullakko, E. Pagounis, *J. Appl. Phys.*, **95**, 8054 (2004).
89. I. Suorsa, E. Pagounis, K. Ullakko, *J. Magn. Magn. Mater*., **272-276**, 2029 (2004).
90. M. Marioni, R.C. O'Handley, S.M Allen, *Appl. Phys. Lett.*, **83**, 3966 (2003).
91. Y. Liu, F. Xiong, E. Pagounis, *J. Magn. Magn. Mater.*, **285**, 410 (2005).
92. F. Xiong, Y. Liu, E. Pagounis, *J. Alloys and Compounds*, in press
93. E. Pagounis, Adaptamat leaflet, private communication, Adaptamat Ltd.
94. S.J. Murray, R.C. O'Handley, S.M. Allen, *J. Appl. Phys.*, **89**, 1295 (2001).
95. S.J. Murray, M. Marioni, A. Kukla, J. Robinson, R.C. O'Handley, S.M. Allen, *J. Appl. Phys.*, **87**, 5774 (2000).
96. O. Heczko, N. Lanska, O. Söderberg, K. Ullakko, *J. Magn. Magn. Mater.*, **242-245**, 1446 (2002).
97. A. Sozinov, Y. Ezer, G. Kimmel, P. Yakovenko, D. Giller, Y. Wolfus, Y. Yeshurun, K. Ullakko, V.K. Lindroos, *J. Phys. IV France*, **11**, Pr8-311 (2001).
98. N. Glavatska, I. Glavatsky, G. Mogylny, V. Gavriljuk, *Appl. Phys. Lett.*, **80**, 3533 (2002).
99. A. Sozinov, A.A. Likhachev, K. Ullakko, *Proc. SPIE*, **4333**, 189 (2001).
100. V.A. Chernenko, V.A. L'vov, M. Pasquale, S. Besseghini, C. Sasso, D.A. Polenur, *Int. J. Appl. Electromag. Mech.*, **12**, 3 (2000).
101. Y. Ge, O. Söderberg, N. Glavatska, K. Ullakko, V.K. Lindroos, *J. Phys. IV France*, **11**, Pr8-317 (2001).
102. K. Ullakko, Y. Ezer, A. Sozinov, G. Kimmel, P. Yakovenko, V.K. Lindroos, *Scripta Mater.*, **44**, 475 (2001).
103. O. Heczko, L. Straka, K. Ullakko, *J. Phys. IV France*, **112**, 959 (2003).
104. W.H. Wang, G.H. Wu, J.L. Chen, S.X. Gao, W.S. Zhan, G.H. Wen, X.X. Zhang, *Appl. Phys. Lett.*, **79**, 1148 (2001).
105. I. Suorsa, J. Tellinen, E. Pagounis, I. Aaltio and K. Ullakko, *Proc. Actuator 2002*, Bremen, Germany, 158 (2002).

106. H.E. Karaca, I. Karaman, B. Basaran, Y.I. Chumlyakov, H.J. Maier, *Acta Mater*., **54**, 233 (2006).
107. S. Chikazumi: Physics of ferromagnetism, 2nd edition, Oxford: Clarendon Press (1997).
108. C.P. Henry, D. Bono, J. Feuchtwanger, S.M. Allen, R.C. O'Handley, *J. Appl. Phys.,* **91**, 7810 (2002).
109. J. Tellinen, I. Suorsa, A. Jääskelainen, I. Aaltio, K. Ullakko, *Proc. Actuator 2002*, Bremen, Germany, 527 (2002).
110. M. Pasquale, *Sensors and Actuators* A, **106**, 142 (2003).
111. I. Suorsa, E. Pagounis, K. Ullakko, *Sensors and Actuators* A, **121**, 136 (2005).
112. J.P. Ahn, N. Cheng, T. Lograsso, K.M. Krishnan, *IEEE Trans. Magn.*, **37**, 2141 (2001).
113. J.W. Dong, L.C. Chen, J.Q. Xie, T.A. Müller, D.M. Carr, C.J. Palmstrom, S. McKernan, Q. Pan, R.D. James, *J. Appl. Phys.*, **88**, 7357 (2000).
114. P.G. Tello, F.J. Castano, R.C. O'Handley, S.M. Allen, M. Esteve, A. Labarta, X. Batlle, *J. Appl. Phys*., **91**, 8234 (2002).
115. S.K. Wu, K.H. Tseng, J.Y. Wang, *Thin Solid Films*, **408**, 316 (2002).
116. M. Kohl, S. Hoffmann, Y. Liu, M. Ohtsuka, T. Takagi, *J. Phys. IV*, **112**, 1185 (2003).
117. H. Rumpf, J. Feydt, D. Lewandowski, A. Ludwig, B. Winzek, E. Quandt, P. Zao, M. Wuttig, *Proc. SPIE*, **5053**, 191 (2003).
118. C.Y. Chung, V.A. Chernenko, V.V. Khovailo, J. Pons, E. Cesari, T. Takagi, *Mater. Sci. Eng.* A, **378**, 443 (2003).
119. J.W. Dong, J.Q. Xie, J. Lu, C. Adelmann, C.J. Palmstrom, J. Cui, Q. Pan, T.W. Shield, R.D. James, S. McKernan, *J. Appl. Phys.*, **95**, 2593 (2004).
120. V. Chernenko, M. Kohl, S. Doyle, P. Müllner, M. Ohtsuka, *Scripta Mater*., **54**, 1287 (2006).
121. T. Kanada, M. Enokizono, E. Nakamoto, *J. Phys. IV*, **8**, 245 (1998).
122. F. Albertini, S. Besseghini, A. Paoluzzi, L. Pareti, M. Pasquale, F. Passaretti, C.P. Sasso, A. Stantero, E. Villa, *J. Magn. Magn. Mater*., **242-245**, 1421 (2002).
123. Z.H. Liu, M. Zhang, Y.T. Cui, Y.Q. Zhou, W.H. Wang, G.H. Wu, X.X. Zhang, G. Xiao, *Appl. Phys. Lett*., **82**, 424 (2003).
124. J. Feuchtwanger, S. Michael, J. Huang, D. Bono, R.C. O'Handley, S.M. Allen, C. Jenkins, J. Goldie, A. Berkowitz, *J. Appl. Phys*., **93**, 8528 (2003).
125. H. Hosoda, S. Takeuchi, T. Inamura, K. Wakashima, *Sci. Technol. Adv. Mater*., **5**, 503 (2004).

9. Shape Memory Thin Films for Smart Actuators

Manfred Koh - Microsystems, Forschungszentrum Karlsruhe, IMT, Germany

Recent progress in research and fabrication of thin films of shape memory alloys (SMAs) has opened the opportunity to develop novel actuators and systems, which are capable to perform smart functions by responding to their thermal, mechanical and magnetic environment in a controllable way [1]. The fabrication and material properties of SMA thin films have been described in a number of books and review articles, see e.g. [1-5]. Until now, demonstrator devices have been developed for a broad range of applications, e.g., in the fields of microfluidics, robotics and information technology. The following section covers the aspects of design, modeling, fabrication and performance of selected examples of smart actuators of SMA thin films. New development trends in this exciting interdisciplinary field of materials research and engineering are highlighted.

9.1 Microfluidic Valves using SMA Thin Films

The development of a SMA thin film microvalve has been pioneered by A.D. Johnson based on silicon technology using a monolithic integration approach [6-8]. Figure 9.1 shows an exploded view of the microvalve structure. It consists of three silicon layers. The top layer is micromachined to form a spring. The middle layer contains a poppet supported by ribbons of NiTi. The valve seat is located in the bottom layer. NiTi ribbons and Si spring form an actuation system with passive biasing mechanism. At room temperature, the microspring forces the poppet against the valve seat to close the valve while the ribbons are stretched. In this condition, the force of microspring determines the maximum controllable pressure difference. Direct heating of the ribbons with electrical current causes the ribbons to contract pulling the poppet back into the plane of the middle Si layer.

Another technological approach has been to hybrid integrate micromachined SMA thin films, which allows the flexible combination with various materials such as thermoplastic substrates [9]. A schematic of such a microvalve is shown in Figure 9.2. The main components are a plastic housing with an integrated valve seat, a polyimide membrane, a spacer, a SMA microactuator and a cover. The SMA microactuator consists of a circular array of micro-bridges.

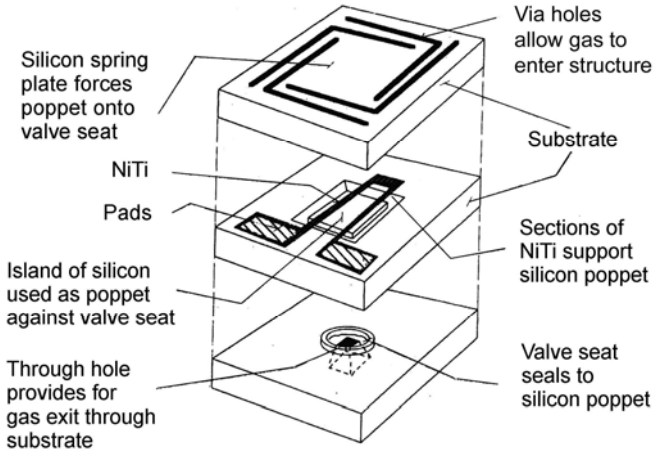

Figure 9.1: Schematic of a NiTi microvalve fabricated in silicon technology by monolithic integration [7].

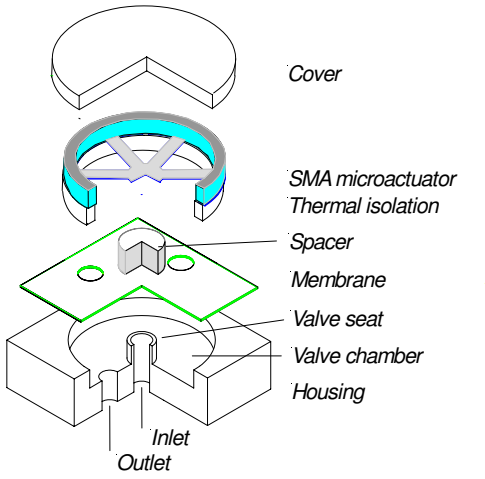

Figure 9.2: Schematic of a NiTi microvalve fabricated by hybrid integration [9].

Fabrication of the SMA microactuator is performed by chemical micromachining of a cold-rolled TiNi sheet of thickness d = 20 µm. In the unheated condition, a pressure difference between inlet and outlet causes a deflection of the membrane and the SMA microactuator. Thus, the valve is in a normally-open condition. By application of an electrical heating current, work is generated, which is used for the control of fluid flow and pressure difference between inlet and outlet. The maximum backpressure for closing the valve is adjusted by the spacer thickness, which prestrains the SMA microactuator. Pressure compensation between the valve chambers above and below the membrane may be achieved by lithographically microfabricated membrane holes.

For an optimum use of the shape memory effect with respect to work output and fatigue, several design criteria have been developed [1]. In short, it is essential to design the geometry and thermal connection to the environment such that homogenous profiles of stress and temperature of the mechanically active parts are created upon loading. Several valve prototypes have been developed, which largely fulfil these criteria [9-13].

Some major specifications of the SMA microvalves are summarized in Table 9.1. These specifications highlight the major advantages and drawbacks of using SMA thin films. The NiTi microvalves are capable to generate large work outputs and power densities in the order of 50 mJ/g and 1W/g, respectively, which can hardly be reached by other actuation principles. By keeping the maximum strain below 1%, large cycling times well above 10^6 are achieved. Due to thermal actuation, however, the frequency for complete actuation cycles is limited to about 10 Hz for the present designs.

The dynamics of TiNi microvalves and temperature range of operation can be improved by using alternative SMA materials with phase transformation temperatures well above room temperature [12]. Alternatives are, for instance, sputtered TiNiPd thin films, whose phase transformation temperatures can be raised by several hundred degrees by increasing the Pd content [1-3]. Figure 9.3 shows time-resolved gas flow characteristics of a NiTiPd microvalve for a pressure difference of 30kPa at various ambient temperatures between room temperature and 120°C. The microvalve is operated by applying periodic heating pulses of 1ms duration. The heating power is adjusted to close

the microvalve within about 10ms. When no extra heating power is supplied after closing the valve, a minimum opening time of 22 ms is observed at 25 °C. Thus, the maximum operation frequency at room temperature is improved by a factor of about 3.5 compared to NiTi microvalves of similar layout.

Figure 9.4 shows typical characteristics of gas flow of a NiTiPd microvalve and corresponding electrical resistance of the microactuator for a fixed pressure difference of 70 kPa. The flow characteristics of the microvalve are determined in a thermostat at various ambient temperatures between room temperature and 120 °C using nitrogen gas. The resistance characteristics indicate that the change of gas flow is caused by the martensitic phase transformation. At 120 °C, the critical heating power required to close the valve is about 80 mW. With decreasing temperature, the power requirements increase reaching about 260 mW at room temperature. At 70 kPa, the maximum leakage rate is less than 0.1 %. The specifications of the NiTiPd microvalve are summarized in Table 9.1.

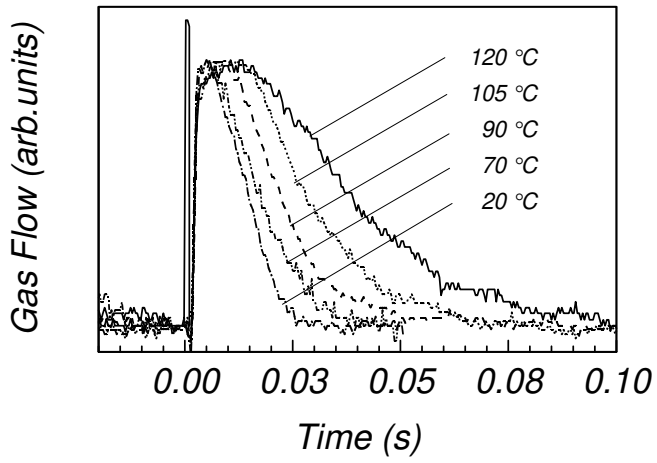

Figure 9.3: Time-resolved gas flow during closing and opening of a TiNiPd microvalve for a pressure difference of 30 kPa at various operation temperatures [16].

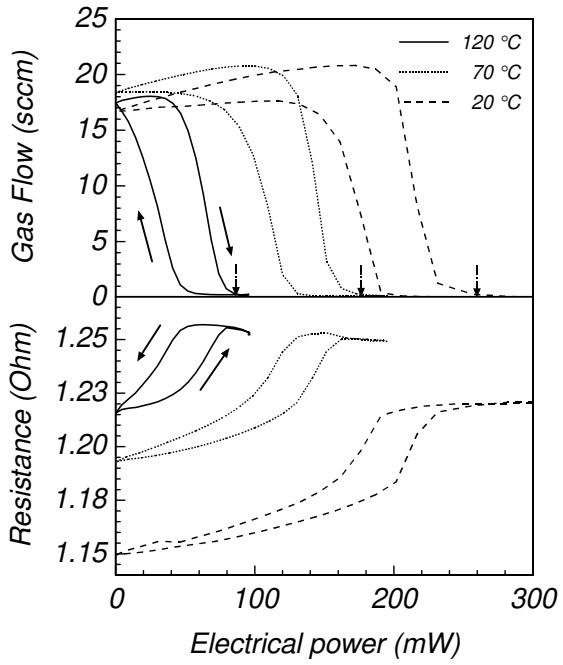

Figure 9.4: Gas flow and electrical resistance characteristics of a TiNiPd microvalve for a pressure difference of 70 kPa at various operation temperatures as indicated [16].

Table 9.1: Specifications of selected SMA thin film microvalves. The abbreviations PMMA and PES denote polymethylmethacrylate and polyethersulfone, respectively.

Materials	Lateral Size (mm^2)	Max. gas flow (standard ccm)	Max. pressure difference (kPa)	Operation frequency (Hz)	Power (DC)	Ref.
NiTi, silicon	10 x 5	800	670	10	< 0.3 W	[8]
NiTi, PMMA	6 x 6	470	500	13	< 0.1 W	[13]
NiTiPd, PES	6 x 6	360	250	35	< 0.26 W	[13]

The microvalve developments demonstrate the significant potential of SMA thin film microactuators. So far, SMA microvalves have only been fabricated in small scale production. For a broad introduction into the market, further developments in the fields of materials research and fabrication technology will be required in order to extend the application range and to minimize fabrication costs. For instance, suitable packaging and interconnection technologies have to be developed on the wafer level using parallel fabrication processes to mass-fabricate SMA microvalves. Apart from competitive stand-alone devices, current developments concentrate on microvalves for modular integration in fluidic systems of higher complexity.

9.2 Robotic Devices using SMA Thin Film Composites

Sputter deposited thin SMA films are also in use as composites in combination with a substrate. In this case, the substrate works as a bias spring and enables the SMA actuator to show a two-way behavior. Actuator motions with large deflections can for instance be generated by SMA thin films deposited onto metallic foils [1-3]. The motion occurs when film stresses induced by annealing treatment are drastically released by the shape memory film upon the martensitic transformation. Since these composites provide their work right after deposition and annealing without training they are promising candidates for microactuators.

By means of the combination of shape memory composites with additional polymer films, also bistable actuators can be realized [1]. Figure 9.5 illustrates the functional principle of such a bistable shape memory actuator. The temperature-dependent stiffness of the polymer is superimposed to the mechanical hysteresis of the shape memory composite, which shows a two way behavior. The essential precondition of bistable behavior is that the glass transition of the thermoelastic polymer takes place within the hysteresis of the shape memory alloy. Recent investigations indicate that combining, e.g., $Ti_{39}Hf_{15}Ni_{46}$/Mo composites with a Lucryl polymer leads to an actuator with a bistable behaviour [20].

Upon heating, first, the polymer becomes soft due to its glass transition at T_g before the SMA starts to undergo the reverse martensitic transformation from martensite to austenite at the austenite start temperature A_s. Due to the low stiffness of the polymer above T_g, the actuator is able to move and since the SMA composite is deflected in the austenitic state the total polymer-SMA composite is bent. Upon cooling, first, the polymer becomes stiff below its glass transition temperature T_g before the SMA starts to undergo the martensitic transformation at M_s. If the thickness of the polymer is high enough, the stiffness of the polymer below T_g is sufficient to keep the SMA-composite in the curved state even after the transformation of the SMA to the martensite.

Therefore, the actuator remains deformed. To switch the bistable actuator to the flat shape, the actuator has to be heated to a temperature between T_g and A_s. Above the glass transition T_g, the polymer becomes soft and therefore releases the shape memory composite, which is still martensitic and tends to go to the flat shape as long as the temperature is below A_s. Upon cooling, the flat shape is fixed again by the polymer.

Figure 9.6 shows a sketch of a microgripper using this mechanism. The gripper can be fabricated by magnetron sputtering and other MEMS-compatible methods on a silicon wafer.

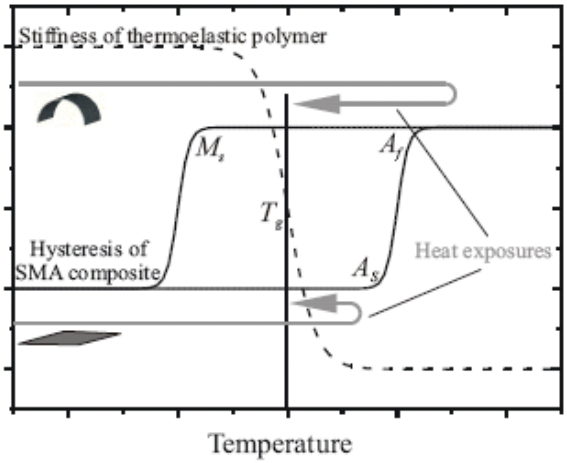

Figure 9.5: Stiffness versus temperature of a thermoelastic polymer and transformation hysteresis of a SMA composite, required for bistability. Arrows indicate the heat exposures to change the curvature of the actuator [20].

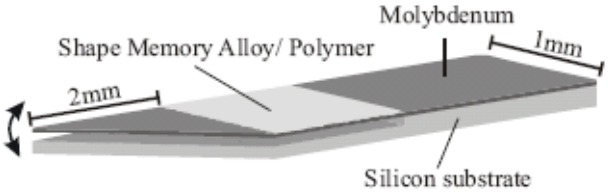

Fiigure 9.6: Principle of a bistable microgripper fabricated by magnetron sputtering [20].

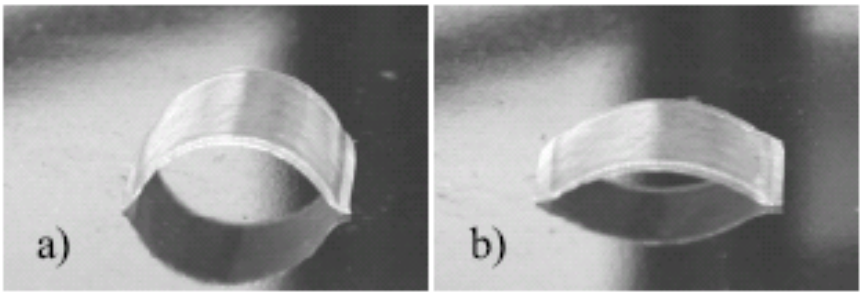

Figure 9.7: Bistable actuator a) after 160°C heat exposure in the bent state and b) after 90°C heat exposure in the flat shape, respectively. Photos taken at room temperature [20].

Figure 9.7 demonstrates that the polymer's stiffness is strong enough to fix the actuator in the bent state (Fig.ure 10.7a) and to allow it to reach the flat state after heating to a temperature between T_g and A_s (Figure 10.7b). The thickness of the polymer layers surrounding the metal is 75 µm and the thickness of the SMA composite is 35µm (25µm Mo + 10µm SMA) in this case.

The transformation behavior of an actuator consisting of two neighbouring SMA thin film composites is automatically phase-coupled by the variation of temperature. Thus,

complex motions can be easily controlled without the need of additional electronics [1]. If the small hysteresis of a certain SMA is embedded within the broad hysteresis of the second SMA, a special transformation sequence can be provided. This mechanism enables the actuator to create a wave-like behavior which is very promising for the motion of microrobots as illustrated by Figures. 9.8 and 9.9. By deposition of the SMA thin films on opposite sides of the substrate, neighbouring SMA thin film composites are created, which work in opposite directions. Figure 9.8 shows that, in this case, the path of deflection upon heating is completely different from the path upon cooling. Figure 9.9 illustrates, how this concept can be used for locomotion of a robot. The cross-section of a robot leg is drawn as a superposition of the four different stages of a complete motion cycle. The SMA B with the broad hysteresis is placed at the upper part and SMA A at the lower part of the actuator. Every motion step corresponds to a different combination of austenite and martensite of the two SMAs. The stages are marked by the four possible phases. At the beginning, both alloys are martensitic and the leg is straight. By means of a single heat pulse, even legs with different initial positions can perform a complete motion cycle since a phase-coupling between these legs can be achieved directly.

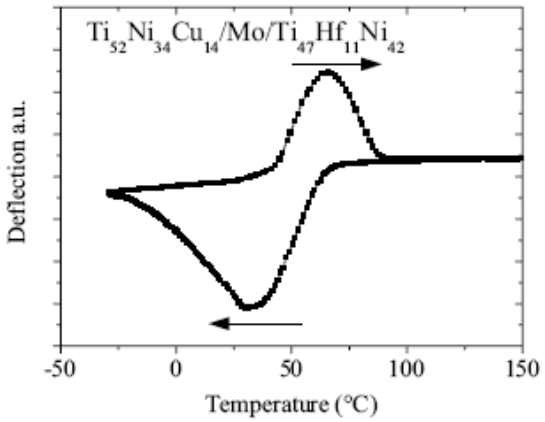

Figure 9.8: Deflection-temperature measurement of a $Ti_{52}Ni_{34}Cu_{14}$/Mo/$Ti_{47}Hf_{11}Ni_{42}$ cantilever [21].

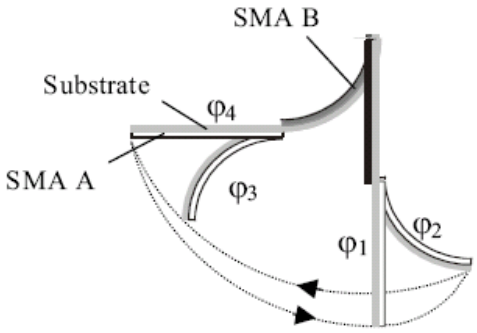

Figure 9.9: Superposition of the cross-section of a robot leg at different phases of a motion cycle [21].

9.3 Microactuators of Ferromagnetic SMA Thin Films for Information Technology

In the last decade, ferromagnetic shape memory alloys (FSMAs) experienced a widespread research boom as they exhibit a unique combination of high energy densities, shape memory and ferromagnetic properties [22]. Of particular interest have been the Heusler ferromagnetic shape memory alloys Ni-Mn-Ga. Recent investigations on bulk NiMnGa single crystals revealed the giant magnetostrain effect showing deformations as large as 10 %, which is based on the magnetic field-induced reorientation of martensite variants [23,24]. In order to exploit these materials for microsystems applications considerable efforts have been undertaken recently to fabricate FSMA thin films [25,30].

The martensitic transformation temperature T_0 of Ni-Mn-Ga thin films can be tuned by the chemical composition in a large range from cryogenic temperatures up to

temperatures above the Curie temperature T_C, which is much less composition-dependent [31]. Thus, an optimum chemical composition with $T_0 \approx T_C$ can be adjusted, where the material shows ferromagnetic thermoelastic martensites at room temperature and a mixed austenitic and ferromagnetic transformation in a relatively small temperature interval. This behaviour is of particular interest as the shape memory effect and the ferromagnetic transition can be induced simultaneously by a relatively small temperature change.

For FSMA thin films, a novel actuation mechanism has been developed, which makes use of both the ferromagnetic transition and the martensitic transformation [31]. The mechanism is illustrated in Figure 9.10 for a Ni-Mn-Ga bending actuator placed in the inhomogeneous magnetic field of a miniature permanent magnet. Depending on the temperature of the microactuator, either magnetic or shape recovery forces occur in opposite directions, while the corresponding biasing forces remain small. Thus, an almost perfect antagonism can be realized in a single component part. By applying an alternating electrical current, a periodic oscillation of the beam can be excited. This motion can be used to control the deflecton of a micromirror attached to the front end of the actuator. For instance, a microscanner prototype has been developed based on the actuation mechanism, see Figure 9.11 [32]. The overall dimensions are 7 x 2 x 5 mm^3.

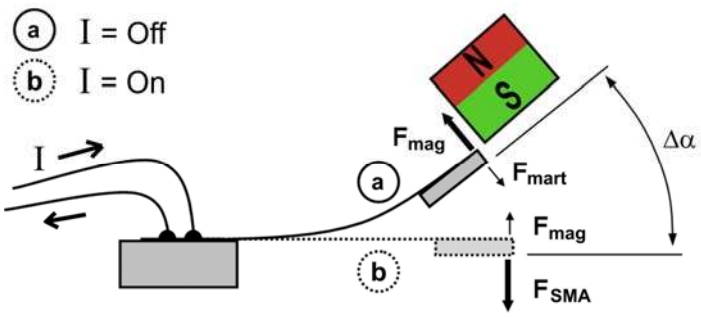

Figure 9.10: Operation principle of the FSMA microactuator. Legend: N,S - north and south pole of a permanent magnet; F_{mag} - magnetic force, F_{SMA} - shape recovery force, F_{mart} - force in martensitic condition, $\Delta\alpha$ - mechanical scanning angle.

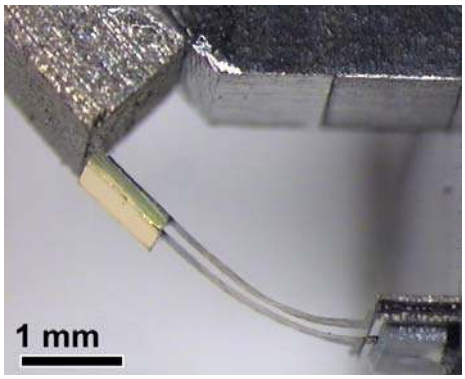

Figure 9.11: Prototype of a FSMA microactuator for control of a micromirror.

Figure 9.12 shows experimentally determined deflection angles of the micoactuator in vertical direction $\Delta\alpha$ as a function of heating power in stationary condition [32]. For a heating power lower than 40 mW, the double-beams remain nearby the magnet. At about 50 mW, the maximum temperature of the actuator reaches the Curie temperature causing a decrease of the deflection angle. This motion is supported by the shape recovery force for a heating power above 70 mW, where already a sufficient fraction of the double-beams is transformed to austenite. Above 100 mW, the flat position is reached.

A typical frequency characteristic is depicted in Figure 9.13 with the optical scanning angle being twice the deflection angle of the FSMA microactuator $\Delta\alpha$ [33]. A pulsed heating signal is applied at a fixed duty cycle of 1:6 and fixed frequency steps of 2 Hz. For each frequency, the driving power is optimized. Surprisingly, it turns out that two

optimum power regimes denoted as P_{opt1} and P_{opt2} exist, which give rise to large scanning angles. Below a critical frequency of about 120 Hz, the scanning angle shows several power-dependent maxima. These features occur due to the phase difference between heating pulses and eigenoscillations, which depend on the heating power [34]. By increasing the driving frequency above the critical frequency, the scanning angle sharply decreases independent of the heating power. This low-pass behavior can be attributed to the dynamics of heat transfer between the double-beam and its environment. The relatively short time constants for the given dimensions are mainly due to the high phase transformation temperatures and the forced convective cooling during scanning motion. Above about 150 Hz, a broad resonance occurs.

These results demonstrate that large scanning angles up to 60° are generated for the given size of the FSMA microactuator. Furthermore, the operation frequency is not fixed but can be tuned in a wide range, which differs from previous developments of microscanners working mostly at resonance [35]. The driving voltage remains below 1.5 V in all cases. Recent developments include extensions of design and technology to generate two-dimensional scanning patterns [36] and to combine the microscanner with a time-of-flight measurement setup for three-dimensional scanning of objects in the environment [33]. On main advantage of such systems is the small size and low moving masses allowing mobile applications with low sensitivity to vibrations and shock.

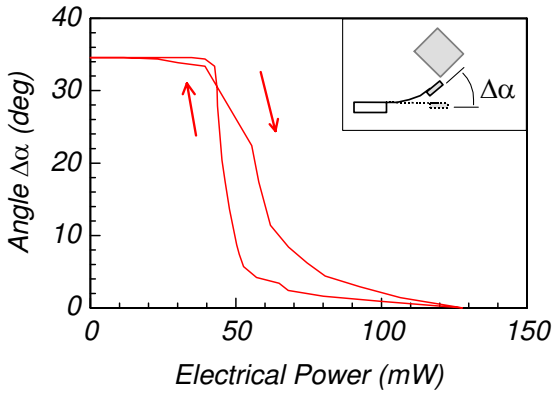

Figure 9.12: Deflection angles Δα as a function of electrical heating power upon heating and cooling [32].

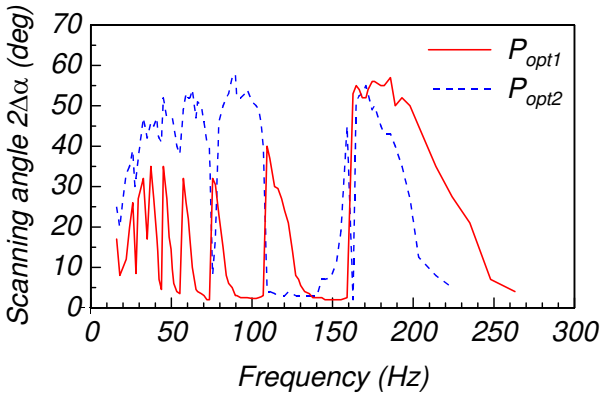

Figure 9.13: Scanning angle versus frequency. Optimum power regimes are indicated by P_{opt1} and P_{opt2} [33].

Various investigations have been undertaken to exploit the giant magnetostrain effect in FSMA thin films. Recent investigations on polycrystalline Ni-Mn-Ga thin films with a fiber texture show that prestrained films show stress-induced prealignment and magnetic field-induced reorientation of martensite variants [37]. However, the effects are relatively small, below 0.1 %. Considerable improvements are expected for highly oriented and single crystalline FSMA thin films. First results on expitaxial Ni-Mn-Ga thin films also show magnetic field-induced reorientation qualitatively [38]. It is expected that functional FSMA thin films with giant magnetostrain effect will be available in the near future opening up the development of novel microdevices with magnetic shape memory.

Conclusions

This review demonstrates that smart actuators fabricated from SMA thin films allow new solutions with remarkable performance reflecting the recent advances in the fields of material development, actuator design and modeling, micromachining, and system integration. Some of the presented microactuators are competitive components, which, however, have been fabricated in small quantities so far. Due to their high energy densities and multifunctional properties, they have a large potential for innovation and may contribute significantly to future developments in microsystems technology.

[1] M. Kohl, *Shape memory microactuators*, Springer book series on Microtechnology and MEMS, Springer-Verlag Berlin Heidelberg, 2004.

[2] K. Otsuka and C.M. Wayman, *Shape Memory Materials*, Cambridge University Press (1998).

[3] S. Miyazaki and M. Kohl, *Recent developments in TiNi-based shape memory alloys*, Int. Symp. on Smart Structures and Materials, San Diego, USA, SPIE Vol. 3324, (1998), pp. 2-12.

[4] S. Miyazaki and A. Ishida, *Martensitic transformation and shape memory behavior in sputter-deposited TiNi-base thin films*, Materials Science and Engineering A273-275 (1999)I 106-133.

[5] M. Kohl, *Shape memory actuators in MEMS,* Proc. SMST 99, Antwerp Zoo, Belgium, (1999), pp. 267-279.

[6] J.D. Bush and A.D. Johnson, Prototype microvalve actuator, Proc. MEMS 90, Napa Valley, California, USA (1990).

[7] C.A. Ray, C.L. Sloan, A.D. Johnson, J.D. Busch and B.R. Petty, A Silicon-Based Shape Memory Alloy Microvalve, Mat. Res. Soc. Symp. Proc. Vol. 276 (1992), pp. 161-166.

[8] A.D.Johnson and E.J. Shahoian, Recent progress in thin film shape memory microactuators, Proc. MEMS 95, Amsterdam, the Netherlands, IEEE Catalog No. 95CH35754 (1995), pp. 216-220.

[9] M. Kohl, D. Dittmann, E. Quandt and B. Winzek, *Thin film shape memory microvalves with adjustable operation temperature,* Sensors and Actuators A83 (2000), pp. 214-219.

[10] K.D. Skrobanek, M. Kohl and S. Miyazaki*, Stress-optimised shape memory devices for the use in microvalves*, J. Phys. IV France 7 C5 (1997), pp. 597-602.

[11] M. Kohl, K.D. Skrobanek and S. Miyazaki*, Development of stress-optimised shape memory microvalves*, Sensors and Actuators A72 (1999), pp. 243-250.

[12] M. Kohl, I. Hürst and B. Krevet, *Time response of shape memory microvalves*, Proc. Actuator 2000, Bremen, Germany, H. Borgmann Ed., (2000), pp. 212-215.

[13] M. Kohl and B. Krevet, *3D Simulation of a shape memory microactuator*, Materials Transactions Vol. 43, No. 5 (2002), pp. 1030-1036.

[14] E. Quandt, C. Halene, H. Holleck, K. Feit, M. Kohl, P. Schloßmacher, A. Skokan and K.D. Skrobanek, *Sputter deposition of TiNi, TiNiPd and TiPd films displaying the two-way shape memory effect*, Sensors and Actuators A 53 (1996), pp. 434-439.

[15] M. Kohl, D. Dittmann, E. Quandt and B. Winzek, *Thin film shape memory microvalves with adjustable operation temperature,* Sensors and Actuators A83 (2000), pp. 214-219.

[16] Y. Liu, M. Kohl, K. Okutsu and S. Miyazaki, *A TiNiPd thin film microvalve for high temperature applications*, Materials Science and Engineering 378 (2004) 205-209.
[17] P. Krulevitch, A.P. Lee, P.B. Ramsey, J. C. Trevino, J. Hamilton, M.A. Northrup, J. of Microelectromechanical Systems, 5 (1996), 270 – 282.
[18] B. Winzek, E. Quandt, Zeitschrift für Metallkunde, 90 (1999) 796 – 802.
[19] B. Winzek, E. Quandt, H. Holleck, Proc. Actuator 2000, Bremen, Germany (2000), pp. 172 – 176.
[20] T. Sterzl, B. Winzek, H. Rumpf and E. Quandt, Bistable shape memory composites for switches, grippers and adjustable capacitors, Proc. Actuator 2002, Bremen, Germany (2000), pp. 91 – 94.
[21] B. Winzek, H. Rumpf, T. Sterzl and E. Quandt, Shape memory composites with phase-coupled motion, Proc. Actuator 2002, Bremen, Germany (2000), pp. 95 – 98.
[22] For a recent review see, e.g., A.N. Vasil'ev, V.D. Buchel'nikov, T. Takagi, V.V. Khovailo and E.I. Estrin, Shape memory ferromagnets, Physics-Uspekhi 46 (6) (2003) 559-588.
[23] S.J. Murray, M. Marioni, S.M. Allen, R.C. O'Handley and T.A. Lograsso, 6% magnetic-field-induced strain by twin-boundary motion in ferromagnetic Ni-Mn-Ga, Appl. Phys. Lett. 77 (2000), pp. 886-888.
[24] A. Sozinov, A.A. Likhachev, N. Lanska, K. Ullakko, Giant magnetic-field-induced strain in NiMnGa seven-layered martensitic phase, Appl. Phys. Lett. 80 (2002), pp. 1746-1749.
[25] M. Ohtsuka, K. Itakagi, Int. J. Appl. Electromagn. Mech. 12 (2000) 49-59.
[26] M. Wuttig, C. Craciunescu, J. Li, Mater. Trans. JIM 41 (2000) 933-37.
[27] S. Isokawa, M. Suzuki, M. Ohtsuka, M. Matsumoto, K. Itagaki, Mater. Trans. JIM 42 (2001) 1886-1889.
[28] P.G. Tello, F.J. Castano, R.C. O'Handley, S.M. Allen, M. Esteve, F. Castano, A. Labarta, X. Battle, J. Appl. Phys. 91 (2002) 8234-8236.
[29] H. Rumpf, J. Feydt, D. Levandovski, A. Ludwig, B. Winzek, E. Quandt, P. Zhao, M. Wuttig, SPIE Proc. Series 5053 (2003) 191-199.
[30] J.W. Dong, J.Q. Xie, J. Lu, C. Adelmann, C.J. Palmstrøm, J. Cui, Q. Pan, T.W. Shield, R.D. James, S. McKernan, J. Appl. Phys. 95, No. 5 (2004) 2593-2600.
[31] M. Kohl, D. Brugger, M. Ohtsuka and T. Takagi, *A novel actuation mechanism on the basis of ferromagnetic SMA thin films*, Sensors and Actuators 114/2-3 (2004) 445-450.
[32] D. Brugger, M. Kohl, and B. Krevet, *Ferromagnetic shape memory microscanner with large deflection angles*, Proc. E-MRS 2005, Symposium C, Warsaw, Poland, (2005), p. 84.
[33] D. Brugger, M. Kohl, U. Hollenbach, A. Kapp and C. Stiller, *Ferromagnetic shape memory microscanner system for automotive applications*, Proc. E-MRS 2005, Symposium C, Warsaw, Poland, (2005), p. 70.
[34] B. Krevet and M. Kohl, *Coupled Simulation of the thermo-magneto-mechanical properties of a Ni-Mn-Ga actuator,* Proc. E-MRS 2005, Symposium C, Warsaw, Poland, (2005), p. 88.
[35] For a recent review see, e.g., T. Gessner, K. Hiller, A. Hübler and S. Kurth, *Micro scanners for spectrum analysis systems*, Proc. Actuator 04, Bremen, Germany, H. Borgmann Ed., (2004), pp. 232-237.

[36] M. Kohl, D. Brugger and B. Krevet, *Ferromagnetic shape memory actuator for large 2D optical scanning*, Proc. MEMS 06, Istanbul, Turkey, (2006), pp. 794-797.

[37] A. Agarwal, M. Kohl, V.A. Chernenko and M. Ohtsuka, Magnetomechanical properties of polycrystalline Ni-Mn-Ga thin film actuators, Proc. E-MRS 2005, Symposium C, Warsaw, Poland, (2005), p. 85.

[38] J.W. Dong, J.Q. Xie, J. Lu, C. Adelmann, C.J. Palmstrom, J. Cui, Q. Pan, T.W. Shield, R.D. James and S. McKernan, Shape memory and ferromagnetic shape memory effects in single-crystal Ni2MnGa thin films, J. Appl. Phys., Vol. 95, No. 5, (2004), pp. 2593-2600.

10 Shape memory materials

Jovan Matovic – Institute of Sensor and Actuator Systems, TUWien, Austria

Shape-memory materials (SMM) are stimuli-responsive materials. They have the capability of changing their shape upon application of an external stimulus such as temperature or magnetic field. A change in shape caused by a change in temperature is called the thermally induced shape-memory effect. There are two main groups of SMM, metallic Shape Memory Alloys (SMA) and Shape Memory Polymers (SPM).

10.1 Shape Memory Alloys

SMAs are characterized by reverse phase transformation between two different crystal structures (phases). At temperature lower than a predefined temperature M_f (martensite finished temperature), the SMA exists in *martensite* phase (Figure 10.1). In *martensite* phase, the SMA material it is soft and ductile and can be easily deformed in an arbitrary shape with deformation up to 8% [7]. When martensitic SMA is heated over *As*, (austenite start temperature*)* it begins to transform into the *austenite* or *parent* phase. The transformation is finished at *austenite finish temperature* (A_f). During *martensite* $\rightarrow$ *austenite* transformation, not-constrained SMA material becomes mechanicallyu hard and returns to the pre-deformed shape. After that, if the temperature falls again under the M_f value, the SMA goes into reverse, austenite to martensite transformation. In reverse transformation the specimen's shape remains unchanged until an external force is applied. If the deformation of specimen in the *martensite* phase is modest, i.e. less than 5%, the process is fully reversible for millions of cycles. The transition temperatures of a SMA sample *Ms*, M_f, , A_s, and A_f are set by metallurgical composition as well as with the thermomechanical treatment history of the sample. Readers are referred to reference [1] for more details.

If the SMA sample is fixed and clamped, i.e. it is prevented from returning to the shape it has in parent phase, the SMA can generate stress up to 800 MPa during transformation cycle. If the SMA material is used in an actuator, it can produce the specific work up to 5 J/g. This is the most energy-dense actuator for MST applications when compared with other actuator materials (electrostatic, electromagnetic, piezoelectric etc.), as illustrated in Figure 10.1b.

The ability of SMA materials to absorb the heat energy from their surroundings and convert it into the mechanical work during the *martensite* $\rightarrow$ *austenite* transformation and the reverse process, to dissipate the heat energy during deformation, can classify the SMA materials as "thermodynamics heat engines". In the future, these characteristics could be applied to create a MEMS thermal engine. Theoretically, a SMA heat engine, using temperature difference from 0 to 100 ^{o}C, has the Carnot efficiency near 20%, close to that of gas turbines with efficiency of 35% [2] These attributes make the SMA useful for many applications beyond the well-lnown memory effect.

In the martensitic phase, SMA has excellent mechanical damping properties due to the energy absorption characteristics of the martensite structure. In addition, the martensitic form of SMA has an extraordinary fatigue resistance [3]. The mechanical energy of deformation is internally transformed to heat via fully revisable structural transformations. This property is known as "superplastic" behavior. The original parent

shape can be recovered at any time simply by heating the sample above its transformation temperature. A thorough analysis of the damping properties of SMAs can be found in [3].

In the austenitic (parent) phase, at temperatures slightly above the transformation temperature, the SMA's show another unusual effect, called "superelastic" or "pseudoelastic" behavior. For large deformations, the applied stress can induce the formation of martensite above the M_s temperature (stress-induced transformation). During deformation the external force remains practically constant as the mechanical work is consumed for the phase transformation. Once a deformation of ~8% is reached, all the available austenite is transformed into the martensite and upon further deformation SMA responds as an ordinary elastic material. Since the stress-induced martensite has been formed above its normal temperature, the martensite reverts immediately to undeformed austenite as soon as the stress is removed. It should be noted here that all of the described effects can occur in the same specimen, depending on the temperature: under the M_s the SMA has superplasticity behavior prevails, between M_s and A_f the material exhibits the memory effect and over A_f behaviour is superelastic. These exciting features of the SMA materials sometime represent the serious drawback: without the serious consideration of all properties of the SMA materials, manufacturing and the learning procedures one may expect more from SMA, than it can offer.

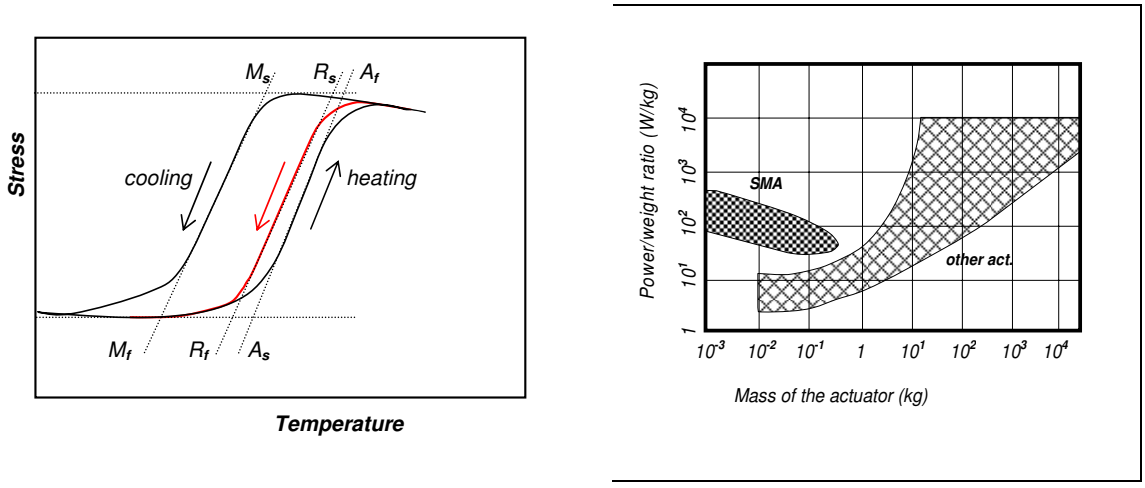

Figure 10.1a – The generic hysteresis loop for the SMA thermal cycling. Upon heating, the martensite → austenite transformation straits at As and at the Af, material is fully austenite. Upon cooling, the austenite → martensite transformation start at Ms and finished at Mf. For the specially treated SMA material, there is an additional phase transformation between austenite and R phase, with very narrow hysteresis loop (red line). Figure 10.1b A schematic representation of the locus of SMA-actuators in a power density versus weight. The area enclosed between the two border lines indicate where other types of actuators are situated [4]

The two major SMA systems that have significance today are the Ni-Ti alloys and the copper-base alloys [5]. Of these, TiNi is better suited for use as a microactuator. The Ni-Ti alloys have greater shape memory strain (up to 8% versus 4 to 5% for the copper-base alloys), have higher ductility and more stable transformation temperatures. Further, Ni-Ti alloys have excellent corrosion resistance, compared to the copper-base alloys;

have better biocompatibility and the ability to be electrically heated for shape recovery [5]

The newly developed FeMnSiCrNi shape memory stainless steels (SMSS) have attracted substantial interest because of their good shape memory effect, mechanical properties, machinability, weldability and corrosion resistance [6].

The Ni-Ti has proven to be the most flexible and beneficial alloy for the micro-actuator application. One property makes Ni-Ti unique among other actuators for MEMS application; its power density rises with mass reduction, up to the nanometer range (Figure 10.1b).

Advantages	Disadvantages
High power/weight (or power/volume) ratio, increased with mass reduction	Low energy efficiency:, max 10 %
Smooth, noiseless and friction free operation	Limited bandwidth due to heating and cooling restrictions:
Excellent corrosion resistance and biocompatibility	Degradation and fatigue under the strain >5 %
Simple and compact actuator mechanics	Complex control. The SMA behavior is influenced by a large number of parameters

Table 10.1: Summary of the basic features of the SMA in micro-actuators [7]

The phase transformation of the Ni-Ti alloy was described in detail in1965, when the term ‘memory’ was first used to describe the shape recovery behavior [8]. During the past four decades, the most of the complex behavior of Ni-Ti alloys was discovered, both practically and theoretically. The modern and comprehensive analysis of the Ni -Ti alloys can be found in [1]. The most of knowledge about the Ni-Ti alloys is connected to the alloy in a bulk form, but many facts can be also applied to the thin film form.

10.2 Micro-scale applications of SMA

When one reviews the “new SMA materials for microsystems technology (MST) actuators”, the issue can be divided in two distinct fields. These are the application of the well known Ni-Ti alloys in the form of thin films, and application and development of the new alloys, not previously used in the MST actuators.

Considering the application of Ni-Ti, MST brings the new challenges in the alloy manufacturing processes. The transition temperature of the Ni – Ti alloy is extremely sensitive to the composition: the shift from proper composition of only 1 % changes the transition temperature for 150^{o}C [1]. Attaining the required composition of Ni – Ti alloy is a difficult task for any thin film deposition technology. Sputtering and laser ablation, the two main manufacturing processes, have the tolerance margins larger then required. Even the characterization techniques of the thin film are accurate of about 1%.

Sputtering deposition remains the principal manufacturing process for the Ti - Ni thin films. The process is MEMS compatible, which includes pattering and etching

processes. The target is usually the Ti - Ni alloy; however, the composition of the sputtered film does not match the composition of the target. The most common solution to this problem is use of the dual phase target NiTi + Ti, or use of multiple sputtering guns. A comprehensive review of manufacturing processes can be found in [9-33].

Considering the use of new SMA materials, most of the materials discovered in the past 40 years have no widespread application. The origin of this situation is complex: the alloy component cost, absence of a notable advantage over Ni-Ti alloy, manufacturing complexity etc.. For MST applications, the cost of the material is not the primary property, enabling materials previously ignored due to their high cost to be considered. Table 10.2 list some of the exotic SMA alloys [34]. The decisive answer about the use and development new shape memory materials for MST applications should be matter for future examination.

Alloy	Composition	Transition temp. (°C)
Ag-Cd	44/49 at.% Cd	-190 to -50
Au-Cd	46.5/50 at.% Cd	30 to 100
Cu-Al-Ni	14/14.5 wt.% Al, 3/4.5 wt.% Ni	-140 to 100
Cu-Sn	approx. 15 at.% Sn	-120 to 30
Cu-Zn	38.5/41.5 wt.% Zn	-180 to -10
Cu-Zn-X (X = Si,Sn,Al)	a few wt.% of X	-180 to 200
In-Ti	18/23 at.% Ti	60 to 100
Ni-Al	36/38 at.% Al	-180 to 100
Ni-Ti	49/51 at.% Ni	-50 to 110
Fe-Pt	approx. 25 at.% Pt	approx.-130
Mn-Cu	5/35 at.% Cu	-250 to 180
Fe-Mn-Si	32 wt.% Mn, 6 wt.% Si	-200 to 150
NbU		
UMo		
Nb_3Sn		
V_3Si		

Table 10.2 List of some Shape Memory Alloys with basic parameters [34]

A SMA actuator can be manufactured by a simple deposition of active material, it is therefore potentially easier to fabricate than electromagnetic or electrostatic actuators. Applications of the SMA to MST and microactuators started in the early 1990s. Since this time, many MST devices with SMA actuation have been developed including microfluidic, microoptic, valves and pumps [35-49]. The SMA actuators are usually heated resistively, but ambient temperature variations are also applied. Figure 10.2 shows an SMA actuator activated by solar energy. When the sun illuminates the structure, the SMA ribs bend and open the highly reflective surface to the sun.

Figure10. 2: SMA actuator activated with solar energy. When the sun illuminates the structure, the SMA ribs bend and open the highly reflective surface (4cm diameter) to the sun. [50].

10.3 Shape memory polymers

Shape memory polymers (SMP) are second important group of shape memory materials. Like SMAs, they have the capability of changing their shape in response to an external stimulus. The most common is temperature and thermo-responsive shape memory polymers typically consist of two polymer components and two phases, one with a higher melting temperature than the other. The glass transition temperature T_g, is the reference point where the higher temperature component starts to melt. When heated above T_g, the SMP, is soft and rubbery and it is easy to change the shape. When subsequently cooled below T_g, it retains the given shape (shape fixing characteristic). When heated again above T_g, the material autonomously returns to the original "parent" shape. [51-53]

The physical of memory effect in polymers is quite different from that in the SMA. The polymeric phase that exisits above T_g, corresponds to the higher melting temperature component. This acts as the physical cross-link that is responsible for the permanent shape. The second component acts as a molecular switch and helps to freeze temporary shapes below the transition temperature, with either the glass transition temperature or the melting temperature serving as the transition/switching temperature. Chemical cross-links can be used in elastomeric shape memory polymers instead of physical cross-links. The T_g of a SMP can be set over a temperature range of several hundred degrees by control of composition and/or the degree of cross-linkage. [53]

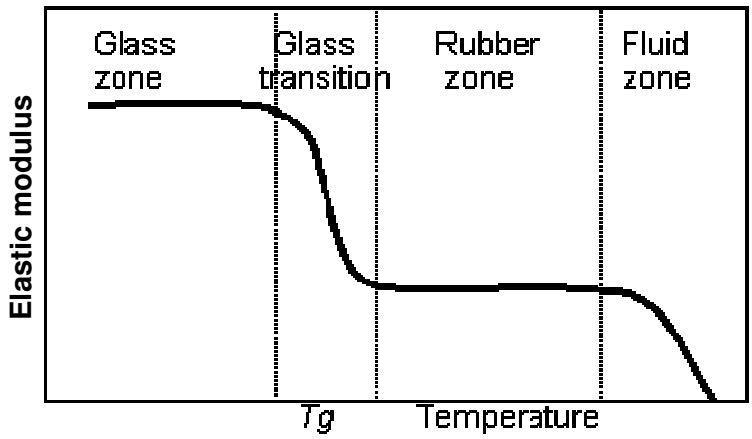

Figure 10.3 Temperature dependency of elasticity modulus of SMP

The shape-memory effect is in principle a behavior inherent to all polymers. However, polymers that exhibit a useful shape-memory effect must demonstrate a sharp transition temperature and a rubbery plateau, along with relatively large strain capacity without local material damage. Only a few polymers that satisfy these criteria are described in the literature [51]. The common SMP's surpass the metallic shape memory alloys in their shape-memory properties of maximum strain. Table 10.3 is a comparison of SMA and SMP materials showing the high maximum strain of the SMP, but with lower stress generating capacity compared to SMAs due to their lower stiffness.

Actuator type	Max. Strain (%)	Max . stress (MPa)	Specific elastic energy density (J/g)	Elastic energy density (J/cm^3)	Maximum efficiency (%)	Specific density (g/cm^3)
NiTi	>5	>200	>15	>100	<10	6.5
Polymer	100 - 400	4	2	2	<10	1

Table 10.3 Comparison of the main properties of the SMA and SMP

The first SMP introduced the 1960s was the polyethylene, which is covalently cross-linked by means of ionizing radiation. However, SMPs was recognized as potentially attractive materials for actuators in the 1990s [52]. The next SMP was copolymer polyurethane along with terephthalate, polystyrene, poly(1,4-butadiene), polyethylene oxide etc. A thorough review of the SMPs can be found in [53].

The range of application of SMP actuation stimuli is far wider than for SMA which generally use heat as the stimulus. Apart from heat, SMP materials can be actuated with light [54], water [55] and magnetic field [56]. This property enables a new opportunities in the advanced MST actuators.

10.4 SMP applications in MST

Due to relatively easy manufacturing processes and simple programming procedures of shape-memory polymers, these materials represent a cheap and efficient alternative to SMA. SMP find the broad spectrum of application that covers an area from minimally invasive surgery, through high-performance textiles, up to self-repairing plastic components. Although SMP materials display attractive properties for the

microactuators, SMP have only limited application in the MST technology to date. One of the few applications of the SMP in micro devices is shown in the Figure 10.4, which show optical images of an active microfluidic reservoir during operation. The shape change of the SMP leads to black fluid travelling along the reservoir. It is expected that SMP will have more important role for microactuators in the future.

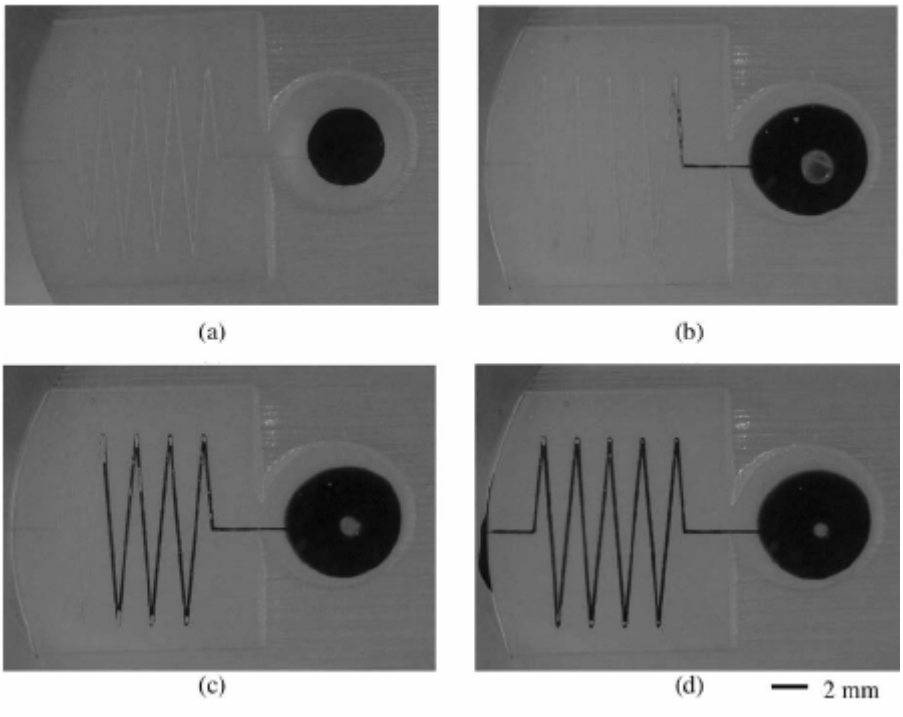

Figure 10.4 Optical images of the active 2mm diameter microfluidic reservoir during operation. [57]

Conclusion

To conclude, a summary of the main properties and the difference between metallic and polymer memory materials will be made. The metallic memory materials (SMA) can deliver high force and have higher energy density. In contrast, the polymer materials (SMP) have a maximum strain that is two orders in magnitude lager than that of metallic materials.

The manufacturing technologies for MST applications are also very different. The metallic materials, mostly the NiTi alloy are made by sputter deposition. The characteristics of the deposited film are extremely sensitive to the processing parameters. The polymer memory materials are often spin coated onto a substrate and polymerized by thermal annealing

The actuation stimulus for metallic materials in MST applications is generally a temperature rise. Note that magnetic shape memory materials are discussed in a separate section. For polymeric materials, specific compositions exists that can be actuated with heat but also with light, magnetic fields, water or they can respond to chemical reagents. This versatility sets them apart and it offers new possibilities in microtechnology for the design of actuators or sensors.

[1] Otsuka, K., Ren X.: Progress in Materials Science 50 (2005) 511–678

[2] Spakovsky, Von M.R. and Olsommer, B., Fuel System Modeling and Analysis, Perspectives for Fuel Cell Development, ECOS, 1999.

[3] Humbeeck J. V., Kustov S.: Active and passive damping of noise and vibrations through shape memory alloys: applications and mechanisms, Smart Mater. Struct. 14 (2005) S171–S185

[4] Ikuta K, et al. Proc. IEEE MEMS Workshop 1991, 103-108.

[5] Leppaniemi, Ari. “Shape Memory Alloys – Applications and Commercial Aspects”. 8/29/04. http://www.ad.tut.fi/aci/courses/76527/seminars2000/sma.pdf

[6] Zhao, C. Shape memory stainless steels. Advanced materials & processes, February. 2001

[7] Stalmans R., et al.: *Adaptive Composites with Embedded Shape Memory Alloy Wires;* ibid, pp. 801-804

[8] Krulevitch P. et al.: *Thin Film Shape Memory Alloy Microactuators*, Jour. of Micromech. Sys. Vol. 4. Dec. 1996

[9] Walker J.A., et al., "Thin-film Processing of TiNi Shape Memory Alloy", Sensors and Actuators, vols. A21-A23, p. 243-246, 1990

[10] Busch J.D., et. al., "Shape-memory properties in Ni-Ti sputter deposited film", J. Appl. Phy., vol. 68 (12), pp. 6224-6228, Dec. 15, 1990

[11] Grummon D.S., et al., "Thermotractive titanium-nickel thin films for microelectromechanical systems and active composites", Mat. Res. Soc. Symp. Proc., vol. 459,pp. 331-342, 1997

[12] Miyazaki S., et al., "Shape memory characteristics of sputter-deposited Ti-Ni base thin films", SPIE, vol. 2441, pp. 156-164, 1995.

[13] Ishida A., et al., "Shape memory behavior of Ti-Ni thin films annealed at various tempertures", Mat. Res. Soc. Symp. Proc., vol. 360, pp. 381-386, 1995

[14] Ishida A., et al., "Effect of heat treatment on shape memory behavior of Ti-rich Ti-Ni thin films", Materials Transactions, JIM, vol. 36, No. 11, pp. 1349-1355, 1995.

[15] Miyazaki S., et al., "Effect of heat treatment on deformation behavior associated with R-phase and martensitic transformations in Ti-Ni thin films", Trans. Mat. Res. Soc. Jpn., vol. 18B, pp. 1041-1044, 1994

[16] Peter J. A., "Deposition parameters for sputter-deposited thin film TiNi", Mat Res. Soc. Symp. Proc., vol. 360, pp. 293-298, 1995

[17] Miyazaki S., et al., "Development of perfect shape memory effect in sputter-deposited Ti-Ni thin films", Proceedings IEEE Micro Electro Mechancial Systems, pp. 176-181, 1994

[18] Gyobu A., et al., "Martensitic transformations in sputter-deposited shape memory Ti-Ni films", Mat. Trans. JIM, vol. 37, No. 4, pp. 697-702, Apr. 1996.

[19] Favalukis J., et al., "An Experimentally Validated Thermal Model of Thin Film NiTi", Proceedings of SPIE, vol. 3668, Part Two, pp. 617-629, Mar. 1-4, 1999

[20] Chernysh V.S., et al., "Angular distributions of Ni and Ti atoms sputtered from a NiTi alloy under He+ and Ar+ ion bombardment", Nuclear Instr. And Methods in Physics Research B 140, pp. 303-310 (1998).

[21] Neshev I., et al., "Sputtering of NiTi alloys: a comparison of experiment and simulation", Vacuum vol. 44, Nos. 3-4, pp. 209-212 (1993).

[22] Ken K. Ho, et al., "Modeling and measuring the response times of thin film TiNi", SPIE Proceedings Smart Mat. Tech., vol. 3040, San Diego, CA, Mar. 3-4 1997, pp. 10-22

[23] Quandt E. et al., Sensors and Actuators A53 (1995) Sputter Deposition of TiNi and TiNiPd Films Displaying the Two Way Shape Memory Effect.

[24] Bendahan Marc et al., "NiTi shape memory alloy thin films: composition control using optical emission spectroscopy", Thin Solid Films 283 (Sep. 1996), pp. 61-66.

[25] Krulevitch, P. et al., "Mixed-sputter deposition of Ni-Ti-Cu shape memory films", Thin Solid Films 274 (Mar. 1996), pp. 101-105.

[26] Miyazaki, S., et al., "Martensitic transformations in sputter-deposited Ti-Ni-Cu shape memory alloy thin films", Thin Solid Films 281-282 (Aug. 1996) pp. 364-367.

[27] Chen, J.Z., "Crystallization behavior of r.f.-sputtered TiNi thin films", Thin Solid Films 339 (Feb. 1999). pp. 194-199

[28] Ho, Ken et al., "Sputter deposition of NiTi thin film exhibiting the SME at room temperatures", Proceedings of the Symposium, 1998 ASME International Mechanical Engineering Congress and Exposition, Nashville TN, Nov. 14-19, 1999

[29] Gabry, B., et al., "Thermodynamic modeling of the recovery strains of sputter-deposited shape memory alloys Ti-Ni and Ti-Ni-Cu thin films", Thin Solid Films 372 (Sep. 2000), pp. 118-133

[30] Ho, Ken K. et al., "Sputter deposition of NiTi thin film shape memory alloy using a heated target", Thin Solid Films 370 (Jul. 2000), pp. 18-29.

[31] Wibowo W, Kwok C Y,: Fabrication and characterization of sputtered NiTi shape memory thin films, J. Micromech. Microeng. 16 (2006) 101–108

[32] Mezzanotti F. and Salvia M.; *Actuation properties of adaptable hybrid composites with embedded wires of shape memory alloys;* in: Smart Materials and Structures edited by G.R. Tomlinson and W.A. Bullough, IoP Publishers, 1998, pp. 801-804

[33] Stalmans R Humbeeck J. V,.: *Shape Memory Alloys: Functional and Smart*, Seminar Smart materials and technologies - sensors, control, systems and regulators, October 1995, Prague, Czech Republik,

[34] Hodgson, D.E.: Shape Memory Alloys, Avaiable from - Shape Memory Applications Inc, Maude Ave., Suite 603, Sunnyvale, CA 94086, USA

[35] Ray C.A., et al., "A Silicon-based shape memory alloy microvalve", Mat. Res. Soc. Symp. Proc., vol. 276, pp. 161-166 (1992)..

[36] Kuribayashi K., et al., "Trial fabrication of micron sized arm using reversible TiNi alloy thin film actuators", Proceedings of the 1993 IEEE/RSJ International Conf. On Intel. Robots and Sys., Yokohama, Japan, pp. 1697-1702, Jul. 26-30, 1993

[37] Kuribayashi K., et al., "Micron sized arm using reversible TiNi alloy tin film actuators". Mat. Res. Soc. Symp. Proc., vol. 276, pp. 167-175, 1992

[38] Bernard W.L., et al., "Thin film shape memory alloy actuated micropumps", J. of Microelectromechanical Systems, vol. 7, No. 2, pp. 245-251, Jun. 1998.

[39] Wolf R.H., et al., "TiNi (Shape Memory) Films on Silicon for MEMS Applications". J. of Microelectromechanical Systems, vol. 4, No. 4, pp. 206-212, Dec. 1995.

[40] Ho C. M, et al., "Mems: Science and Technology," Application of Microfabrication to Fluid Mechanics, FED V. 197, ASME 1994, pp. 39-49, 1994.

[41] Su Q, et al., "Martensitic transformation in Ni50Ti50 films", SPIE vol. 2189, pp. 409-412 (1994).

[42] Surbled, P. et al., "Shape memory alloys for micromembranes actuation", LIMMS/CNRS-IIS, Institute of Industrial Science, University of Tokyo 7-22-1 Roppongi, Minato-ku, Tokyo 106-8558, Japan,

[43] Ken K. Ho, John. J. Gill and Gregory P. Carman, "Sputter deposited NiTi thin film SMA for active flow control",

[44] Johanson A, : Thin film shape-memory technology: A tool for MEMS, Micromachine Devices 4(12), 1999, 1 - 3

[45] Buchaillot L, Nakamura Z,. Nakamura S,. Fujita H, Miyazaki S, “Thin film SMA actuators for MEMS applications”, Mecatronics’96, 2, pp. 627-630, Besançon, France, 1996

[46] E. Makino E, Mitsuya T, Nakatsuji T,. Shibata T, “Patterning and bonding of TiNi shape memory thin film for fabrication of micropump”, Symposium on Design, Test and Microfabrication of MEMS/MOEMS, SPIE, Paris, France, pp. 1030-1037, 1999

[47] Kahn H. et al: *The TiNi shape-memory alloy and its applications for MEMS*, J. Micromech. Microeng. 8 (1998) pp. 213–221

[48] Barth P.W., “Silicon microvalves for gas flow control”, 8th Conference on Solid-State Sensors and Actuators, Transducers’95, Stockholm, Sweden, 2, pp. 276-279, 1995

[49] Gill, J J, et al: Manufacturing issues of thin film NiTi microwrapper, Sensors and Actuators, A 93 (2001) 148 - 156

[50] Matovic J. , Vujanic A,. Kment C., Reichenberger K.; Space Flower: the bionic system for satellite thermal regulation, Second International Conference on Design & Nature, Rhodes 2004

[51] Sillion B.: Shape memory polymers, Act. Chimique, vol. 3, pp.182–188, 2002
[52] Osada Y., and A. Matsuda, Shape-Memory Gel with Order-Disorder Transition, Nature, 376, 219, 1995

[53] Lendlein A.., Kelch S. *Shape-Memory Polymers,* Angew. Chem. Int. Ed. 2002, 41, pp. 2034 / 2057 WILEY-VCH Verlag GmbH, 69451 Weinheim, Germany

[54] Lendlein A, Jiang H, Ju O, Langer R,: Light-induced shape-memory polymers, Nature, Vol. 434, 14 April 2005
[55] Huang, WM, Yang, B, An, L, Li, C and Chan, YS, Water-driven programmable polyurethane shape memory polymer: demonstration and mechanism, Applied Physics Letters, Vol. 86, 2005, 114105

[56] Conti S., Lenz M., Rumpf M, Modelling and simulation of magnetic shape-memory polymer composites, to be published 2006

[57] Gall K, Kreiner P, Turner D, Hulse M, :Shape-Memory Polymers for Microelectromechanical Systems, J. of Microelectromechanical Sys., Vol 13, No. 3, June 2004

11 Expandable microsphere composites

Björn Samel, Wouter van der Wijngaart – Microsystem Technology, School of Electrical Engineering, Royal Institute of Technology (KTH), Stockholm, Sweden.

Expandable microspheres are small plastic particles, which expand when heat is applied. The microspheres consist of a gas tight thermoplastic shell, which encapsulates a small amount of a liquid hydrocarbon, e.g. isobutane or isopentane. The dramatic expansion of the microspheres when heated is due to the fact that the liquid hydrocarbon is transformed into a gas. The shell of the expandable microspheres is made of copolymer precursors (monomers), for example, vinylidene chloride and acrylonitrile together with methylmethacrylate. When the microspheres are heated the thermoplastic shell softens and the liquid hydrocarbon inside the shell transforms into a gas, which increases its pressure. This results in a dramatic irreversible expansion of the microspheres (typical diameter values: from 10 to 40 μm), with a corresponding dramatic decrease of the density (typical values: from 1000 to 30 g/l). When fully expanded, the volume of the microspheres increases more than 60 times (Figure 11.1a). After cooling down, the microspheres do not shrink because the thermoplastic shell hardens again and thus, the dramatic volume increase is irreversible.

The expandable microspheres are commercially available with expansion temperatures in the range of 80–190degC, see Figure 11.1b [1]. At temperatures above the temperature at which the highest expansion is obtained the microspheres gradually collapse. The expandable microspheres can be used in contact with many chemicals, including solvents without negative effects on expansion. The available microsphere sizes range from 6 to 90 μm in diameter (weight average diameter). Expandable microspheres are today used in a wide variety of applications in the macro-scale. Some examples include printing inks used to form topographical patterns on paper, in reaction injection moulding to counteract the shrinkage of polyurethane, and in a method to decrease the density of plastics through a controlled and predictable foaming process [1].

Expandable microspheres are manufactured by a number of industrial groups, including Expancel and Sekisui [1]. All experiments described in this section were performed with Expancel® beads.

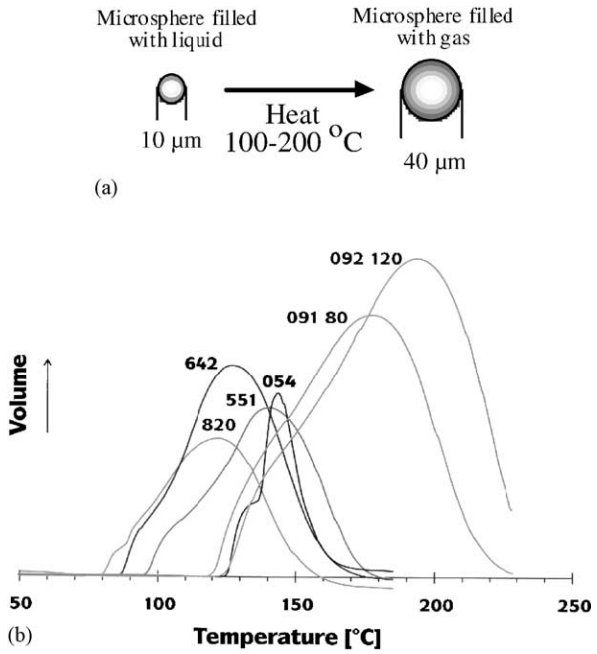

Figure 11. 1 (a) A schematic of the expansion principle of the expandable microspheres; (b) A graph showing the different expansion intervals for different types of expandable microspheres [1].

In 2002, expandable microspheres were introduced as a novel actuator material within microsystem technology. This novel microactuator material has especially proven its performance in the field of microfluidics. Five specific technologies for the system integration of the actuator have been proposed: 1) direct mixing of the microspheres in liquid, 2) surface immobilization of the microspheres by incorporation in photoresist or 3) through self-assembly on a chemically altered surface, 4) through incorporation in a paste and 5) through incorporation as a composite in a polymer matrix.

In this section we will discuss these five methods and some of the applications realized with them, including single-shot valves and pumps.

11.1 Direct mixing of the microspheres in liquid

The perhaps most straightforward approach to incorporate expandable microspheres as a microfluidic actuator material involves the mixing of the expandable microspheres in liquid prior to addition to a microfluidic system. A mechanical barrier in the microchannel traps, i.e. localizes the position of the actuator beads to a predefined area on-chip. Heating the liquid, either locally via a built-in heater or by heating the entire system, triggers the expansion of the microspheres and accomplishes the microfluidic actuation.

This method was proven successful for both pumping and valving of liquid [2]. The pump and valve system can be realized with nearly identical microstructures. They consist of a channel that contains a mechanical barrier (filter) for the microbeads, thus localizing them in a predefined area on-chip. The exact layout of the microfluidic device determines whether such a system works as a pump or as a valve, as illustrated in Figure 11.2.

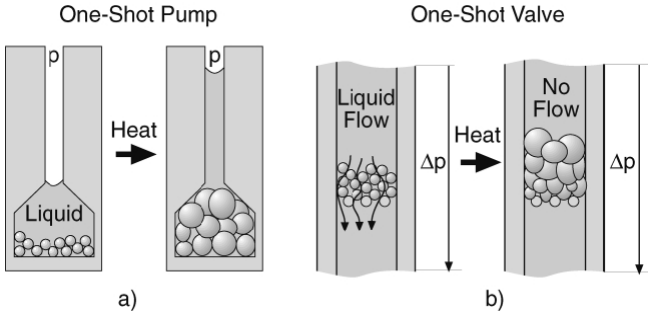

Figure 11.2: Two concepts for liquid handling by Expandable microspheres: (a) is a one-shot pump; (b) a normally open one-shot valve [2].

Test structures consisting of silicon microchannels covered by a glass lid were evaluated as valves where each channel has openings on both sides. Pumps were configured by sealing one opening of the microchannel with UV curing epoxy (Epotek OG 198).

The width of the inlet channel is typically 100 or 200 µm, the width of the outlet 20 or 50 µm. The depth of both channels is 50 µm.

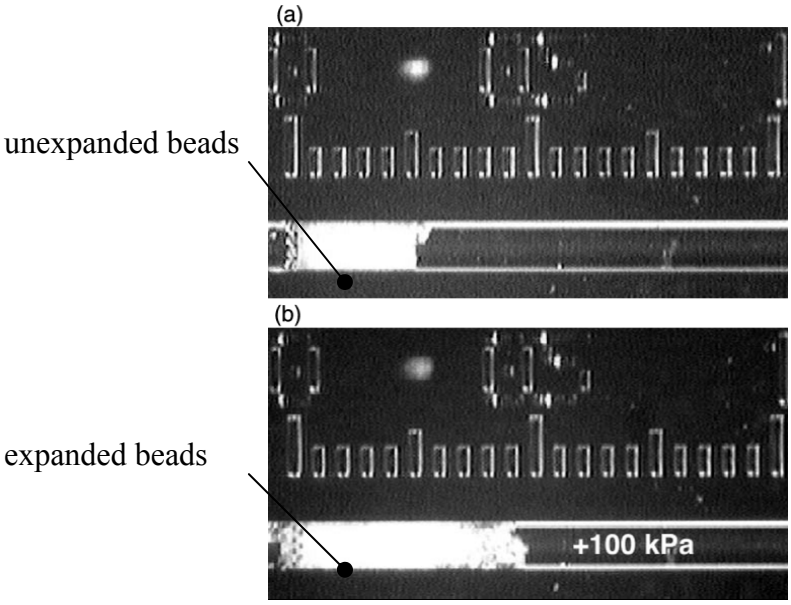

Figure 11.3 Micrographs showing a bead pack before (a) and after (b) a 70 °C heat treatment at 100 kPa counter pressure in a 200µm wide channel. The total expansion is 1.4 nl.

Liquid handling in microfluidic channels has been demonstrated as shown in figure 11.3. Water in the nanoliter range was displaced in a microchannel against a counter pressure of 100 kPa (*i.e.*, the microspheres act as a one-shot pump). The flow of water in a microchannel was completely blocked (*i.e.*, the microspheres act as a one-shot normally open valve).

11.2 Surface immobilization of the microspheres by incorporation in photoresist

The microspheres can also be patterned and immobilized on a surface. Two technologies were developed for this purpose. In a first approach, the microspheres can be mixed in photoresist, and subsequently patterned. Best results were obtained using a lift-of process in a two-step spin process, see Figure 11.4.

Two methods for selective immobilization of expandable microspheres without the use of mechanical barriers have been studied for their application in microfluidics, including patterning by photolithography and microcontact printing combined with self-assembly based on surface chemistry.

The microspheres were deposited on the surface of silicon wafers by a process based on a positive photoresist from Shipley (Microdeposit S1813).

Some of the microspheres remained on the exposed area even though the photoresist was dissolved as can be seen in Figure 11.4a. The remaining microspheres could be removed by overdeveloping the wafer, however the selectivity to the unexposed area is then drastically decreased. Therefore, a layer of pure S1813 photoresist was first deposited, to serve as a release layer for the microspheres in the exposed area. This enabled removal of all microspheres from an exposed area after a development of 1.25 min, see Figure 11.4b. The expandable microspheres were found to be transparent to the UV light used during the exposure. Hence, the microspheres did not shadow the photoresist and no distortion of the pattern was observed

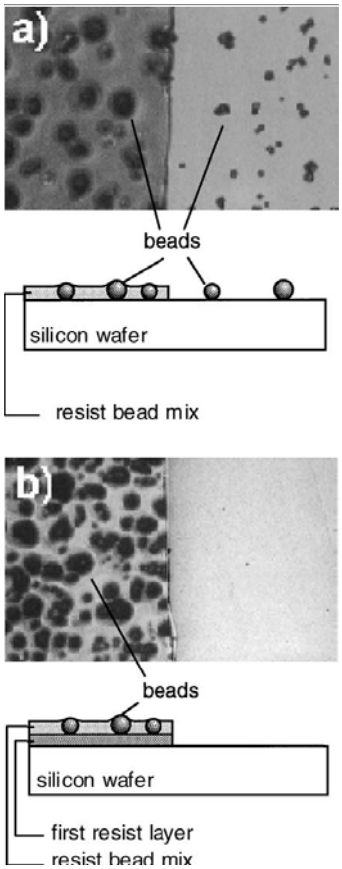

Figure 11.4. (a) Photo showing that some microspheres remained on the unexposed area even though the photoresist was dissolved. (b) When using a pure photoresist layer as release layer all microspheres were successfully removed in the exposed area [3].

Figure 11.5 shows selectively deposited expandable microspheres on a silicon wafer, using the photoresist technique described above, before (a) and after expansion, (b) and (c). The shown pattern is a test pattern consisting of 100 μm pitched stripes. The expansion of the microspheres increases the thickness of the microsphere layer and alters the pattern-features to some extent as depicted in Figure 11.5c. It was found that

the density of deposited microspheres, i.e. the number of microspheres per area, can be influenced by varying the amount of microspheres per photoresist volume or by varying the spin speed. This technique can also be applied to form patches of photoresist/microspheres on structured substrates, i.e. in etched channels. The channels can then be sealed, using a low temperature bonding technique which does not activate the immobilized microspheres, e.g. a PDMS film.

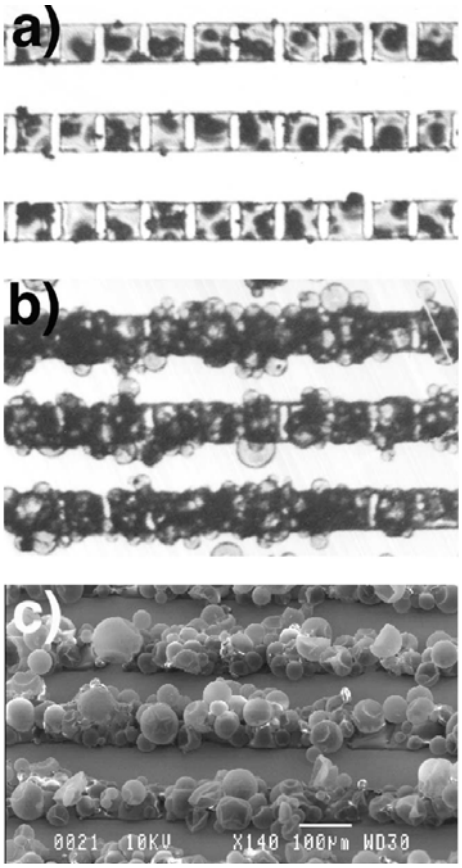

Figure 11.5 Photos showing selectively deposited expandable microspheres before (a) and after (b/c) expansion. The horizontal lines are 100 µm wide and the vertical short lines are 15 µm wide [3].

11.3 Surface immobilization of the microspheres through self-assembly on a chemically altered surface

Alternatively, the microspheres can also be patterned using self-assembly based on surface chemistry [4] utilizing micro contact printing technology. Hydroxy-functionalized beads have previously been immobilized on silicon substrates by means of surface chemistry. The beads were thought to be covalently bound to the substrate via ester bond formation between the anhydride-functionalized surface and the hydroxy groups on the beads. This assumption was corroborated by the fact that the beads did not attach when the printed 4-(chlorosulfonyl) benzoic acid is not transformed into anhydride. The surface chemistry of the expandable microspheres is currently not known. However, the same methodology as for the hydroxy-functionalized beads was applied for immobilization of the expandable microspheres. In Figure 11.6, a scanning electron microscope (SEM) photo of an immobilized monolayer of (unexpanded) expandable microspheres is shown. No microspheres were found outside the printed

anhydride pattern showing that the microspheres can be patterned using this methodology. In Figure 11.7, a SEM photo of expanded microspheres is shown. The microspheres remained bound to the substrate during and after the expansion. The immobilized microspheres (both unexpanded and expanded) could withstand rigorous washing in water. Preliminary experiments show that it is also possible to immobilize monolayers of expandable microspheres in deep reactive ion etched channels.

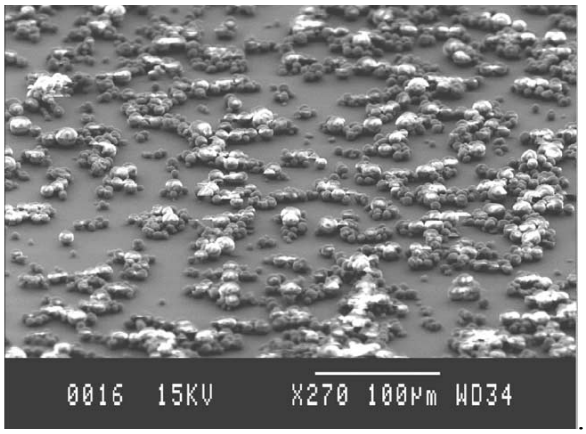

Figure 11.6: A SEM photo of an immobilized monolayer of unexpanded microspheres by using self-assembly based on surface chemistry [3].

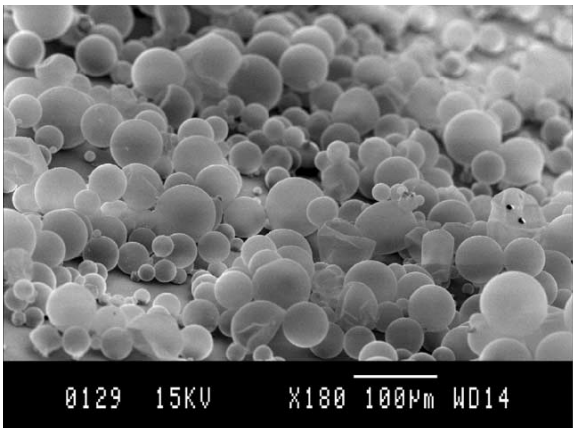

Figure 11.7: A SEM photo of microspheres, expanded after immobilisation by surface chemistry [3].

In such an application the expandable microspheres might be used to coat the internal walls of microfluidic channels in order to enlarge the reactive surface area. It should also be possible to chemically modify the surface groups on the microspheres in a variety of ways for screening and analysis within the fields of biochemistry and organic chemistry.

11.4 Incorporation of the microspheres in a paste

For mesoscopic applications (mm-range to cm-range), the microspheres can be incorporated in a paste. Such “active paste” is suited for integration during device assembly. A successful actuator approach was shown by mixing of microspheres and glycerine [5]. Fabrication and testing of a thermally actuated one-shot liquid dispenser as an uncomplicated, fully functional, low cost device for use in medical disposables was shown.

The dispenser was designed for one-shot usage and made to meet requirements of disposable drug delivery system. Hence, all device components are made out of low cost materials and adapted for processes with the potential for high volume batch fabrication. Figure 11.8 shows a schematic view of the device. A small portion of an expandable paste containing Expancel ® microspheres and Glycerine is heated from the bottom side. When the paste reaches a temperature of 70 degC it gradually expands into the liquid container. The liquid, separated from the paste by a thin elastic membrane, is pushed out as the expanded paste fills the whole container. Since volume expansion of the paste is manyfold, the heat conduction in the paste gradually drops to a considerably lower level, preventing the dispensed liquid from extensive heating. Figure 11.9 depicts the disassembled device before and after expansion.

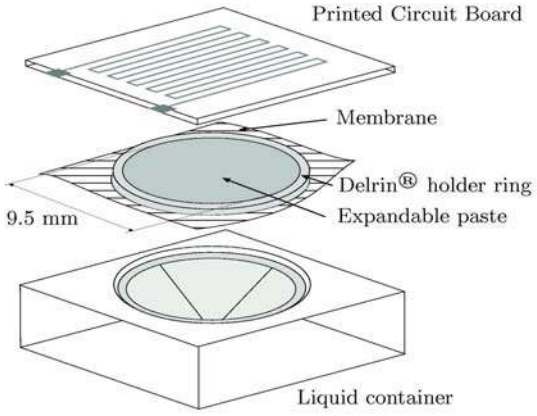

Figure 11.8 Schematic view of the device. The ring with the expandable paste together with the membrane is clamped into the liquid container, thereby stretching the membrane to become flat [5].

Figure 11. 9: Photographs showing the paste a) unexpanded (state before actuation), b) expanded (state after actuation; liquid container removed for visualization) and c) expansion without constraining liquid container results in a volume expansion of seven times the original volume [5].

11.5 Incorporation of the microspheres as a composite in a polymer matrix

For Large Scale Integration (LSI) of microfluidic actuators, it was proposed [6] that expandable microspheres are mixed in an elastomeric polymer matrix prior to application to the system. When incorporating the expandable microspheres (XB) in Poly(dimethylsiloxane) (PDMS) as the matrix the resulting composite material (PDMS-XB) entails the merits of both PDMS and expandable microspheres.

In order to investigate replication molding techniques a master for replica molding was photolithographically manufactured using the positive photoresist AZ-4562 from Clariant. 35µm deep structures were fabricated using standard lithography equipment to

evaluate whether the composite retains the characteristic of pure PDMS to replicate features of the master with high fidelity. In the liquid pre-polymer state the composite was poured onto the mold, degassed for 5 minutes in vacuum, cured and eventually peeled off the master. Figure 11.10 shows the high-resolution imprint of the replica-molded structure in the novel composite. Apparently, the novel composite is well suited for replica molding techniques, which significantly increases the design freedom of microfluidic components.

The basic property of the composite was investigated by means of a fluidic application and evaluated whether the composite completely fills out voids upon heating. A thin film of the composite was spun on a wafer and covered with a plastic replicated diffuser micropump with a depth of 80µm serving as a precisely defined volume. To simplify matters expansion was effectuated all-over using a hot plate. The reservoir volume was consequently filled out. Subsequent removal of the rigid reservoir revealed the expanded composite showing both its expansion potential and its capability of filling out deep as well as small voids. The latter was verified by the fact that the height of the expanded composite conforms to the depth of the reservoir (Figure 11.11).

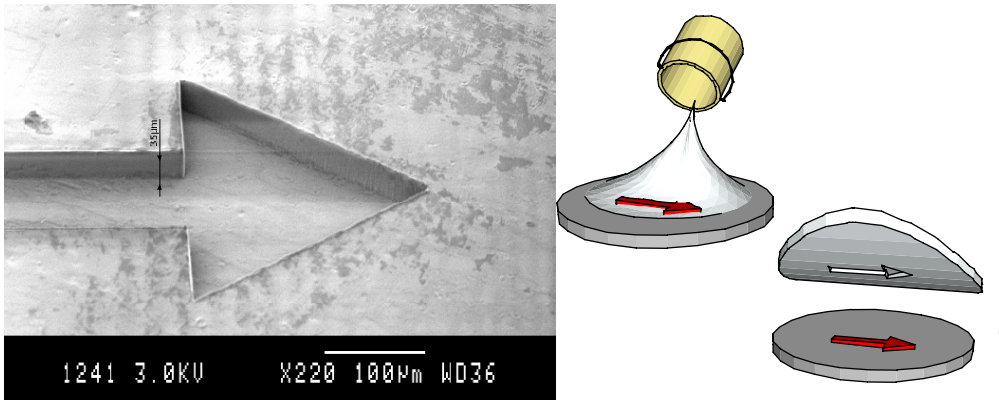

Figure 11.10: SEM picture of the unexpanded PDMS-XB composite after imprinting an arrow-shaped mold into the composite [6].

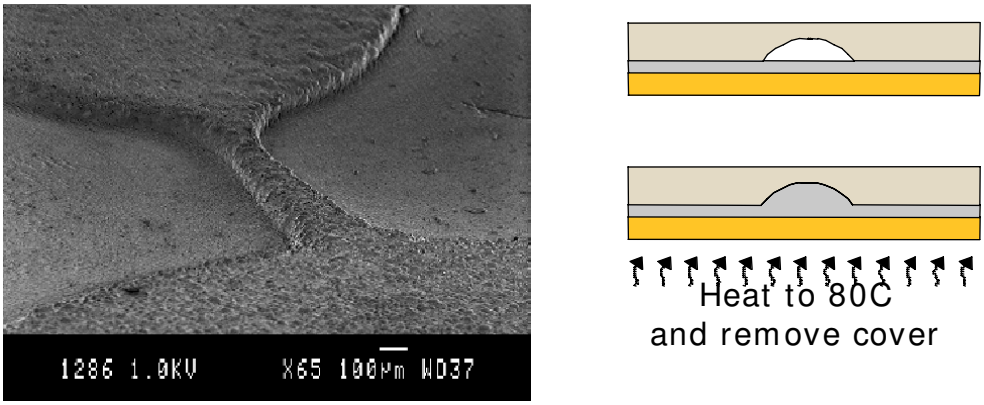

Figure 11.11: SEM picture of the expanded composite after expansion inside another, 80 µm deep mold and subsequent removal of the mold [6].

Single-use microfluidic pumps were fabricated in a multilayer fashion and show the displacement of liquids in the nanoliter range [7]. Localized heating is achieved through resistive heating elements patterned on a printed circuit board (PCB). All photolithographical fabrication steps use high-resolution transparencies. The PDMS-

XB composite is obtained by thoroughly mixing PDMS base, curing agent (typically at 10:1 (v/v) base:curing agent) and XB at a concentration of 250mg/ml liquid PDMS pre-polymer. A layer of the PDMS-XB composite is spun onto the patterned PCB at 750rpm and subsequently degassed in vacuum and crosslinked at room temperature. An additional thin layer of the liquid PDMS pre-polymer is spun on top of the cross-linked composite at 2500rpm.

Microfluidic channels and reservoirs are formed in PDMS by replica molding. The master was fabricated using Shipley SJR 5740 photoresist on a silicon wafer to yield inverse structures. Subsequent heating to 200°C makes the inverse structures reflow which results in structures that are curved at the edges. Liquid PDMS pre-polymer is spun onto the master at 500rpm, cured at 110°C for 20min and eventually peeled off the master.

The molded PDMS channels and reservoirs were bonded to the previously fabricated stack of PDMS/PDMS-XB/PCB by oxidizing both surfaces in oxygen plasma and bringing them into conformal contact.

Access holes were punched out of the elastomeric layers and aligned to fluidic ports in a PMMA plate. For increased structural stability, an additional PMMA plate was attached to the bottom. The multilayer structure was tightened with screws providing sufficient backing for the flexible PDMS layers.

An on-chip liquid reservoir was filled with small amounts of water and green dye under vacuum. As sufficient power is applied to the system, the composite locally expands upon dissipated heat from the integrated heater and liquid stored in the reservoir is consequently released into the microchannel as shown in Figure 11.12.

Moreover, liquid flow in microchannels is entirely blocked by means of integrated valves. The devices are fabricated using low cost materials only and the concept allows for wafer-level processing. This microfluidic liquid handling concept with on-chip active components is highly integrable and does not require external actuators.

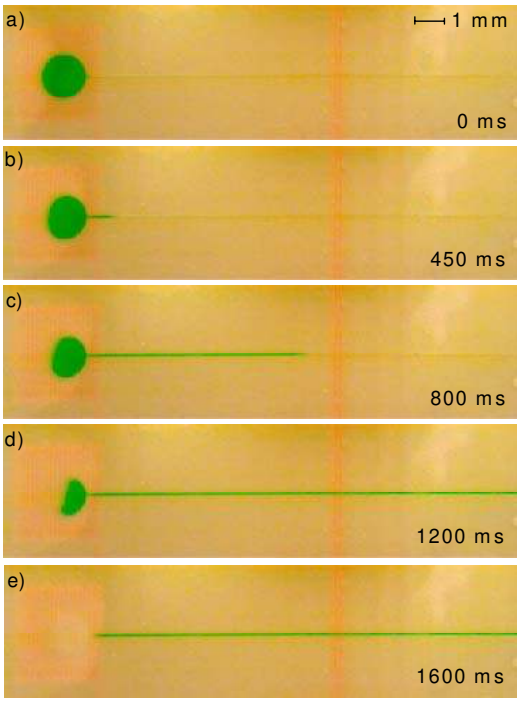

Figure 11.12: Picture sequence (a-e) showing the release of 24 nl of liquid from a reservoir. The reservoir is completely depleted after 1.6 seconds [7].

[1] Expancel Microspheres, "An Introduction", www.expancel.com ; http://www.sekisui.com.sg/product_pages/adp/

[2] Griss, P., Andersson, H., Stemme, G. "Expandable Microspheres for the Handling of Liquids." *Lab-on-a-Chip* 2002, 2 (2), 117-120.

[3] H. Andersson, P. Griss, and G. Stemme, "Expandable microspheres – surface immobilization techniques", *Sensors and Actuators B: Chemical*, vol. B84, no. 2–3 (2002) 290–295.

[4] A. Kumar, H. Biebuyck, G. Whitesides, "Patterning self-assembled monolayers: applications in material science", *Langmuir 10* (1994) 1498–1511.

[5] N. Roxhed, S. Rydholm, B. Samel, W. van der Wijngaart, P. Griss and G. Stemme, "Low Cost Device for Precise Microliter Range Liquid Dispensing", *17th IEEE International Conference on Micro Electro Mechanical Systems, MEMS2004*, pp. 326–329

[6] B. Samel, P. Griss, and G. Stemme, "Expandable microspheres incorporated in a pdms matrix: A novel thermal composite actuator for liquid handling in microfluidic applications," in *Transducers'03 The 12th International Conference on Solid-State Sensors, Actuators and Microsystems*, pp. 1558–1561.

[7] B. Samel, J. Melin, P. Griss, G. Stemme, "Single-use Microfluidic Pumps and Valves Based on a Thermally Responsive PDMS Composite" *18th IEEE International Conference on Micro Electro Mechanical Systems, MEMS2005,* pp.690-693.

12 Electro-active Polymers – A General Introduction

Chantal Khan Malek – Laboratoire FEMTO-ST, Département LPMO, Besançon, France

Active polymer systems can be used to create smart structures that can be elastically deformed in three dimensions in a controlled manner through a variety of stimuli to produce forces and displacements. Due to the convenience and practicality of electrical stimulation, substantial interest exists in Electro Active Polymers (EAP) which exhibit large shape and/or size changes in response to electrical excitation [1-4].

Two families of electro-active polymers exist namely electronic polymers and ionic polymers. Electronic polymers (‘*dry’ polymers*) are characterised by a high dielectric breakdown strength and in operation they require a high activation field (> 150 V/mm), which is applied directly to the polymer. The efficiency of electro-mechanical coupling is strongly influenced by the mechanical properties of the polymers themselves. They can maintain an induced displacement under activation of a DC electric potential and they can be operated in air, which is compatible with robotic applications. Examples of such polymers are: dielectric elastomers, ferroelectric polymers [e.g. poly-(vinylidene fluoride-trifluoroethylene, PVDF-TFE] and some electrostrictive polymers. In contrast, so-called ionic polymers rely on the mobility of ions and electro-chemo-mechanical coupling. They generally require a wet environment; hence they are referred to as *‘wet’ polymers.* The applied electric potential acts on an electrolyte, involving motion of both ions and solvent in the actuation process. This effect is exploited to create a structural and volume changes. Ionic polymers can be operated at relatively low driving voltages (1-10 V/mm). Large displacements and large forces are possible and whilst they are more versatile, such systems tend to be much more complicated than electronic polymers, mainly due to the wet environment and the complexity of the compounds used to provide electro-chemo-mechanical coupling Ionic polymers encompass a large variety of materials such as: polyelectrolyte gels; ionomeric polymers and conducting polymers (CP), featuring conjugated structures such as polyacetylene, polyaniline, polypyrrole, and polythiophene (and its derivatives). A composite form of ion-exchange polymer films with metal electrodes called Ion-Metal Polymer Composites (IMPC) (Kim et al. 2004)] are receiving attention for applications such as artificial muscles. Other systems in research include polymer nano-composites (PNC), carbon nanotubes in an electrolyte and molecular actuators [8,9].

Some examples of ionic ‘wet’ polymer systems include:

i) Electroactive-conjugated (CP) polymers. Although these are poor electrical conductors in their natural state, they can be made to incorporate delocalised bonds. This leads to an increase in their conductivity from insulating to semi-conducting to metallic via redox doping, hence their application in electronic circuits. Electrochemically changing the oxidation state leads to changes in charge distribution and ion diffusivity. This can be exploited to produce changes in volume, shape and mechanical properties.

ii) Ionomeric polymers. These consist of ion-exchange membranes such as Nafion® (or Flemion®) are the key components in proton exchange membrane fuel cell and they are commercially available. Nafion is also used as a high performance electroactive polymer gel actuator or sensor. In some

systems the method of operation involves replacement of protons by another cation. This can provide a mechanism for large, rapid bending movements upon an applied voltage [10,11]

Many EAPs require specialized processing methods that prevent them from being co-fabricated with other more traditional materials. Currently this limits and restricts their application. Conducting polymers are an exception in this respect as they can be produced using low temperature techniques and they are rapidly being commercialized. For example polypyrrole can be produced electrochemically and patterned by ink-jet printing methods. Other methods for producing these materials are being explored, including free-form fabrication, which potentially can enable greater geometric freedom in designs and control spatial heterogeneity in material compositions. This offers a possible means of producing electroactive polymer actuators with novel geometries and/or integration with ancillary mechanisms to give both linear and more complex termotions [12]. In addition to process integration, the assessment of the long-term reliability of some electroactive-based components is another issue that remains to be resolved. For example, hydrogels are delicate materials and they often suffer from a limited active lifetime owing to dehydration and leakage during actuation [12].

[1] K. J. Kim and S. Tadokoro (Eds.) "Electroactive Polymers for Robotic Application", Springer (London) November 2006 ISBN 1-84628-371-X
[2] Y. Bar-Cohen, WorldWide Electroactive Polymer Actuators Webhub (on line): http://ndeaa.jpl.nasa.gov/nasa-nde/lommas/eap/EAP-web.htm, JPL NDEAA Technologies Lab (2004).
[3] P. Sommer-Larsen, "Polymer actuators – how do they work?", Proc. Actuator 2004, 9th Int. Conf. on New Actuators, 14-16 June 2004, Bremen, Germany, pp. 681-685.
[4] J. Madden, "Properties of electroactive polymer actuators" Proc. Actuator, 9th Int. Conf. on New Actuators, 14-16 June 2004, Bremen, Germany, pp.338-343, 2004.
[5] S. P. Lacour, H. Prahlad, R. Pelrine, and S. Wagner, "Mechatronic system of dielectric elastomer actuators addressed by thin film photoconductors on plastic", Sensors and Actuators A 111 (2004) 288-292.
[6] J. Bobacka, A. Ivaska, A. Lewenstam, "Potentiometric ion sensors based on conducting polymers", Electroanalysis 15(5-6) (2003) 366-374.
[7] K. J. Kim, J. W. Paquette, D. Leo, and K. M. Farinholt "Ionic Polymer-Metal Composite for Sensory Applications," a review chapter in Encyclopedia of Sensors, Ed. C. A. Grimers and E. C. Dickey, American Scientific Press (ASP), accepted for publication, 2005.
[8] J. D. Nam, H. R. Choi, Y. S. Tak, K. J. Kim, "Novel electroactive silicate nanocomposites prepared to be used as actuators and artificial muscles", Sensors and Actuators A105(1) (2003) 83-90.
[9] J. Chung, K.-H. Lee, J. Lee, "Microfabricated glucose sensor based on single-walled carbon nanotubes", Proc. 17th IEEE Int. Conf. on Micro electro Mechanical Systems (MEMS), Maastricht, 617- 620, January 2004.
[10] K. J. Kim and M. Shahinpoor, Ionic polymer-metal composites: II, Manufacturing techniques", Smart Materials and Structures 12(1) (2003) 65-79.

[11] H. Tamagawa, F.Nogata, T. Watanabe, A. Abe, K. Yagasaki, J.-Y. Jin, “Influence of metal plating treatment on the electric response of Nafion”, Journal of Materials Science, 38(5), pp. 1039-1044 (2003).
[12] E. Malone, H. Lipson “Freeform Fabrication of Electroactive Polymer Actuators and Electromechanical Devices”, Proc. of the 15th Solid Freeform Fabrication Symposium, Austin TX, 697-708, Aug. 2004.

13 Electro-active Polymer Microactuators

Edwin W. H. Jager, Daniel Carlsson - Micromuscle AB, Linköping, Sweden

Electroactive polymers (EAP) are a novel class of active materials that can be used in micro-actuator systems. Commonly the EAPs are divided into two classes: electronic EAP and ionic EAP. *Electronic EAP* comprise dielectric elastomers and electrostrictive polymers [1]. They are dry materials often characterized by their high operating voltages. *Ionic EAP* on the other hand depend on mobile ions to provide the main actuation mechanism. These materials are generally wet and they require relatively low driving potentials. Ionic EAP comprise Ion Polymer Metal Composites (IPMC) [2,3], conducting polymers (CP) [4], carbon nanotubes [5], and electroactive gels. For more details on EAP actuators and devices we refer to [6].

Most of the micro-actuators based on electroactive polymers use conducting polymers (CP) as the active material. These will be reviewed in this section together with some other EAP miniature devices. Pelrine *et al* describe an electrostrictive linear microactuator [7]. Kwok and co-workers have presented sub-millimeter Ionic Polymer Metal Composite actuators [8]. These were made by laser ablation of Nafion® sheets. The smallest actuators that they were able to fabricate were 300µm wide and 3000µm long with 200µm thick fingers. By improving the IPMC processing and using micromachining techniques the same group were able to reduce the size of the IPMC actuators to 100µm wide, 1200µm long and 0,4µm thick [9].

Conducting polymers have a number of properties that make them attractive as EAP microactuators. Some advantages are the low opertating voltages and low power consumption, biocompatibility [10,11], ease of manufacturing and integration with common microfabrication processes [12].

13.1 Conjugated Polymer Actuators

CP microactuators are based on conducting or conjugated polymers that undergo a volume change upon oxidation or reduction of the material. The first devices based on conjugated polymers as the active material were demonstrated in the early 1990's, mostly as bilayer devices [4,13-19]. One layer of the bilayer was typically a passive substrate onto which the electroactive conjugated polymer layer was applied, commonly by electrochemical deposition.

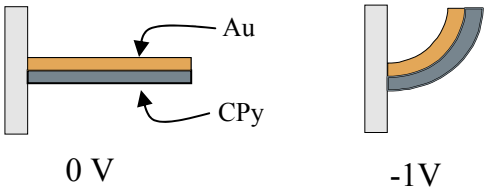

Figure 13.1 - A bilayer actuator consisting of a passive gold layer and a conducting polymer layer, such as polypyrrole. Upon reduction of the CP (-1V) the CP layer expands and the bilayer bends. Upon oxidation, the CP layer contracts and the actuator returns to its previous position.

These bilayer devices were initially used to determine the amount of volume change and to identify the volume change mechanism [19,20]. Bilayers thereby provided a simple way to study conjugated polymers, such as polypyrrole, polyaniline [21,22], and polythiophenes [23]. Under electrochemical oxidation and reduction, the volume change of the active layer causes the entire assembly to bend. The direction of the volume change as well as its magnitude can be deduced from the direction and degree of bending. Such bilayer structures were typically a few centimeters long and a few millimeters wide. Studies showed that the volume change in the conjugated polymer is dominated by ionic movement into and out of the polymer.

Other studies have been done on single conducting polymer fibers or strips submerged in a liquid electrolyte and connected to force/elongation measuring equipment. Speed of actuation, stress and strain were measured, verifying the results from the earlier bilayer studies [16,17,24,25].

As mentioned above, the volume change of conjugated polymers is controlled by the electrochemical processes that cause ion insertion and de-insertion. There are two mechanisms for the ionic flow. For a polymer P doped with large, immobile anions A^- in contact with an electrolyte containing small mobile cations M^+:

$$P^+(A^-) + M^+(aq) + e^- \leftrightarrow P^0(A^-M^+) \quad (1)$$

that is to say, cations can inserted and de-inserted into the polymer. For a polymer P doped with small, mobile anions (a^-) in contact with an electrolyte containing both mobile cations and anions:

$$P^+(a^-) + e^- \leftrightarrow P^0 + a^-(aq) \quad (2)$$

In this case ions inserted and de-inserted are anions. In the former case, the volume expands in the reduced state of the polymer (a negative potential), and in the latter case the volume typically expands in the oxidized state (a positive potential). In the latter case however, there may be two moving species. This is because not only reaction (2) but also reaction (1) may occur. This can lead to “twitching” behavior [20]. For a smooth actuation movement, it is preferred to have only one ionic species transferred. For microactuators, polypyrrole (PPy) doped with the large immobile anion dodecylbenzene sulfonate (DBS) has most commonly been used. This system provides smooth motion, as only cations are used as the moving species, as well as stability and a long life time.

The volume change is brought about by changing the applied electrical potential; in this way changing the oxidation or reduction state of the conjugated polymer. This is not just a bistable system; however, intermediate potentials can also be applied, leading to intermediate redox states and this can produce intermediate volume changes and intermediate bending angles or strains. The potential can be applied both statically and dynamically and the volume change can be repeated a large number of times.

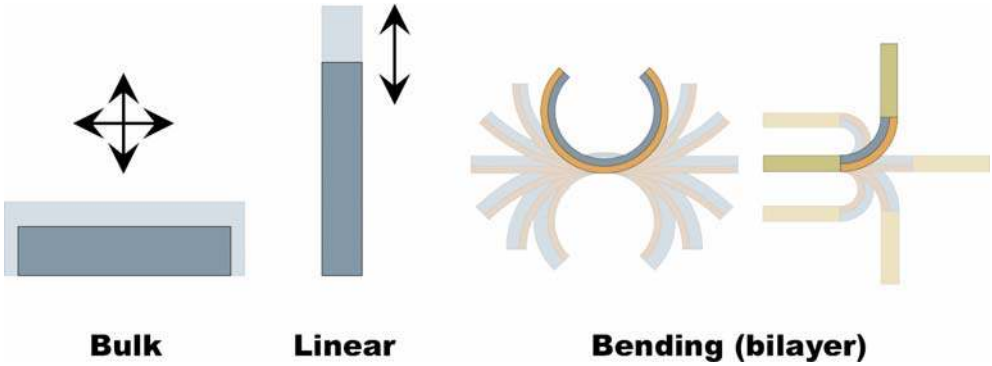

Figure 13.2. The volume change may be utilized in different actuation modes: the bulk expansion can be used as a piston like actuator; the linear strain for linear actuators; and bending motion as a sheet or hinge in bi- or multilayer devices.

Multiple mechanisms are involved in the physical swelling of CPs. The macroscopic volume change of the polymer is mainly due to the combined effect of the insertion of ions and their solvent/hydration shell, which occupies free space within the polymer matrix [19,20]. Moreover, there is also an inflow of solvent, governed by osmosis, with acts to balance the altered ionic concentration inside the polymeric matrix [26]. Thirdly, there are conformational changes and coulombic repulsion acting on the existing polymer backbones which provide an additional contribution to the structural changes [27,28]. The degree of volume expansion and its speed is thus dependent on a number of factors. These include ion types and sizes, ionic concentration, the solvent, the thickness of the CP film and the external voltage applied [26,29,30].

A critical factor for the performance of CP actuators is the ion transport through the film which controls the swelling behaviour. The ion transport process is controlled by ion diffusion but also involves ion migration in response to the electric field [32].

In order to activate the actuators an ion source/sink is needed. In the main aqueous electrolytes have been used and hence these systems are often referred to as being *wet*. These fluids can be salt solutions such as those containing NaDBS or NaCl, and they have analogues in physiological solutions such as cell culture media and blood. In some cases it is preferred to have a "dry system", that is a system that can be operated in air, instead of a liquid. Several ideas for this have been proposed and polymer electrolytes have been demonstrated in macroactuators [33,34]. In these devices, the polymer electrolyte is sandwiched between two CP layers, which generate the bending force. Encapsulation of a complete device using the CP layer, a hydrogel electrolyte, and a counter electrode has been demonstrated [35].

The first PPy based microactuators were PPy/gold bilayer devices made on silicon wafers using standard photolithography. These "fingers" with lateral dimensions in the range of a few millimeters curled when activated [36]. After this initial demonstration, the fabrication process was further developed and the PPy-microactuators were integrated into more complex microsystems such as self-assembling boxes [37], cell clinics [38] and microrobots [39]. A millimeter-scale actuator using polyaniline as the conductive polymer has been presented by Zhou *et al*. [9]. Using standard microfabrication techniques they fabricated bending actuators with dimensions of 0,5mm by 2,5mm and 1mm by 5mm.

13.2 Fabrication of PPy-Microactuators

Standard photolithography and microfabrication methods, including surface and bulk micromachining, are used to fabricate PPy-microactuators. For more details on microfabrication of conducting polymers we refer to reviews such as [40-42].

Conjugated polymers can be deposited in several ways such as casting, dip coating, or spin coating. However, in many cases this approach is limited by the insolubility of the polymer. Alternatively the polymer can be electro-synthesized in-situ from a liquid electrolyte containing the monomer and a dopant salt. The electro-polymerization and deposition of conjugated polymers occurs via monomer oxidation, monomer addition or dimerization and subsequent growth of oligomers and polymers of the oxidized monomer [43]. The chain precipitates out of solution and forms a deposit on the electrode surface where the initial oxidation occurred. The polymer is deposited in the oxidized form, with compensating counter ions incorporated from the electrolyte.

Typically, for the PPy-microactuators, PPy(DBS) is electrochemically deposited onto Au-coated Si wafers from an aqueous electrolyte containing 0.1 M pyrrole and 0.1 M NaDBS. To initiate growth, a potential between 0.5 and 0.6 V vs. Ag/AgCl is applied to the electrode. A higher potential results in faster deposition but also in non-uniform thickness. As a counter electrode, another Au coated Si wafer is used, and as a reference electrode, an Ag/AgCl electrode.

The lateral dimensions of the conjugated polymer components are determined by the patterning step. Standard photolithography can be used in many ways to define the lateral dimensions (Figure 13.3). One can pattern holes or openings in a layer of photoresist that is applied on a conducting surface to protect parts of the surface. The polymer only "grows" on the surface areas that are exposed to the solution. Alternatively one can synthesize the conducting polymer on the whole surface area and remove parts of the polymer by covering the layer with photoresist and subsequent Reactive Ion Etching (RIE) in an O_2/CF_4 plasma. Also one can pattern the electrodes areas first and polymerize the conducting polymer on these patterned electrodes.

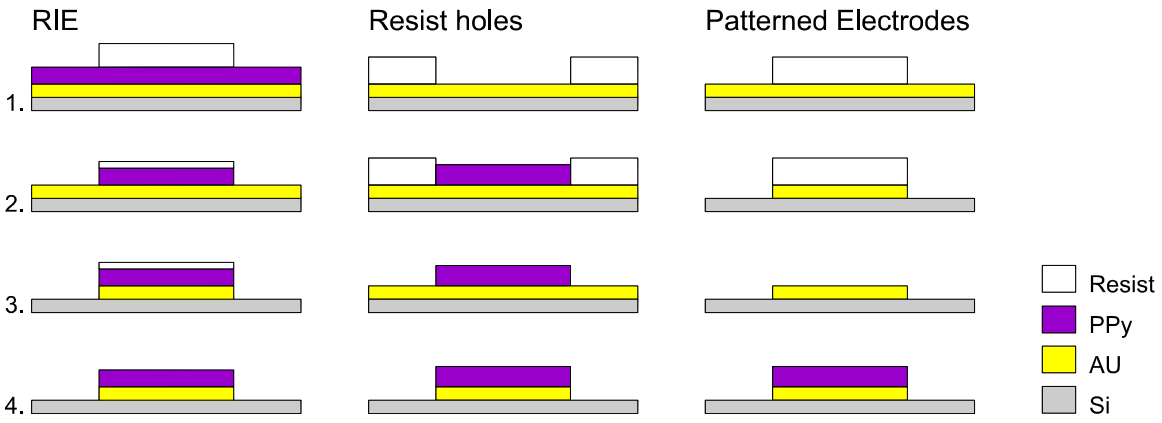

Figure 13.3 Different patterning methods of PPy.

The lower limits to the lateral dimensions of the microactuators are currently enforced by the photolithographic equipment. The smallest actuators that have been made were 10 μm wide and 40 μm long.

After fabrication of the actuators (or complete microsystems) the actuators have to be released. For the release of PPy microactuators three methods have been demonstrated: Differential adhesion, sacrificial layer, and bulk etching (Figure 13.4). The differential adhesion method [44] is based on the poor adhesion between Au and Si. A Cr layer on a Si surface is patterned, resulting in adhesive and non-adhesive areas. Over this surface, an Au layer is deposited, and PPy is electrochemically deposited as described above. The PPy is patterned so that a minor part of the Au/PPy bilayer is in contact with the adhesive Cr layer, and this part functions as an anchor holding the actuator to the surface. The major part of the bilayer is in contact with the Si, to which the Au does not adhere. Activating the bilayer causes it to pull itself free.

Although the differential adhesion method is easy and fast, it is not suited for all designs. For example, it cannot be used to fabricate some individually controlled microactuators. To make individually controlled actuators, the metallic layer of the microactuators is patterned into segments, one for each actuator. These segments are mechanically connected by a resin layer (Benzocyclobutene, BCB, which is a rigid, transparent, conventional polymer similar to polyimide for micromachining applications). This step will cause the resin layer to be in contact with the Si-substrate, and as this resin is adhesive, the microactuators cannot release. For instance, to fabricate the micro-robot [39] the sacrificial layer method had to be used. This is a common method to release object in microsystems. On a SiO_2 covered wafer, a support layer of Ti (the sacrificial layer) was patterned. Next, Cr, Au, and PPy layers were deposited. The microactuators were patterned with a small part overlapping the Si as the anchor point and the rest overlapping the sacrificial layer. Removing the sacrificial layer by under etching resulted in a free-hanging bilayer that could be activated. The advantage of the sacrificial layer method is that one can build more complex microactuator devices. Disadvantages include a long under etching time and potential damage to the PPy, depending on the etchant.

The third method is bulk etching. First, the PPy-microactuator or the complete microsystem is built. In one of the last steps a part of the substrate is removed by etching thus freeing the actuators [45,46].

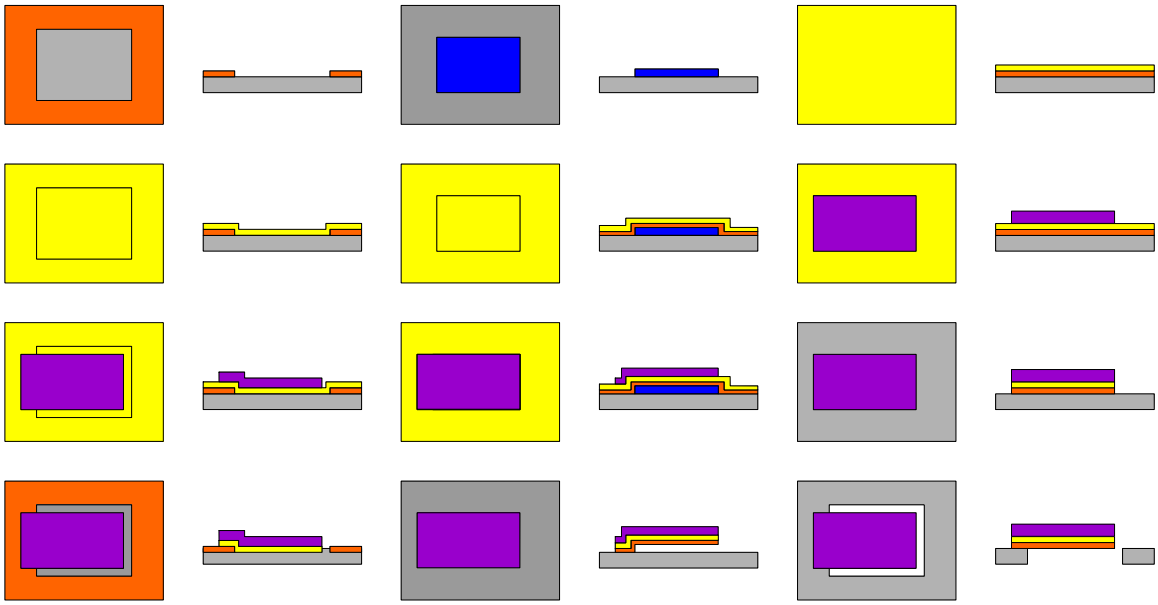

Figure 13.4: Different fabrication methods - Differential adhesion, sacrificial layer, and bulk etching.

13.2 Operation and Performance

In order to actuate the devices an electrochemical cell has to be used. This comprises a control unit, an electrolyte, a working electrode, that is the PPy-microactuator(s), a counter electrode, and possibly a reference electrode. As a counter electrode typically an Au-coated Si wafer, Au wire or Ti/Pt mesh is used. As a reference electrode a commercial Ag/AgCl reference electrode can be used. For miniaturization all these electrodes can be integrated on-chip [47]. A microactuator with 100 µm by 150 µm Au counter electrode and a 50 µm by 100 µm Ag/AgCl quasi-reference electrode has been demonstrated. For the control unit one can use apparatus ranging from a simple battery to commercial research grade potentiostat/galvanostats. Also, integration of the potentiostat in the device that comprises the PPy-microactuators is being developed [48].

The performance of PPy microactuators has been characterized for microfabricated bilayer actuators. Bending angles, strain, speed and force are some important performance metrics [45,49]. For bilayer actuators the performance is largely influenced by geometric parameters. The length and width of the actuator are naturally influential as well as the total bilayer thickness and the individual thicknesses and ratios of the PPy and Au layers. For PPy(DBS) microactuators the optimum thickness ratio of PPy:Au for minimum curvature has been found to be 5:1 [50].

A key aspect for actuator performance and long life time is to avoid delamination of PPy from the underlying substrate. Significant interfacial stresses are generated when the PPy expands and contract [51]. Adding porous layers of Au has been a successful method promoting mechanical interlocking of the different layers [50,52].

The actuation strain of the PPy is critical a critical parameter that characterizes the performance of the actuators. For bilayer actuators the strain has been calculated based on mechanical models to be 0.45 to 3.4% in polypyrrole doped with various anions

[19,21]. Bay et al. have also measured strain directly and reported strains of up to 4 % for PPy doped with various alkyl benzene sulfonates [29]. The strain varies for different film thicknesses and a strain gradient through the PPy film thickness has also been reported [50].

Bending is a response only to in-plane volume change. The volume change of PPy has shown to be highly anisotropic The out-of-plane volume change has been measured for PPy(DBS) and an expansion of >35% in the reduced state has been reported [53]. This out-of-plane volume change is sufficiently large that it can in principle be exploited directly in bulk type microactuators that do not need to be released from the surface. Such devices could be used as micropumps and valves.

Force measurements on PPy microactuators have been performed by measuring the mass that microactuators could reversibly lift. For a device with a PPy thickness of 0.9 μm, the ratio of the mass lifted to the mass of the hinge was 43,000:1. The radius of curvature was 5.6 μm, and it took 2 s to bend or straighten a bilayer 1 μm thick. Energy efficiencies were ~ 0.2%. [45].

13.3 Applications and Devices

Bending actuators

The simplest devices are benders or fingers: bi- or multilayer strips of PPy/Au or PPy/Au/polyimide that curl and straighten under activation [36,54]. These can be used to grab small objects. For example, the cylindrical object in Figure 13.5 could be a synthetic analogue of a nerve fiber.

Figure 13.5 - Three bilayer actuators (500 μm wide) grabbing a 0.5 mm wire

In these fingers rigid beams can be added at different angles relative to the long side of the actuator in order to control the motion [55]. These stiff beams can turn the curling fingers into spirals with either a right hand or left hand turn (Figure 13.6).

Figure 13. 6 Spiral motion of a PPy-microactuator with rigid elements.

One can add other micromachined elements to the PPy-microactuators. This will result into more complex structures. Rigid plates can be added to the ends of the bilayers so that they function as hinges. These rigid plates can be made of BCB (Benzocyclobutene) [56], SU8 [38], or "bulk" silicon showing that one may potentially move and position anything that can be fabricated on silicon [45]. The plates can be rotated from 0 over 270° until they hit the surface of the substrate, depending on the device design, and might be used as mirrors or to change the surface of a device by exposing either one or another side of a flap. They have been combined in series, generating self-opening and closing boxes [56].

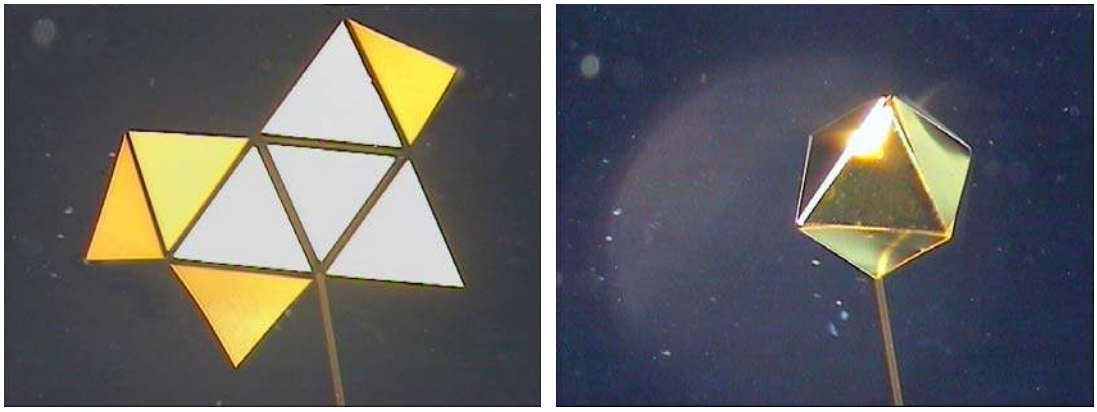

Figure 13.7. A self assembling octahedron controlled by several hinge actuators

It is possible to deliver power to the plate and for instance build a moving pixel [57]. Lids can also be constructed to close and re-open microcavities or microvials that might contain drugs or cells. [38]. These sealable microcavities might also be used as small vessels for nano- and picoliter chemistry. The *cell clinic* is one such device. This is microcavity with integrated electrodes on the bottom and a lid operated by PPy-hinges (Figure 13.8). It has been used to study cell behavior. Frog melanophores (*Xenopus laevis* melanophores) have been added to the cell clinic. It was possible to determine cell spreading on the surface and covering of the electrodes at the cell clinic bottom, and subsequent measurement of intra-cellular effects of stimuli added to the cells [58]. This work is continued with the addition more sensors to the cavity, resulting in what now is called a laboratory-on-a-chip [59].

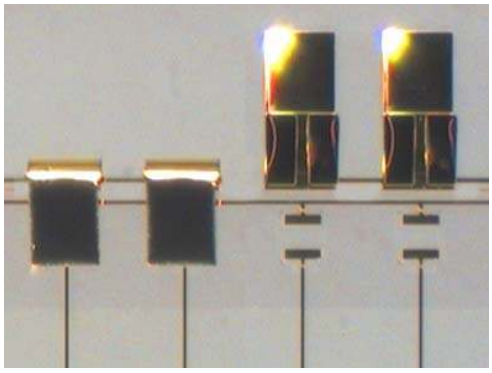

Figure 13.8 Two cell-clinics in the closed and opened state. In the latter picture, two electrode pairs on the bottom of the transparent cavity are visible as well as the PPy-microactuator hinges (black).

Several individually-controlled actuators can be combined in a single device to create more complex structures. A microrobot has been fabricated and operated [39]. PPy microactuators were combined with stiff elements formed from the resin BCB to generate a “robot arm” consisting of an “elbow”, a “wrist”, and a “hand” with 2 to 4 “fingers”. The arm was only 670 μm long. With this robot arm 100 μm glass beads could be picked up, lifted, and moved over a surface. In another design, two connected hinges have been placed perpendicular to each other to create an actuator that could move in plane, perpendicular to the surface [60]. By intelligently combining such microactuators or hinge elements, new activation schemes in 3D space are possible.

A microgripper for underwater manipulation based on IPMC is under development by Zhou and co-workers, although these have not yet reached the small dimensions of PPy-microactuators [9].

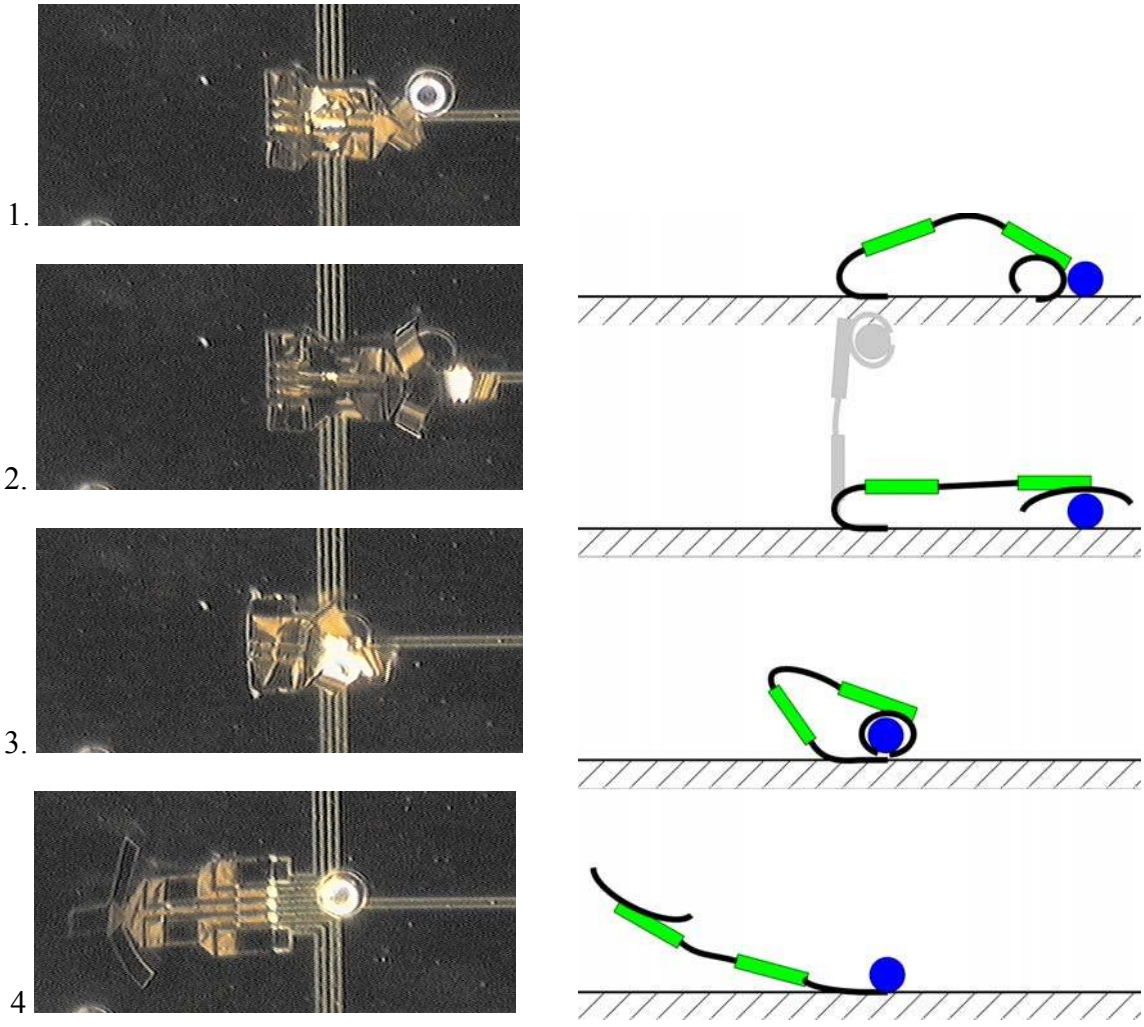

Figure 13.10 Photos (left) showing the grabbing and lifting of a 100 m glass bead and a schematic drawing of this movement (right). The microrobot arm had three PPy-microactuator ‘fingers’, placed at 120° of each other, two PPy-microactuators formed the “wrist” and two formed the “elbow”. The photos do not illustrate that the glass bead is actually lifted from the surface before it is placed at the base of the robot arm. This is illustrated in grey in the second sketch to the right.

Valves

PPy-microactuators are also commonly used as the active element in microfluidic valves. Several constructions have been demonstrated. The afore mentioned plates activated by hinge-type PPy-microactuators have been used to control flows in microchannels made of a silicone rubber (PDMS) slab assembled on a silicon wafer [61] and to open containers for a drug delivery device ("smart pill") [62].

The out-of-plane volume change in these materials is found to be higher and this has been exploited in a valve [62,63]. In [62] it was proposed as the valve for the "smart pill". In [63] it was used to open and close a microfluidic channel made in silicone rubber. The microfluidic channel was fabricated in assembled silicone slabs. The PPy-microactuator was a piston-like device mounted under the channel. Upon activation the PPy-piston pushed the bottom wall of the channel up, thus blocking the flow. An advantage was that the electrolyte chamber was separated from the flow channel. Yet, another type of PPy valve is used in an implantable drug delivery device called IntelliDrug (www.intellidrug.org) [64]. Here, a buckling PPy membrane is used to control a flow in a microfluidic channel, in order to control the drug release.

Yamada and co-workers have also demonstrated a PPy-microactuator based on the bulk expansion of PPy [65]. A 30 μm thick PPy film was synthesized on comb shape electrodes and covered with a solid polymer electrolyte. Upon activation the PPy expanded 2 μm.

The nature of CP microactuators makes them good candidates for applications in medical devices, in-vitro diagnostics and biomedicine [66]. Medical device applications, for example for use during vascular interventional procedures are for instance being developed by companies such as Micromuscle AB (www.micromuscle.com). The CP microactuators are being incorporated as parts of medical devices and enable new functionality by performing a range of functions, such as controlling the movement and mechanical properties of medical devices, holding and releasing objects inside vascular areas etc (Figures 13.11 and 13.12).

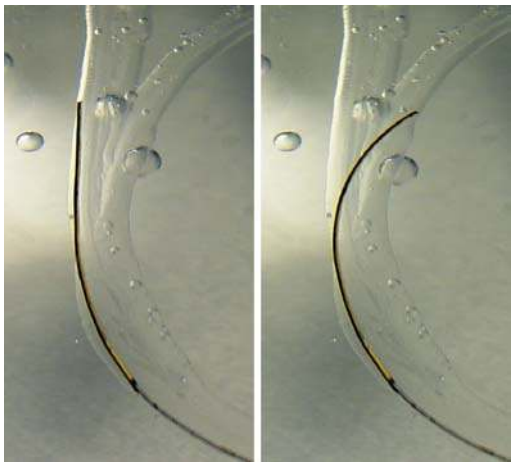

Figure 13.11. EAP-steerable vascular device for maneuvering in vessels, demonstrated in a bench set-up.

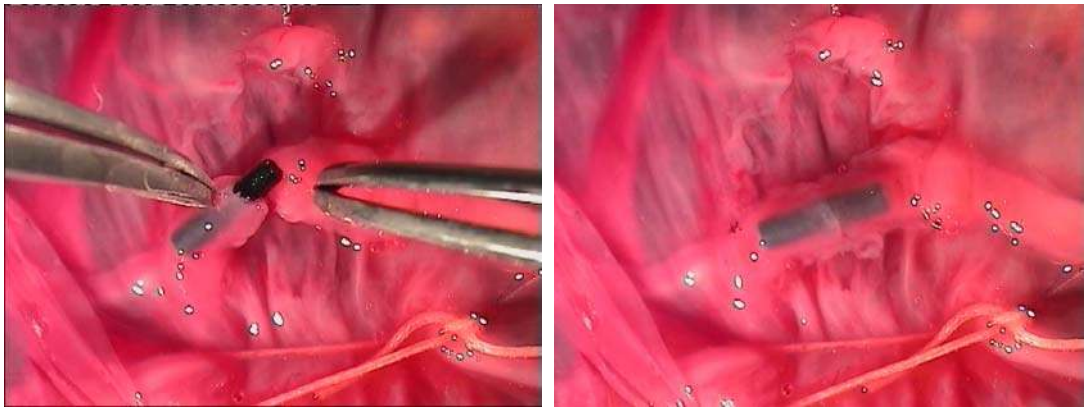

Figure 13.12. A micro-anastomosis connector is an implantable tube with contractible and expandable features using EAP. It is intended for reconnecting cut mm sized blood vessels.

The knowledge of CP material properties and of the mechanisms that control actuator performance increases constantly. This development will enable new and improved CP actuators for future (commercial) applications.

[1] R. Pelrine, R. Kornbluh, Q. Pei, J. Joseph, Science 287 (2000) 836.
[2] K. Onishi, S. Sewa, K. Asaka, N. Fujiwara, K. Oguro, Biomimetic Micro Actuators Based on Polymer Electrolyte/ Gold Composite Driven by Low Voltage, IEEE-MEMS 2000, Miyazaki, Japan, 2000.
[3] M. Shahinpoor, Y. Bar-Cohen, J. O. Simpson, J. Smith, Smart Materials and Structures 7 (1998) R15.
[4] Q. Pei, O. Inganäs, Advanced materials 4 (1992) 277.
[5] R. H. Baughman, C. X. Cui, A. A. Zakhidov, Z. Iqbal, J. N. Barisci, G. M. Spinks, G. G. Wallace, A. Mazzoldi, D. De Rossi, A. G. Rinzler, O. Jaschinski, S. Roth, M. Kertesz, Science 284 (1999) 1340.
[6] Y. Bar-Cohen (Ed.), Electroactive Polymer (EAP) Actuators as Artificial Muscles - Reality, Potential, and Challenges - 2nd edition, SPIE Press, Bellingham, Washington, USA, 2004.
[7] R. Pelrine, R. Kornbluh, J. Joseph, S. Chiba, Electrostriction of polymer films for microactuators, IEEE proceedings of Tenth Annual International Workshop on Micro Electro Mechanical Systems, MEMS ' 97 (1997) 238.
[8] M. Y. F. Kwok, W. Zhou, W. J. Li, Y. Xu, Micro Nafion Actuators for Cellular Motion Control and Underwater Manipulation, in: D. Rus, S. Singh (Eds.), Experimental Robotics VII (Lecture notes i control and information sciences 271), Springer Verlag, Berlin, 2001, 471.
[9] J. W. L. Zhou, H.-Y. Chan, T. K. H. To, K. W. C. Lai, W. J. Li, IEEE/ASME Transactions on Mechatronics, 9 (2004) 334.
[10] X. Wang, X. Gu, C. Yuan, S. Chen, P. Zhang, T. Zhang, J. Yao, F. Chen, G. Chen, J. Biomed. Mater. Res. 68A (2004) 411.
[11] P. M. George, A. W. Lyckman, D. A. LaVan, A. Hegde, Y. Leung, R. Avasare, C. Testa, P. M. Alexander, R. Langer, M. Sur, Biomaterials 26 (2005) 3511.
[12] E. W. H. Jager, E. Smela, O. Inganäs, Science 290 (2000) 1540.

[13] R. H. Baughman, L. W. Shacklette, R. L. Elsenbaumer, E. J. Plichta, C. Becht, Micro electromechanical actuators based on conducting polymers, in: P. I. Lazarev (Ed.), Molecular Electronics, Kluwer Academic Publishers, Dordrecht, 1991, 267.
[14] R. H. Baughman, Synthetic metals 78 (1996) 339.
[15] T. F. Otero, J. Rodriguez, E. Angulo, C. Santamaria, Synthetic Metals 57 (1993) 3713.
[16] M. R. Gandhi, P. Murray, G. M. Spinks, G. G. Wallace, Synth. Met. 73 (1995) 247.
[17] A. Della Santa, D. D. Rossi, A. Mazzoldi, Synthetic Metals 90 (1997) 93.
[18] T. F. Otero, J. M. Sansinena, Bioelectrochemistry and Bioenergetics 38 (1995) 411.
[19] Q. Pei, O. Inganäs, Journal of physical chemistry 96 (1992) 10507.
[20] Q. Pei, O. Inganäs, Journal of Physical Chemistry 97 (1993) 6034.
[21] Q. Pei, O. Inganäs, Conjugated polymers as smart materials: bending bipolymer strips, in: V.K.Varadan (Ed.), Smart Materials and Structures, SPIE Proceedings Vol 1916, Albuquerque, 1993, 28.
[22] K. Kaneto, M. Kaneko, Y. Min, A. G. MacDiarmid, Synthetic Metals 71 (1995) 2211.
[23] Q. Pei, O. Inganäs, Synthetic metals 55-57 (1993) 3724.
[24] J. D. Madden, R. A. Cush, T. S. Kanigan, I. W. Hunter, Synthetic Metals 113 (2000) 185.
[25] T. W. Lewis, S. E. Moulton, G. M. Spinks, G. G. Wallace, Synthetic Metals 85 (1997) 1419.
[26] L. Bay, T. Jacobsen, S. Skaarup, K. West, J. Phys. Chem. B 105 (2001) 8492.
[27] T. F. Otero, H. Grande, J. Rodriguez, Electrochimica Acta 41 (1996) 1863.
[28] T. F. Otero, J. Padilla, J. Electroanal. Chem. 561 (2004) 167.
[29] L. Bay, N. Mogensen, S. Skaarup, P. Sommer-Larsen, M. Jörgensen, K. West, Macromolecules 35 (2002) 9345.
[30] Y. Sonoda, W. Takashima, K. Kaneto, Synthetic Metals 119 (2001) 267.
[31] K. P. Vidanapathirana, M. A. Careem, S. Skaarup, K. West, Solid State Ionics 154-155 (2002) 331.
[32] X. Wang, B. Shapiro, E. Smela, Advanced Materials 16 (2004) 1605.
[33] T. W. Lewis, G. M. Spinks, G. G. Wallace, D. D. Rossi, M. Pachetti, Polymer Reprints 38 (1997) 520.
[34] J. M. Sansiñena, V. Olazabal, T. F. Otero, C. N. Polo da Fonseca, M.-A. De Paoli, Chemical Communications 22 (1997) 2217.
[35] J. Madden, R. Cush, T. Kanigan, C. Brenan, I. Hunter, Synthetic Metals 105 (1999) 61.
[36] E. Smela, O. Inganäs, Q. Pei, I. Lundström, Advanced Materials 5 (1993) 630.
[37] E. Smela, O. Inganäs, I. Lundström, Self-opening and closing boxes and other micromachined folding structures, in: Transducers '95, vol 2, Stockholm, Sweden, 1995, 350.
[38] E. W. H. Jager, C. Immerstrand, K. H. Petersson, K.-E. Magnusson, I. Lundström, O. Inganäs, Biomedical Microdevices 4 (2002) 177.
[39] E. W. H. Jager, O. Inganäs, I. Lundström, Science 288 (2000) 2335.
[40] E. Smela, J. Micromech. Microeng. 9 (1999) 1.
[41] J. W. Schultze, T. Morgenstern, D. Schattka, S. Winkels, Electrochimica Acta 44 (1999) 1847.

[42] M. Angelopoulos, Conducting polymers in microelectronics, in: T. A. Skotheim, R. L. Elsenbaumer, J. R. Reynolds (Eds.), Handbook of Conducting Polymers, Marcel Dekker, Inc, New York, 1998, 921.
[43] J. Heinze, Synthetic Metals 41-43 (1991) 2805.
[44] E. Smela, O. Inganäs, I. Lundström, Differential adhesion method for microstructure release: an alternative to the sacrificial layer, in: Transducers '95, vol 1, Stockholm, Sweden, 1995, 218.
[45] E. Smela, M. Kallenbach, J. Holdenried, Journal of Microelectromechanical Systems 8 (1999) 373.
[46] E. Jager, M. Krogh, Method for producing a micromachined layered device, Swedish patent 526 192, 2004.
[47] E. W. H. Jager, E. Smela, O. Inganäs, Sensors & Actuators B: Chemical 56 (1999) 73.
[48] S. B. Prakash, P. Abshire, M. Urdaneta, M. Christopherson, E. Smela, A CMOS Potentiostat for Control of Integrated MEMS actuators, ISCAS, 2005.
[49] M. Christopherson, E. Smela, Polypyrrole-gold bilayer microactuators; response time and temperature effects, in: Smart Structures and Materials; Electoactive Polymer Actuators and Devices (EAPAD), San Diego, CA, USA, 2006.
[50] M. Christopherson, B. Shapiro, E. Smela, Subm. Sensors & Actuators B. (2005).
[51] B. Shapiro, E. Smela, J.Intell.Mater.Syst.Struct. In press (2005).
[52] C. C. Bohn, M. H. Pyo, E. Smela, J. R. Reynolds, A. B. Brennan, Polymeric Materials:Science & Engineering 86 (2002) 26.
[53] E. Smela, N. Gadegaard, Advanced Materials 11 (1999) 953.
[54] A. P. Lee, K. C. Hong, J. Trevino, M. A. Northrop, Thin film conductive polymer for microactuator and micromuscle applications, in: Dynamic and Systems and Control Session, International Mechanical Engineering Congress, vol DSC-2, ASME publications, Chicago, USA, 1994, 725.
[55] M. Krogh, O. Inganäs, E. Jager, Fibre-reinforced microactuator, Swedish patent 525 649, 2003.
[56] E. Smela, O. Inganäs, I. Lundström, Science 268 (1995) 1735.
[57] E. Smela, Advanced Materials 11 (1999) 1343.
[58] C. Immerstrand, E. W. H. Jager, K.-E. Magnusson, T. Sundqvist, I. Lundström, O. Inganäs, K. H. Peterson, Medical & Biological Engineering & Computing 41 (2003) 357.
[59] M. Urdaneta, Y. Liu, M. Christopherson, S. Prakash, P. Abshire, E. Smela, Integrating Conjugated Polymer Microactuators with CMOS Sensing Circuitry for Studying Living Cells, in: Smart Structures and Materials; Electoactive Polymer Actuators and Devices (EAPAD), San Diego, CA, USA, 2005.
[60] E. W. H. Jager, O. Inganäs, I. Lundström, Advanced Materials 13 (2001) 76.
[61] F. Pettersson, E. W. H. Jager, O. Inganäs, Surface Micromachined Polymer Actuators as Valves in PDMS Microfluidic System, in: IEEE-EMBS Special Topic Conference on Microtechnologies in Medicine & Biology, Lyon, France, 2000, 334.
[62] L.-M. Low, S. Seetharaman, K.-Q. He, M. J. Madou, Sensors and Actuators B:Chemical 67 (2000) 149.
[63] Y. Berdichevsky, Y.-H. Lo, Polymer Microvalve Based on Anisotropic Expansion of Polypyrrole, in: Mat. Res. Soc. Symp. Proc., vol 782, Materials Research Society, 2004, A4.4.1.
[64] T. Göttsche, A. Wolff, MST news 1/06 (2006) 36.

[65] K. Yamada, Y. Kume, H. Tabe, Japanese Journal of Applied Physics Part 1-Regular Papers Short Notes & Review Papers 37 (1998) 5798.
[66] C. Immerstrand, K. H. Peterson, K.-E. Magnusson, E. Jager, M. Krogh, M. Skoglund, A. Selbing, O. Inganäs, MRS bulletin 27 (2002) 461.

14. Electrochromic and electroluminescent polymers

Zoran Djinovic – Institute of Sensor and Actuator Systems, TUWien, Austria

The discovery of conductivity in plastic materials [1] has been a significant breakthrough in the field of engineering science since it has led to new avenues and applications. For example, a special type of electro-conductive plastics known as conjugated polymers [2,3] are today emerging as a material for the production of electrochromic (EC) and electroluminescent (EL) devices [4,5]. These devices are already at or near market for thin flexible displays, "smart" windows, rear-view mirrors, chameleon camouflaged clots, light-emitting diodes (LED), field-effect transistors (FET), chemical sensors, solar cells end even coloured fingernails [4-8]. The main reason for such a broad area of application is the versatility of polymer science and organic chemistry that enables a wide range of functionalities. From the market point of view, EC and EL devices are potentially much lower cost compared to common inorganic semiconducting devices, mainly due to easier processing technologies of the polymers. An expected price decrease per polymer EC/EL device in the near future and a large market potential attracted the attention of academia, large international companies and small start up companies.

Both phenomena, electrochromism and electroluminescence in polymers, are based on the unique property of the conductivity of conjugated polymers. Conjugated polymers have a backbone composed of alternating single and double carbon-carbon bonds. Single bonds known as σ– bond are made by overlapping two hybridized sp^3 orbitals, while double bonds known as π-bonds are made by overlapping two hybridized sp^2 orbitals. The remaining out-of-plane p_z orbitals also overlap each-other, forming an electron cloud above and below the main backbone. It is depicted in figure 14.1 for the case of ethylene molecule [9]. This cloud is though to contain delocalized electrons capable of carrying charge, if polymer is exposed to the external field [1].

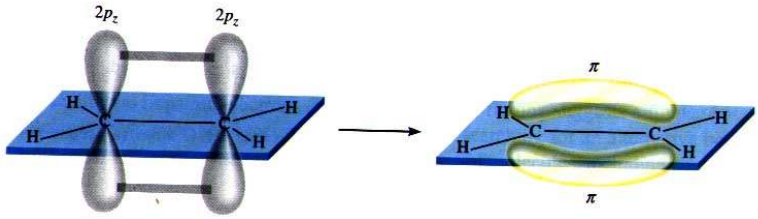

Figure 14.1 - a π-bond in ethylene molecule [9]

In comparison to solid state electronics, this situation is similar to the electronic structure of common inorganic semiconductors, e.g. silicone. Hence, we can now consider two energetic bands of conjugated polymers, the valence band (π state), also known as high occupied molecular orbital (HOMO) and the conductive band (π^* state) which corresponds to the lowest unoccupied molecular orbital (LUMO) [4]. The conductive band has a larger energy potential than the valence band so that electrons must jump from the lower to the upper band. The energy gap, E_g , is a fingerprint of every conjugated polymer that is dependent on the chemical composition and steric architecture of the polymer chain [4]. Good knowledge of organic synthesis is the main key for fine-tuning of the E_g and the resulting electrical properties. Typically, most

conjugated polymers have the energy gap between 1.5-3eV, which corresponds with visible to near-infrared electromagnetic radiation, i.e. from 400 – 1200 nm.

On application of a voltage to the polymer it can be switched between a neutral (undoped) state and a conducting (doped) state. Some conjugated polymers show distinct electrochromic behaviour in that the doped and undoped states have different colors. The mechanism of reversible colour switching in elctrochromic materials is based on oxidative (loss of electrons, 'p-doping') and reductive (gain of electrons, 'n-doping') processes occurring at the anode/cathode interface. Upon electrochemical doping the band structure of the neutral polymer is modified, generating lower energy intraband transitions and creating charged carriers, which are responsible for increased conductivity and optical modulation.

Electroluminiscence is an optoelectronic phenomenon whereby the material emits light when an electrical current passed through it, usually in response to a strong electric field. The main mechanism is radiative recombination of electrons and holes in material, e.g. as in a semiconductor [5]. When electrons and holes are injected from electrodes into an organic film or several organic layers, organic electroluminiscence occurs and the devices are called organic light-emitting diodes. The cathode injects electrons in the lowest unoccupied molecular orbital (LUMO), i.e. in conduction or π^* band of the polymer. Simultaneously, the anode injects holes in the highest occupied molecular orbital (HOMO), i.e. in valence or π band of the polymer. Under the voltage these charges, named polarons, travel towards the opposite electrodes and are mutually annihilated by multi-phonon emission or surface recombination. As a result of the electron-hole interaction, a neutral space (exciton) has been formed. The exciton can be in the singlet or triplet state, depending on spin state. Only the singlet state can contribute to the photon emission and since the singlet state to triplet state ratio is 1/3, the maximum quantum efficiency with luminescent polymers can be 25 % [10]. The remainder of the electrons will annihilate by some non-radiative means, for example in causing photo-oxidation of the polymer.

14.1 Electrochromic materials

Early electrochromic (EC) materials and devices were demonstrated on inorganic materials such as metal oxides and wide-band-gap semiconductors, mainly WO_3 [11,12]. Electrochromism in organic materials was initially discovered using small molecules such as bipyridiliums (viologens), but it has also been observed in conjugated polymers such as those compounds based on poly(thiophene) (PTh), poly(pyrrole) (PPy) and poly(aniline) (PANI) [13]. These materials are the prime candidates for display technology, due to their high contrast ratio (electrochromic contrast), short response times (switching speed) and long lifetimes (stability) [4].

There are three main groups of EC materials. The first group comprises materials with two distinctive optical states, colored and bleached (transmittive) state. They find their application in so-called absorption/transmission EC devices such as "smart" windows and optical shutters. The most frequently used organic polymer in this group is poly(3,4-ethylenedioxythiophene) (PEDOT). The second group encompasses those materials used for display applications, since they have two clearly defined colored states. For example, PTh can change colour from red to blue under oxidation [4]. The third group consists of materials known as multi-colour polymers. These have more than two optical states such as poly(3,4-propilendioxypyrrole) (PProDOP) and the

above-mentioned PANI. These materials also find application in display technology as conductive layers [14].

One of the main advantages of the conjugated polymers, particularly multicolour polymers, is the unlimited possibility to tailor EC properties by changing the polymer structure. A large number of synthetic techniques are involved for fine-tuning of the E_g of conjugated polymers [15] and ultimately their response to the applied electric fields. In the simplest method it is possible to substitute the parent heterocycle causing steric and electronic influence on the E_g of polymer. Homo-polymerization of co-monomers or co-polymerization of different monomers also results in modification of the main backbone of the polymer, providing it with new properties. Electro-synthesis has been frequently used to produce structurally different polymers [16]. In addition to these chemical techniques there are several physically based techniques for altering the electrochromic properties of the polymer, for example, polymers can be utilized in blends, laminates or composites [17-19].

A large number of different compounds are produced by relatively small structural changes of the starting monomers such as PTh, PPy and PANI, providing new colours in their neutral or doped forms. For example, Gaupp et al, [20] slightly modified the structure of the PPy to include an additional aromatic ring and they obtained several new derivates, such as PEDOP and PProDOP with E_g of 2.0 and 2.2eV respectively. Hence, PEDOP gained in its neutral state a red colour, while in its oxidized state the polymer was transmissive blue. Moreover, PProDOP achieved three coloured states, an orange neutral, an intermediate brown and a grey/blue oxidized state. The effect of substitution of the H atom in the NH-group with a sulfonato-propoxy group was even stronger causing a significant increase of the E_g, to more than 3.0eV in N-PrS-PProDOP (poly(N-sulfonatopropoxy-ProDOP)) derivate. Consequently, the polymer changed its colour from its transmissive colourless neutral state to an absorbing light grey oxidized state [21]. This was a direct consequence of the steric interaction of the rather bulky substituted groups with the rest of the polymer chain. The involvement of more rings into the basic repeated unit, as well as combining the thiophene and pyrole rings, drastically increased the number of possible derivates. Depending on the doping level, they demonstrated multi-colour ability, resulting from variability in the energy gap, from 1.2eV with PBEDOT-PyrPyr (poly-bis-EDOT-pyridopyrazine) to more than 3eV [22]. By inclusion of the Si atom as a link between the two bithiophene rings in the repeated unit, an extremely low E_g of about 0.85eV was obtained [23] enabling the material to be used for near infra-red (NIR) applications. This significant decreased of E_g is explained by shortening of the conjugated length of the polymer chain.

14.2 Electrochromic devices

Electrochromic devices (ECDs) have the sandwich structure that is schematically presented in Figure 14.2a. Figure 14.2b shows the electrochromic effect of one absorption/transmission-based ECD composed of PProDOT-Me_2 and N-PrS-PProDOP polymers [4]. The active elctrochromic material is coated onto a transparent glass or plastic substrate and driven by a low voltage source of +/-1.5V. An electrochemical reaction (redox reaction) then takes place between the cathode and anode via oxidative or reductive processes. Electrochromic behaviour depends on the diffusion of ions from one layer to another.

ECDs based on inorganic materials are relatively slow to change to their two-colour states, with timescales that are typically of the order of several seconds. Liquid Crystal Displays (LCDs) are much faster, but they suffer from a limited viewing angle and they lack the multi-colour effect. Hence, the current need in the display technology is to have much faster, stable and higher contrast displays. Based on the latest developments, electrochromic polymers are promising materials that can meet the above mentioned demands. For example, Auber et al. [24] were able to achieve a switching rate in the order of 5-10 Hz, with about 60 % of contrast ratio in the visible region and they maintained stable ECD performance over 180,000 cycles. The polymers used included those mentioned above, such as PXDOT poly(3,4-alkylenedioxythiophene), PEDOT , PProDOT as well as some derivates of these polymers, changing blue and red neutral state colours to a bleached oxidative state.

Despite the evident successes, the problem of long-term stability has remained a major challenge for the polymer based ECDs. However, the use and development of novel classes of polymers, blends, copolymers, composites and laminates and new ionic media have enabled fabrication of ECDs with increased stability against environmental conditions especially in air and oxygen interaction. Furthermore, the colouration efficiency, i.e. the amount of charge required to produce the optical change, will in all likelihood reach 500-3,000 cm^2/C very soon [4]. Finally, it is possible to contemplate the production of large-area flexible ECDs due to relatively simple processing technology involved. This is primarily based on solutions of the polymers and readily compatible with current ink jet technology.

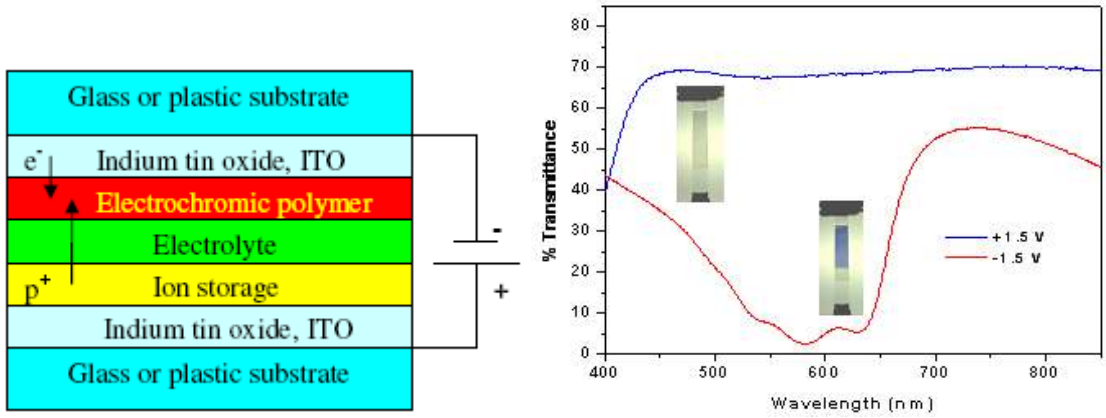

a) b)

Figure 14.2: a) Schematic presentation of an ECD, b) example transmittance spectra of absorption/transmission electrochromic devices [4]

In practice there are two main types of ECDs, the absorption/transmission (A/T) type and the reflective type. The first group is composed of two complementary polymers, deposited onto the cathode and anode respectively and separated by an electrolyte. Usually this is a viscous gel. The electrodes are typically made of a transparent solid such as indium tin oxide (ITO)/glass or flexible ITO/polyethyleneterephthalate (PET) materials. When a voltage is applied between the electrodes, a high-band gap polymer becomes oxidized by the anode and changes the transmissive state to a coloured state. At the same time a low-band gap polymer, which is deposited on the cathode and is coloured in the neutral state, becomes transmissive upon oxidation. Hence, the ECD switches between two states, coloured and transmissive. This is the main functionality

necessary for “smart” windows and optical shutters. Figure 14.2b shows these events when two complementary polymers PProDOT-Me_2 and N-PrS-PProDOP have been driven by only +/- 1.5 VDC [4]. Reflective ECDs have a similar structure to that presented in Figure 14.2a with the exception that one electrode is non-transmissive, usually made of Mylar foil coated by gold. When a thin film of PProDOT-Me_2 is applied on the gold electrode it is possible to obtain switching from a deep blue to a reflective gold state. However, these devices can be active not only in the visible region but also in the near-infrared, mid-infrared and even micrometer regions, yielding a contrast ratio as high as 90 % at 1.8μm. This functionality is very important for thermal emissive control, often demanded in military applications, for example for camouflage purposes [25].

High volume production of low-price ECDs will be feasible in the near future due to comparatively simple polymer production technologies. For example the solvent state of the active polymers is compatible with well known and mature screen printing techniques with resolution values of about 10-100 μm. Micro-coating printing (μCP) and inkjet printing can also be utilised [26]. Fine electrode structures can be obtained by line patterning, which combines metal-vapor deposition and inkjet printing [27]. ECDs most certainly have a large market potential, not only in microtechnology, but also for much larger scale applications. An example of this would be in the building industry for the production of so-called ‘smart windows’. Electrochromic windows can help save energy by automatically controlling of the light and solar energy that can pass through the window. The US Solar Energy Industries Association estimates that smart windows could save as much as 50 % of building’s energy. This is based on the premise that they can lower cooling loads in the summer months by reducing solar heat gain [28]. At present electrochromic windows are usually made of inorganic EC materials [29].

14.3 Electroluminescent materials

Electroluminescence (EL) is the generation of light in response to an externally applied voltage. EL was first observed in an inorganic material, zinc sulphide, in 1936 by Destriau [30]. In 1950, Bernanose observed the effect in organic compounds when thin films of acridine orange and qinacrine [31] were exposed to a high alternating voltage. The same effect was observed 1963, when Pope et al. applied a voltage of ~ 400 V to an anthracene film which generated a blue light [32]. Leading on from these valuable initial observations, two-layer structures composed of p-type aromatic diamine and n-type of emitting layer of aluminium chelate tris-hydroxyquinoline (Alq_3), were created and this represented the first real example of organic light emitting diodes (OLEDs) capable of working at a relatively low voltage of ~10 V.

In 1990, Friend [33] made a dramatic breakthrough in the field of EL materials reporting that the conjugated polymer poly(*p*-phenylene vinylene) PPV showed green-yellow electroluminescence with E_g of ~2.5eV. Although the first simple device had an EL efficiency (the number of generated photons per number of injected electrons) of only 0.01%, this discovery heralded the beginning of polymer light emitting diode (PLEDs) or OLED technology. Heeger and co-workers also discovered that a PPV soluble derivate, poly[2-methoxy-5-(2’-ethylhexyloxy)-1,4-phenylenevinylene], or MEH-PPV in short, [34,35] generated a red EL colour with an E_g of ~2.2eV. Since MEH-PPV was a soluble conjugated polymer it offered a number of advantages in processing technology. However, it rapidly became clear that this particular EL polymer

is highly sensitive to photo-oxidation [36], which was a significant disadvantage for further development.

PPV was soon recognised as being unsuitable for the fabrication of PLEDs, mainly due to difficulties of processing the solid phase of the polymer. Significant effort has been made within the scientific community [37-39] to synthesise a number of soluble PPV derivates involving different side groups such as alkoxy, alkyl and cyano groups. It was also shown [40] that side groups have a significant influence on the magnitude of the energetic gap, electron and hole mobility and luminescence efficiency. As a result, the PPV derivate, MEH-PPV, gained about 1% of the EL efficiency at 3 to 4V, due to alkoxy substitution in side chains of the PPV backbone. Alkyl substitution produced a shift of the luminescence colour from yellow to blue with an increase of efficiency of approximately 2.5% [41]. Cyano side groups improved electron mobility in CN-PPV derivatives, while triphenylamine and carbazole molecular fragments increased hole mobility.

Poly(*p*-phenylene) PPP is a new EL active polymer, derived from PPV, which has a higher E_g, between 2.8 and 3.5eV. PPP materials have received a lot of attention with regard to the creation of blue PLEDs. Unsubstituted PPP, like PPV, is insoluble in organic solvents and this makes fabrication procedures for PLEDs difficult. Trials [42] to deposit thin PPP film by vacuum deposition have been undertaken, but generally this technique requires a pre-polymeric precursor. Like PPV, PPP can either be modified in soluble derivates by incorporating of alkyl-, aryl-, alkoxy-, or perfluoroalkyl-groups. sulfonate-, carboxy functional groups and ammonium have the effect of making PPP water-soluble [43].

In the past 10-15 years there have been over a thousand different polymers [44] developed for ELD applications, mostly these are based on parent monomers such as thyophene and phenylene. The goal has been to tailor the colour of the EL polymer in the same way to the methods described above. For example, Yoshio et al. prepared the wide-bandgap polymer polyfluorene to emit a rich blue EL colour [45]. Researchers at Dow Chemical Co. [46] synthesized a family of 9,9-dialkylfluorenes with a molecular weight in the range of 50 to 600kDa, indicating a degree of branching in the polymer chain, with E_g of 3.68eV and a blue EL colour corresponding to a primary emission peak at 436 nm. Many high-efficiency, high-brightness and long-living devices have been constructed from these materials. For example, Friend et al. [47] succeeded in fabricating an optimized green LED with very pure fluorine-based polymers. They obtained light emission of 10000cd/m^2 by applying less than 6V. Peak efficiency was 22lm/W. Table 14.1 presents the most important achievements obtained for three different colours at Cambridge Technology Display:

Table 14.1: Performance for red, green and blue emitting polymers [48]

Colour	Efficiency at 100 cd/m^2 (monthly average)	Voltage at 100 cd/m^2 (monthly average).	Lifetime initial from 100 cd/m^2
red	1,7	2,4	>40,000
green	9,0	2,7	>20,000
blue	2,0	3,9	3,500

At the same time, collaboration between Donetsk University, Ukraine and the University of Durham in the UK, has produced new stable variants of PF. The Durham–Donetsk collaboration replaced the carbon at the 9-position in PF with SO_2 to prepare dibenzothiophene-S,S-dioxide, which was then formed into co-oligomers with 9,9-dihexylfluorene [9]. This improved electron transport and stopped it degrading. Kim et al. [50] recently achieved high purity of the blue color emitted by the poly [2,7-(9,9-di-*n*-dioctylfluorene) (PF) by incorporating gold nanoparticles (Au NPs) into the host PF polymer. At the same time the stability of the blue color was greatly improved by Au NPs that suppressed the photo-oxidative and degenerative processes of the PF.

Recently, Shen et al. [51] reported the combination of two polymers, PF and MEH-PPV in order to get efficient white-polymeric light emitting diodes (WPLED) with brightness from 200 cd/m^2 to 10,000 cd/m^2 as the forward bias increases from 5 V to 10 V. The EL turn-on voltage is below 4 V and the maximum luminance reaches 10270cd/m^2 at the bias of 10 V. The luminous power efficiency and luminous efficiency were found to be about 1.8 lm/W and 2.3 cd/A, respectively for the bias of 4 V.

14.4 Electroluminescent devices

Basic device architecture is presented in Figure 14.3a. This shows a polymer thin film, between two electrodes on a substrate. Figure 14.3b presents the electroluminescent spectra of previously mentioned MEH-PPV in combination with PMMA [52]. An OLED or PLED consists of a light-emitting polymer film, an optically transparent anode and a metallic cathode, together with a DC or AC power source. The anode is most often indium tin oxide (ITO) coated glass. This material has a relatively high work function (4.8-5.2eV), and is a good material for injecting holes into the active polymer layer. The hole mobility in PPV is of the order of 10^{-4} $cm^2V^{-1}s^{-1}$ allowing transport across a 1000 Å layer with typical fields of $5x10^5$ Vcm^{-1} in 0.5 μs. The cathode material is typically a low work-function metal, such as Ca, Mg or Al. For example, Ca has about 2.8eV of work function that is very close to the value of LUMO of PPV. They are very efficient at injecting electrons from the cathode into the polymer layer. The polymer may be deposited on the ITO by spin- or dip-coating from solution, and is typically of the order of 100nm thick. The cathode metal is evaporated onto the polymer film in vacuum. In order to improve injecting of holes there is very often an intermediate layer between the ITO and active polymer, e.g. PEDOT polymer. The efficiency of electron injections from the cathode side could be achieved by deposition of one intermediate layer between the cathode and polymer, such as PF-N2 (aminoalkyl substituted polyfluorene). More complex structures of PLED can involve multilayer composition of several active polymers and one or more transport layers.

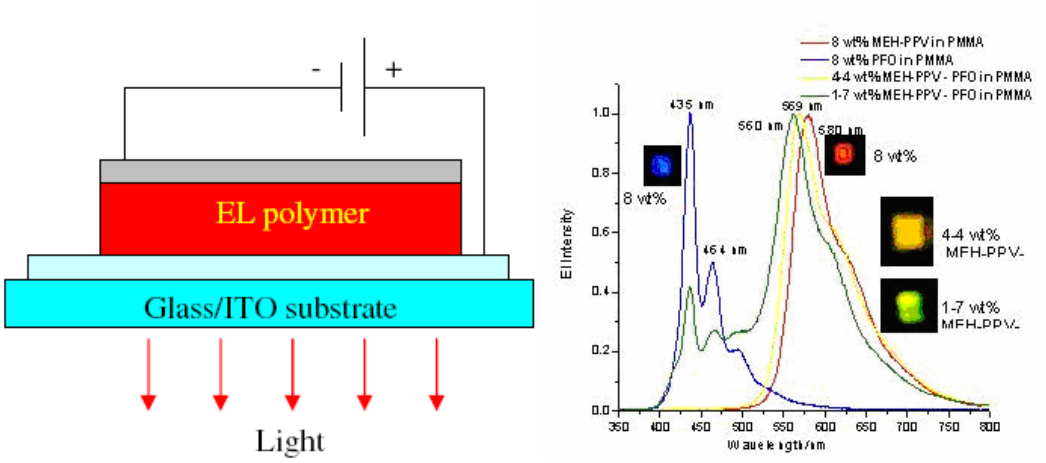

a) b)

Figure 14.3 - a) Basic structure of PLED; b) Electroluminescent spectra of MEH-PPV with PMMA [52]

PLEDs are currently approved devices for high-volume production of low cost video and graphic displays. They can be processed in a relatively simple way by applying some of the well matured technologies such as spin coating or inkjet printing (see Figure 14.4a) [47] onto the ultra thin, large and flexible plastic substrates. Using these techniques it is possible to define complex light emission patterns with high pixel resolution. Figure 14.4b shows such a structure [53]. Completed devices provide 180 degree viewing angle without loss of aperture, backlight, colour filter, and polarizer. The devices consume low amounts of power, working on DC current under the voltage lower than 5 V. Hence, they do not generate any significant heat during operation. These properties, combined with a light, flexible structure and high switching speed, make the PLEDs highly attractive structures for innovative designs and new products.

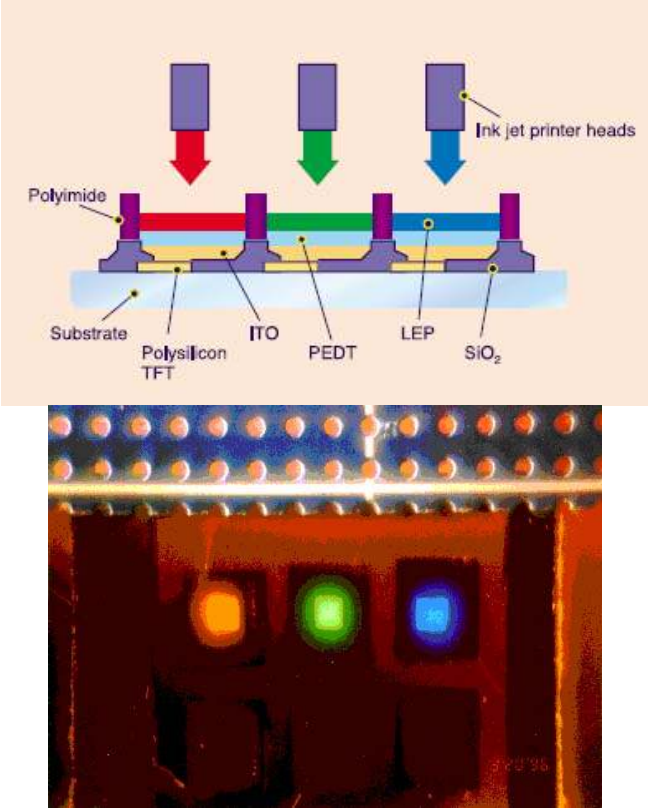

a) b)

Figure 14.4 - Ink-jet printing of EL polymers [47], b) Integrated red-green-blue devices [53]

Despite the promising results that have been obtained in reliability, efficiency and usability of EL polymers [30,39], there are still a lot off challenges that have to be overcome. The most important of these relate to: short lifetime, colour stability, modest efficiency and manufacturing technology. It is a well known that some of these organic compounds are very sensitive to their environmental conditions, for example to moisture, air, heat or UV radiation [54]. The influence of these factors induces ageing of the polymer and deterioration of their useful properties, shortening the lifetime of the ELDs. The lifetime of an ELD is defined as time it takes for the device luminance to drop to half of its initial value. Typically it has to be more than 10,000 hours for most consumer electronic displays. Cambridge Display Technology (CDT) has recently announced the achievement of an extrapolated lifetime of over 100,000 hours for laboratory devices with brightness 100 cd/m² at room temperature [47]. These are colour displays composed of three adjacent pixels emitting red, green and blue light (RGB). Current red and green polymers can meet the stability requirements for displays. However, a significant challenge still exists in terms of the stability of the blue EL polymers. Finally, there are some particular problems concerning the fabrication procedure, such as patterning of the light emitting area, encapsulation of PLED and in the use of organic solvents [55].

Progress has been made in micro-fabrication of PLED pixel arrays by reduction of the active area to 0,8 μm, and by employing ultra-thin and self-assembling polymer coating techniques such as Langmuir-Blodgett deposition [56]. In this way it has been possible to fabricate perfectly assembled layer-by-layer thin film multilayer hetero-structures.

The main benefit has been precise control of the structural features and thickness of the single layers at the molecular scale. It is well known that on this scale, at the interface of the multilayer contacts, it is possible for quantum effects to emerge [10]. For example, a multi-layer structure composed of an aluminium cathode, sulfonium PPV and sulfonated polyaniline (SPAn) deposited on ITO (anode)/glass substrate emitted blue light instead of the greenish-yellow light that is typical for a single SPAn/PPV layer structure. This has been explained as being due to a confinement effect of carriers in the superlattice multilayer structure of SPAn/PPV [57].

Conclusions

Electrochromic (EC) and electroluminescent (EL) devices have already found applications for 'smart' windows and video displays. This has been made possible due to the unusual semiconducting properties of the conjugated polymers. Unlike inorganic semiconductors, these polymeric materials can be processed using simple and low cost techniques, such as spin coating, ink-jet printing and casting. This may result in a significant decrease of the production cost, increased flexibility in design and the ability to create devices in a large range of sizes. Furthermore, their low power consumption operating potentials below 5VDC, high switching speed, good colour brightness, a broad viewing angle of 180^{o} and long lifetime in the range of 100,000 hours (PLEDs) will enable these materials to compete for high volume production of graphic and video displays. Fine tuning of the electronic band gap and colour of the active polymer has been reached by structural modification of monomers, changing the composition of copolymers, involving substitutions and additions to the host polymer, e.g. Au nano particles, or simply by mixing two or more polymers. To-date, good purity and long time stability of the red and green colour of EL polymers has been obtained. However, some challenges remain to achieve stable blue-emitting colours from electroluminescent polymers.

1. C. K. Chiang, C. R. Fincher, Jr., Y. W. Park, A. J. Heeger , H. Shirakawa, E. J. Louis, S. C. Gau, and Alan G. MacDiarmid, "Electrical Conductivity in Doped Polyacetylene", Phys. Rev. Lett.**,** 39 (1977) 1098–1101
2. G. G. Wallace, G. M. Spinks, L. A.P. Kne-Maguire, P. R. Teasdale, "Conductive Electroactive Polymers", CRC Press, Taylor & Francis Group, Boca Raton, 2003
3. R. H. Friend, "Conjugated polymers. New materials for optoelectronic devices", Pure Appl. Chem.,73 (2001) 425-430
4. A. A. Argun, P. H. Aubert, B. C. Thompson, I. Schwendeman, C. L. Gaupp, J. Hwang, N. J. Pinto, D. B. Tanner, A. G. MacDiarmid, J. R. Reynolds, „Multicolored Electrochromism in Polymers: Structures and Devices", Chem. Meater., 16 (2004) 4401-4412
5. Z. H. Kafafi, "Organic Electroluminescence", CRC press, Taylor & Francis Group, Bocka Raton, 2005
6. B. D. Reeves, C. R. Grenier, A. A. Argun, A. Cirpan, T. D. McCarley, J. R. Reynolds, „Spray Coatable Electrochromic Dioxythiophene Polymers with High Coloration Efficiencies", Macromolecules, 37 (2004) 7559-7569
7. C. J. Brabec, N. S. Sariciftci, J. C. Hummelen, "Plastic Solar Cells", Advanced Functional Materials, 11 (2001) 15-26

8. R. V. Gregory, T. Hanks, R. J. Samuel, “Chameleon Fibers: Dynamic Color Change From Tunable Molecular and Oligomeric Devices”, National Textile Center Research Briefs-Materials Competency, 2001
9. nanotech.sc.mahidol.ac.th/ genchem/bonding1/pi.jpg
10. L. Akcelrud, “Electroluminiscent polymers”, Progress in Polymer Science, 28 (2003) 875-962
11. M. Macek, B. Orel, “Electrochromism of sol-gel derived niobiumoxidefilms”, Tr. J. of Chemistry, 22 (1988) 67-72
12. T. J. Richardson, J. L. Slack, M. D. Rubin, “Electrochromism in copper oxide thin films”, Proc. of the 4th International Meeting on Electrochromism, August 21-23, 2000, Uppsala, Sweden
13. D. R. Rossiensky, R. J. Mortimer, “Electrochromic Systems and the Prospects for Devices”, Adv. Mater., 13 (2001) 783-793
14. H. Antoniadis, “Overviewof OLED display technology”, Opto semiconductors, Osram, http://www.ewh.ieee.org/soc/cpmt/presentations/cpmt0401a.pdf
15. J. Roncali, “Conjugated Poly (thiophenes): Synthesis, Functionalization and Applications”, Chem. Rev., 92 (1992) 711-738
16. J. Roncali, R. Grreau, A. Yassar, P. Marque, F. Garnier, M. Lemarie, “Effect of Steric Factors on the Electrosynthesis and Properties of Conducting Poly(3-alkylthiophenes)”, J. Phys. Chem., 91 (1987) 6706-6714
17. D. L. Meeker, M. S. K. Dhurjati, J. Osborn, D. C. Loveday, J. P. Ferraris, “Electrochromic properties of Blends based on Poly(N-vinylcarbazole) and Poly(N-phenyl-2-(5*-vinyl-2*thienyl)-5-(2*-thienyl)pyrrole)” Macromolecules, 31 (1998) 2943-2946
18. J. L. Boehme, D. S. K. Mudigonda, J. P. Ferraris, “Electrochromic Properties of Laminate Devices Fabricated from Polyaniline, Poly(ethylenedioxythiophene) and Poly(N-methylpyrrole)”, Chem. Mater., 13 (2001) 4469-4472
19. D. M. DeLongchamp, M. Kastantin, P. T. Hammond, “High-Contrast Electrochromism from Layer-by-Layer Polymer Films”, Chem. Mater., 15 (2003) 1575-1586
20. C. L. Gaupp, K. Zong, P. Schottland, B. C. Thompson, Ch. A. Thomas, J. R. Raynolds, “Poly(3,4-ethylenedioxypyrrole): Organic Electrochemistry of a High Stable Electrochromic Polymer”, Macromolecule, 33 (2000) 1132-1133
21. G. Sonmez, I. Schwendeman, P. Schottland, K. Zong, J. R. Reynolds, „ N-Substituted Poly(3,4-propylenedioxypyrrole)s: Haigh Gap and Low Redox Potential Switching Electroactive and Electrochromic Plymers“, Macromolecule, 36 (2003) 639-647
22. C. J. DuBois, J. Reynolds,"3,4-Ethylenedioxythiophene-Pyridine-Based Polymers: Redox or N-Type Electronic Conductivity”, Adv. Mater., 14 (2002), 1844-1846
23. G. A. Sotzing, K. Lee, “Poly(thieno[3,4-*b*]thiophene); a P- and N-dopable Polythiophene Exhibiting High Optical Transparency in the Semiconducting State**”,** Macromolecules, 35 (2002) 7281-7286
24. P. H. Aubert, A. A. Argun, A. Cirpan, D. B. Tanner, J. R. Reynolds, „Microporous Patterned Electrodes for Color-Matched Electrochromic Polymer Displays“, Chem. Mater., 16 (2004) 2386-2393
25. E. Yablonovtich, “Electrochromic adaptive infrared camouflage” http://www.ee.ucla.edu/~eamuri/vu-graphs/yablonovitch/yablonovitch10.html

26. S. Holdcroft, “Patterning π-conjugated polymers”, Advanced Materials, 13 (2001) 1753-1765
27. J. P. Coleman, A. T. Lynch, P. Madhukar, J. H. Wagenknecht, “Antimony-doped tin oxide powders: - Electrochromic materials for printed displays”, Solar Energy Materials and Solar Cells, 56 (1999) 395-394
28. Switchable Glazing Windows, http://www.toolbase.org/techinv/techDetails.aspx?technologyID=187
29. G. Tulloch, I. Skryabin, G. Evans, J. Bell, „Operation of electrochromic devices prepared bysol-gel methods”, Proc. of SPIE, Sol-Gel Optics IV, 3136 (1997) 426-432
30. G. Destriau, “Recherchers sur les Scintillations des Sulferes de Zinc aux Rayons”, J. Chem. Phys., 33 (1936) 587-625
31. C. W. Tang, S. A. Van Slyke, “Organic Electroluminiscent Diodes”, Appl. Phys. Lett., 51 (1987) 913-915
32. M. Pope, H. P. Kallmann, P. Magnate, „Electroluminiscence in Organic Crystals“, J. Chem. Phys., 38 (1963) 2042-2043
33. J. H. Burroughes, D. D. C. Bradley, A. R. Brown, R. N. Marks, K. Mackay, R. H. Friend, P. L. Burn, A. B. Holmes, “Light-emitting Diodes Based on Conjugated Polymers”, Nature, 347 (1990) 539-541
34. D. Braun, A. J. Heeger, “Visible Light Emission from Semiconducting Polymer Diodes”, Appl. Phys. Lett., 58 (1991) 1982-1984
35. M. R. Andersson, G. Yu, A. J. Heeger, “Photoluminescence and Electroluminescence of films from soluble PPV”, Synth. Metals, 85 (1997) 1275-1276
36. D. G. J. Sutherland, J. A. Carlisle, P. Elliker, G. Fox, T. W. Hagler, I. Jimenez,H. W. Lee, K. Pakbaz, L. J. Terminello, S. C. Williams, F. J. Himpsel, D. K. Shuh, W. M. Tong, J. J. Jia, T. A. Callcott, D. L. Ederer,“Photo-oxidation of electroluminescent polymers studied by core-level photoabsorption spectroscopy“, Appl. Phys. Lett., 68 (1996) 2046-2048
37. A. Greiner, B. Bolle, P. Hesemann, J. M. Oberski, R. Sander, “Preparation and Structure-Property Relationships of Polymeric Materials Containing Arylenevinylene Segments – perspectives for new light-emitting materials”, Macromol. Chem. Phys. , 197 (1996) 113–134
38. J. L. Segura, “The chemistry of electroluminescent organic materials”, Acta Polymerica, 49 (1998) 319-344
39. R. H. Friend, R. W. Gymer, A. B. Holmes, J. H. Burroughes, R. N. Marks, C. Taliani, D. D. C. Bradley, D. A. Dos Santos, J. L. Bredas, M. Loeglund, W. R. Salaneck, “Electroluminescence in conjugated polymers”, Nature, 397 (1999) 121-128
40. A.Kraft, A. C. Grimsdale, A. B. Holmes, „Electroluminescent Conjugated Polymers - Seeing Polymers in a New Light”, Angew. Chem. Int. Ed., 37 (1998) 402-428
41. B. Liu, G. C. Bazan, “Chemistry of electroluminescent conjugated polymers” in Organic Luminescence, ed. Z. H. Kafafy, CRC Press, boca Raton, 2005
42. C. H. Lee, G. W. Kang, J. W. Jeon, W. J. Song, S. Y. Kim, C. Seoul, Photoluminescence and electroluminescence of vacum-deposited poly(p-phenylene) thin film, Synthetic Metals, 117 (2001) 75-79

43. P. B. Balanda, M. B. Ramey, J. R. Reynolds, “,Water-soluble and blue luminescent cationic polyelectrolytes based on poly (p-phenylene)”, Macromolecules, 32 (1999) 3970-3978
44. D. F. Perepichka, I. G. Perepichka, H. Meng, F. Wudl, “Light Emitting Polymers”, in “Organic Light Emitting Diodes”, ed. Z. R. Li, Marcell-Dekker Inc., 2006 (in press)
45. Y. Ohmori, M. Uchida, K. Muro, K. Yoshio, “Blue Electroluminescent Diodes Utilizing Poly(alkylfluorene)”, Jpn. J. Apll. Phys., 30 (1991) 1941-1943
46. M. Inbasekaran, E. P. Woo, W. Wu, M. Bernius, L. Wujkowski, „Fluorene Homopolymers and Copolymers“, Synth. Met., 111-112 (2000) 397-401
47. http://www.cdtltd.co.uk/technology/36.asp
48. M. Leadbeater, “Polymers Shine the Light”, SPIE Oe Magazin, 2002
49. I. I. Perepichka, I. F. Perepichka, M. R. Bryce, L. O. Palsson, “Dibenzothiophene-S,S-Dixide-Fluorene co-Oligomers. Stable, Highly-Efficient Blue Emitters with Improved Electron Affinity”, Chemical Communications, (2005) 3397-3399
50. J. Y. Kim, S. H. Park, K. Lee, „High-Efficiency Bipolar Electroluminescent Polymer Containing an Oxadiazole Pendant Group“, J. Korean Phys. Soc., 47 (2005) 167-170
51. F. Shen, F. He, D. Lu, Z. Xie, W. Xie, Y. Ma, B. Hu, „Bright and Colour Stable White Polymer Light-Emitting Diodes“, Semicond. Sci. Technol. 21 (2006) L16-L19
52. http://www.chem.ufl.edu/~reynolds/
53. http://www.princeton.edu/~polymer/elelumpoly.html
54. H. Wang, X. Tao, E. Newton, “Thermal degradation kinetics and lifetime prediction of a luminescent conducting polymer”, Polymer International, 53 (2004) 20-26
55. M. B. Wolk, “Patterning of OLED device materials” in Organic Luminescence, ed. Z. H. Kafafy, CRC Press, boca Raton, 2005
56. J.A. Rogers, Z. Bao and L. Dhar, “Fabrication of patterned electroluminescent polymers that emit in geometries with feature sizes into the submicron range”, Appl. Phys. Lett., 73 (1998) 294–296
57. M. Onoda, K. Yoshino, “Fabrication of self-assembled multilayer heterostructure of poly(*p*-phenylene vinylene) and its use for an electroluminescent diode”, J. Appl. Phy., 78 (1995) 4456–4462

15 Ferroelectrets – Cellular piezoelectric polymers

Michael Wegener – Department of Physics, University of Potsdam, Germany

Ferroelectrets are a new class of piezoelectric polymers. They consist of non-polar space-charge electrets with cellular foam structures. An electret is a material which can exhibit an internal polarization due to (i) trapped charges e.g. in non-polar space-charge electrets, (ii) oriented molecular dipoles in polar electrets, or a combination of both of these effects [1]. A well-known polar piezoelectric polymer is polyvinylidene fluoride (PVDF) in which the piezoelectric activity arises from the change of dipole density during the application of a mechanical stress or an electric field. Details of classical ferroelectric polymers are given in a book edited by Nalwa [2].

In the case of the new non-polar ferroelectrets, the microscopic origin of the piezoelectric activity is completely different compared to that of well known polar ferroelectric polymers. In ferroelectrets charge separation exists, effectively creating upper and lower void surfaces that are oppositely charged (Figure 15.1). This is the origin of the breakdown of symmetry, which is required for piezoelectric characteristics to emerge. Each void can be considered as a macroscopic dipole. An applied mechanical stress leads to the decrease of void sizes accompanied by the generation of an electrical signal. Therefore piezoelectricity in ferroelectrets results from changes of dipole sizes.

The development of ferroelectret materials (previously referred to as cellular electro-mechanical films) was initiated in Finland during the late eighties [3,4] and strengthened in the late nineties [5,6]. Several groups entered this research field and today ferroelectrets are established as a major form of piezoelectric polymer, along with ferroelectric polymers. The mechanisms, preparations, properties and applications of ferroelectrets have been described in recent reviews [7-9].

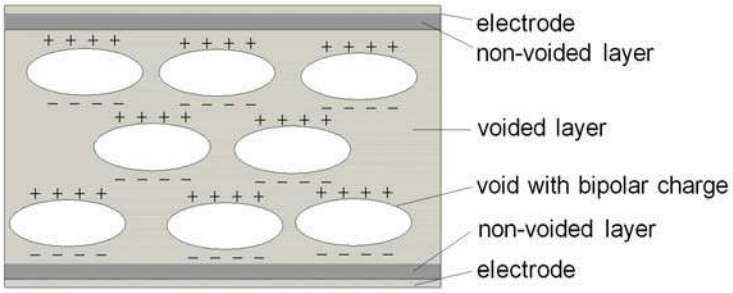

Figure 15.1: Schematic sketch of a cellular polymer film with trapped bipolar charge.

To-date piezoelectric foams of polypropylene PP [8, 9]), polyethylene terephthalate PETP [10-12], a variety of compounds of cyclo-olefine polymers COP, copolymers COC [13-16] and Teflon®AF [17] have been developed. Ferroelectrets prepared from PP, PETP and COP form the basis of the following brief overview, which is focused on the preparation of cellular foams, the internal charging of the voids, the resulting piezoelectric properties, and concluding with a discussion of demonstrated applications.

15.1 Foam preparation and optimization

In the design of a ferroelectret, a cellular void structure is required as the starting point to obtain piezoelectric properties from non-polar space-charge electrets. The optimal cellular structures consist of lens-like voids with diameters of approximately 10 to 100 µm and widths of approximately 1 to 100 µm. Typical cellular structures of PP, PETP and COP ferroelectrets are shown in the scanning electron microscopy (SEM) images in Figure 15.2, adapted from the references [18, 10, 15]. Recently, a non-destructive 3D-scan of a cellular ferroelectret was performed with optical coherence tomography (OCT), which yields additional information e.g. about the form and dimensions of the cell walls [19].

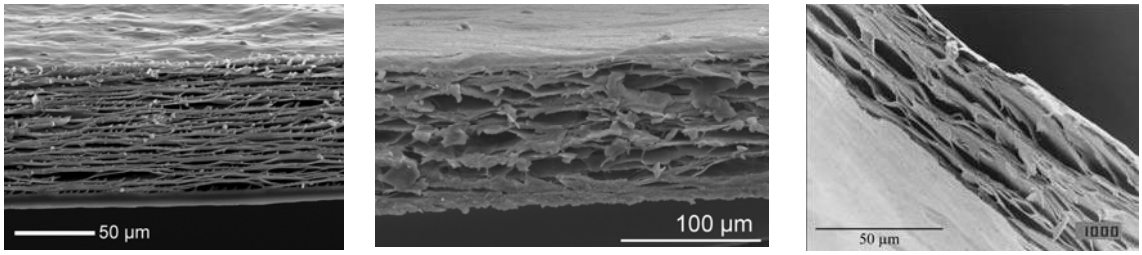

Figure 15.2: Scanning electron microscopy (SEM) images of PP (left), PETP (middle) and COP (right) ferroelectrets, after [18, 10, 15].

Different foaming procedures with separate preparation steps were developed in order to obtain optimized cellular structures. The first step is the initial foaming obtained either by extrusion of filler loaded polymers or by treatment in gases or supercritical fluids (SCF). The extrusion method often leads to cracks and void formation during the manufacturing process (schematically shown in [20]). The latter treatment utilizing gases, e.g. in carbon dioxide or supercritical carbon dioxide, during or after the extrusion leads to diffusion of the gas into the polymer. When the pressure is suddenly released, the gas expands violently, which leads to a voided structure. This process is supported by a heat treatment. Ferroelectret foaming by SCF and heat treatment is described in [11, 12] the principle of their methods and their application to other materials is described in [21]. With this approach, approximately round voids are obtained depending on the base material. After forming the porous polymer, lens-shaped voids are formed by a biaxial stretching of the foamed polymer films. The void heights (which represent the size of the macroscopic dipoles) can be subsequently adjusted by an inflation process [9]. A variety of inflation procedures have been studied in detail [22-28] where suitable inflation parameters, the resulting void structures and their influence upon the piezoelectric properties were examined. As a result, the void sizes in filled-loaded, extruded, stretched and inflated polymers can be adjusted and tailored from flat lens-shaped up to large round voids with diameters of approximately 100µm [26].

The variety of cellular structures that can be formed result in different piezoelectric and elastic properties, which in turn depend significantly upon the foam porosity. The foam porosity can be determined by the film density. The interdependencies are shown schematically (Figure 15.3a) along with experimental data in Figure 15.3b. A low elastic stiffness of the foam is essential for a high piezoelectric activity (see Figure 15.3a). For PP ferroelectrets the optimized void length and height ratio is approximately

4 to 5, which corresponds to lens-like voids. However, the cell-wall thickness must be taken into consideration [29]. Furthermore, there is a lower limit on the elastic modulus since deformation during use of the material as a transducer should be reversible. The above-mentioned experimental conclusions regarding manufacture of cellular materials are also supported by numerical calculations [30] and by recently performed experiments [31]. Therefore, these dependencies find great use in the development and application of new ferroelectrets.

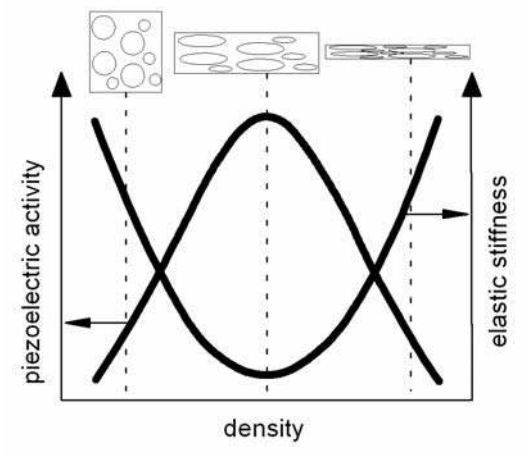

(a)

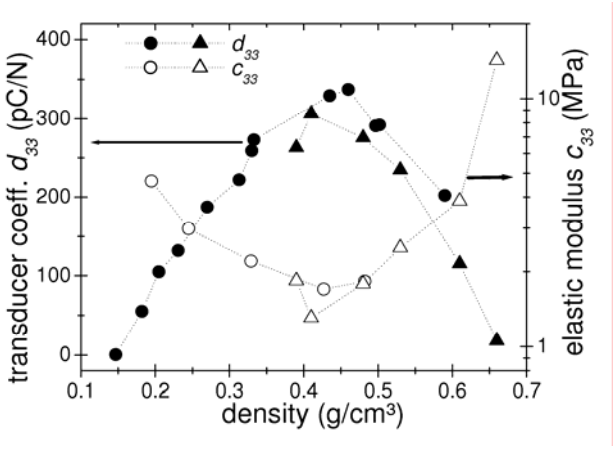

(b)

Figure 15.3: Schematic sketch and experimental data (obtained on PP ferroelectrets) of piezoelectric d_{33} coefficient and elastic stiffness c_{33} as function of the foam density, after [10] and [29].

15.2 Void charging in cellular space-charge electrets

Non-voided electrets were traditionally charged electrically by means of a corona discharge. Initially, the corona discharge method was also preferred for charging of foamed electrets and it is now the accepted method for charging of large-scale ferroelectret transducers. However, the detailed understanding of the mechanism of charging cellular structures was obtained by examining a range of charging techniques, along with the variation of charging parameters.

Cellular films are charged by corona discharge or direct application of high electric fields in the range from tens to hundreds MV/m. The large field across the film thickness leads to dielectric barrier micro-plasma discharges inside the voids, which results in trapping of charges with opposite polarities on the top and bottom sides of the voids, as schematically shown in Figure 15.1. Evidence for the nature of this mechanism is provided by several experimental results. An electric field above a threshold is necessary to initiate the micro-

plasma discharges, which was seen during charging experiments with varying electric fields applied by means of a corona discharge [32] as well as during direct-contact charging [20, 33]. The electric charging depends significantly on the ambient atmosphere in the sample chamber and in the sample itself [11, 18, 22]. The micro-plasma discharges can be visually observed, and were recorded in-situ during direct-contact charging via transparent electrodes [34].

Charge patterns were measured by scanning electron microscopy (SEM) on obliquely cut cellular PP films and this constitutes direct proof of the internal void charging [35]. Furthermore, the switching of the internal polarization was demonstrated by means of direct-contact charging [20, 34], which gives rise to a hysteresis curve of the polarization or the piezoelectric activity as a function of the applied electric field. In summary, the charging of ferroelectrets is significantly different from the charging of non-cellular space-charge electrets. Charging of ferroelectrets leads to two different stable polarization states and is therefore comparable to the charging of ferroic materials, which was also the reason for the development of the name 'ferroelectrets' (for further details see the reviews [7-9]).

15.3 Piezoelectric properties

In general, ferroelectrets show high piezoelectric activity after suitable foaming and optimized electric charging. Typically, piezoelectric d_{33} coefficients of several hundred pC/N or pm/V were reported for the direct and inverse piezoelectric effect in cellular PP films [22, 25-28, 36-38]. The recently developed PETP ferroelectrets and COC and COP ferroelectrets, which were prepared by extrusion of filler loaded polymer, exhibit a lower piezoelectric activity, at least under the current manufacturing conditions [10, 11, 13-16].

Ferroelectrets exhibit significant thickness-extension resonances [10, 25, 36, 37]. Bauer and co-workers found length-extension resonances, but with a piezoelectric activity two orders of magnitude lower than for the thickness extension [37]. Furthermore, they showed that the pyroelectricity of ferroelectrets is very small and approximately two orders of magnitude below that of classical pyroelectric materials such as ferroelectric PVDF. Table 15.1 summarises typical values of the piezoelectric coefficient d_{33}, the elastic stiffness c_{33} and the thickness-extension resonance frequency f_{TE} for different ferroelectrets. An extended comparison of piezoelectric and elastic properties of PP ferroelectrets and ferroelectric PVDF is given in [39]. A direct comparison of the d_{33} coefficient of ferroelectrets and ferroelectrics such as PVDF can give a misleading view of their relative performance due to the large difference in their elastic stiffeness, by a factor of 1000 or more (and therefore the dependence of their piezoelectric activity on pre-pressure), pyroelectricity and d_{31} activity.

Ferroelectret	Elastic	Piezoelectric	Resonant

material	stiffness c_{33} (MPa)	coefficient d_{33} (pC/N)	Frequency f_{TE} (kHz)	Ref
PP	1.3 ... 14	up to 340	600 ... 2000	[25]
PETP	7	up to 23	560	[10]
COC / COP		up to 25		[13]

Table 15.1: Piezoelectric and elastic properties of ferroelectrets

It should be mentioned that specialised preparations or treatments can lead to significantly higher piezoelectric coefficients of 790pC/N [22] or 2000pC/N [27] in PP and approximately 476pC/N in PETP [12] ferroelectrets.

The thickness-extension resonance in the high kHz up to the low MHz region is the basis for the application of especially PP ferroelectrets in the audible and ultrasonic frequency range as microphones [38, 40, 41] or as loudspeakers [42-44]. A further advantage of PP ferroelectrets driven in the audible and ultrasonic frequency range is their low quadratic and cubic distortion, which is found to be typically 20 dB below the fundamental sound [40, 42].

PP ferroelectrets show high piezoelectric activity, however, in the optimization of the transducer properties various approaches such as stacking of individual layers were attempted. A layer system can be arranged by folding or bending a ferroelectret film [45, 46], by stacking or gluing ferroelectret films on top of each other [38, 44] or connecting the ferroelectrets via a spacer air gap [14]. For PP and COP ferroelectrets, the piezoelectric activity increases linearly with the number of active layers [38, 44], however, only for the first approximately 5 to 10 layers, since the foam weight eventually influences the piezoelectric activity of the lower films in the stack [15, 44].

A critical property in terms of applications of ferroelectrets is the thermal stability of their piezoelectric activity. For PP ferroelectrets the thermal stability of the high piezoelectric activity is limited to approximately 60°C [37, 47, 48]. Annealing at elevated temperatures decreases the piezoelectric activity, due to loss of polarization within the voids and changes of void geometry. However, the resulting lower activity is thermally stable up to approximately 80°C. Therefore, PP ferroelectrets can be made to fulfill some application requirements, as discussed below. In comparison to PP ferroelectrets, a slightly increased piezoelectric activity is found in PETP ferroelectrets [10]. A significant improvement in thermal stability is obtained with the cyclo-olefine polymers and copolymers. Excellent thermal stability up to at least 110°C was demonstrated for some COP compounds [13, 15].

For PP ferroelectrets in particular other environmental influences such as UV radiation and higher humidity were tested. UV radiation decreases the piezoelectric activity slightly [49]. Storage in higher humidity and at temperatures of up to 50°C for 12 days leads to a 25% decrease of the piezoelectric coefficient [48]

15.4 Applications of ferroelectrets

Several applications were suggested and demonstrated for PP ferroelectrets as described in the reviews [7] and [9]. These applications are often similar to those of other thin piezoelectric films such as e.g. ferroelectric polymers. However, the difference in the structural properties of ferroelectrets and ferroelectrics allow them to support different applications. The disadvantages of ferroelectrets are their strong dependence of the piezoelectricity upon the applied static pre-stress [43, 48, 50, 51] whereas the very low pyroelectric activity is in direct comparison, for example, with the ferroelectric PVDF. Thus, in ferroelectrets the piezoelectric signal will not be super-imposed with a pyroelectric current if a temperature change occurs.

Some examples of applications are quasistatic sensors for motion detection used in factory buildings for safety reasons, as well as for traffic control of cars and other vehicles as suggested in [52]. Another application area is pressure monitoring for sports and orthopedic diagnostics [53]. Applications, which are already implemented and currently served by PP ferroelectrets, are push buttons for keyboards for a variety of equipment (for details see the description in [9]). A new development in this area is the combination of ferroelectrets with integrated field-effect transistors [54].

As discussed above, PP ferroelectrets are suitable as microphones, which were already realized in the early nineties and used to record the respiration of human patients [55]. Furthermore, sensors working in the frequency range from 50Hz to 23kHz are produced to function as pickups for musical instruments by the company EMFIT in Finland. This application is probably the largest currently, in terms of manufactured quantities.

The application of ferroelectrets as sensors and actuators in ultrasonic applications such as material testing and industrial gas-flow measurements is a current area of research and development. An unusual ultrasonic application was realized with the implementation of PP ferroelectrets as a transducer to mimic the echo-detection capabilities of a bat in flight [41, 56].

Conclusions and outlook

Ferroelectrets are a new class of piezoelectric polymers. They exhibit outstanding piezoelectric activities compared to ferroelectric polymers and enable applications such as quasistatic sensors and as transducers at audible and ultrasonic frequencies. Some applications such as keyboards and pick-ups for musical instruments are already implemented industrially. Until now, ferroelectrets of three different electret polymers, i.e. PP, PETP and compounds of different cyclo-olefine polymers or copolymers were developed. Extensive knowledge about the processing of PP ferroelectret allows for a wide range adjustment of piezoelectric and elastic properties.

The new processing possibilities of PETP ferroelectrets by treatment with supercritical fluids offer better lab-scale investigation of the basic foaming mechanisms. The most thermally stable ferroelectret transducers are prepared from compounds of cyclo-olefine polymers. Investigations of suitable compounding of cyclo-olefine polymers are still running. Furthermore, the expansion of the ferroelectret concept to fluorinated polymers is

under development. Based on the excellent electret properties of fluorinated polymers [1], a high thermal stability of fluorinated ferroelectrets is expected.

[1] G.M. Sessler (Ed.), Electrets, 3rd Edition, Volume 1, Laplacian Press, Morgan Hill, CA, 1999
[2] H.S. Nalwa (Ed.), Ferroelectric Polymers, Marcel Dekker Inc., New York, 1995
[3] K. Kirjavainen, U.S. Patent No. 4,654,546 (1987)
[4] A. Savolainen, Polym. Eng. Sci. 30 (1990) 1258
[5] M. Paajanen, H. Välimäki., and J. Lekkala, J. Electr. 48 (2000) 193
[6] M. Paajanen, J. Lekkala, and K. Kirjavainen, Sens. and Act. 84 (2000) 95
[7] R. Gerhard-Multhaupt, IEEE Trans. Dielectr. Electr. Insul. 9 (2002) 850
[8] S. Bauer, R. Gerhard-Multhaupt, and G.M. Sessler, Phys. Today 57 (Febr. 2004) 37
[9] M. Wegener and S. Bauer, ChemPhysChem 6 (2005) 1014
[10] M. Wegener, W. Wirges, and R. Gerhard-Multhaupt, Adv. Eng. Mat. 7 (2005) 1128
[11] M. Wegener, W. Wirges, J.P. Dietrich, and R. Gerhard-Multhaupt, Proceedings 12th International Symposium on Electrets (ISE 12), IEEE Service Center, Piscataway NJ (2005) 28
[12] W. Wirges, M. Wegener, O. Voronina, L. Zirkel, and R. Gerhard-Multhaupt, Adv. Fun. Mat. in press (2006)
[13] A.-M. Savijärvi, M. Paajanen, E. Saarimäki, and H. Minkkinen, Proceedings 12th International Symposium on Electrets (ISE 12), IEEE Service Center, Piscataway, NJ (2005) 75
[14] E. Saarimäki, M. Paajanen, A.-M. Savijärvi, and H. Minkkinen, Proceedings 12th International Symposium on Electrets (ISE 12), IEEE Service Center, Piscataway, NJ (2005) 220
[15] M. Wegener, M. Paajanen, O. Voronina, R. Schulze, W. Wirges, and R. Gerhard-Multhaupt, Proceedings 12th International Symposium on Electrets (ISE 12), IEEE Service Center, Piscataway NJ (2005) 47
[16] G.C. Montanari, D. Fabiani, F. Ciani, A. Motori, M. Paajanen, R. Gerhard-Multhaupt, and M. Wegener, IEEE Trans. Dielectr. Electr. Insul. submitted (2006)
[17] A. Mellinger, M. Wegener, W. Wirges, and R. Gerhard-Multhaupt, Appl. Phys. Lett. 79 (2001) 1852
[18] X. Qiu, M. Wegener, W. Wirges, X. Zhang, J. Hillenbrand, Z. Xia, R. Gerhard-Multhaupt and G. M. Sessler, J. Phys. D: Appl. Phys. 38 (2005) 649
[19] K. Wiesauer, M. Pircher, E. Götzinger, S. Bauer, R. Engelke, G. Ahrens, G. Grützner, C.K. Hitzenberger, and D. Stifter, Opt. Expr. 13 (2005) 1015
[20] M. Wegener and W. Wirges, Optimized electromechanical properties and applications of cellular polypropylene, a new voided space-charge electret material, in: H.-J. Fecht and M. Werner (Eds), The Nano–Micro Interface: Bridging the Micro and Nano Worlds, Wiley-VCH, Weinheim (2004) 303
[21] A.I. Cooper, Adv. Mat. 15 (2003) 1049
[22] M. Paajanen, M. Wegener, and R. Gerhard-Multhaupt, J. Phys. D: Appl. Phys. 34 (2001) 2482

[23] M. Paajanen, H. Minkkinen, and J. Raukola, Proceedings, 11th International Symposium on Electrets (ISE 11), IEEE Service Center, Piscataway, NJ (2002) 191
[24] M. Wegener, W. Wirges, R. Gerhard-Multhaupt, M. Paajanen, H. Minkkinen, and J. Raukola, Annual Report, Conference on Electrical Insulation and Dielectric Phenomena (CEIDP), IEEE Service Center, Piscataway, NJ (2003) 36
[25] M. Wegener, W. Wirges, R. Gerhard-Multhaupt, M. Dansachmüller, R. Schwödiauer, S. Bauer-Gogonea, S. Bauer, M. Paajanen, H. Minkkinen, and J. Raukola, Appl. Phys. Lett. 84 (2004) 392
[26] M. Wegener, W. Wirges, J. Fohlmeister, B. Tiersch, and R. Gerhard-Multhaupt, J. Phys. D: Appl. Phys. 37 (2004) 623
[27] X. Zhang, J. Hillenbrand, and G.M. Sessler, J. Phys. D: Appl. Phys. 37 (2004) 2146
[28] X. Zhang, J. Hillenbrand, and G.M. Sessler, Appl. Phys. Lett. 85 (2004) 1226
[29] M. Wegener, E. Tuncer, W. Wirges, R, Gerhard-Multhaupt, M. Dansachmüller, S. Bauer-Gogonea, R. Schwödiauer, and S. Bauer, Proceedings IEEE Ultrasonics Symposium 2004, IEEE Service Center, Piscataway, NJ (2004) 1138
[30] E. Tuncer and M. Wegener, Mat. Lett. 58 (2004) 2815
[31] J. Hillenbrand, G.M. Sessler, and X. Zhang, J. Appl. Phys. 98 (2005) 06410
[32] M. Wegener, M. Paajanen, W. Wirges, and R. Gerhard-Multhaupt, Proceedings 11th International Symposium on Electrets (ISE 11), IEEE Service Center, Piscataway, NJ (2002) 54
[33] R. Gerhard-Multhaupt, M. Wegener, W. Wirges, J.A. Giacometti, R.A.C. Altafim, L.F. Santos, R.M. Faria, and M. Paajanen, Annual Report, Conference on Electrical Insulation and Dielectric Phenomena (CEIDP), IEEE Service Center, Piscataway, NJ (2002) 299
[34] M. Lindner, S. Bauer-Gogonea, S. Bauer, M. Paajanen, and J. Raukola, J. Appl. Phys. 91 (2002) 5283
[35] J. Hillenbrand and G.M. Sessler, Annual Report, Conference on Electrical Insulation and Dielectric Phenomena (CEIDP), IEEE Service Center, Piscataway, NJ (2000) 161
[36] G.S. Neugschwandtner, R. Schwödiauer, M. Vieytes, S. Bauer-Gogonea, S. Bauer, J. Hillenbrand, R. Kressmann, G.M. Sessler, M. Paajanen and J. Lekkala, Appl. Phys. Lett. 77 (2000) 3827
[37] G.S. Neugschwandtner, R. Schwödiauer, S. Bauer-Gogonea, S. Bauer, M. Paajanen and J. Lekkala, J. Appl. Phys. 89 (2001) 4503
[38] J. Hillenbrand and G.M. Sessler, J. Acoust. Soc. Am. 116 (2004) 3267
[39] M. Wegener and R. Gerhard-Multhaupt, Ferroelectrets: polymer foams for piezoelectric transducers, in R.F. Singer, C. Körner, V. Altstädt and H. Münstedt (Eds), Cellular Metals and Polymers 2004, Trans Tech Publications, Uetikon-Zurich, Switzerland, 2005
[40] R. Kressmann, J. Acoust. Soc. Am. 109 (2001) 1412
[41] A. Streicher, R. Müller, H. Peremans, M. Kaltenbacher, and R. Lerch, Proceedings IEEE International Ultrasonics 2004, IEEE Service Center, Piscataway, NJ (2004) 1142
[42] M. Wegener, S. Bergweiler, W. Wirges, A. Pucher, and Reimund Gerhard-Multhaupt, Proceedings 116th Conference of the Audio Engineering Society 2004, Berlin May 8-11, 2004

[43] J. Hillenbrand and G.M. Sessler, IEEE Trans. Dielectr. Electr. Insul. 11 (2004) 72
[44] M. Wegener, S. Bergweiler, W. Wirges, A. Pucher, E. Tuncer, and R. Gerhard–Multhaupt, IEEE Trans. Ultrason., Ferroelectr, Freq. Contr. 52 (2005) 1601
[45] A. Savolainen and K. Kirjavainen, J. Macrom. Sci. – Chem. A26 (1989) 583
[46] M.K. Hämäläinen, J.K. Parviainen, and T. Jaaskelainen, Rev. Sci. Instr. 67 (1996) 1598
[47] D. M. Taylor and O. Fernández, IEEE Trans. Dielectr. Electr. Insul. 12 (2005) 768
[48] A. Mellinger, M. Wegener, W. Wirges, R.R. Mallepally, and R. Gerhard-Multhaupt, Ferroelectrics 331 (2006) 189
[49] A. Mellinger, F. Camacho Gonzalez, and R. Gerhard-Multhaupt, Appl. Phys. Lett. 82 (2003) 254
[50] R. Kressmann, J. Appl. Phys. 90 (2001) 3489
[51] M. Dansachmüller, R. Schwödiauer, S. Bauer-Gogonea, S. Bauer, M. Paajanen and J. Raukola, Appl. Phys. Lett. 86 (2005) 031910
[52] M. Paajanen, J. Lekkala, and H. Välimäki, IEEE Trans. Dielectr. Electr. Insul. 8 (2001) 629
[53] J. Lekkala and M. Paajanen, Proceedings of the 10th International Symposium on Electrets (ISE 10), IEEE Service Center, Piscataway, NJ (1999) 743
[54] I. Graz, M. Kaltenbrunner, C. Keplinger, R. Schwödiauer, S. Bauer, S.P. Lacour and S. Wagner, Flexible ferroelectret field-effect transistor for large-area sensor skins and microphones, Appl. Phys. Lett. in press.
[55] J. Siivola, K. Leinonen, and L. Räisänen, Med. Biolog. Eng. & Comp. 31 (1993) 634
[56] A. Streicher, R. Müller, H. Peremans, and R. Lerch, Proceedings, IEEE Ultrasonics Symposium 2003, IEEE Service Center, Piscataway, NJ (2003) 1364

16 Conductive Polymers

Carmen Moldovan, Rodica Iosub – IMT - National Institute for Research and Development in Microtechnologies, Bucharest, Romania

Conductive polymers are sometimes called 'synthetic metals' because they present electric, electronic, magnetic and optical properties inherent to metals or semiconductors, while preserving the mechanical properties of conventional polymers.

Until about 30 years ago, all carbon-based polymers were rigidly regarded as insulators. The notion that polymers could be made to conduct electricity would have been considered to be absurd. They were used, for example, as inactive packaging and insulating materials. Alan J. Heeger, Alan G. MacDiarmid and Hideki Shirakawa changed this conception with their discovery that a polymer, polyacetylene, can be made conductive almost like a metal.

They managed to make polyacetylene films that were 109 times more conductive than they were in their original state by oxidation with chlorine, bromine or iodine vapour, and they received the Nobel Prize in chemistry for this achievement in 1977 [1].

Since that time some interesting applications of these materials have been developed [2,3], such as light emitting diodes, solar cells, transistors, diodes, holographic storage media, chemical and biological sensors, capacitors, batteries, anti-static coatings, electromagnetic shielding, anti-corrosive coatings, gas and liquid separation membranes, artificial muscles, lithography and metallization, photo-electrochromic devices, xerographic photoreceptors and all-polymer electronic circuits.

Several companies involved in commercialisation of conjugated polymer devices include, Pioneer, Dupont, Cambridge Display, Infineon, Kodak, Sanyo, Philips and TDK.

Conductive polymers have found extensive potential application in the fields of micro-sensors and micro-actuators, providing cheaper, accurate and faster alternatives to devices already on the market. Chemical sensors and biosensors with remarkable specifications have been developed and some of them are already being used in medicine for fast bio-diagnostic systems. Conductive polymer-based actuators also seem to hold great promise for the future, owing to their high strength and low energy consumption. Models of actuator response are being tested [4-11], but the relationship between input electrical energy and mechanical output has yet to be fully described.

In the sections to come, a brief description of some conductive polymers will be made, followed by a discussion of their conductivity mechanism. The focus will then shift onto applications of conductive polymers in sensor and actuator systems, including some noable examples of recent achievements.

16.1 Mechanism of polymer conductivity – role of doping

Polymers that have been studied extensively since the early 1980s include polypyrrole, polythiophene (and various polythiophene derivatives) and polyaniline. Polyacetylene, the original conductive polymer, exhibits the highest crystallinity of this group, but itwas not the first conductive polymer to reach commercial production. The reason for this is its

sensitivity both to atmospheric oxygen and to humidity. Polypyrrole and polythiophene, however, differ from polyacetylene most notably in that they may be synthesized directly in the doped form and they are very stable in air.

In intrinsically conductive polymers, conductivity is atributed to delocalization of π-bonded electrons, in conjugated double bonds, over the polymeric backbone. These materials also exhibit unusual electronic properties, such as low energy optical transitions, low ionization potentials and high electron affinities [12]. Figure 16.1 shows the structure of some conductive polymers.

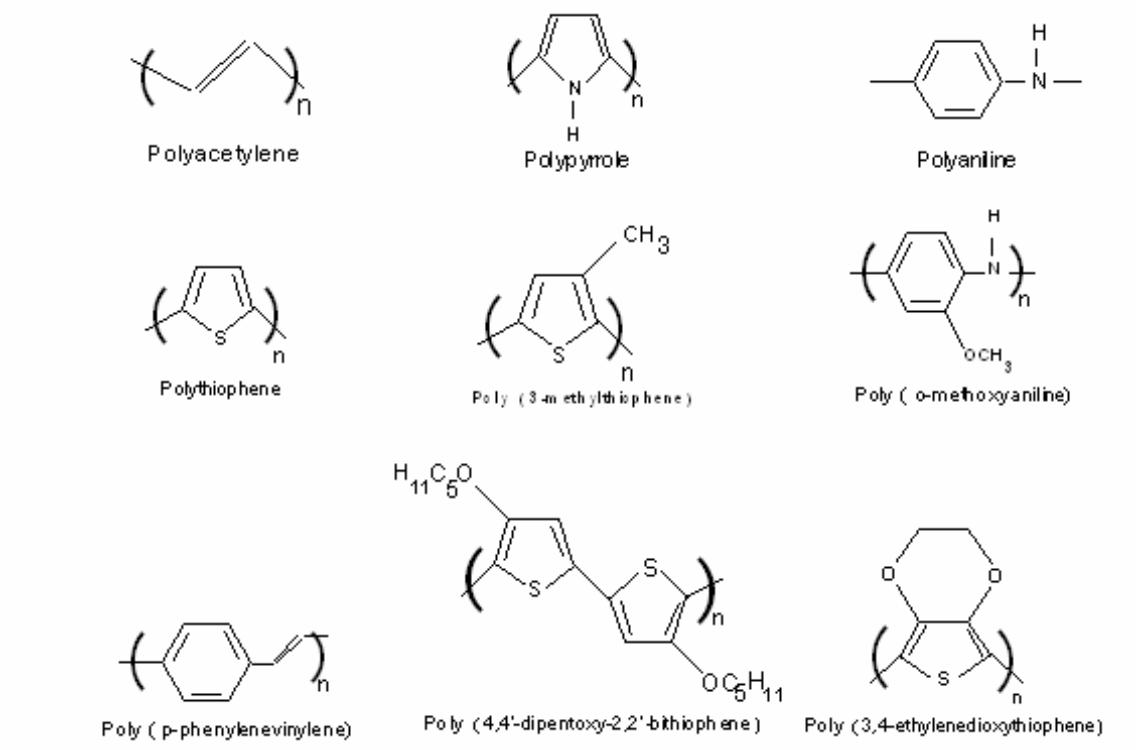

Figure 16.1 - Structure of some commonly used conductive polymers

Steric (conformational) factors and charge interactions can easily limit the degree of delocalization, leading to the formation of energy gaps analogous to conventional semiconductors such as Si or Ge. To become electrically conductive, the polymers have to be disturbed-either by removing electrons from (oxidation), or by inserting electrons into (reduction), the material. This process is known as *doping*. Depending on the dopant, conductive polymers exhibit either p-type or n-type conductivity. For example, treatment with halogens has been termed 'doping' by analogy with the doping of semiconductors. During this process, an organic polymer, either an insulator or semiconductor having a small conductivity, typically in the range 10^{-10} to 10^{-5} Scm^{-1} is converted into a polymer which is in the 'metallic' conductive regime (~1 to 10^4 Scm^{-1}). Conductivities are relatively low in comaprison to metals at around $10^4 Scm^{-1}$, but this is enough for many practical purposes.

Dopant ions are generally introduced into the polymer system during chemical or electro-chemical polymerization and they play an important role in balancing the charge distribution within the polymer. The dopant ion influences the distribution of positive charge on the polymer backbone and, when constrained over a small area, this can cause additional closely spaced electronic levels to form within the band gap. Small lattice distortions occur locally so that conformational changes as well as charge inequalities are induced in the polymer backbone. The net effect is that the oxidation state changes and the equivalent of free radicals can be formed. A charged site interacting with a free radical forms a polaron. These are normally highly unstable but they can be stabilized by further oxidation of the polymer to form a bipolaron. Polarons are radical cations or anions that are generated during the doping process, but if the doping level is sufficiently high, a radical dication (a spinless defect) can be generated on the same polymer segment [13]. This is termed a bi-polaron. These defects lie within the band gap of the material and it is these defects that make conductive polymers interesting for chemical sensing.

The introduction of dopants and the creation of bipolarons influence the electrical conduction mechanism. It can be assumed that the attraction of an electron in one repeat unit of the polymer backbone to the nuclei in neighboring units leads to carrier delocalization along the polymer chain and to charge carrier mobility. This is further extended into three dimensions through inter-chain electron transfer. Primary dopants are used to change the electronic, optical, magnetic, and/or structural properties of the polymer and this is accompanied by a large increase in conductivity. Secondary dopants also exist. These are substances that, when applied to a primary-doped polymer, induce further changes in its properties. The interactions of such molecules with the polymer, whether by hydrogen bonding, Van der Waals forces or even covalent interaction, modulate its electronic, optical, or magnetic properties. These changes can be sensed, for example, using external circuitry. Hence the polymers can act as chemical transducers and they can be tailored to detect particular substances. The precise interactions of an external molecule with the polymer can modulate electronic coupling in different ways, but typically they lead to changes in conformation and charge transfer. The molecule being sensed can be thought of as a secondary dopant, where a charge transfer complex is formed between the polymer and the secondary dopant. If the forces involved are low, then the modulation of the electrical properties of the dopant can be reversible [14].

16.2 Conductive polymeric materials - examples

The science of conductive polymers has advanced rapidly in recent years he most commonly used conductive polymers and their derivates will be discussed.

Polypyrrole

Polypyrrole has excellent electrical, thermal and mechanical properties and it can be synthesis is relatively straightforward. The response of a polypyrrole film is determined by the electrochemical deposition conditions used and, in particular, the choice of the electrolyte/solvent system. Extensive studies of polypyrrole indicate that the main charge carriers are spinless bipolarons formed by the combination of two polarons [15]. In the fully oxidized, or doped state there is on average about one positive charge for every three

or four monomer units in the polymer chain. These counter-anions make up a significant portion of the polymer and they play a major role in determining the properties of the polymer [15].

In the case of pyrrole and its derivatives, coupling in the alpha or 2-position produces a polymer with extended conjugation [15]. Partial oxidation of the polymer chains induces electrical conductivity because the resulting positive charge carriers (polarons and bipolarons) are mobile along the chains.

The most commonly applied method for the deposition of polypyrrole onto sensor structures is electro-chemical polymerization. Polypyrrole film can be generated from either aqueous or non-aqueous solutions, but it is thinner and more homogeneous when produced in an aqueous environment.

Polyaniline

English and German chemists described the polyaniline structure at the end of the 19^{th} century but it has recently come back into prominence [16, 17]. Although Jozefowicz and coworkers noticed in 1968 a considerable raise in the electric conductivity of polyaniline, it was only after 1980 that it's physical, chemical and electrical characterization became a subject of intense study. Polyaniline became the first dispersible inherently conductive polymer and it has been commercialised by Zipperling Kessler & Co.

Polyaniline was chemically synthesized by oxidation of xylene or alcohol with ammonium peroxydisulfate, doped with different acids and dispersed in water. Polyaniline can be switched very quickly between insulating and conductive forms when exposed to an acidic or alkaline environment. The interest in polyaniline is also motivated by the fact that the monomer is cheap and readily accessible, chemical and electrochemical polymerization techniques are relatively simple and undemanding and the polymer is stable in ambient conditions. Chemical polymerization of aniline can also be performed in water or in various organic solvents, in acid, neutral or basic environments, using chemical oxidants.

Polyaniline has one further advantage in it can be doped into its conductive state using various protonic, anorganic and organic acids. If the organic acid has a macromolecular structure a conductive compound can be obtained. Polyaniline can be made conductive by a protein acid-treatment that does not involve irreversible protonation of the polymer backbone [18]. Protonic doping of polyaniline has also been achieved using inorganic acids such as HCI, H_2S0_4**,** HNO_3 and organic acids such as CF_3SO_3H and CF_3COOH [19].

Polythiophene

This compound has recently gained special attention as a conductive polymer because of its thermal and oxidative stability, its optical nonlinear properties and its high electrical conductivity in doped state. Because the oxidation potential of thiophene is greater than that of pyrrole, the number of chemical oxidants that can be used for polymerization is much smaller.

As in the case of other polyheterocycles, synthesis of polythiophene may be performed both chemically and electrochemically. Although chemical synthesis is a method that yields a larger quantity of polymer, electrochemical polymerization of heterocycles is more

effective, because in this case the final polymer is free of impurities such as catalyzers and metallic salts. It can be deposited electrochemically as adherent films whose thickness can be controlled and the electro-polimerization may be performed in either potentiostatic or galvanostatic conditions. The substituent(s) and the side group(s) attached to thiophene allow more extensive electron delocalization, which helps to lower the band gap energy and reduces the energy required for the polymer to be charged. The ideal structure is made up by coupling of the thiophenic rings in α,α' or the 2,5 positions. Substituents may alter the properties of polythiophene in two ways:

a) by introducing photo-conductive, chiralic or liquid crystal, groups which may subsequently complex with various ions or organic compounds

b) the volume of the substituent may also determine the torsion angle between the thienyl groups, hence the length of the conjugation and the position of the absorption π-π.

Polythiophenes having alkoxy groups as substituents are very interesting because they promote solubility and increased hydrophilic character. They can complex with cations to make chemical sensors. Moreover, when the alkoxy group is chiralic, the polymer can form complexes with enantiomers out of mixtures of optical isomers. Polythiophenes with macrocyclic ether groups (crown ethers) are very important because of the possibility of cation complexion and self-assembly. These macrocycles may be attached:

(a) by a spacer in position 3 of thiophene;

(b) by monomers containing two tiophenic groups, connected in positions 3,3' by

poly-etheric groups or thiophene with polyetheric groups introduced in position 3.

Polythiophene derivatives can be made highly conductive by treatment with $FeCl_3$, $AuCl_3$, I_2 or H_2S0_4. Oxidized films exposed to ambient light and air showed a loss in conductivity. The lifetime of the conductivity was dependent upon the stability of the oxidizing agent used.

Polysiloxane

Polysiloxane $[Si(R)_2\text{-}O]_n$ is the most studied and most importantof the inorganic polymers. Due to its very strong bonding between silicon and oxygen, polysiloxane is generally extremely stable. The characteristics of the polymer depend on the reaction conditions during synthesis. Basic catalysts and high temperatures lead to the preferential formation of linear polymers with high molecular mass. Polysiloxane polymer hosts with branched and crown ether side chains exhibit high ionic conductivities [20]. Most recently work has split into two directions: respectively lower viscosity liquid siloxanes and siloxanes that are incorporated into freestanding gels. Polymethylsiloxane polymers with an oligo(ethylene glycol)methyl ether side chain are lower molecular weight hosts and liquids. The doped electrolytes have ionic conductivities between 10^{-5} Scm^{-1} and 10^{-4} Scm^{-1}.

Polyphthalocyanine

Phthalocyanine is a macrocyclic compound having an alternating nitrogen atom-carbon atom ring structure, Figure 16.2 [21]. It was probably discovered by accident in 1907, as a by-product during synthesis of o-cyanobenzamide, but it was not until almost 20 years later that a patent was filed describing a manufacturing process.

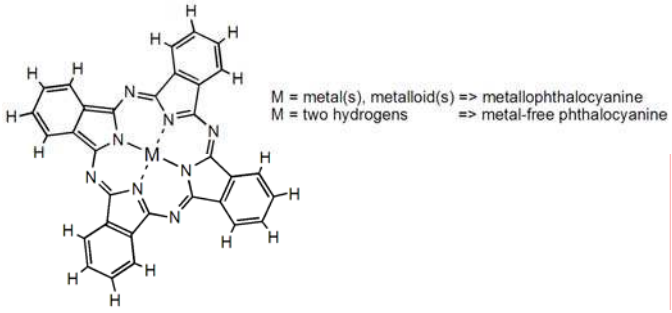

Figure 16.2: Molecular structure of metallophtalocyanine, metal-free phtalocyanine

The molecule is able to coordinate hydrogen and metal cations in its center by bonding to the four isoindole nitrogen atoms. The central atoms are able to carry additional ligands. Most elements are able to coordinate to the phthalocyanine macrocycle and therefore, a variety of useful phthalocyanine complexes can exist. The structure of a phthalocyanine molecule is closely related to that of the naturally occurring porphyrin systems. Complex investigation of electric and gas-responsive properties of a series of synthesized metal-free and metal-containing oligo and polyphthalocyanines (OPc and PPc, respectively) has been reported.

16.2.6 Fullerene

The 1996 Nobel Prize in Chemistry was awarded for the discovery of fullerenes, which are one of only four types of naturally occurring forms of carbon. The fullerenes are molecules composed entirely of carbon, taking the form of a hollow sphere, an ellipsoid, or a tube. Spherical fullerenes are sometimes called buckyballs, while cylindrical fullerenes are called buckytubes or nanotubes**.** Fullerenes are similar in structure to graphite, which is composed of a sheet of linked hexagonal rings, but they contain pentagonal (or sometimes heptagonal) rings that prevent the sheet from being planar. The smallest fullerene is C_{60} (buckminsterfullerene) and it is also the most common.

The buckminsterfullerene molecule, a closed cage structure molecule with carbon network, is shown in Figure 16.3 [22]. The structure of C_{60} is that of a truncated icosahedron, which resembles a round soccer ball of the type made of hexagons and pentagons, with a carbon atom at the corners of each hexagon and a bond along each edge.

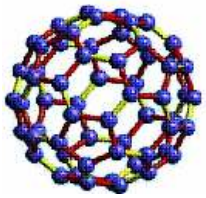

Figure 16.3 The structure of a buckminsterfullerene molecule

Novel electrical and optical characteristics have been observed in conductive polymers doped with molecular dopants such as fullerenes ($C_{60,}$ C_{70}). The C_{60}/conductive polymer junction can be interpreted as donor-acceptor (D-A) type photocell rather than the conventional p-n junction common in organic semiconductors [23].

16.3 Applications of conductive polymersin sensors and actuators

The development of biological and chemical sensors based on conductive polymers has been investigated extensively during the past ten years. Esentially they can function in two different ways: as conductive materials for the construction of various devices and as selective layers in chemical sensing applications [24]. In both cases, the interaction with ambient gases is an important factor to consider. On one hand it may compromise the performance of a device based on conductive polymers. Conversely it may be beneficial in a sensor. Conductivity has been the primary focus of recent interest. Work function, which is related to conductivity but in principle a different property, has received only scant attention.

The advantages in using conductive polymers as sensing materials over conventionally used materials [25] include: a) the availability of a diverse range of monomer types and synthetic monomer analogues; b) electrochemical preparation readily allowing mass production and miniaturization of the sensors; c) the ease with which biomaterials, such as enzymes, antibodies and whole cells, may be incorporated in the polymer; d) the ability to change the oxidation state of the polymer after deposition and thereby tailor the sensing characteristics of the film; and e) the ability to obtain a reversible response at ambient temperature.

Sensors

A variety of conductive polymers have been evaluated using microelectronic devices, such as chemoresistors (interdigitated array transducers), quartz crystal microbalances (QCMs) and field-effect transistors (FETs). Kunugi et al. [26] utilized a specially modified QCM for making electrical and microgravimetric measurements of the uptake of alcohols onto polypyrrole thin films. Josowicz and Janata investigated the measurement of work-function changes using a polypyrrole-coated FET for the detection of lower aliphatic alcohols [27]. Several companies, including Neotronics [28] and AromaScan [29], manufacture “electronic noses” comprising arrays of chemoresistor-based conductive polymer sensors.

Conductive polymers are an effective medium for chemical sensing, based upon the electronic changes that are induced in the polymeric films due to gas-phase adsorption. The conductivity changes are commonly attributed to the interaction of analytes with either the

polymer backbone itself or with dopant molecules incorporated within the film, thereby modulating the mobility and/or the number of free charge carriers available [30].

Conductive polymer sensors can be applied in a number of different modes, [31]:

- pH-based (change in pH);
- conductometric mode (change is conductivity);
- amperometric mode (monitoring the variation in current),;
- potentiometric mode (change of open circuit potential).

Gas sensors are often operated in conductometric mode, whereby changes in the conductivity or resistivity are measured while exposing the polymer to the gas molecules of interest (electronic noses).

To-date, most research on biosensors has focused on devices that consist of a metal layer to conduct electrons as the signal, an enzyme or antibody to sense the presence of a particular analyte, and a membrane to immobilize the enzyme and also possibly aid in transducing the signal to the electrode. Conductive polymers are used in biosensors in three main areas: signal detection, transmission of signal to a measuring electrode or response element and controlling the feedback response to the signal. They are characterised by their exceptional versatility and at the present moment in time they promise to revolutionize chemical sensing

Chemical microsensors

Two types of sensor, developed at Sandia National Laboratory, were tested at the Nevada Test Site as part of the Advanced Monitoring Systems Initiative program in late 2002. These were a chemo-resistive sensor and a surface-acoustic-wave (SAW) sensor. Both sensors utilize the adsorption of chemicals onto polymer films to produce a change in an electrical signal, which is recorded and calibrated. The results showed that both sensors could be operated remotely and continuously for long-term monitoring applications using commercial data-acquisition systems and custom-designed packaging. Both the chemo-resistive and the SAW sensors experienced drift in the signal and the readings were impacted by fluctuations in temperature and humidity. The chemoresistor, however, showed that exposure to large concentrations of contaminants overwhelmed the fluctuations caused by temperature and humidity variations. It was also demonstrated that the chemoresistive sensor exhibited better stability and sensitivity than the SAW sensor for the conditions and analytes thet were tested and this was contrary to initial theoretical predictions [32]. The chemoresistor sensors used in the field tests at the Nevada Test Site detect volatile orgaic compound (VOC) vapours with conductive polymer films deposited onto micro-fabricated circuits. The polymers used were: a 75% phenyl : 25% methylpolysiloxane (OV25); an alkylaminopyridyl-substituted polysiloxane (SXPYR); a hexafluoro-2-propanol-substituted polysiloxane (SXFA); polybis(cyanopropyl)-siloxane (SXCN); poly(vinyltetradecanal) (PVTD) and poly(trifluoropropyl)methylsiloxane (OV-202). The variety of compounds that could be detected in this way included aromatic hydrocarbons (benzene), chlorinated solvents (trichloroethylene, carbon tetrachloride), aliphatic hydrocarbons (hexane, iso-octane), alcohols, and ketones (acetone).

In order to fabricate this type of sensor, the chemically sensitive polymer is dissolved in a solvent and mixed with conductive carbon particles. The resulting ink is then deposited onto a solid substrate, between some platinum tracks and dried. When chemical vapour comes into contact with the surface it is absorbed by the polymer, causing it to swell. The swelling changes the electrical resistance which can be measured and recorded. The amount of swelling corresponds to the concentration of the chemical vapor in contact with the chemoresistor and the devices can be calibrated by exposing them to known concentrations of target analytes. In the Nevada tests the SAW sensor probe was placed alongside the chemoresistor probe (Figure 16.4), according to [32].

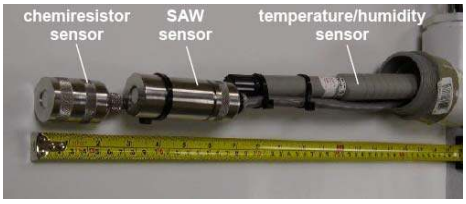

Figure 16.4. Sensors deployed during side-by-side test of chemoresistor and SAW sensors, Nevada Test Site [32]

The conductivity of polyaniline is highly sensitive to chemical vapours and, besides polysiloxane, this is another promising material for manufacture of chemical sensors. An example is given in [33], where oriented polyaniline nanowires, with diameters on the order of 100 nm were deposited on gold electrodes. The devices showed a rapid and reversible resistance change upon exposure to NH_3 gas at concentrations as low as 0.5ppm. The well-defined single-wire geometry allows for accurate characterization of the device response. The response times of nanowire sensors with various diameters correspond to radius-dependent differences in the diffusion time of ammonia gas into the wires. The nanowires were deposited, using a particular scanned micro-fabricated electrospinning source which presents a general method for interfacing polymeric nanowire devices with microfabricated structures. The method could ultimately be used to make a device that has an array of wires sensitive to different chemicals. Such a device would be able to rapidly detect and analyze the composition of gasses in the air [34].

Other chemical sensors based polyaniline are ammonia sensors fabricated on a dielectric substrate using microelectronic planar technology. A sensitive layer based on polyaniline is deposited onto interdigitated metallic electrodes. The principle of operation lies in the variation of the electrophysical characteristics of the film (conductivity, charge carriers concentration) that is induced by the reversible ammonia adsorption process and its chemical interactions [35]. In practice, the sensors are found to be high selective to ammonia in mixtures with different active toxic gases (nitrogen dioxide, hydrogen, methane, hydrogen sulfide, carbon monoxide, carbon dioxide). The sensitivity threshold is 0.1÷0.5 ppm and the range of measurement is between 0.1 and 1000 ppm. Response time is 10-15 s and the sensor can operate at room temperature. These sensors are suitable for measurement of ammonia content in an industrial environmental monitoring system, for some agricultural applications, in medical and biological research.

Electronic noses

Polymer membrane sensor arrays, also called ‘electronic noses’, have been in research for several years and they could provide a simple alternative to many complex instrumental techniques, such as chromatography and ultra-violet spectroscopy, which are both expensive and time-consuming. Some successful trials of the technology have taken place at hospitals in Manchester and London to diagnose bacterial vaginosis, BV).

A company called Osmetech has designed the electronic nose customized to smell out gases emitted by the bacteria that cause BV. This ‘nose’ is as accurate as other methods and tests can be perfromed in very much less time. The analyser instrument consists of an array of 48 of these conductive polymer sensor elements, made using wafer-scale technology. Arrays can be selectively tailored to match the particular application: for example a narrow range of sensor types would be chosen to obtain very high sensitivity where only a few chemical species need to be assayed. A module containing a broad range of different sensors would be used where many different responses are needed to detect a wider range of analytes, (Figure 16.5) [36].

Figure 16.5 - The analyzer instrument consists of conductive polymer sensor elements, made using wafer scale technology [36]

Conductive polymers are made by ‘electropolymerisation’ of complex organic dyes-specifically, derivatives of the substances polypyrrole, polyaniline and polythiophenes.

Osmetech have discovered how to give each of these polymers different conductive behavior, through variations in chemical structure, so that it has managed to build up a proprietary library of 80 to 100 sensor materials, each applicable to a particular molecular type and each sensitive to variations in concentration. The responses of indvidual sensing elements are picked up by signal processing circuits and compiled into a response profile (or ‘scent’) that characterises the atmosphere around the sensor.

An electronic nose also has many industrial applications and important amongst these is detection of aroma. Food producers and manufacturuers of toiletries use panels of people to assess the smell of their products, Naturally, human factors ensure that the panels can never be entirely objective or in fact reproducible. Electronic noses can provide objective data, and polymeric sensors are now being used to sniff out the amount of ethanol in mouthwash, monitor odour levels in sodium bicarbonate for toothpaste, check the stability of fragrances in soap tablets, and to assess the smell of fixatives used in hair sprays.

Another application is in cereal quality assurance. Specialty trained human snifters have been used for hundreds of years to detect the presence of mould and contaminants in bulk grain stores. This is particularly important in the Far East, with its large rice consumption;

rice stored for a long time can acquire unpleasant tastes and smells, which significantly affect its price. The polymer sensor array can perform this sensing role and supply some consistency in assessing the quality and value of the rice.

Polymer sensor arrays are also being used to check the usability of recycled plastics, which are nowadays-popular materials for manufacturing car interiors. Such plastics can retain traces of smells from their previous uses, which are not necessarily welcome inside a car on a hot day. Sensors are available that can assess these trace odours much more rapidly than is possible using gas chromatography - and in a real vehicle environment, too, not just in the lab. [37].

FET type devices

Electronic devices can be made, for example, by forming tracks of PEDOT (poly-3,4-ethylenedioxythiophen) on a substrate using a solvernt evaporation, line patterning, technique. Two electrodes were prepared in this way, comprising a source/drain electrode and a gate electrode [38,39] (Figure 16.6).

Figure 16.6 FET-type device - Prof. A. G. MacDiarmid, Department of Chemistry of University of Philadelphia

Line Patterning is a novel process that provides a simple and cheap way to prepare patterns of conductive polymers. It exploits differences in selected physical and/or chemical properties between a substrate and insulating lines that have been printed onto it by a conventional copying or printing process. The substrate and printed lines react differently or at different rates with a solvent (or vapor) to which they have been exposed and, hence, the conductive polymer can be selectively deposited as a film after evaporation of the solvent. Line Patterning has the advantages that no photolithography is involved; no printing of conductive polymer is involved; it uses only, for example, a standard office laser printer, which is not modified in any way. Commercially available flexible, transparent plastic or paper substrates can be used and solutions of conductive or non-conductive polymers are commercially available.

Biosensors

An enzyme electrode is a combination of any electrochemical probe (amperometric, potentiometric or conductometric) with a thin layer (10 to 200nm) of immobilized enzyme. In these devices, the function of the enzyme is providing selectivity by virtue of its biological affinity for a particular substrate molecule. For example, an enzyme is capable of

catalyzing a particular reaction of a given substrate even though other isomers of that substrate or similar substrates may be present. The progress of the enzyme reaction (which is in turn related to the concentration of the analyte) is monitored by either the rate of formation of product or the disappearance of a reactant.

The method of analysis used depends on several properties of the enzyme such as: the existence of redox active groups on the enzyme, the electrical properties of the products of the biochemical reaction, the electrical characteristics of the substrates or cofactors, the required speed of response and ultimately the intended application of the sensor. The first three of these criteria will depend largely on the system under investigation. The latter three depend on the requirements and application of the sensor under consideration. If the enzyme does not contain any redox groups, then the method of analysis will be restricted to monitoring either the release of products or the consumption of substrate by their reaction at the transducing electrode. The current produced can then be related directly to the concentration of analyte [40].

The Glucose Sensor is one of the most successful commercial biosensors, used to monitoring blood sugar levels for diabetics. An enzyme depostited on an electrode surface acts as the bio-recognition element to identify glucose molecules. When an enzyme recognizes the glucose molecules, it acts as a catalyst to produce gluconic acid and hydrogen peroxide using oxygen from the air. The electron transfer due to hydrogen peroxide/oxygen coupling is easily detectable and the electron flow is proportional to the number of glucose molecules that are present in blood.

A new type of glucose sensor uses the hydrogen-specific gas sensing capability of single walled carbon nanotubes (SWCNT) assembled on a micro-electrode. The conductivity of SWCNT's effectively changes due to adsorption of hydrogen owing to a shift in the energy band structure. Such devices could be minimally invasive and possibly non-invasive, relying only upon a small sample quantity of blood or other body fluid. It could also be highly sensitive, very fast immune to false positives and it would not require any calibration. It has been demonstrated that a signal-readout is proportional to glucose levels within a clinically significant range. (Figure 16.7) [41]. Each device requires a few thousand-carbon nanotubes on an area of a ~ 1mm by 1mm in size). Only electrical resistance needs to be measured, and the sensor can be easily operated without specific training.

Microtubule sensors for glucose, urea, and triglyceride have been fabricated based on poly (styrene sulfonate)-polyaniline (PSS-PANI) composites. These were synthesized within the pores of track-etched polycarbonate membranes and arrays were fabricated by immobilization of three different sets of enzymes on three closely spaced devices. The sensors for urea and tri-glyceride were found to have a higher linear range of response, better sensitivity, improved multiple-use capability, and faster response time in comparison to potentiometric and amperometric sensors based on polyaniline. Response was found to be free from cross-interference when a sample containing a mixture of the above analytes was analyzed in a single measurement [42].

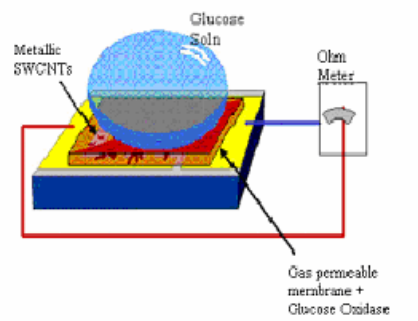

Figure 16.7 The schematic of the glucose sensor [41]

Actuators

Conductive polymer actuators are rapidly advancing from promising laboratory research [43-50] towards full-fledged engineering materials [51,52]. Most studies to-date have investigated the contractile properties of either of two conductive polymers, polypyrrole and polyaniline. These conductive polymer actuators are of technological interest due to their low operating voltages, high forces, moderate strain and controllability. The operating voltage range is typically less than 1 V, with short bursts of up to 10 V being used to increase power [53]. Such voltages are readily provided by batteries and of course this is of particular value for micro-scale devices applications [54], The fact that displacement is proportional to charge transfer in conductive polymer actuators makes them relatively easy to control, giving then a potential advantage over shape memory alloys [55]. Unlike mammalian muscle and electromagnetic motors, conductive polymers do not expend significant energy when holding a load in place, greatly reducing losses in static applications such as switches and valves [56]. Conductive polymers show great potential as electro-mechanical actuator materials although efficiency curently tends to be low at around 1%.

Conductive polymers actuate via the reversible counter-ion insertion and expulsion that occurs during redox cycling. Significant volume changes occur through oxidation and reduction reactions at corresponding electrodes through exchanges of ions with an electrolyte. Electrodes are commonly fabricated from polypyrrole (Ppy) or polyaniline (PAN), or PAN doped with HCl. Polypyrrole actuators in particular can generate a strain of 1%-3% under electro-chemical excitation and the forces generated are 100-1000 times greater than skeletal muscle. They require low voltage for actuation (1V or less), are biocompatible and operate ideally in liquid electrolytes (including bio-fluids). Such features make them very promising for biomedical applications.

Responsive drug delivery applications of polymer actuators have been studied at UC Irvine. In this case drug reservoirs were incorporated with small polymer valves, biosensors control the opening and closing of these valves and the required amount of drug is released [57]. An example of actuator made using conductive polymers is shown in Figure 16.8.

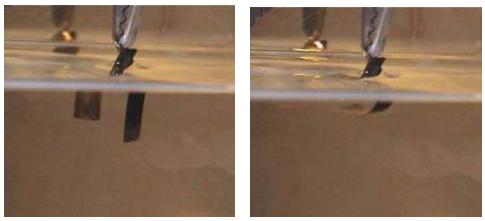

Figure 16.8: Movement of an actuator made of one layer of polypyrrole and one layer of Au. Left) The bilayer is straight under no current; Right) The bilayer is bent to the liquid surface after -1V applied for 4 seconds. Actuator size: 4mmx12mm; film thickness: polypyrrole-20um, Au-200nm; working solution: 0.1M NaDBS (sodium dodeclybenzenesulfonate) [57]

The applications for conductive polymer actuators include microtweezers, microvalves, micropositioners for microscopic optical elements, and actuators for micro-mechanical sorting (such as the sorting of biological cells). Furthermore these materials offer the possibility of creating devices at the nano-scale. Nano-electromechanical systems (NEMS) devices and machines are an extension of present-day micro-machines and micro-actuators into the nano-scale domain. Notable achievements in this field of activity are protein motors, capable of linear or rotary motion, DNA and active devices such as nanowires, switches, motors and tweezers [58].

Conclusions

Although implementation of these materials is still at its beginning, it is becoming clear that they will permit important (if not radical) changes in future electronic systems. Conjugated polymers are expected to play, for example, a crucial role in the fabrication of molecular electronic circuits. In the future, the dimensions of electronic circuits could be reduced well below the current minimum pattern dimensions used in advanced integrated circuits on silicon wafers, perhaps reaching as small as 1 nm. A reduction in circuit size of this magnitude could increase the speed and the dynamic memory capacity of computers by several orders of magnitude ($\sim 10^6$). Sensitive detectors have been made that can detect low ppm levels of toxic gases. These can be inexpensive, compact, simple to operate and they can potentially be incorporated within a fabric-based sensor system.

A number of enzymes have been covalently attached or integrated into conductive polymers as dopants. Interestingly enzyme activity is dependent on the potential applied to the conductive polymer, and this can be used to modulate its behaviour. In a similar way, antibodies can be incorporated into conductive polymers as dopants. Application of a potential to the polymer can change the conformational characteristics of the antibody so that reversible affinity biosensors can be constructed.

Conductive polymer actuators require voltages in the range of 1 to 5 V. Relatively high mechanical energy densities of over 20 J/cm^3 are attained with these materials, however, they posses low efficiencies at levels of 1%.

[1] a) A. J. Heeger, S., Kivelson, J. R. Schrieffer, and W. P. Su,., *Rev. Mod Phys*., **1988**, *60*, 781; b) T. A. Skotheim, R. L. Elsenbaumer, and J. R. Reynolds (eds), *Papers in Handbook of ConductingPolymers*, Dekker, New York, **1998**, 2nd edn.

[2] Nalwa, H. S (ed.), *Handbook of Organic Conductive Molecules and Polymers*, Wiley, New York, **1997**.
[3] C. J. Dury, C. M. J. Mutsaers,., C. M. Hart,., M. Matters, and de D. M Leeuw, *Appl. Phys. Lett*. **1998**, 73, 108
[4] J.D. Madden, "Conducting Polymer Actuators", *Ph.D. Thesis*, Massachusetts Institute of Technology, Cambridge, MA, **2000.**
[5] J.D. Madden, C. J. Brenan, J. Dubow, *Accession Number AD-A332 030/6/XAB,* NTIS, Springfield,VA, **1997**.
[6] J. D. Madden, R. A. Cush, T. S. Kanigan, I. W. Hunter, *Synthetic Metals,* **2000,** *113*, 185**.**
[7] E. W. H. Jager, E. Smela, O. Inganas, *Science,* **2000,** *290*, 1540.
[8] I. W. Hunter and S. Lafontaine, *Technical Digest IEEE Solid State Sensors and Actuators Workshop*, **1992,** 178.
[9] H.Baughman, *Synthetic Metals,* **1996,** *78*, 339.
[10] T. F. Otero, *Handbook of organicand conductive molecules and polymers*, H. S. Nalwa Ed., **4**, 517-594, John Wiley & Sons, Chichester, **1997**.
[11] Bohwon Kim, Vladan Koncar and Eric Devaux, *Autex Research Journal,* **2004**, **4**, No.1.
[12] A. O. Patil, A. J Heeger, F. Wudl, *Chem. Rev.*1**988**, *88*, 183.
[13] C.K. Chiang, M.A. Druy, S.C. Gau, A.J. Heeger, E.J. Louis, A.G. MacDiarmid and Y.W Park*, J. Am. Chem. Soc*., **1978,** *100*, 1013.
[14] A.C. Patridge, P. Harris and M.K. Andrews, *Analyst*, **1996,** *121*, 1349**.**
[15] Julian W. Gardner and Philip N. Bartlett, *Electronic Noses Principles And Applications,* Oxford Science Publications, p.79, **1999**.
[16] E. M. Genies, , M. Lapkowski, si C. Tsintavis, *New J. Chem.,* **1988,** *12*, 181.
[17] C. I. Simionescu, I. Cianga, si M. Grigoras, *Roum. Chem. Quater. Rev.,* **1995,** *3*, 3.
[18] J-C Chiang, , A.G. MacDiarmid, *Synth.Met*. **1986,** *13*, 193.
[19] I.V. Krvoshei, V.M. Skorobogatov,.***Polyacetylene and*** *Polyarylenes*, ***Synthesis and*** *Conductive Properties*, Gordon and Breach Science PubIishers, Philadelphia, Pennsylvania, **1991**.
[20] Hooper, R.; Lyons, L. J.; Moline, D.; West, R. *Silicon Chemistry,* **2002**, *1,* 121.
[21] Veena Vijayanathan, S.Venkatachalarn, V.N.Krishnamurthy, *Synthetic Metals*, **2000** *114*, 273.
[22] Dresselhaus Group home page, http://www.godunov.com/Bucky/fullerene.html.
[23] Katsumi Yoshino, Kazuya Tada, Kenji Yoshimoto, Masayoshi Yoshida, Tsuyoshi Kawai, Hisashi Araki, Maki Hamaguchi, Anvar Zakkidov, *Synthetic Metals*, **1996,** *78*, 301.
[24]Jiri Janata and Mira Josowicz, *Nature Materials,* **2003**, *2*, 19.
[25] A.C.Patridge, P. Harris and M.K. Andrews, *Analyst*, **1996,** *121*, 1349.
[26] Y. Kunugi, K. Nigorikawa, Y. Harima and K. Yamashita, *J. Chem Sot., Chem. Commrtn*., **1994,** 873.
[27] M. Josowicz and J. Janata, *Anal. Chem*. **1986,** *58*, 514.
[28] T.C. Pearce, J.W. Gardner, S.Friel, P.N.Bartlett and N.Blair, *Analyst*, **1993,** *118*, 371.
[29] J.V. Hatfield, P. Neaves, P.J. Hicks, K. Persaud and P. Travers, *Sensors and Actuators B*, **1994,** *18-19*, 221.

[30] G.E. Collins, L.J. Buckley, *Synthetic Metals* **1996,** *78*, 93.
[31] P.Chandrasekhar, *Conducting Polymers, Fundamentals and Applications,* **1999,** 484.
[32] Clifford K. Ho, Jerome Wright, Lucas K. McGrath, Eric R. Lindgren, K. Scott Rawlinson, Sandia National Laboratories Albuquerque, New Mexico, *Field Demonstrations of Chemoresistor and Surface Acoustic Wave Microchemical Sensors at the Nevada Test Site*, **2003**.
[33] Jiaxing Huang, Shabnam Virji, Bruce H. Weiller, Richard B. Kaner, *A European Journal*, **2004,** 11(6), 1314.
[34] Haiqing Liu, Jun Kameoka, David A. Czaplewski, and H. G. Craighead, *Nano Letters*, **2004,** 4, 671.
[35] Krutovertsev S.A., Ivanova O.M., Sorokin S.I. *Joint Stock Company "Practic-NC", 103460, Moscow, Russia;* Russian Federation's Patent No 2133029 "Ammonia sensor" (patented by JSC "Practic-NC") with priority dated on **08.05.1998**.
[36] www.sensorland.com, Link
[37] Biological Science, University of Paisley, http://www-biol.paisley.ac.uk/marco/ Enzyme_Electrode/Chapter1/introduction.htm
[38].“*Synthetic Metals*”: A Novel Role for Organic Polymers (Nobel Lecture), Copyright The Nobel Foundation 2001; *Angew. Chem. Int. Ed*. **2001**, *40*, 2581
[39] IMS Lab, http://ims.postech.ac.kr/ims/main/main.php
[40] Chung Jaehyun, Lee Kyong-Hoon, Lee Junghoon, *17th IEEE International Conference on Micro Electro Mechanical Systems (MEMS)*, Maastricht MEMS 2004, *Technical Digest*, **2004**, 617.
[41] Technology Transfer Program, Northwestern. University, http://ttp.northwestern.edu/abstracts/viewabs.php?id=233&cat=96, Link
[42] Kanungo M, Kumar A, Contractor AQ., *Anal Chem*., **2003**, 75, 5673.
[43] R. H. Baughman, R. L. Shacklette, R. L. Elsenbaumer, *Topics in Molecular Organization and Engineering: Molecular Electronics*, P. I. Lazarev Ed., **1991,** ***7***, 267, Kluwer, Dordrecht,.
[44] M. R. Gandhi, P. Murray, G. M. Spinks, G. G. Wallace, *Synthetic Metals,* **1995,** *73*, 247.
[45] Q. Pei and O. Inganas, *Journal of Physical Chemistry* **1992,** *96*, 10507.
[46]. E. Smela, O. Inganas, I. Lundstrom, *Science* **1995,** *268*, 1735**.**
[47] T. E. Herod and J. B. Schlenoff, *Chemistry of Materials* **1993,** *5*, 951.
[48] T. F. Otero, J. Rodriguez, E. Angulo, C. Santamaria, *Synthetic Metals* **1993,** *55-57*, 3713
[49] K. Kaneto, M. Kaneko, Y. Min, A. G. MacDiarmid, *Synthetic Metals* **1995,** *71*, 2211
[50] J. D. Madden, S. R. Lafontaine, and , I. W. Hunter, *Proceedings - Micro Machine and Human Science* **1995,** *95*, Nagoya, Japan,.
[51]. A. Mazzoldi, A. Della Santa, D. De Rossi, *Polymer Sensors and Actuators*, Y. Osada and D. E. De Rossi, Eds., Springer Verlag, Heidelberg, **1999.**
[52] J. D. Madden, "Conducting Polymer Actuators", *Ph.D. Thesis*, Massachusetts Institute of Technology, Cambridge, MA, **2000**.
[53] J. D. Madden, R. A. Cush, T. S. Kanigan, I. W. Hunter, *Synthetic Metals* **2000,** *113*, 185.
[54] E. W. H. Jager, E. Smela, O. Inganas, *Science* **2000,** *290,* 1540**.**

[55] I. W. Hunter,S. Lafontaine, *Technical Digest IEEE Solid State Sensors and Actuators Workshop*, **1992,** 178.
[56] John D.W. Madden, Peter G.A. Madden and Ian W. Hunter, *Electroactive Polymer Actuators and Devices* conference, *SPIE 8th Annual International Symposium on Smart Structures and Materials*, Newport Beach, CA.
[57] Biomems Research Group University of California Irvine, http://mmadou.eng.uci.edu/Research/PA.htm, Link
[58] I. Chun, D. H. Reneker, H. Fong, X. Fang, J. Deitzel, N. B. Tan, K. Kearns, *J. Adv. Mater.,* **1999**, *31*, 36; D. Hohnholz, A. G. MacDiarmid, *Synth. Met*., **2001**, *121*, 1327

17 Photo-patternable polyimides

Estefania Abad – Fundación Tekniker, Eibar, Spain

Polyimides (PI) are part of a group of high-temperature polymers that have been applied in microelectronics and microelectromechanical systems (MEMS). They constitute an important class of materials because of their low dielectric constants, high breakdown voltage, good planarization, wear resistance, radiation resistance, inertness to solvents, good adhesion properties, low thermal expansion, long-term stability and excellent mechanical properties.

Due to their outstanding features, polyimides, photosensitive and non-photosensitive, have found many applications both in integrated circuitry(IC) and microfabrication. In these areas PI films are being used as structural materials, passivation layer, interlayer dielectric or protection layer. In addition, an important commercial application of PI is the construction of multilayer flexible circuits used in the realisation of Multi Chip Modules (MCMs). On the other hand, photosensitive PI precursors, called polyamic acids, can also be used as new photoresists with promising sensor and microfabrication applications.

PI films are supplied either as films (obtained by lamination) or as solutions that can be applied by spin coating, afterwards curing over 275ºC to convert to PI.

17.1 Properties of polyimides

PI film has a unique combination of properties that make it ideal for a variety of applications in many different industries. PI film can maintain its excellent balance of electrical, thermal, mechanical, physical and chemical properties over a wide range of temperatures. In MEMS structures and flexible circuits, the most widely used are 25-50 μm thick flexible Kapton from DuPont [1] and Upìlex from Ube Industries [2] PI films. Han et al. in ref [3] gathers comparative tables that show the mechanical, chemical and electrical properties of Kapton and Upilex PI films. These tables can be extremely useful in order to make a good choice of materials for applications. Both the Kapton and Upilex PI films possess very strong mechanical properties, sufficient chemical resistance, and excellent thermal and electrical characteristics. However, Upilex PI film is relatively stronger mechanically, and shows higher chemical resistance and dimensional stability over a wide range of temperatures than Kapton PI film, while Kapton is stronger in folding endurance, and shows higher electrical resistance and lower thermal conductivity than Upilex PI film.

17.2 Processing of polyimides

The conventional methods to pattern PI films are by laser, NC drilling or punching, wet-etching (achieved using chemicals) or dry-etching (using plasma or reactive-ion etching) and photolithography, in the case of using photosensitive solutions. In principle, the laser, mechanical and wet etching processes produce coarse features whereas the dry etching and the photosensitive polyimides allow for finer features. Figure 17.1 shows the established methods for wet etch, dry etch and the use of photosensitive polyimide.

Both wet-etch and photo-definable polyimides are patterned prior to final cure. Whereas, dry etch processing requires the polyimide layer to be fully cured prior to the etching process.

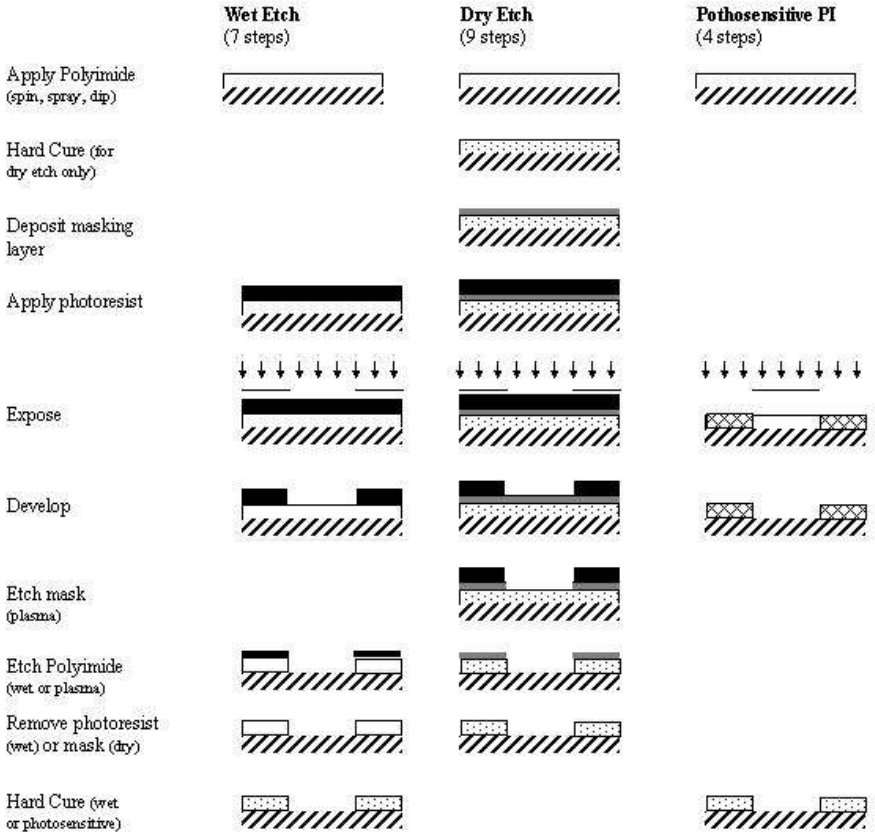

Figure 17.1 - Methods for polyimide patterning.

Wet Etch Patterning

Wet etch patterning uses wet chemistry in conjunction with a liquid photoresist to define the desired pattern in the polyimide layer. Wet etch processing is typically used to pattern coarse features such as bond pads or large vias. An aspect ratio of 1 to 5 can be achieved reliably.

The base process involves spin coating and partial curing of the polyimide layer, using one or more in-line hot plates or sometimes a convection oven. A layer of positive photoresist is deposited, baked and imaged. The photoresist is then developed with a standard developer. A TMAH-based developer can simultaneously wet etch the underlying polyimide in the imaged areas. Otherwise alkaline solutions, like the TPE 300 from Toray [3] or the Kapton polyimide film etchant from Transene [4] can be used. After develop/etch and a water rinse, the photoresist is stripped using a liquid photoresist stripper. The patterned polyimide wafer is then fully cured to complete the imidization process and remove residual solvent.

Dry Etch Patterning

Dry etch patterning is typically used when an aspect ratio greater than 1 to 1 is required for very fine feature sizes. The process begins with the application and full cure of the polyimide layer. After curing, a dry etch mask is applied over the polymer layer. Thin films of aluminium or CVD oxide are typically used for this purpose. Photoresist is applied and imaged over the etch mask to define the desired pattern. The wafer or substrate is then placed in a plasma or reactive-ion etcher, typically of parallel plate configuration. Process parameters and gas mixture are then optimised to pattern the etch mask. The gas mixture is switched to an oxygen/CF_4 blend and parameters are set to etch the underlying polyimide and remove the photoresist. The etch mask is then stripped by switching back the etch parameters or by using a wet process.

Photodefinable Polyimides

The use of photosensitive polyimides simplifies the process complexity by reducing the number of steps as shown in Figure 17.1, as well as improving the sidewall profile. Photosensitive polyimides permit the patterning of relatively fine features. An aspect ratio of 1 to 1 can be achieved in fully cured films. HD Microsystems is a global supplier of liquid polyimide materials [5].

The basic process involves the spin coating of the polyimide and a drying step, using one or more in-line hot plates or a convection oven. The polyimide layer is then exposed on a standard I or G line lithography tool. A negative tone photo mask is usually required since most photodefinable polyimides are negative acting. However, positive aqueous soluble photosensitive polyimides have been formulated recently [6]. After imaging, the wafer is developed on a traditional track line and rinsed. Finally, the polyimide layer is cured, both to imidize the film and to remove the photo package.

Laser Ablation

Laser ablation also begins with a fully cured film. The wall profile of the vias formed with a laser is V-shaped and it is not aspect-ratio limited. The specific patterning process depends upon the laser tool configuration. Most of the reported works on laser processing of polyimides, in particular for flex interconnect applications, use excimer or Nd:YAG laser [7]. However, kapton processing using other types such as CO_2 or femto-second laser is also possible. The advantage of using femto-second laser equipment is that it combines the use of UV light along with the femto-second pulses, to avoid the creation of heat affected zones on the polymer [8].

The process starts by transferring a DXF file to the code of the equipment. The process parameters that need to be optimised are power, focal length, advance (which determines the line width) and the thickness of material to be ablated. When these parameters have been established, the system can operate unattended. Figure 17.2 shows blind via holes 760 μm diameter and through holes fabricated in the same femtosecond laser ablation process. The material employed is Pyralux AP 8525R double-sided, copper-clad laminate from DuPont. It is an adhesiveless laminate for flexible printed circuit applications. The kapton has a thickness of 50 μm and the copper layer has a thickness of 18 μm on each side.

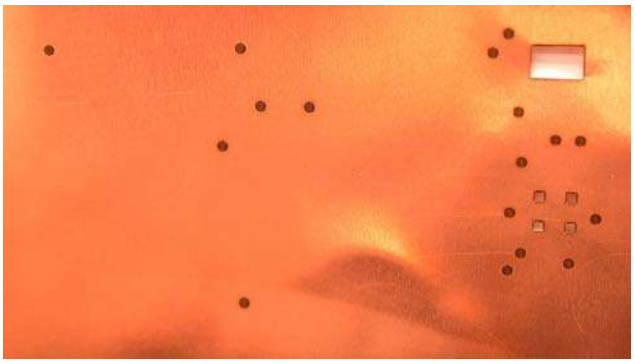

Figure 17.2 - Via holes blind via holes of 760 μm diameter and windows fabricated by femtosecond laser ablation in a Pyralux composite from DuPont.

17.3 Polyimide applications

HighDensity Interconnection flexible substrates

Sophisticated high density interconnection (HDI) flexible substrates are experiencing a strong demand for advanced applications such us implantable medical devices [9,10], as well as for new products in the printing and telecommunications industry.

Flexible substrates offer some unique advantages when compared to their rigid counterparts and in particular they are lighter, thinner and in some applications they are adaptable to more flexible packages. To create such a HDI flex circuit a multilayer construction is needed. Either thin film or laminate technology can be used. Thin film technology is based on polyimide spin coating, patterning, metal deposition and patterning of successive layers. Laminate technology is used to make polyimide sandwich structures with layers of copper. Each layer has to be individually fabricated, assembled by multilayer construction (alignment and bonding) and Z interconnected through vias. The main advantage of using the laminated approach is its lower cost in comaporison to the thin film approach, which is a relatively immature technology.

MEMS devices

Polyimide is a useful material for MEMS fabrication. The use of polyimides in this field is quite recent but it includes some interesting applications as it can be seen from the following examples.

Humidity sensors

Polyimide films have been recently introduced for the fabrication of capacitive humidity micro sensors [11-13]. The principle of a humidity capacitive sensor lies on the increase of the dielectric permitivity of a sensitive layer due to the moisture absorption or in the change of capacitance due to moisture dependent bending of a movable electrode. Polyimide films can be used either as a sensing layer or as a vapour absorbent polymer coating for the movable electrode. The sensitivity of this polyimide layer can be amplified by patterning the layer to increase the active surface area or by treating the surface in a oxygen plasma to raise the roughness. Polyimide is a polymer particularly suitable for this application thanks

to its high permeability to water, its great chemical stability and its full compatibility with IC process.

Implantable flexible electrodes

Neural prostheses are systems that partially substitute for the neural functions of the body that have been lost after traumatic lesions or neurological disorders. This loss can be partially replaced by implantable flexible electrodes for functional electrical stimulation of the remaining nerves or muscles. The most well-known examples of this type of devices are cardiac pacemakers and cochlear implants. These types of systems are usually a combination of flexible micromachined substrates with monolithically integrated electrodes, hybrid assemblies of electronics and encapsulation materials. Polyimide substrates are frequently used because they are flexible, light and can be easily patterned [14].

Flexible tactile sensor skins

Tactile sensing is an area of MEMS research that has potential applications in robotics, medicine and industrial automation. A tactile skin is a two-dimensional array of flexible sensor substrate with a high density of sensors of the following types: a hardness sensor, a temperature sensor, a sensor for thermal conductivity, and sensor for surface roughness measurement. The realization of multimodal tactile skin involves the application of MEMS technology on polymer materials such a polyimide. Figure 17.3 shows a novel fabrication process of a skin containing a two dimensional array of tactile sensors using polyimide and metal strain gauges developed by Engel et al. [15]. The result is a flexible, robust, monolithical polyimide-based sensor with embedded metal-film strain gauges and interconnects to detect force distribution. Sensor fabrication, on oxidized silicon wafers or Pyrex wafers with recessed regions (Figure 17.3(a) to (c)), consists of the deposition, patterning and curing of three layers of photosensitive polyimide with embedded metal thin films patterned by lift off (Figure 17.3(d) to (h)). Finally, the polyimide devices are released from the wafers Figure 17.3(i) and packaged on flexible copper-clad substrates.

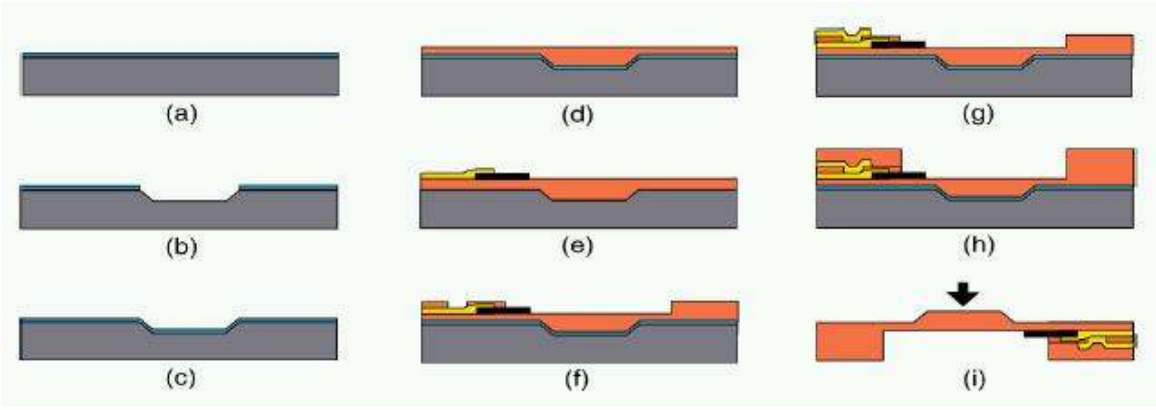

Figure 17.3. Schematic diagram of the fabrication process of a single taxel [15].

Piezoelectric polyimide MEMS process

Recently, a series of novel high-temperature piezoelectric polyimides have been synthesized and evaluated for potential use in MEMS devices [16]. Typical piezoelectric materials are crystalline ceramics that are brittle. Alternatively polyvinyldenefluoride (PVDF) has attained a widespread use as piezoelectric material in low cost flexible structures. However, the temperature range over which the piezoelectric properties of PVDF are maintained is limited to less than 80ºC. For applications at higher temperatures, as for example in the aerospace field, the introduction of this type of piezoelectric polyimides is of great interest. In order to demonstrate sensor and actuator utility of piezoelectric polyimides a low temperature (<120ºC) surface miocromachined process has been developed by Atkinson et al. [17]. This process consists of conventional lithographic and metallisation steps and uses a sacrificial layer of photoresist.

Polyimide joints

Creation of 3-D structures is a very important issue in the field of MEMS and several different techniques have been proposed. However many of them have drawbacks. Eberfors et al. [18] developed a novel and simple technology for making robust, small radius micro-joints (or micro-hinges) based on thermal shrinkage of polyimide in V-grooves. The structures can be used in both static-mode, for 3-D sensor applications and dynamic mode for use as actuators. Polyimide is and excellent micro-joint material because of its flexibility, high thermal shrinkage and high thermal expansion.

Polyimide sacrificial layers for surface micromachining

Compatibility of surface micromachining with conventional IC processing is essential for MEMS devices. Several post-process approaches have been developed in recent years, including some that use polyimide as a sacrificial layer [19]. Micromachining post processes require deposition and patterning of mechanical and sacrificial layers at temperatures below 400ºC. To avoid stiction problems during the release of the sacrificial layer, dry steps as oxygen plasma etching have been used to eliminate the polyimide.

In addition to these illustrations of polyimide applications, many other examples exist, such as a polyimide membrane with ZnO piezoelectric thin film pressure transducer, for use as a differential pressure liquid flow sensor [20]; high-resolution polyimide-based double-layered coils on flexible Kapton support for miniaturized power inductors [21]; or the mould transfer fabrication of polyimide SPM probes [22]. All these examples reveal the exceptionally wide fiefd of applications that polyimides can cover.

[1] http://www.dupont.com/kapton/
[2] http://www.ube.com/
[3] J. Han, Z. Tan, K. Sato, M. Shikida, J. Micromechanics and Microengineering. 2004, 14, 38.
[4] http://www.transene.com/kapton.html/
[5] http://www.hdmicrosystems.com/
[6] W.W. Flack, S.Kulas, C. Franklin, Proc. SPIE 2000, 3999, 452.

[7] B. Chou, S Beilin, H. Jiang, D. Kudzuma, M. Lee, M. McCormack, T. Massingill, M. Peters, J. Roman, Y. Takahashi, V, Wang. Proc. SPIE 1999, 3830, 270.
[8] E. abad, V.S. Raffa, B. Mazzolai, S. Marco, A. Krenkow, T. Becker, Proc. SPIE 2005.
[9] S. Corbett, J. Strole, B. Ross, P. Jordan, J. Kettrl, T. Hugues, Proc. IMAPS 2000
[10] J. Strole, S. Corbett, W. Lee, E. Light, S. Smith, Proc. IMAPS 2002
[11] J. Laconte, V.Wilmart, J.-P. Raskin, IEEE Sensors Conference 2003, 372.
[12] C-Y Lee, G-B Lee, J. Micromech. Microeng. 2003, 13, 620.
[13] T. Suzuki, P. Tanner, DV. Thiel, Analyst. 2002, 127(10), 1342
[14] A. Schneider, T. Stieglitz, Medical Device Technology 2004 16.
[15] J. Engel, J. Chen, L. Chang, J. Micromech. Microeng. 2003, 13, 350.
[16] C.Park, Z. Ounaies, J. Su, J.G. Smith, J.S. Harrison, Materials Research Society symposia proceedings 2000. 600, 153.
[17] G.M.Atkinson, R:E: Pearson, Z. Ounaies, C. Park, J.S. Harrison, W.C: Wilson, J.A. Midkiff, Proc. of the NASA VLSI Sympossium 2003.
[18] T. Ebefors, J. U. Mattsson E. Kälvesten, G. Stemme, Proc. SPIE 1999. 3892, 118
[19] L.S Pakula, H.Yang, H. T. M. Pham, P. J. French, P. M. Sarro, J. Micromech. Microeng. 2004, 14, 1478.
[20] A. Kuoni, R. Holzherr, M, Boillat, N. F: de Rooij, J. Micromech. Microeng. 2003, 12, S103.
[21] M. Saidani, M. A. M. Gijs, J. Micromech. Microeng. 2002, 12, 470.
[22] J. Zou, X. Wang, D. Bullen, K. Ryu, C. Liu, C. A. Mirkin, J. Micromech. Microeng. 2004, 14, 204.

18 Structural polymers

Michael Wendlandt - Micro and Nanosystems, ETH Zurich, Switzerland

In recent years silicon has been the dominant mechanical material for micro-electromechanical systems (MEMS) fabrication [1]. However other materials such as glass, ceramics and metals are equally useful at this scale and they have also been used as structural or functional materials with great success [2, 3]. The term 'structural' usually denotes those materials that are used solely for mechanical purposes. Moving parts in mechanisms also fall into this category. Despite the great benefits of using traditional materials such as silicon, it is not always true that they are the best choice for structural applications in micro-systems. In particular, their high modulus and related stiffness restricts the development of micro-sensors and actuators that would gain in sensitivity and performance, or could be further miniaturized by having moving parts with reduced stiffness [4-6]. Soft materials, such as synthetic polymers, are also excellent candidates for structural use in micro-scale sensors and actuators, since they are available with tailored moduli in the range <1 MPa up to several GPa [7, 8]. For example, the modulus of chemically cross-linked elastomers may be tuned over one or even several orders of magnitude by controlling the amount of cross-linking between the polymer chains [9-12]. In addition to the wide range of mechanical properties available, the transparency of many polymers is an advantage if visual control is necessary, for example in micro assembly processes [4]. Furthermore, many polymers offer good biocompatibility [13], which is either necessary or desirable for some biomedical applications such as actuated micro valves in micro-fluidic systems [14, 15].

On a macroscopic scale, synthetic structural polymers have become the most widely used material in terms of volume production [16-18]. Here, the main requirements for a structural polymer are mechanical stability and low material costs [19]. Nowadays, the so-called 'commodity' or 'standard' polymers such as high and low-density polyethylene (HDPE, LDPE/LLDPE), polypropylene (PP), polystyrene (PS), or polyvinylchloride (PVC) have gained over 80% share of the industrial structural polymer market [18]. On a microscopic scale, the requirements for structural polymers are somewhat different. Apart from good mechanical properties, their ease of processing plays an important role in the materials selection for micro-scale devices. Recently significant advances have been made in lithographic technologies for polymers, which make use of their low softening temperature or their sensitivity to radiation. In particular photosensitive polymers such as SU-8 [20] have attracted great attention for the fabrication of microstructures with high aspect ratios [21-24]. Micro-molding [25-27], rapid prototyping [28], and the so-called "soft-lithographic" techniques [29-36] such as hot-embossing have been developed and refined so that they are now well suited for micro and nano-fabrication of non-photosensitive, thermoplastic polymeric components. In addition to soft lithographic techniques, most polymers can be structured by established surface micromachining techniques such as dry etching [37, 38].

Release of free-standing micro-structures can be achieved by sacrificial-layer techniques, whereby a sacrificial layer is deposited below the structural element that will be released.

Subsequently this sacrificial layer is dissolved or removed by selective etching. The correct selection of the sacrificial layer material needs great care, since ideally the release step should not affect the structural polymer. This can be a challenge [37, 39], particularly for polymers with poor chemical resistance. In this case, water-soluble sacrificial polymer layers might present a potential alternative [40].

For moving structures there is a challenge related to the fact that polymers, particularly thermoplastics, can exhibit enhanced viscoelastic behavior [41-43]. This has consequences for resonant applications and for the long-term stability of dynamic microstructures. The viscoelastic nature of polymers can cause high energy dissipation by enhanced damping, or by creep deformation under load. Therefore, polymers intended for structural use in micro-scale sensors and actuators require a thorough evaluation and characterization of their viscoelastic behavior.

In the following paragraphs, those polymers will be discussed that have been already used as structural materials in micro-scale sensors and actuators, which are currently under investigation or which have high potential for applications in MEMS. The reader is referred to references [44-47] for further background information.

18.1 Selection of structural polymers for micro-scale devices

A summary of important material properties of polymers in this section can be found in Table 18.1.

Thermosets

Thermosetting plastics (thermosets) are polymeric materials that form cross-linked networks on curing. Curing is an energy-activated process that can in different cases be initiated by heating, through a chemical reaction, or by irradiation. Low molecular-weight precursor materials can be used that can be deposited as very smooth layers of varying thickness by solution spin casting [48] and subsequent curing. Generally, this yields materials that have a high modulus and high thermal stability in comparison to most non-thermosetting polymers. In the following paragraphs, the most well developed thermosetting polymers for structural use in microsystems, SU-8 and polyimide, are described. These both combine excellent micro-machining capabilities with outstanding thermal and mechanical properties. Non-photosensitive thermosetting epoxy resins can also be used for applications in this field and a few of these materials are also described [14, 49].

SU-8, is a low-cost, negative photo-resist developed by IBM in 1982 [50]. It is based on a multi-functional glycidyl ether derivate of bisphenol-A novolac. EPON® SU-8 from Shell Chemical currently provides the highest functionality that is commercially available [51]. This low-molecular weight resin can be dissolved in a variety of organic solvents up to very high concentrations (85 weight %) and it can be photo-sensitized with triaryl sulfonium salt [20]. Upon exposure to near UV (350-400 nm), electron-beam, or X-rays, a Lewis acid is generated which induces cationic polymerization. In common with other photo-resists, SU-8 can be structured by partial exposure and the unexposed areas are subsequently removed by dissolution in a developer/solvent. The high functionality of SU-8 provides fast and extremely dense cross-linking, which suppresses diffusion of the photo-initiator from

exposed to unexposed regimes. High contrasts can be achieved enabling structures to made that have at aspect ratios up to 50:1 [52, 53]. The precursor has good solubility in organic solvents and, by varying solution viscosity, film thicknesses up to 700μm can be deposited with a single coating [22]. Layers of up to 2mm thickness can be obtained by multilayer spin-coating [54]. Limitations for the structural use of SU-8 may arise from the large mismatch between the thermal expansion coefficient with most substrates, e.g. silicon. This can lead to large stresses along the layer-substrate interface after processing and delamination of the SU-8 layer from the substrate [54, 55]. SU-8 is a highly brittle material in its fully cured state [56]. Fracture samples have shown almost no plastic deformation [21]. The Young's modulus of SU-8 lies within the range of 0.7-5GPa, depending on curing conditions, which can be varied to give different cross-link densities [21, 55-58]. A great advantage for high temperature applications is the inherent high thermal stability of SU-8 featuring a degradation temperature of ~380°C and a glass transition temperature above 200°C at maximum cross-link density [20, 56, 59]. Excellent chemical resistance is reported for SU-8 [21]. There are some indications that SU-8 can be classified as biocompatible material, however, to-date it is not clear if this material meets the tight requirements of certain standards for medical applications, for example the ISO 10993 requirements for medical implants [60, 61].

Photosensitive polyimide was first reported in 1971 by Kerwin and Goldrick [62]. As polyimide is generally insoluble in many solvents, it is usually prepared by imidization of photo-sensitive precursors based on poly(amic acid)s or poly-isoimides, via thermal or chemical treatment [63, 64]. Spin casting solutions of varying viscosity yields films with thicknesses up to 50μm with a single coating [65, 66]. Structuring of polyimide films is described in detail in a previous section of this review and structures with aspect ratios of 20:1 have been reported [67]. Polyimide is a ductile material which allows for maximum elongation up to 70 % [63]. The Young's modulus of photosensitive polyimide is usually within the range of 2.5–4.7GPa for commercially available materials [68], but it can be greater than 7 GPa using optimized photosensitive groups [63]. The most noteworthy characteristics of polyimide are its excellent thermal stability and high toughness. It can be elongated up to 45 % before break at 200 MPa in tension [68], and it exhibits a glass transition temperature as high as 290-350°C in the fully cured state [68]. Thermal degradation of polyimide starts at temperatures above 420°C [62, 68]. In addition, polyimide also offers superior chemical and electrical barrier properties [69].

Thermoplastics

Thermoplastics refer to those polymeric materials (including the above mentioned 'standard' polymers) which soften or melt upon the application of heat. They are further separated into those which are (semi-) crystalline and transfer into a viscous liquid above their melting temperature, and those which are amorphous and transfer into a viscous liquid above their glass transition temperature. They can be processed at the micro-scale by soft-lithographic techniques at an appropriate temperature, for example by embossing, molding, or imprinting. The feature size of the micro-structures then replicates the feature size of the embossing or imprinting stamp, or the mould. Moulds are usually made from Si-based materials, metals, or thermosets. In this way, feature sizes in the sub-micron regime can be

achieved [30, 34, 70]. Most thermoplastic polymers can be also be structured by etching with reactive gases such as O_2 or CF_4 plasma [37, 38]. In strict comparison with SU-8 or polyimide, thermoplastics have the general disadvantage that their long chain nature (and thus low solubility) does not allow deposition of smooth, thick films by spin casting.

Polymethylmethacryltae (PMMA) is the best characterized and most well developed thermoplastic polymer for microsystems in terms of surface micromachining [66]. However, to-date PMMA has only been used rarely as structural polymer in micro-scale sensors or actuators. Spin casting of solutions of high molecular weight PMMA results in films of thickness up to 5μm with a single coating [71]. Thicker film deposition can be achieved by multi-layer spinning [71], or by chemical bonding of thick PMMA sheets (0.5-1mm) onto a substrate [66]. Structuring of PMMA can be achieved by e-beam, X-ray, or UV radiation, all of which cause chain scission. Afterwards a chemical development process is employed which selectively dissolves the lower molecular weight PMMA in the exposed areas. The lower molecular weight fractions dissolve much faster than the higher weight material, and variously shaped profiles can be created by careful selection and layering of differently molecular-weighted polymer. High resolution structures with feature sizes far below 1μm can be achieved using X-ray lithography [71]. Micro-structures of PMMA can also be fabricated by soft lithographic techniques such as hot-embossing [70]. The modulus of PMMA (~1.9-3.3 GPa [7, 43, 66]) is a little lower than most epoxy resins. Glass transition temperature is low, at around 105°C and degradation temperature around 160°C, making this a rather thermally unstable material [72]. As already pointed out, thermoplastic materials exhibit comparatively poor mechanical stability due to their visco-elastic nature. This can lead to undesirable plastic deformation of the micro-structure, particularly when the operating temperature approaches the softening temperature of the polymer.

Conjugated polymers, such as polypyrrole (PPy) and polyaniline (PANI), are widely used as structural materials in micro-actuators. The actuation of conjugated polymers is based on reversible switching between the oxidized and the reduced state, which can be accompanied by significant changes in the volume of the polymer. This process can be driven electrochemically by small changes in cell voltage (~1V) (please refer to the section on ionic electro-active polymers in this review). Typically, conjugated polymers are doped by ion implantation to maintain charge neutrality. The volume changes can be ascribed to mass transport of charge-balancing ions or associated solvent molecules between the polymer and the surrounding electrolyte. Owing to their low solubility, a common way of thin film deposition of PPy is monomer oxidation and the subsequent growth of polymers of the oxidized monomer [37, 73, 74]. Thin films also have been deposited by micro-contact-printing [75]. In contrast, PANI can be dissolved and thin films deposited by spin-casting [76, 77]. Micro-patterning can be achieved by soft-lithographic methods [75] or reactive ion etching [73, 74]. The modulus of conjugated polymers depends on the degree of doping, the applied potential and on the surrounding environment, for example the composition of the electrolyte solution [77-79]. Moduli within the range of 0.1-2GPa [77, 79-81] and 0.3-4.3GPa [78, 79, 82-88] have been reported for PANI and PPy, respectively. The glass transition temperature of PANI lies in the range of 100-160°C dependent on the

amount of solvent in the material [79, 89]. For PPy, a glass transition temperature of 42-55°C has been reported [90, 91].

Elastomers

Elastomers refer to cross-linked rubbery polymeric materials that can be stretched easily to very high extensions (usually 3 to 10 times original dimensions) and then rapidly recover to their original dimensions upon unloading. Usually the modulus of elastomers can be tuned over a wide range by chemically controlling the amount of cross-linking between the precursor chains or monomers [9].

Among the most widely used elastomers in MEMS is polydimethylsiloxane (PDMS). This elastomer is usually synthesized by mixing a liquid monomer and a cross-linker and shaped by casting into the desired shape. Upon heating, the polymerization reaction starts and a solid elastomer is formed. Thin films of PDMS can be deposited by spin casting of the precursor liquid with thicknesses ranging from below 100μm to 1 mm [12, 92]. Structuring of PDMS can be achieved by replica molding into any desired shape [10, 93]. The modulus can be tuned over a wide range (0.5-10MPa) by varying the amount of cross-linking and the curing conditions [10-12]. PDMS is chemically inert, thermal stable, permeable to gases, low-cost and simple to handle [93]. In particular, it is an attractive material for applications in micro-fluidics, for example as an actuated membrane, or as structural polymer in BioMEMS [12, 92, 93].

18.2 Applications

At a research level numerous examples of micro-scale sensors and actuators exist which benefit from the low modulus and great elasticity of structural polymers as well as from the cost-efficiency of micro-fabrication processes. However, they are restricted to only a few polymers, usually not including standard polymers. This may be due to the fact that implementation of micro-machining techniques for non-photosensitive polymers is still at an early stage of development.

Micro-scale sensors

The use of structural polymers for micro-scale sensors has been successfully demonstrated for chemical mass-sensing applications. These sensors make use of the low modulus and stiffness of free-standing structural polymer cantilevers. Immobilization of a monolayer of molecules on one side of the cantilever induces a difference in surface stress between the opposite sides, which results in a deflection as shown in Figure 18.1. In order to promote selective binding of specific molecules, such as DNA or antibodies, the surface of the cantilever is coated in an appropriate reagent. Read-out of the sensors is usually achieved by integrated piezo-resistors [94, 95]. These sensors are usually disposable and cost-efficient fabrication using structural low-cost polymers is therefore of great benefit [6]. A six times higher sensitivity can be achieved by using SU-8 as the structural polymer, compared to Si-nitride cantilevers [6]. Potential applications of thermoplastic polymers with even lower modulus and greater cost-efficiency have not yet been evaluated systematically to the current knowledge of the authors.

Limitations may arise due to electron migration in the piezo-resistive layer at high supply voltages, leading to an increase in the minimum deflection that can be detected [94]. Self-heating of the cantilever could result in plastic deformation of the structural polymer [94] if the operating temperature approaches the softening temperature.

Micro-scaled sensors cantilever arrays have been fabricated using Epo-tek UVO-114, an optically transparent epoxy, which mimic the biological front-end processing in the mammalian cochlea. They are intended for use in auditory prostheses. Fabrication of the epoxy cantilevers was achieved by microinjection-molding using a flexible PDMS mould [96].

Another application of structural polymers for micro-scale sensing applications is the fabrication of epoxy soft tips for scanning force microscopy [97, 98]. The reduced modulus of SU-8, compared to conventional Si-based tips, allows for a low-cost fabrication of soft tips with non-critical dimensions. SU-8 has also been utilized as structural material for wells suitable for large volume deposition of gas sensitive films onto a constrained area [99].

Micro-scale actuators

Micro-scale actuators can also make use of the low modulus of structural polymers and larger displacements at smaller actuation forces can be achieved. Actuated polymer-microstructures can be divided into two groups. The first group comprises polymer structures that can be directly actuated using some special electrical, electrochemical, or thermal properties of the structural polymer. Electronically conducting polymers or conjugated polymers, such as polypyrrole (PPy) [37, 100-103], or polyaniline (PA) [77, 81, 103-105], have been used as structural materials for biomedical devices. The applications are in cell manipulation [77], mimicking of muscle-like movements [74, 102, 106, 107], or actuation of micro-valves in microfluidic systems [14]. The great advantage of these actuators, compared to the widespread piezoelectric actuator devices, lies in the low voltages that are required to drive them [103]. Underwater applications are possible since electrolysis due to high voltages is no longer a concern [77]. The excellent thermal properties of highly cross-linked epoxies, such as SU-8, can be used for thermal actuation [108]. Due to their large thermal expansion coefficient, SU-8 structures can be actuated at low voltages < 1–2 V and at low ambient temperatures (10–32°C), which allows for actuation even in physiological solutions [109]. Actuators incorporating piezoelectric polyvinylidene fluoride (PVDF) have also been reported [110].

The second, larger, group of actuated polymer micro-structures comprises the majority of structural polymers. These exhibit rather poor electrical, electrochemical, or thermal properties and thus they have to be actuated indirectly. For example, metal coated polymer structures made from polyimide or SU-8, can be actuated electrostatically by using the metallic layer as an electrode [111, 112]. Pneumatic actuation of SU-8 micro-grippers has been reported which benefit from the low modulus and the good transparency of SU-8 for visually controlled micro-assembly applications [4, 113], figure 18.2. Low-modulus (0.75 MPa) elastomeric membranes of polydimethylsiloxane (PDMS) with attached magnetic

Permalloy (Ni80Fe20) films can be actuated magnetically, enabling large displacements for applications of tetherless micro-pumps in microfluidic systems [92].

Although numerous instances of structural polymers used in micro-scale actuators can be found in literature, the general benefits that polymer materials offer through their exceptional variety of properties have not been exploited to full capacity. A novel actuation mechanism is now under investigation which permits direct actuation of non-conductive structural polymers [114]. This uses the so-called Kelvin polarization force, which acts on a dielectric structural polymer in the presence of an electric field gradient. A new fabrication process for polymer micro-cantilevers (figure 18.3) and micro-bridges has been developed, which is based on conventional micro-machining techniques. Using a combination of photolithography and sacrificial layer etching, similar to the approach for structuring of PMMA-based micro-bridges [38], this fabrication process can be applied to virtually any polymer. Finally, a new micro-scale, wireless, passive strain sensor for biomedical applications has been proposed, which can be built entirely from low-cost thermoplastic polymer materials [115].

Table 18.1: Material properties of selected structural polymers

Material	Young's modulus [GPa]	Tensile strength [MPa]	Glass Transition [°C]	Thermal Degradation [°C]	Thermal conductivity [W / (m K)]	Thermal expansion [μm / (m K)]
SU-8	0.7 - 5 [21, 55-58]	15-53 [56, 116]	>200 [20, 56, 59]	> 380 [20, 56, 59]	0.2 [108]	52 [109]
Photo-sensitive polyimide	2.5 – 7.2 [63, 68]	120 - 428 [63, 68, 117]	290 - 350 [68]	> 420 [62, 68]	0.88 - 1.7 [62, 69]	16 - 57 [62, 68]
PMMA	1.9 - 3.3 [7, 43, 66]	72 - 84 [7]	105 -115 [7, 8, 43]	> 160 [72]	0.15 - 0.2 [7, 8]	50 - 70 [7, 8]
PDMS	0.0005 - 0.01 [10-12]	4-10 [12]	-123 [7]	> 339 [118]	0.2 [93]	310 [93]
PPy	0.3 - 4.3 [78, 79, 82-88]	4 - 49 [78, 79, 83, 87, 119]	42 - 55 [90, 91]	> 100 [120]	0.62 - 1.12 [121]	n.a.
PANI	0.1 - 2 [77, 79-81]	0.5 - 50 [122, 123]	100 - 160 [79, 89]	> 200 [124, 125]	0.01 [77]	n.a.

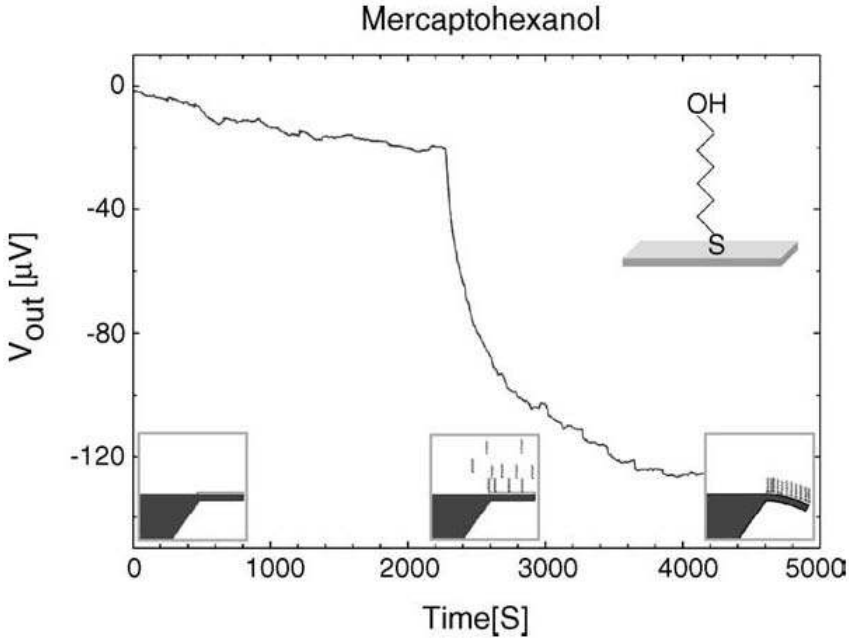

Figure 1: The response in output voltage of a SU-8 cantilever when 6-mercapto-1-hexanol is immobilized on the gold coated surface [95]. Reprinted from with permission.

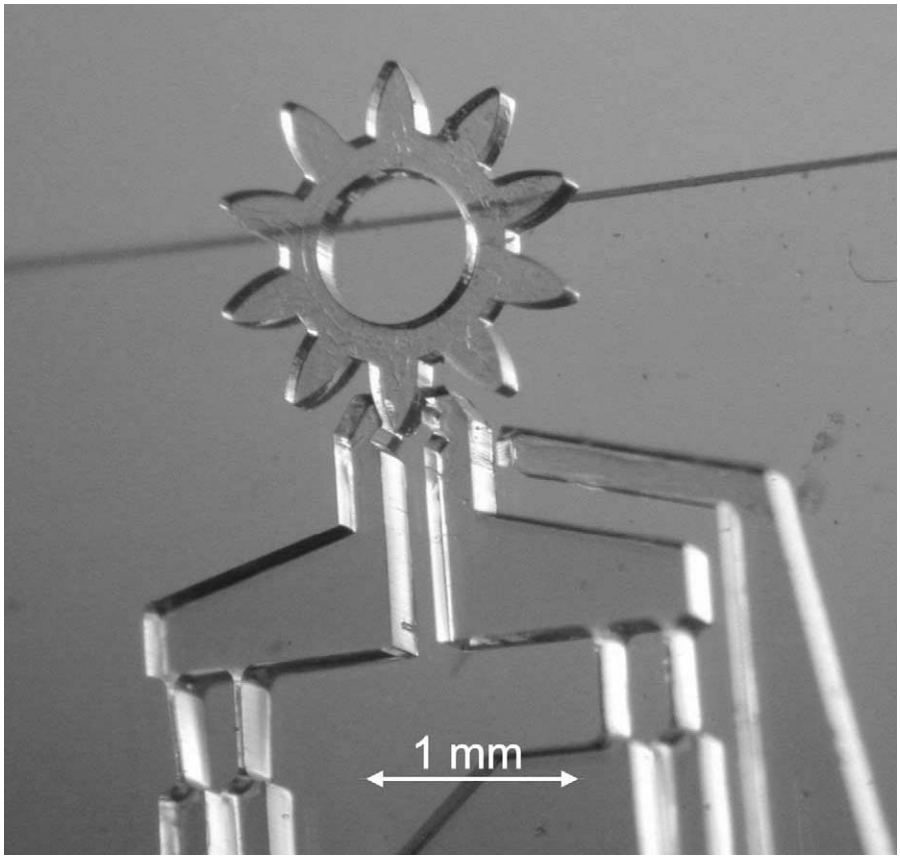

Figure 2: A SU-8 microgripper grasping a micro-mechanical object [4]. Reprinted with permission.

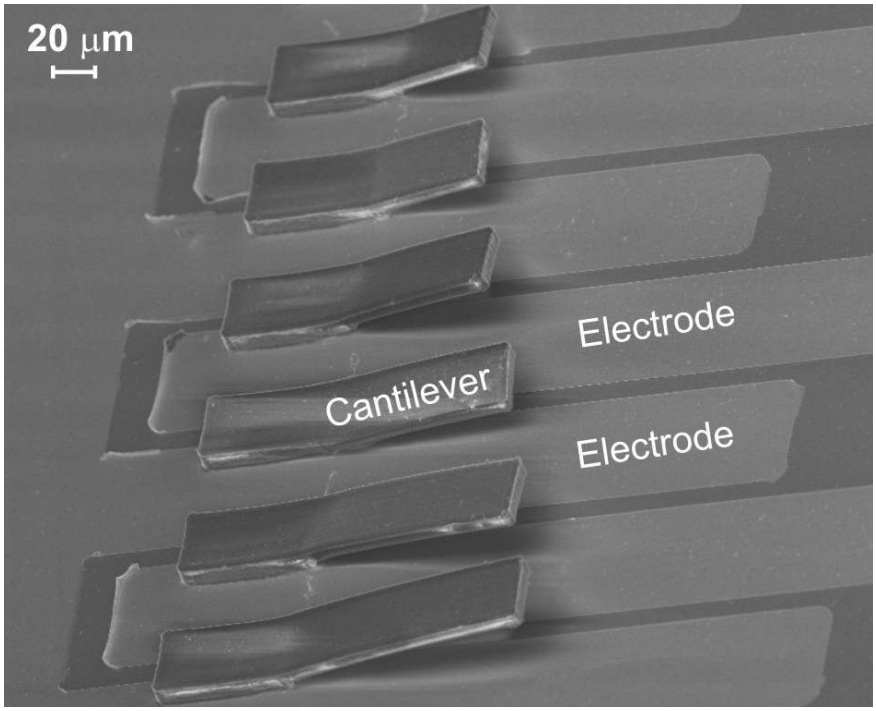

Figure 3: Array of free-standing SU-8 cantilevers of thickness 3.5 μm and different length within the range of 20-60 μm. The cantilevers are placed above a combination of electrodes, which produce an electric field-gradient and thus, a net (Kelvin polarization) force on the dielectric cantilevers [114].

[1] K. E. Petersen, Proc. IEEE 70 (1982) 420.
[2] S. M. Spearing, Acta Materialia 48 (2000) 179.
[3] V. T. Srikar, S. M. Spearing, J. Microelectromech. Syst. 12 (2003) 3.
[4] S. Butefisch, V. Seidemann, S. Buttgenbach, Sens. Actuator A-Phys. 97-8 (2002) 638.
[5] V. T. Srikar, S. M. Spearing, Sens. Actuator A-Phys. 102 (2003) 279.
[6] M. Calleja, M. Nordstrom, M. Alvarez, J. Tamayo, L. M. Lechuga, A. Boisen, Ultramicroscopy 105 (2005) 215.
[7] B. Ellis (Ed.) Polymers. A Property Database., Chapman and Hall / CRC, Boca Raton, USA, 2000.
[8] J. Bandrup, E. H. Immergut, E. A. Grulke, A. Abe, D. R. Bloch, Polymer Handbook, John Wiley & Sons, 2003.
[9] L. R. G. Treloar, The Physics of Rubber Elasticity, Oxford university press, Oxford, 1975.
[10] D. Armani, C. Liu, N. Aluru, Twelfth IEEE International Conference on Micro Electro Mechanical Systems, Orlando, USA, 1999.
[11] K. M. Choi, J. A. Rogers, J. Am. Chem. Soc. 125 (2003) 4060.
[12] A. Mata, A. J. Fleischman, S. Roy, Biomedical Microdevices 7 (2005) 281.
[13] J. B. Park, J. D. Bronzino (Eds.), Biomaterials, CRC Press, Boca Raton, FL, 2003.
[14] C. Goll, W. Bacher, B. Bustgens, D. Maas, R. Ruprecht, W. K. Schomburg, J. Micromech. Microeng. 7 (1997) 224.
[15] S. R. Quake, A. Scherer, Science 290 (2000) 1536.
[16] V. Warzelhan, Polymers for Advanced Technologies 8 (1997) 210.
[17] L. Y. Ljungberg, Materials & Design 24 (2003) 383.
[18] V. Warzelhan, F. Brandstetter, Macromol. Symp. 201 (2003) 291.
[19] E. Winkler, H. Pielartzik, A. Schneller, Angewandte Makromolekulare Chemie 244 (1997) 161.
[20] K. Y. Lee, N. LaBianca, S. A. Rishton, S. Zolgharnain, J. D. Gelorme, J. Shaw, T. H. P. Chang, Journal of Vacuum Science & Technology B 13 (1995) 3012.
[21] H. Lorenz, M. Despont, N. Fahrni, N. LaBianca, P. Renaud, P. Vettiger, J. Micromech. Microeng. 7 (1997) 121.
[22] H. Lorenz, M. Despont, N. Fahrni, J. Brugger, P. Vettiger, P. Renaud, Sens. Actuator A-Phys. 64 (1998) 33.
[23] M. B. Chan-Park, W. K. Neo, Microsyst. Technol. 9 (2003) 501.
[24] J. X. Gao, M. B. Chan-Park, D. Z. Xie, Y. H. Yan, W. X. Zhou, B. K. A. Ngoi, C. Y. Yue, Chemistry of Materials 16 (2004) 956.
[25] L. Vogelaar, J. N. Barsema, C. J. M. van Rijn, W. Nijdam, M. Wessling, Adv. Mater. 15 (2003) 1385.
[26] M. Heckele, W. K. Schomburg, J. Micromech. Microeng. 14 (2004) R1.
[27] L. Vogelaar, R. G. H. Lammertink, J. N. Barsema, W. Nijdam, L. A. M. Bolhuis-Versteeg, C. J. M. van Rijn, M. Wessling, Small 1 (2005) 645.
[28] M. F. Jensen, J. E. McCormack, B. Helbo, L. H. Christensen, T. R. Christensen, O. Geschke, Lab Chip 4 (2004) 391.
[29] Y. N. Xia, G. M. Whitesides, Annu. Rev. Mater. Sci. 28 (1998) 153.
[30] H. Becker, U. Heim, Sens. Mater. 11 (1999) 297.
[31] H. Becker, U. Heim, Sens. Actuator A-Phys. 83 (2000) 130.
[32] N. Stutzmann, T. A. Tervoort, C. W. M. Bastiaansen, K. Feldman, P. Smith, Adv. Mater. 12 (2000) 557.

[33] G. Fichet, N. Stutzmann, B. V. O. Muir, W. T. S. Huck, Adv. Mater. 14 (2002) 47.
[34] V. Studer, A. Pepin, Y. Chen, Appl. Phys. Lett. 80 (2002) 3614.
[35] M. Brehmer, L. Conrad, L. Funk, Journal of Dispersion Science And Technology 24 (2003) 291.
[36] J. P. Rolland, E. C. Hagberg, G. M. Denison, K. R. Carter, J. M. De Simone, Angewandte Chemie-International Edition 43 (2004) 5796.
[37] E. W. H. Jager, E. Smela, O. Inganas, Science 290 (2000) 1540.
[38] G. Zhang, J. Gaspar, V. Chu, J. P. Conde, Appl. Phys. Lett. 87 (2005).
[39] Y. J. Kim, M. G. Allen, IEEE Transactions on Components and Packaging Technologies 22 (1999) 282.
[40] V. Linder, B. D. Gates, D. Ryan, B. A. Parviz, G. M. Whitesides, Small 1 (2005) 730.
[41] J. D. Ferry, Viscoelastic Properties of Polymers, John Wiley and Sons, New York, 1980.
[42] I. M. Ward, Mechanical Properties of Solid Poylmers, John Wiley and Sons Ltd, Chichester, 2004.
[43] M. Wendlandt, T. A. Tervoort, U. W. Suter, Polymer 46 (2005) 11786.
[44] A. B. Frazier, M. G. Allen, J. Appl. Phys. 73 (1993) 4428.
[45] M. D. Frogley, D. Ravich, H. D. Wagner, Composites Science and Technology 63 (2003) 1647.
[46] Q. H. Zeng, A. B. Yu, G. Q. Lu, D. R. Paul, Journal of Nanoscience and Nanotechnology 5 (2005) 1574.
[47] N. Damean, B. A. Parviz, J. N. Lee, T. Odom, G. M. Whitesides, J. Micromech. Microeng. 15 (2005) 29.
[48] D. W. Schubert, T. Dunkel, Mater. Res. Innov. 7 (2003) 314.
[49] C. Friese, F. Goldschmidtboing, P. Woias, Transducers, 2003.
[50] H. Ito, C. G. Willson, J. M. J. Fréchet, Proceedings of the SPE Regional Technical Conference on Photopolymers, The Nevele Country Club, Ellenville, New York, 1982.
[51] J. M. Shaw, J. D. Gelorme, N. C. LaBianca, W. E. Conley, S. J. Holmes, IBM Journal of Research and Development 41 (1997) 81.
[52] J. Zhang, K. L. Tan, G. D. Hong, L. J. Yang, H. Q. Gong, J. Micromech. Microeng. 11 (2001) 20.
[53] J. Zhang, K. L. Tan, H. Q. Gong, Polym. Test 20 (2001) 693.
[54] E. H. Conradie, D. F. Moore, J. Micromech. Microeng. 12 (2002) 368.
[55] H. S. Khoo, K. K. Liu, F. G. Tseng, J. Micromech. Microeng. 13 (2003) 822.
[56] R. Feng, R. J. Farris, J. Micromech. Microeng. 13 (2003) 80.
[57] L. Dellmann, S. Roth, C. Beuret, L. Paratte, G. A. Racine, H. Lorenz, M. Despont, P. Renaud, P. Vettiger, N. F. de Rooij, Microsyst. Technol. 4 (1998) 147.
[58] F. E. H. Tay, J. A. van Kan, F. Watt, W. O. Choong, J. Micromech. Microeng. 11 (2001) 27.
[59] N. C. LaBianca, J. D. Gelorme, 1995.
[60] G. Kotzar, M. Freas, P. Abel, A. Fleischman, S. Roy, C. Zorman, J. M. Moran, J. Melzak, Biomaterials 23 (2002) 2737.
[61] G. Voskerician, M. S. Shive, R. S. Shawgo, H. von Recum, J. M. Anderson, M. J. Cima, R. Langer, Biomaterials 24 (2003) 1959.
[62] R. E. Kerwin, M. R. Goldrick, Polym. Eng. Sci. 11 (1971) 426.
[63] M. Ree, T. L. Nunes, K. J. R. Chen, J. Polym. Sci. Pt. B-Polym. Phys. 33 (1995) 453.

[64] D. K. Yoo, S. J. Shim, D. H. Lee, J. H. Kim, Y. K. Lee, Y. J. Kim, S. W. Kim, D. Kim, Journal of Chemical Engineering of Japan 38 (2005) 615.
[65] M. Hiro, C. C. Schuckert, Advanced Packaging Volume (2000). Retrieved from http://ap.pennnet.com.
[66] M. Gad-el-Hak (Ed.) The Mems Handbook, CRC Press, Boca Raton, 2002.
[67] A. B. Frazier, IEEE Trans. Ind. Electron. 42 (1995) 442.
[68] HDMicrosystems. Retrieved 01.03.2006 from http://www.hdmicrosystems.com/conn/data/HDMPSG.pdf.
[69] HDMicrosystems. Retrieved 01.03.2006 from http://www.hdmicrosystems.com/conn/data/PI2720.pdf.
[70] Y. J. Zhao, T. H. Cui, J. Micromech. Microeng. 13 (2003) 430.
[71] MicroChem. Retrieved 01.03.2006 from http://www.microchem.com/products/pdf/PMMA_Data_Sheet.pdf.
[72] E. H. Vieweg (Ed.) Kunststoffhandbuch, Carl Hanser Verlag, München, 1975.
[73] E. Smela, J. Micromech. Microeng. 9 (1999) 1.
[74] E. Smela, Adv. Mater. 15 (2003) 481.
[75] Z. N. Bao, J. A. Rogers, H. E. Katz, Journal of Materials Chemistry 9 (1999) 1895.
[76] D. Chinn, J. Janata, Thin Solid Films 252 (1994) 145.
[77] J. W. L. Zhou, H. Y. Chan, T. K. H. To, K. W. C. Lai, W. J. Li, IEEE-ASME Transactions on Mechatronics 9 (2004) 334.
[78] P. Murray, G. M. Spinks, G. G. Wallace, R. P. Burford, Synthetic Metals 84 (1997) 847.
[79] G. G. Wallace, G. M. Spinks, L. A. P. Kane-Maguire, P. R. Teasdale, Conductive Electroactive Polymers, CRC Press LCC, Boca Raton, USA, 2003.
[80] O. Oka, O. Kiyohara, S. Morita, K. Yoshino, Synthetic Metals 55 (1993) 999.
[81] J. M. Sansinena, J. B. Gao, H. L. Wang, Adv. Funct. Mater. 13 (2003) 703.
[82] M. Satoh, K. Kaneto, K. Yoshino, Synthetic Metals 14 (1986) 289.
[83] T. Shimidzu, A. Ohtani, T. Iyoda, K. Honda, Journal of Electroanalytical Chemistry 224 (1987) 123.
[84] P. Chiarelli, A. Dellasanta, D. Derossi, A. Mazzoldi, Journal of Intelligent Material Systems and Structures 6 (1995) 32.
[85] A. Della Santa, D. De Rossi, A. Mazzoldi, Smart Mater. Struct. 6 (1997) 23.
[86] A. Della Santa, A. Mazzoldi, C. Tonci, D. De Rossi, Materials Science & Engineering C-Biomimetic Materials Sensors and Systems 5 (1997) 101.
[87] G. M. Spinks, G. G. Wallace, L. Liu, D. Zhou, Macromol. Symp. 192 (2003) 161.
[88] L. Bay, K. West, P. Sommer-Larsen, S. Skaarup, M. Benslimane, Adv. Mater. 15 (2003) 310.
[89] A. J. Milton, A. P. Monkman, J. Phys. D-Appl. Phys. 26 (1993) 1468.
[90] J. C. Thieblemont, A. Brun, J. Marty, M. F. Planche, P. Calo, Polymer 36 (1995) 1605.
[91] C. N. Van, K. Potje-Kamloth, J. Phys. D-Appl. Phys. 33 (2000) 2230.
[92] M. Khoo, C. Liu, Sens. Actuator A-Phys. 89 (2001) 259.
[93] J. C. McDonald, G. M. Whitesides, Accounts of Chemical Research 35 (2002) 491.
[94] J. Thaysen, A. D. Yalcinkaya, P. Vettiger, A. Menon, J. Phys. D-Appl. Phys. 35 (2002) 2698.
[95] A. Johansson, M. Calleja, P. A. Rasmussen, A. Boisen, Sens. Actuator A-Phys. 123-24 (2005) 111.
[96] T. Xu, M. Bachman, F. G. Zeng, G. P. Li, Sens. Actuator A-Phys. 114 (2004) 176.

[97] G. Genolet, J. Brugger, M. Despont, U. Drechsler, P. Vettiger, N. F. de Rooij, D. Anselmetti, Review of Scientific Instruments 70 (1999) 2398.
[98] M. Hopcroft, T. Kramer, G. Kim, K. Takashima, Y. Higo, D. Moore, J. Brugger, Fatigue & Fracture of Engineering Materials & Structures 28 (2005) 735.
[99] F. Zee, J. W. Judy, Sens. Actuator B-Chem. 72 (2001) 120.
[100] E. W. H. Jager, E. Smela, O. Inganas, Sens. Actuator B-Chem. 56 (1999) 73.
[101] E. W. H. Jager, E. Smela, O. Inganas, I. Lundstrom, Synthetic Metals 102 (1999) 1309.
[102] J. D. Madden, R. A. Cush, T. S. Kanigan, I. W. Hunter, Synthetic Metals 113 (2000) 185.
[103] M. Roemer, T. Kurzenknabe, E. Oesterschulze, N. Nicoloso, Anal. Bioanal. Chem. 373 (2002) 754.
[104] E. Smela, W. Lu, B. R. Mattes, Synthetic Metals 151 (2005) 25.
[105] E. Smela, B. R. Mattes, Synthetic Metals 151 (2005) 43.
[106] R. H. Baughman, Synthetic Metals 78 (1996) 339.
[107] R. H. Baughman, Science 308 (2005) 63.
[108] N. T. Nguyen, S. S. Ho, C. L. N. Low, J. Micromech. Microeng. 14 (2004) 969.
[109] N. Chronis, L. P. Lee, J. Microelectromech. Syst. 14 (2005) 857.
[110] Y. Fu, M. K. Ghantasala, E. Harvey, L. J. Qin, Smart Mater. Struct. 14 (2005) 488.
[111] G. M. Atkinson, R. E. Pearson, Z. Ounaies, C. Park, J. S. Harrison, S. Dogan, Transducers, Boston, USA, 2003.
[112] C. Friese, H. Zappe, Transducers, Seoul, Korea, 2005.
[113] V. Seidemann, S. Butefisch, S. Buttgenbach, Sens. Actuator A-Phys. 97-8 (2002) 457.
[114] S. Schmid, M. Wendlandt, D. Junker, C. Hierold, submitted for publication (2006).
[115] F. Umbrecht, M. Wendlandt, D. Junker, C. Hierold, J. Neuenschwander, IEEE Conference on Sensors, Irvine, USA, 2005.
[116] L. Dellmann, S. Roth, C. Beuret, G. A. Racine, H. Lorenz, M. Despont, P. Renaud, P. Vettiger, N. F. de Rooij, Solid State Sensors and Actuators, Chicago, USA, 1997.
[117] J. L. Wyant, C. C. Schuckert, Solid State Technology Volume (2000). Retrieved from http://sst.pennnet.com.
[118] G. Camino, S. M. Lomakin, M. Lazzari, Polymer 42 (2001) 2395.
[119] N. Bates, M. Cross, R. Lines, D. Walton, Journal of the Chemical Society-Chemical Communications (1985) 871.
[120] P. S. Abthagir, R. Saraswathi, Materials Chemistry and Physics 92 (2005) 21.
[121] B. A. Lunn, J. Unsworth, N. G. Booth, P. C. Innis, J. Mater. Sci. 28 (1993) 5092.
[122] A. Kitani, M. Kaya, S. I. Tsujioka, K. Sasaki, Journal Of Polymer Science Part A-Polymer Chemistry 26 (1988) 1531.
[123] P. J. Laughlin, A. P. Monkman, Synthetic Metals 84 (1997) 765.
[124] K. G. Neoh, E. T. Kang, K. L. Tan, Polymer Degradation and Stability 43 (1994) 141.
[125] X. H. Lu, C. Y. Tan, J. W. Xu, C. B. He, Synthetic Metals 138 (2003) 429.

Acknowledgements

The Authours gratefully acknowledge the EU 4M Network of Excellence for their support in the preparation of this article. Particlular thanks go to the leader of the Sensors and Actuators group, Dr Paul Kirby. Thanks also go to Enza Giaracuni for her work in preparing the manuscript and to Drs Cristina Rusu and Katrin Person at Imego.

E. Pagounis would like to thank Dr. Herbert Schmidt from Robert Bosch GmbH for providing the Figure 8.5 in the text.

Michael Wegener is indebted to Prof. Dr. Reimund Gerhard-Multhaupt, Dr. Axel Mellinger, Werner Wirges, Dr. Guggi Kofod, Andreas Pucher (Potsdam), Dr. Enis Tuncer (formaly Potsdam), Prof. Dr. Siegfried Bauer, Dr. Simona Bauer-Gogonea, Dr. Reinhard Schwödiauer (Linz), Prof. Dr. G. M. Sessler, Dr. R. Kressmann, Dr. J. Hillenbrand (Darmstadt), Dr. M. Paajanen, Dr. J. Raukola (Tampere), Prof. Dr. Gian Carlo Montanari, Dr. Davide Fabiani (Bologna), Prof. Dr. Zhongfu Xia, and Xunlin Qiu (Shanghai), for exciting and fruitful discussions on the topics of this paper and the excellent co-operation in joint research projects. Partial financial support from the German Science Foundation, the Volkswagen Foundation, the German Academic Exchange Service, the German Federal Ministry of Economy and Labor, and the European Commission is gratefully acknowledged.